UNIVERSIDADE DE LISBOA

INSTITUTO SUPERIOR TÉCNICO

Bioengineering strategies towards the *in vitro* fabrication of hierarchical and biomimetic cartilage constructs

João Carlos Fernandes da Silva

Supervisor: Doctor Frederico Castelo Alves Ferreira

Co-Supervisor: Doctor Robert J. Linhardt

Thesis approved in public session to obtain the PhD Degree in

Bioengineering

Jury final classification: Pass with Distinction and Honour

2019

UNIVERSIDADE DE LISBOA
INSTITUTO SUPERIOR TÉCNICO

Bioengineering strategies towards the *in vitro* fabrication of hierarchical and biomimetic cartilage constructs

João Carlos Fernandes da Silva

Supervisor: Doctor Frederico Castelo Alves Ferreira
Co-Supervisor: Doctor Robert J. Linhardt

Thesis approved in public session to obtain the PhD Degree in
Bioengineering

Jury final classification: Pass with Distinction and Honour

Jury

Chairperson: Doctor Joaquim Manuel Sampaio Cabral, Instituto Superior Técnico, Universidade de Lisboa

Members of the Committee:

Doctor Joaquim Manuel Sampaio Cabral, Instituto Superior Técnico, Universidade de Lisboa

Doctor José Paulo Sequeira Farinha, Instituto Superior Técnico, Universidade de Lisboa

Doctor Frederico Castelo Alves Ferreira, Instituto Superior Técnico, Universidade de Lisboa

Doctor Ioannis Papantoniou, KU Leuven, Bélgica

Doctor Teresa Catarina Páscoa Madeira, Nova Medical School / Faculdade de Ciências Médicas, Universidade Nova de Lisboa

Funding Institutions

FCT – Fundação para a Ciência e Tecnologia

CBIS – Center for Biotechnology & Interdisciplinary Studies, Rensselaer Polytechnic Institute

2019

ABSTRACT

Cartilage regeneration upon injury or joint disease remains a challenge mainly due to its intrinsic avascular nature, low cellularity and highly complex multizonal architecture. Cartilage tissue engineering (CTE) approaches combining cells, biomaterial matrices and biochemical/physical stimuli aim to generate tissue substitutes with native-like properties and long-term functionality. However, despite the existence of studies with promising results, fully functional cartilage constructs with physiologic structural and biomechanical properties are yet to be achieved, which has limited their clinical translation.

The main objective of this thesis was to contribute towards the development of novel bioengineering strategies for the *in vitro* fabrication of native-like cartilage tissue through a closer mimicry of some of its specific biochemical/physical, structural and mechanical features. The glycosaminoglican (GAG) composition of the main cells used for CTE (chondrocytes and bone marrow/synovium-derived mesenchymal stem/stromal cells-hBMSC/hSMSC), their cell-secreted extracellular matrix (ECM), and of the respective chondrogenic aggregates generated under normoxic (21% O_2) / hypoxic (5% O_2) conditions was determined using highly sensitive mass spectrometry techniques. It is noteworthy that external supplementation with main cartilage GAGs, particularly, chondroitin sulfate (CS) and hyaluronic acid (HA), showed favorable effects in the MSC chondrogenic differentiation on porous biodegradable scaffolds. Additive manufacturing technology was employed to fabricate a customizable perfusion bioreactor able to provide fluid-induced shear stress stimuli to MSC-based cartilage constructs, which resulted in enhanced chondrogenesis and reduced hypertrophy. Different scaffold structures, namely 3D MSC-ECM decorated-scaffolds and kartogenin-loaded coaxial electrospun nanofibers were developed to target the regeneration of specific zonal regions within the osteochondral tissue. Finally, we introduced the concept of a tri-layered hierarchical scaffold to mimic the architecture of different articular cartilage zones (3D porous polycaprolactone (PCL) scaffold as deep zone layer, a GAG-based hydrogel in the middle zone and aligned PCL/Gelatin nanofibers as superficial zone layer) and its ability to support the chondrogenic differentiation of MSC was evaluated. Such biomimetic scaffolds provide a closer mimicry of the complex structure of articular cartilage and are promising for the repair of full-thickness cartilage defects and as more reliable *in vitro* models for research and drug screening.

Keywords: Cartilage tissue engineering (CTE); Extracellular matrix (ECM); Glycosaminoglycans (GAG); Hierarchical scaffolds; Mesenchymal stem/stromal cells (MSC).

RESUMO

A regeneração da cartilagem após lesão ou doença articular é limitada pela sua natureza avascular, baixa densidade celular e ainda pela sua complexa arquitetura hierarquizada. Abordagens de engenharia de tecidos combinando células, biomateriais e estímulos bioquímicos/físicos têm como objectivo gerar cartilagem com propriedades similares ao tecido nativo e com funcionalidade a longo prazo. No entanto, apesar de muitas estratégias terem originado resultados promissores, ainda não foram gerados substitutos de cartilagem totalmente funcionais e com propriedades estruturais e biomecânicas semelhantes às observadas fisiologicamente, o que limita a sua translação para um contexto clínico.

Esta tese tem como objectivo principal contribuir para o desenvolvimento de novas estratégias de bioengenharia para a fabricação *in vitro* de cartilagem semelhante ao tecido nativo através de um mimetismo mais aproximado de algumas das suas propriedades bioquímicas/físicas, estruturais e mecânicas. As composições da matriz extracelular (ECM), em termos glicosaminoglicanos (GAG) produzidos pelos principais tipos de células usadas para engenharia de tecidos de cartilagem (condrócitos e células estaminais mesenquimais derivadas da medula óssea e da membrana sinovial – hBMSC/hSMSC) bem como de agregados condrogênicos produzidos em ambiente de normoxia (21% O_2) / hipóxia (5% O_2) foram determinados usando técnicas de espectroscopia de massa. De notar que a suplementação do meio de cultura com GAGs constituintes da cartilagem, nomeadamente sulfato de condroitina (CS) e ácido hialurónico (HA), demonstrou um efeito positivo na diferenciação condrogênica de MSC, cultivadas em "scaffolds" porosos biodegradáveis. O uso de bioreactores de perfusão, produzidos usando tecnologias de fabricação aditiva permitiu controlar as condições hidrodinâmicas de culturas de MSC cultivadas em "scaffolds", o que resultou em tecidos com superior potencial condrogênico e hipertrofia reduzida. "Scaffolds" com diferentes estruturas, nomeadamente "scaffolds" obtidos por extrusão decorados com MSC-ECM e nanofibras alinhadas e coaxiais incorporando cartogenina produzidos por electro-fiação, foram desenvolvidos para promover a regeneração de zonas específicas do tecido osteocondral. Por fim, foi introduzido um novo conceito de "scaffold" hierárquico com três camadas para mimetizar a arquitetura das diferentes zonas da cartilagem articular e avaliada a sua capacidade de promover a diferenciação de MSC em cartilagem. Estes "scaffolds" biomiméticos são mais semelhantes à estrutura complexa da cartilagem articular, sendo assim promissores para a reparação de lesões osteocondrais e para uso como modelos *in vitro* para investigação científica e triagem de novas moléculas.

Palavras-chave: Engenharia de tecidos de cartilagem; Matriz extracelular; Glicosaminoglicanos; "Scaffolds" hierárquicos; Células estaminais mesenquimais.

After climbing a great hill, one only finds that there are many more hills to climb.

Nelson Mandela (1918-2013)

Dedication

To my girlfriend, Ana Teresa, for all the support, love and strength that helped me to thrive through the most difficult times of this journey.

To my parents, Mário and Maria de Fátima, and brother, Luís, for the constant understanding and motivation.

To my grandmother Amelia, who I believe is in a better place smiling proud of me.

I want to express my gratitude and dedicate this thesis to them, who were essential for the achievement of this important goal in my life.

ACKNOWLEDGEMENTS

Throughout these 4 years of my PhD adventure, I had a great number of valuable people that shared with me this journey and contributed decisively for the fulfilment of this thesis. Therefore, I sincerely want to highlight and acknowledge here the importance that all of you had for the completion of this significant chapter of my life.

First of all, I would like to express my gratitude to Professor Joaquim Cabral for all the effort in putting together such a challenging and cross-disciplinary PhD Program in Bioengineering – Cell Therapies and Regenerative Medicine in which I was fortunate to enrol. I would also like to thank for the opportunity of developing my PhD project at the Stem Cell Engineering Research Group (SCERG) from iBB-IST, for stimulating the collaboration with the Rensselaer Polytechnic Institute (RPI) where I developed a great part of my research work, and specially, for the constant availability, support and for believing in me and in the potential of this work.

A very special thanks needs to be awarded to my supervisors, Professor Frederico Ferreira and Professor Robert J. Linhardt for being always supportive, enthusiastic and motivated during all this PhD. I thank you both for believing in my ideas and for giving me the independence and all the conditions that I needed to develop this work. I believe you both complemented each other very well in this co-supervision and I am truly glad for the opportunity of working and learning with both of you.

Professor Frederico, I am extremely grateful for your constant support and encouragement to do better throughout this entire journey. Thanks for valuing my opinions and for giving me the liberty to pursue the research topics that I was most interested in, which I truly believe was crucial to keep me motivated. Thank you also for the trust deposited in me, for letting me engage in different projects that allowed me to expand my knowledge in the biomaterials/tissue engineering field and for all your creative research ideas (sometimes too many to manage!). I really valued your optimism and practical management of problems, your transparency to your students and your constant willingness to help (no matter how late in the night) whenever I needed.

Professor Linhardt, I am very thankful for the way I was received in your lab at CBIS-RPI by you and all your lab members. Everyone was so nice and helpful to me, that I quickly felt confortable at RPI and part of the “Linhardt Labs” team. Thank you for all the opportunities you gave me, for always stimulating me to improve, for your highly efficient and goal-oriented

guidance and for all the support during these years. I want you to know your great role in keeping me “on-track” with this thesis work and that I learned a lot from you about how to conduct scientific research in a correct and efficient manner. I believe that the great scientific/social environment with constant meaningful brainstorming among the entire group that you promoted in your lab was really important for my scientific and personal development. I can honestly say that one of my greatest achievements was to be able to integrate and perform in such a renowned and high-standard lab as yours.

Professor Fuming Zhang and Karen Coonrad, thank you for your kindness and availability to help during all my stay at RPI. Also, I am so grateful to Dr. Brigitte Arduini, Professor Xing Wang, Dr. Sergey Pryshchep, Dr. Joel Morgan, Dr. Deniz Rende and Mr. Ray Dove for all the help and for teaching me many different techniques needed for the development of this project.

I would like to acknowledge the other research institutions that were involved in this project, namely, the Centre for Rapid and Sustainable Product Development (CDRSP) from Polytechnic Institute of Leiria and also to Centro de Investigação Interdisciplinar Egaz Moniz (CiiEM). A special thanks to Dr. Carla Moura for establishing this line of research at SCERG, for your constant availability to help and for the assistance with the scaffold fabrication, μ-CT analysis, CFD modelling; and to Professor António Alves de Matos, Gonçalo Borrecho and Pedro Henriques for the help in the histological and electronic microscopy analysis.

Many thanks to all Linhardt Labs members for receiving me so nicely and for all the cooperation, support and good moments during my stay at RPI. Thank you Ke and Xiaorui for the great help with the GAG analysis by LC-MS/MS, Jianle for the assistance with the HPLC and Xing for all the discussions and knowledge shared about chemical synthesis. A special thanks to the Nanogroup team, particularly to Chiara, Paiyz, Randi and Fábio. I really enjoyed working and becoming friends with all of you. Randi, I truly appreciated getting to know you and Jack and I really wanted you to know the great contribution that you had for this thesis, not only with your work and scientific input, but also with your kindness, friendship and support.

To my SCERG/iBB lab colleagues and friends, thanks for your companionship, cooperative spirit and for creating a healthy and fun work environment. I am honoured of being part of such a great team and for making great friends that made these PhD years much more pleasant. Particularly, I should thank Marta Costa for all your friendship and willingness to help, for the great discussions and for sharing the record of 8:10 PM shuttle

losing events; to Sílvia Gonella for the amazing work and perseverance during your MSc thesis; to Teresa Silva for being always so helpful and supportive during the all the journey since the PhD classes; and to Carlos Rodrigues for all your help, for your incursions into the cartilage tissue engineering field and for all the scientific and SCP-related meaningful discussions.

A special thanks to André Nascimento, Tânia Baltazar and Marta Carvalho. I am really glad for developing a good friendship with you and for all the great moments we shared in Troy. I believe the fact that such a strong group of people that was going through the same experience both personally and professionally, made us support each other and thrive through the most difficult times. André, thanks for the positive vibes and for your proactive action to make things in Troy much more smoother and fun. Marta, thank you for giving me also the opportunity to share with you also my research work and for enrolling in some "crazy" projects. I truly appreciate your creativity, focus and efficiency and I want you to know that some parts of this project were only possible with your support and cooperation.

I would also like to acknowledge Fundação para a Ciência e Tecnologia (FCT) – Portugal for funding received under the PhD scholarship (SFRH/BD/105771/2014).

To all my friends, thank you for your unconditional support and encouragement. I am sorry for the regular absence during these last years. I believe it's not about the quantity but more the quality of the moments that we shared, and that has been always undeniable great. Nevertheless, I promise I will compensate you for all that time.

A huge thanks to my family, specially to my parents and brother for always encouraging me to work hard to achieve my goals, for understanding my absence and for all the support, patience and love that were crucial for the completion of this PhD.

Ana, thank you for always believing in me (even when I don't) and for encouraging me to follow my dreams, even when it meant we had to go through difficult times. Thank you for being always there for me, for listen and help me in everything and for your patience and love. I want you to know that without your strength and support, the accomplishment of this PhD wouldn't be possible. I truly believe true happiness needs to be shared and I am lucky for having the possibility of sharing all our achievements, good moments and memories with you during all these years.

TABLE OF CONTENTS

LIST OF FIGURES

LIST OF TABLES

ABBREVIATIONS

#

µ-CT – Micro-computed tomography

$\mathbf{Y_{Lac/Gluc}}$ – Aparent yield of lactate from glucose

A

ABS – Acrylonitrile butadiene styrene

ACAN – Aggrecan

ACI – Autologous chondrocyte implantation

ALP – Alkaline phosphatase

AM – Additive Manufacturing

AMAC – 2-aminoacridone

Anti-Anti – Antibiotic-Antimycotic

ATR-FTIR – Attenuated total reflectance – Fourier transform infrared

B

BF – Bright field

BM – Bone marrow

BMP – Bone morphogenetic proteins

BMSC – Bone marrow-derived mesenchymal stem/stromal cells

BSA – Bovine serum albumin

BTE – Bone tissue engineering

C

CAD – Computer-aided design

CBFβ – core-binding factor β

CFD – Computational fluid dynamics

COL I – Collagen type I

COL II – Collagen type II

COL X – Collagen type X

CS – Chondroitin sulfate

CTE – Cartilage tissue engineering

D

DAPI – 4,6-diamino-2-phenylindole

DMEM – Dulbecco's Modified Eagle Medium

DMMB – Dimethylmethylene blue

DMSO – Dimethylsulfoxide

DNA – Deoxyribonucleic acid

DS – Dermatan sulfate

DSC – Differential scanning calorimetry

E

ECM – Extracellular matrix

EDX – Energy dispersive X-ray

ESC – Embryonic stem cell

F

FACS – Fluorescent activated cell sorting

FBS – Fetal bovine serum

FDA – Food and Drug Administration

FDM – Fused deposition modelling

FGF – Fibroblast growth factor

FTIR – Fourier transform infrared

G

GAG – Glycosaminoglycan

GAPDH – Glyceraldehyde 3-phosphate dehydrogenase

H

H_2O_2 – Hydrogen peroxide

HA – Hyaluronic acid/hyaluronan

hBMSC – Human bone marrow-derived mesenchymal stem/stromal cells

HC – Human chondrocytes

HCL – Hydrochloric acid

H&E – Hematoxylin & Eosin

HFIP – 1,1,1,3,3,3-hexafluoro-2-propanol

HLA-DR – Human leukocyte antigen D related

HPLC – high performance liquid chromatography

HS – Heparan sulfate

hSMSC – Human synovial-derived mesenchymal stem/stromal cells

HUVEC – Human umbilical vein endothelial cell

I

IGF – Insulin growth factor

iPSC – Induced pluripotent stem cell

ISO – International Organization for Standardization

ITS – Insulin-transferin-selenium

K

KGN – Kartogenin

KS – Keratan sulfate

L

LC-MS/MS – Liquid chromatography-tandem mass spectrometry

M

MMP – Matrix metalloproteinase

MSC – Mesenchymal stem/stromal cells

MRM – Multiple reaction monitoring

MTT – 3-(4,5-dimethylthiazol-2-yl)-2,5-Diphenyltetrazolium bromide

N

NaCl – Sodium chloride

$NaCNBH_4$ – Sodium cyanoborohydrade

NH_4OH – Ammonium hydroxide

O

OA – Osteoarthritis

OPN – Osteopontin

P

PBS – Phosphate buffered saline

PCL – Poly (ε-caprolactone)/polycaprolactone

PCR – Polymerase chain reaction

PDMS – Polydimethylsiloxane

PEGSSDA– Disulfide-containing polyethylene glycol diacrylate

Pen-strep – Penicillin-streptomycin

PFA – Paraformaldehyde

PGA – Polyglycolic acid

PGS – Poly (glycerol) sebacate

PLA – Polylactic acid

PLGA – Poly (lactic-co-glycolic acid)

PLLA – Poly (L-lactic acid)

PRG4 – Proteoglycan 4 or lubricin

R

RGD – Arg-Gly-Asp sequence

RNA – Ribonucleic acid

RT – Room temperature

RT-qPCR – Real-time quantitative polymerase chain reaction

Runx1 – Runt-related transcription factor 1

Runx2 – Runt-related transcription factor 2

S

SD – Standard deviation

SDS – Sodium docecyl sulfate

SEM – Scanning electron microscopy

SEM – Standard error of mean

sGAG – Sulfated glycosaminoglycan

SMSC – Synovial-derived mesenchymal stem/stromal cells

SZP– Superficial zone protein

T

TCPS – Tissue culture polystyrene

T_c – Crystallization temperature

TEM – Transmission electron microscopy

TFE – 2,2,2-Trifluoroethanol

TGF-β – Transforming growth factor- β

T_m – Melting temperature

U

UCB – Umbilical cord blood

UCM – Umbilical cord matrix

UTS – Ultimate tensile strength

X

XRD – X-ray diffraction

Chapter I

INTRODUCTION

CHAPTER I – INTRODUCTION

I.1. Thesis concept

I.1.1. Motivation

Articular cartilage is a highly specialized connective tissue with a crucial biological importance for healthy articular motion as it provides a smooth and lubricated surface in the synovial joints and facilitates mechanical load dissipation. Due to the absence of vascularization, low cell density and low proliferative potential, articular cartilage has a poor self-healing capacity after injury or degeneration through prevalent debilitating diseases such as osteoarthritis (OA) and rheumatoid arthritis. OA is a major health concern as it is the most common joint disorder and a major cause of pain and disability in adults. In fact, it is estimated that more than 10% of men and 18% of women over 60 years old are affected by OA worldwide (Vinatier and Guicheux, 2016). These numbers are predicted to be aggravated considerably in the following decades due to the global population aging and as result of a multi-factorial etiology, which also includes obesity and heredity (Chen et al., 2017). In US alone, OA afflicts more than 9% of the population over 30 years and comprises approximately $100 billion of healthcare and socioeconomic annual costs (Tan and Hung, 2017). Previous reports conducted in US predicted the number of OA patients to rise from 47.8 million in 2005 to more than 67 million by the year of 2030 (Hootman and Helmick, 2006; Lawrence et al., 2008). OA pathology is characterized by a progressive destruction of articular cartilage, thickening of the subchondral bone and various degrees of synovial inflammation. Despite its relevance, the molecular mechanisms underlying OA pathogenesis remain poorly understood and there are no current clinical interventions to fully restore degraded cartilage and revert disease progression (Chen et al., 2017; Kim et al., 2018). Despite advances in the field of orthopedic surgery, the current procedures for articular cartilage repair including chondroplasty, microfracture, mosaicplasty and autologous chondrocyte implantation (ACI) (estimated > 250.000 procedures/year in US alone with a 5% annual incidence growth) are not able to consistently produce functional tissue with proper mechanical and structural properties (McCormick et al., 2014). In fact, such methods present numerous limitations such as donor site morbidity, graft instability, incomplete defect filling and often lead to the formation of fibrocartilaginous and calcified tissue (Huang et al., 2016; Makris et al., 2015; Vinatier and Guicheux, 2016). Therefore, there is an urgent unmet need for alternative therapeutic methods to address the challenging process of articular cartilage regeneration. Additionally, from an economic perspective, a successful therapeutic option for OA management will enter as advantageous competitor in a market that is expected to

increase nearly 2.2 times in 10 years (according to GlobalData, Pharma Intelligence Center report that predicts the worldwide OA market will increase from $1.6 billions in 2016 to $3.5 billions by 2026).

The inefficiency of current clinical options combined with the increasing numbers of cartilage disease patients motivated the development of new therapeutic strategies based on stem cell therapy and tissue engineering. Such strategies combining principles of engineering, material science and biology aim to develop tissue substitutes that can fully restore the functions of the injured cartilage tissue. Cartilage tissue engineering (CTE) often follows the "tissue-engineering triad" paradigm, i.e., the combination of cells (chondrocytes or stem cells), biomaterials and biochemical/physical/environmental factors (Bernhard and Vunjak-Novakovic, 2016; Makris et al., 2015; Vinatier et al., 2009). It is believed that the proper combination of these factors holds the promise for the generation of functional long-term articular cartilage substitutes with structure and mechanical behavior similar to the native tissue. Recent discoveries in material science engineering and new technologies for scaffold fabrication together with a better understanding of the role of stem cells and certain molecules in cartilage development and maintenance have greatly benefited the CTE field. Interestingly, when Langer and Vacanti first introduced tissue engineering nearly 25 years ago (Langer and Vacanti, 1993), articular cartilage was predicted to be one of the first tissues to be successfully regenerated as a result of being composed by a single cell type (the chondrocyte, embedded in a extracellular matrix (ECM) mainly composed of proteoglycans and collagen) and of its thin structure and avascular nature (Huey et al., 2012). However, such thought was proven incorrect not only because of articular cartilage intrinsic poor self-regeneration capacity, but also because of it's highly complex, multilayered structure with different cell densities, ECM composition and mechanical properties in each of the different layers of the tissue. Many tissue engineering strategies creating homogeneous tissue replacements and not considering the structural and environmental features (i.e. oxygen tension, biochemical signaling, mechanical stimuli) of articular cartilage niche have failed to achieve clinical effectiveness. Considering that cartilage main properties and functions are dictated by its spatially-varying architecture and proper microenvironment, new approaches should focus in mimicking these features *in vitro* in order to achieve engineered tissues with improved functionality.

Glycosaminoglycans (GAGs) are major components of cartilage tissue and therefore global quantification of their production is one of the principal outcomes considered when evaluating the success of a tissue engineering strategy. However, little is known about its exact composition in the final engineered tissues. Additionally, changes in GAG composition, structure and sulfation patterns have been associated with different tissue maturation stages and with arthritic diseases (i.e. OA) (Hasehira et al., 2017; Plaas et al., 1998; Sharma et al.,

2017). Therefore, in this thesis, we will use a highly sensitive liquid chromatography tandem mass spectrometry (LC-MS/MS) approach to unravel a more accurate GAG composition of *in vitro* generated chondrogenic tissues, cell-derived ECM and respective undifferentiated cells from sources often used in CTE approaches.

Despite the great number of high quality research and pre-clinical studies performed in CTE, the clinical translation of these approaches on a scale that may improve patients' quality of life has not been achieved yet. The current trend in the field to target cartilage regeneration is the development of new integrated CTE strategies that can enhance the functionality and properties of the engineered tissues by a closer mimicry of the *in vivo* conditions of native articular cartilage. Herein, we will focus on the development of biomimetic bioengineering strategies combining scaffolds, mesenchymal stem/stromal cells (MSC) and different cues (i.e. biochemical through supplementation with glycosaminoglycans and small molecules; physical using perfusion bioreactors to provide mechanical stimulation; and environmental through the modulation of oxygen tension) to generate *in vitro* cartilage constructs. In particular, we will study the effects of recreating some of articular cartilage *in vivo* features to promote MSC chondrogenic differentiation in 3D culture systems *ex vivo*.

One of the major unsolved challenges in CTE is the inability of creating engineered tissues with structure, mechanical properties and functionality resembling the ones of healthy native articular cartilage. Therefore, the fabrication of hierarchical multilayered tissue constructs to mimic the structure of the native tissue is now becoming a hot topic in the field of regenerative medicine, particularly for CTE applications (Ansari et al., 2019; Atesok et al., 2016; Correia et al., 2015; Gadjanski, 2018). Herein, we will introduce a concept of a novel hierarchical tri-layered scaffold aiming to enhance MSC chondrogenesis through a closer mimicry of each one of the native articular cartilage layers, and consequently, of their zone-variable cell density, ECM composition and mechanical properties.

I.1.2. Scope, aim of studies and research questions

This PhD thesis was developed under the framework of the PhD Program in Bioengineering – Cell Therapies and Regenerative Medicine and resulted from a collaborative project between the Stem Cell Engineering Research Group (SCERG, iBB-IST, Portugal) and the Linhardt Labs – Center for Biotechnology and Interdisciplinary Studies (CBIS) from the Rensselaer Polytechnic Institute (RPI, NY USA). The objective was to bring together specific expertise from both labs (stem cell culture and differentiation, bioreactor technology and tissue engineering scaffold development from SCERG and GAG disaccharide analysis and electrospinning technique from Linhardt Labs) to develop a project addressing one of the primary unsolved challenges in the fields of tissue engineering and

regenerative medicine: the development of a functional engineered tissue that mimics the highly organized multizonal architecture and mechanical properties of articular cartilage.

Taking into consideration the motivation of this thesis, we aim to improve our understanding of the *in vivo* features and composition of articular cartilage and use that information to develop different biomimetic CTE strategies for the *in vitro* fabrication of stem cell-based engineered cartilage tissues. Specifically, this thesis aims to answer to the following research questions:

1. What is the **GAG disaccharide composition** of ECM produced by cells (MSC and chondrocytes) often used in CTE strategies? How are the GAG types and amounts affected by the **decellularization** method?

2. How **GAG composition changes** during the chondrogenic differentiation of MSC? Are these changes **dependent of the MSC source** used and how they compare with **chondrocytes**? Is the **chondrogenic differentiation** of these cells and their **GAG remodelling** affected by the **oxygen tension** (**normoxia - 21% O_2** *vs.* **hypoxia** - **5% O_2**)?

We propose that a highly sensitive LC-MS/MS approach might contribute to address these two first questions, providing a more accurate quantification (while accounting for different types of GAGs and respective disaccharides) than the standard methods usually used for measuring GAG content in stem cell-based engineered tissues.

Following on these topics, we hypothesize that main native tissue components, such as GAGs or the whole decellularized cell-derived ECM, can be integrated in tissue engineering approaches to improve MSC differentiation towards different components of the osteochondral tissue. In that sense, the following research questions were then addressed in this thesis:

3. Can **GAGs** be used as culture **meddium supplements** to enhance the chondrogenic differentiation of MSC in **3D porous scaffolds**? How different are the **responses to GAG supplementation**, in terms of chondrogenic differentiation, of **two distinct MSC sources**: **bone marrow-derived MSC** and **synovial-derived MSC**?

4. Is **decoration with MSC-derived ECM** an **effective** way to **enhance the bioactivity** and **osteoinductive potential** of synthetic 3D porous scaffolds? Can

these **ECM-decorated scaffolds improve** the **proliferation** and **osteogenic differentiation of MSC** in comparison to pristine scaffolds?

These last two research questions arise from the hypothesis that we can improve cellular processes such as proliferation and differentiation through a closer mimicry of the cell-ECM signaling present in tissues *in vivo*.

Articular cartilage is constantly under the action of mechanical forces resultant from articular motion. These mechanical stimuli have been associated with the maintenance of cartilage homeostasis and also described to have a role in the regulation of MSC differentiation (Li et al., 2017; Panadero et al., 2016; Steward and Kelly, 2015). Concordantly, we hypothesized that additive manufacturing technology could be used to fabricate custom-made and versatile perfusion bioreactor systems to address the following research question:

5. Can we develop a **custom-made perfusion bioreactor system** suitable for **CTE applications**? Does the **perfusion bioreactor culture** play an **enhancing role** in the **MSC chondrogenenic differentiation** on 3D porous scaffolds?

Mimicking the properties of native tissue ECM is an important factor for the success of a tissue engineering strategy. This becomes crucial and a major challenge when considering CTE approaches due to the highly stratified and multizonal architecture of articular cartilage. Accordingly, appropriate scaffold fabrication techniques should be used to develop scaffolds mimicking the structural and mechanical properties of each individual zone/layer of the cartilage tissue.

Regarding the regeneration of defects in the superficial zone of articular cartilage, we hypothesized that nanofibrous scaffolds mimicking the size and alignment of collagen fibrils in the native tissue can be produced by electrospinning, and combined with a drug delivery strategy to promote MSC chondrogenesis.

Finally, we propose the combination of different scaffold fabrication tecnhiques to produce a hierarchical tri-layered scaffold able to closely resemble the multizonal structure of articular cartilage. Considering the abovementioned, two additional research questions were addressed under the scope of this thesis:

6. Can we produce **electrospun nanofibers** able to **mimic** the **size and alignment** of collagen fibrils within the **superficial layer of articular cartilage**? Could a **coaxial fiber configuration** allow the **controlled delivery of a small molecule** and **enhance scaffold's chondroinductive potential**?

7. How can we **combine different scaffold fabrication techniques** to produce a **tri-layered hierarchical scaffold** able to **mimic** the **stratified multizonal architecture of articular cartilage**, considering its zone-varying cell density, ECM composition and mechanical properties? Would such scaffold **support the chondrogenic differentiation of MSC**?

The last research question addresses one of the primary unsolved challenges in CTE. The *in vitro* fabrication of engineered tissues with zone-varying properties similar to the native articular cartilage would be a major achievement in the field as a promising curative therapy for repairing full-thickness cartilage defects. Additionally, this will allow the production of high-quality *in vitro* 3D models for the screening of new therapeutic molecules and for study the mechanism of cartilage degenerative diseases.

I.1.3. Research strategy

Although several different research lines could have been followed to address our research questions, in the next paragraphs, we explain the rationale behind some of the strategies adopted throughout this PhD thesis.

Cell sources

MSC are an attractive source for tissue engineering approaches due to their high availability as they can be isolated from several tissues, their low immunogenicity, their advantageous immunomodulatory/trophic properties and their ability to differentiate into cartilage, bone and adipose tissues (Le Blanc, 2003; Pittenger et al., 1999; Tan and Hung, 2017). To date, human bone marrow MSC (hBMSC) are the most used stem cell source in clinical trials and in cartilage tissue engineering settings (Heathman et al., 2015; Makris et al., 2015). However, since their first isolation by De Bari et al (De Bari et al., 2001), several studies have suggested human synovial-derived MSC (hSMSC) as a superior source for cartilage regeneration due to their higher chondrogenic potential compared to other MSC sources (Fan et al., 2009; Ogata et al., 2015; Sakaguchi et al., 2005). Therefore, owing to their clinical relevance and superiority for chondrogenesis, we selected hBMSC and hSMSC as cell sources in our CTE strategies. In some of the studies performed, human articular chondrocytes were used for comparison. In addition, as hBMSC are present in bone tissue, they were used in the strategy addressing bone repair.

All the MSC donors used in this thesis were characterized following the criteria for MSC definition (Dominici et al., 2006) and different donors were used to account for batch-to-batch

cellular heterogeneity. Moreover, all the human cells used in this thesis were obtained with donor consent either as result of collaboration with hospitals or acquired from specialized companies.

Materials

To produce the scaffolds tested in this thesis, we selected biocompatible and biodegradable materials that can be easily processed to generate the desired structures for each study. Polycaprolactone (PCL) was used to produce 3D extruded porous scaffolds and electrospun nanofibers, as it is a previously FDA-approved material for different medical applications and possess desirable biodegradability rates and mechanical properties (Low et al., 2009; Woodruff and Hutmacher, 2010). Poly (glycerol sebacate) (PGS) used to fabricate coaxial electrospun fibers is a non-toxic elastomeric material synthesized by the mixture of glycerol and sebacic acid, both of them approved by FDA (Loh et al., 2015; Rai et al., 2012).

LC-MS/MS as a technique to determine GAG composition

GAGs, such as chondroitin sulfate (CS) and hyaluronic acid (HA), are main cartilage constituents with a crucial role in the resistance of the tissue to mechanical loads, as well as mediators in important cellular functions. Thus, the quantification of GAG amounts is one the main measures used to assess chondrogenic differentiation and the performance of a CTE strategy. Most of GAG measurements in CTE strategies use the dimethylmethylene blue (DMMB) assay (or equivalent) and are limited to the determination of total sulfated GAG content, being unable to discriminate among different GAG types. In fact, only very few studies used electrophoresis or high-performance liquid chromatography (HPLC) methods to evaluate GAG disaccharides composition in engineered cartilage tissues (Mouw et al., 2005; Wan et al., 2016). Moreover, these methods lack the sensitivity of liquid chromatography tandem mass spectrometry (LC-MS/MS), which might be critical when dealing with low amounts usually generated in microscale culture strategies. Therefore, we propose the use of a highly sensitive and selective LC-MS/MS method using multiple reaction monitoring (MRM) detection mode developed in Linhardt Labs to provide an accurate analysis of the GAG and disaccharide composition of the different cell sources and respective engineered tissues. This method was previously successfully used to study the GAG disaccharide composition of different types of tissues and biological samples (Gasimli et al., 2014; Li et al., 2015; Liu et al., 2018; Schmidt et al., 2016; Sun et al., 2015; Weyers et al., 2012).

Different types of scaffolds

Throughout this thesis, we exploited the use of different scaffold configurations such as 3D extruded porous scaffolds, GAG-based hydrogels and electrospun fibers.

- *3D extruded porous PCL scaffolds*

Additive manufacturing extrusion process has been widely used in tissue engineering due to their ability of fabricating scaffolds with highly controlled size, structure and porosity, which can be tailored to perfectly match the patient's defect site (Melchels et al., 2012). Herein, we explore this technology to produce 3D porous PCL scaffolds with high porosity and interconnectivity to favor cell infiltration and migration, efficient nutrient supply and gas exchange. These scaffolds were used as 3D-culture platforms in several strategies developed throughout this thesis.

- *GAG-based hydrogels*

Hydrogels are attractive platforms for CTE applications due to their ability to mimic the hydrated environment of cartilaginous tissues and to be used as minimally invasive injectable systems (Oliveira and Reis, 2011). In order to provide a closer resemble of articular cartilage biochemical composition, the main cartilage GAG CS was mixed with a commercially available semi-synthetic HA-based HyStem™ hydrogel system to develop the middle zone layer of the hierarchical scaffold. The HyStem hydrogel system was selected based on its previously successful application in MSC-based CTE strategies (Aleksander-Konert et al., 2016; Mikael et al., 2017).

- *Electrospun fibers*

Electrospinning has been widely used in tissue engineering applications due to its ability to fabricate fibrous and porous 3D mesh scaffolds with high surface area from a great variety of materials (Agarwal et al., 2009; Khorshidi et al., 2016). Electrospinning is particularly advantageous for CTE applications because it allows the production of fibrous scaffolds with the nanometer scale and alignment of the collagen fibrillar structures present in the native articular cartilage ECM (Wise et al., 2009). Coaxial electrospinning is a development of the traditional technique, which uses two concentrically aligned nozzles (inner and outer nozzle) each one connected to a different spinning solution to produce fibers with a core-shell structure. The main advantages of coaxial electrospinning include the encapsulation of

nonspinnable polymers and nonpolymeric materials such as drugs and biologically active molecules in the fiber core, which allow for the protection and more controlled-release kinetics of such agents (Jiang et al., 2014; Sperling et al., 2016). Core-shell fibers have been extensively used o deliver drugs, genes and growth factors to target different tissue engineering applications (Ji et al., 2011). Within the scope of this thesis, we used drug-encapsulating monoaxial and coaxial aligned electrospun nanofibers to address the regeneration of the superficial zone of articular cartilage.

Enhancing scaffold's biological performance

In this thesis, we explore different strategies to enhance the bioactivity and performance of synthetic-based scaffolds towards specific applications.

- *Cell-derived ECM decoration of synthetic scaffolds*

In the recent years, decellularized cell-derived ECM has been proposed as a promising material for tissue engineering applications as it serves as a reservoir of multiple cytokines and growth factors, providing biochemical and physical cues that can recreate the *in vivo* microenvironment of cells and tissues (Cheng et al., 2014; Fitzpatrick and McDevitt, 2015). However, the application of cell-derived ECM in the repair of bone defects is hampered by their weak mechanical properties and fast degradation (Bracaglia and Fisher, 2015). Therefore, in this thesis, we propose the combination of MSC-derived ECM (hBMSC were selected as cell source due to their presence in native bone tissue and, consequently, superior ability to recapitulate features of bone niche) with 3D custom-made porous PCL scaffolds to generate MSC-ECM decorated PCL scaffolds with appropriate mechanical support and improved bioactivity/oisteoinductive properties for bone tissue engineering applications.

- *Chondroinductive factor release*

Electrospun scaffolds have been explored to allow the delivery of chondroinductive proteins and molecules in CTE (Man et al., 2014; Wang et al., 2017). Accordingly, we developed coaxial electrospun aligned nanofibers for the controlled delivery of the small molecule kartogenin. Kartogenin is a recently discovered small molecule known to promote MSC chondrogenic differentiation, maintain chondrocyte phenotype and protect cartilage ECM from degradation (Cai et al., 2019; Johnson et al., 2012). Thus, we expect that our coaxial electrospun scaffolds will be able to offer structural support, mimic the structure of

cartilage ECM and promote the controlled release of a chondroinductive factor that can efficiently enhance MSC chondrogenesis towards improved CTE strategies.

In vitro **recreation of articular cartilage niche environmental/biochemical/physical features to promote MSC chondrogenic differentiation**

Within the scope of this thesis, we explore the *in vitro* mimicry of the features of the *in vivo* articular cartilage microenvironment as a strategy to enhance the MSC chondrogenic differentiation in CTE approaches.

- *Low oxygen tension (hypoxic) environment*

Inside the human body, articular cartilage is naturally exposed to hypoxic conditions (compared to atmospheric air), which ranges from 1% O_2 tension in the deep zone to 6% O_2 observed at the superficial zone (Zhou et al., 2004). Considering this and several studies reporting a beneficial role of low oxygen environments in promoting MSC chondrogenesis (Adesida et al., 2012; Leijten et al., 2014; Pattappa et al., 2019), we exploited the use hypoxia conditions (5% O_2) to enhance the quality of our *in vitro* engineered cartilage tissues.

- *GAG supplementation as biochemical cues*

GAGs, particularly CS and HA, are main components of articular cartilage with a critical role in the maintenance of tissue biomechanics and as regulators of signaling pathways controlling cellular processes such as cell growth and differentiation (Gasimli et al., 2012; Linhardt and Toida, 2004; M. Wang et al., 2017). Herein, aiming to recapitulate relevant biochemical cues and cell-ECM signaling observed *in vivo*, we develop a strategy based on GAG supplementation as culture medium additives, assessing its effects on the chondrogenic differentiation of different MSC sources in 3D porous scaffolds.

- *Bioreactor perfusion culture of engineered cartilage constructs*

During normal joint movement, articular cartilage is under a variety of different physical stimuli. *In vitro*, these physiological mechanical stimuli are often replicated through the use of bioreactors (Choi et al., 2018; Tan and Hung, 2017). Among these stimuli, bioreactor-based fluid-induced shear stimulation is reported to favor cartilage ECM production, however too high shear environments might result in increased cell death, compromising the CTE strategy (Darling and Athanasiou, 2003). Moreover, it was previously reported that low fluid-induced

shear stress stimuli (often bellow 0.5 Pa) favors the maintenance of a chondrogenic phenotype, whereas higher magnitudes promote the formation of cartilage hypertrophic tissue (Carter and Wong, 2003; Salinas et al., 2018). Several studies have used perfusion bioreactors to promote MSC chondrogenic differentiation in biomaterial scaffolds (Alves da Silva et al., 2011; Gonçalves et al., 2011; Kock et al., 2014; Mahmoudifar and Doran, 2010). However, such bioreactor platforms are often complex and expensive systems lacking versatility, which represents a limitation for the widespread use of bioreactors in personalized tissue engineering strategies (Costa et al., 2014). Accordingly, we used additive manufacturing technology (i.e. 3D-extrusion/Fused deposition modeling) to design and fabricate a simple, cost-effective and versatile bioreactor platform for the perfused culture of MSC-scaffold constructs. Using this approach, both bioreactor and scaffold can be fabricated with the desired size and shape in a rapid and reproducible manner while being fully compliant with a personalized CTE approach. The produced perfusion bioreactor was tested in terms of their ability to promote MSC chondrogenic differentiation on porous scaffolds under fluid-induced shear stress stimulation.

Mimicking the hierarchical stratified structure of articular cartilage

Articular cartilage presents a highly complex stratified structure consisting of four spatially distinct zones, namely the superficial/tangential zone, the middle/transitional zone, the deep/radial zone and the calcified zone. Each individual zone is characterized by specific cell density and phenotype, ECM composition and organization, and therefore distinct mechanical properties (Correia et al., 2015; Fox et al., 2009). In fact, the fabrication of an engineered cartilage tissue that can recapitulate the stratified structure and zone-varying properties of native articular cartilage tissues remains a major challenge in the CTE field. As the strategies producing homogeneous tissue replacements for cartilage repair failed to produce functional tissue, the trend has shift to approaches aiming to reproduce *in vitro* the native architectural features of cartilage. Such approaches include the use of multilayered scaffolds with different fiber alignments and diameters (Camarero-Espinosa et al., 2016; McCullen et al., 2012), different polymer scaffold morphologies (Steele et al., 2014) and pore size gradients (Woodfield et al., 2005; Zhang et al., 2013), multilayered hydrogels (Nguyen et al., 2011; Zhu et al., 2017) and the use of zone-specific chondrocytes isolated form different cartilage regions (Ng et al., 2009). However, the production of native-like engineered cartilage tissues with long-term functionality that can be translated into clinical use was not achieved yet. Thus, in this thesis, we propose the combination of different scaffold fabrication technologies to produce a new concept of hierarchical tri-layered scaffold consisting of a 3D porous PCL scaffold as deep zone layer, a GAG-based hydrogel to mimic the middle zone

and aligned PCL/Gelatin nanofibers as superficial zone layer. The obtained hierarchical scaffold will be then evaluated in terms of its ability to support MSC chondrogenic differentiation considering a cell density ratio of 3:2:1 for the superficial:middle:deep zone as previously described for normal adult articular cartilage (Hunziker et al., 2002; Ren et al., 2016).

I.1.4. Thesis outline

This thesis is organized in 9 chapters, a first introductory chapter (Chapter I), 7 chapters containing the original experimental research work developed during the time course of the PhD (Chapters II to VIII) and a final chapter highlighting the main conclusions and future trends (Chapter IX). The chapters presenting experimental work are composed by a general outline stating the aim and main findings of the study, an introduction with relevant background for the respective work, a section comprising the results obtained and a discussion section, in which those results are explained and compared to other relevant studies in the field.

Figure I.1 provides a schematic representation of the general structure of the main issues (and their relations) addressed throughout this thesis.

In **Chapter I**, we present the main motivations for the development of this PhD thesis, the main objectives and research questions to address, as well as the research strategies to follow.

In **Chapter II**, we produce and characterize cell-derived ECM produced by cell sources often used in CTE strategies: MSC two different human sources (hBMSC and hSMSC) and chondrocytes. We further used a highly accurate LC-MS/MS method to determine the GAG and disaccharide composition of the different cell-derived ECM in comparison to their respective cell cultures prior to decellularization.

In **Chapter III**, we assess the effects of oxygen tension (normoxia – 21% O_2 *vs.* hypoxia-5% O_2) on the chondrogenic differentiation of hBMSC and hSMSC as micromass aggregates. We also used a LC-MS/MS approach to evaluate the GAG remodeling during the chondrogenic differentiation of MSC, from each of the two sources considered, and compare it with chondrocytes cultured under normoxic/hypoxic conditions. The work developed in chapters II and III provides important information about the GAG composition of the cell sources, cell derived-ECM and respective chondrogenic engineered tissues derived from them. Such information was taken into consideration in the development of the scaffold-based CTE strategies.

In **Chapter IV**, we explore the use of main cartilage GAGs, CS and HA, as biochemical cues added to culture medium to enhance the chondrogenic differentiation of

hBMSC/hSMSC in custom-made 3D porous PCL scaffolds. Prior to GAG supplementation studies, the hBMSC/hSMSC culture conditions on PCL scaffolds were optimized in terms of chondrogenic culture medium and oxygen tension used.

In **Chapter V**, we use additive manufacturing technology (fused deposition modeling) to fabricate a new custom-made perfusion bioreactor platform able to provide fluid-induced shear stress stimuli to cartilage tissue engineered constructs. Furthermore, we demonstrate that the perfusion bioreactor culture enhances the chondrogenic differentiation of hBMSC in PCL scaffolds, generating engineered constructs with superior quality than non-perfused conditions.

In **Chapter VI**, we exploit the concept of decellularized cell-derived ECM presented before as a strategy to enhance the bioactivity and osteoinductive properties of 3D porous PCL scaffolds for bone tissue engineering applications. Therefore, we decorate the scaffolds with cell-derived ECM and investigate their ability to enhance MSC proliferation and osteogenesis in comparison to pristine PCL scaffolds.

In **Chapter VII**, we fabricate and characterize coaxial aligned electrospun fibers intended for the regeneration of the superficial zone of articular cartilage. We also investigate the ability of these fibers to promote the controlled delivery of a small molecule (kartogenin), known to promote MSC chondrogenesis. Thus, we evaluate the produced kartogenin-loaded fibers in terms of their ability to promote MSC proliferation, cartilage-ECM production and chondrogenic gene expression.

In **Chapter VIII**, we propose a new concept of a hierarchical tri-layered scaffold produced by the combination of different scaffold fabrication techniques (3D-extrusion, hydrogel synthesis and electrospinning) with the aim of mimicking the complex multizonal architecture of articular cartilage. Furthermore, we investigate the capacity of the hierarchical scaffold to support MSC chondrogenic differentiation in comparison with the individual layer scaffolds composing it.

Finally, in **Chapter IX**, we summarized the main achievements of this PhD thesis, highlighting their relevance and contribution to the Tissue Engineering field. We also refer the main limitations identified in this work and suggest some future research lines that can be further addressed.

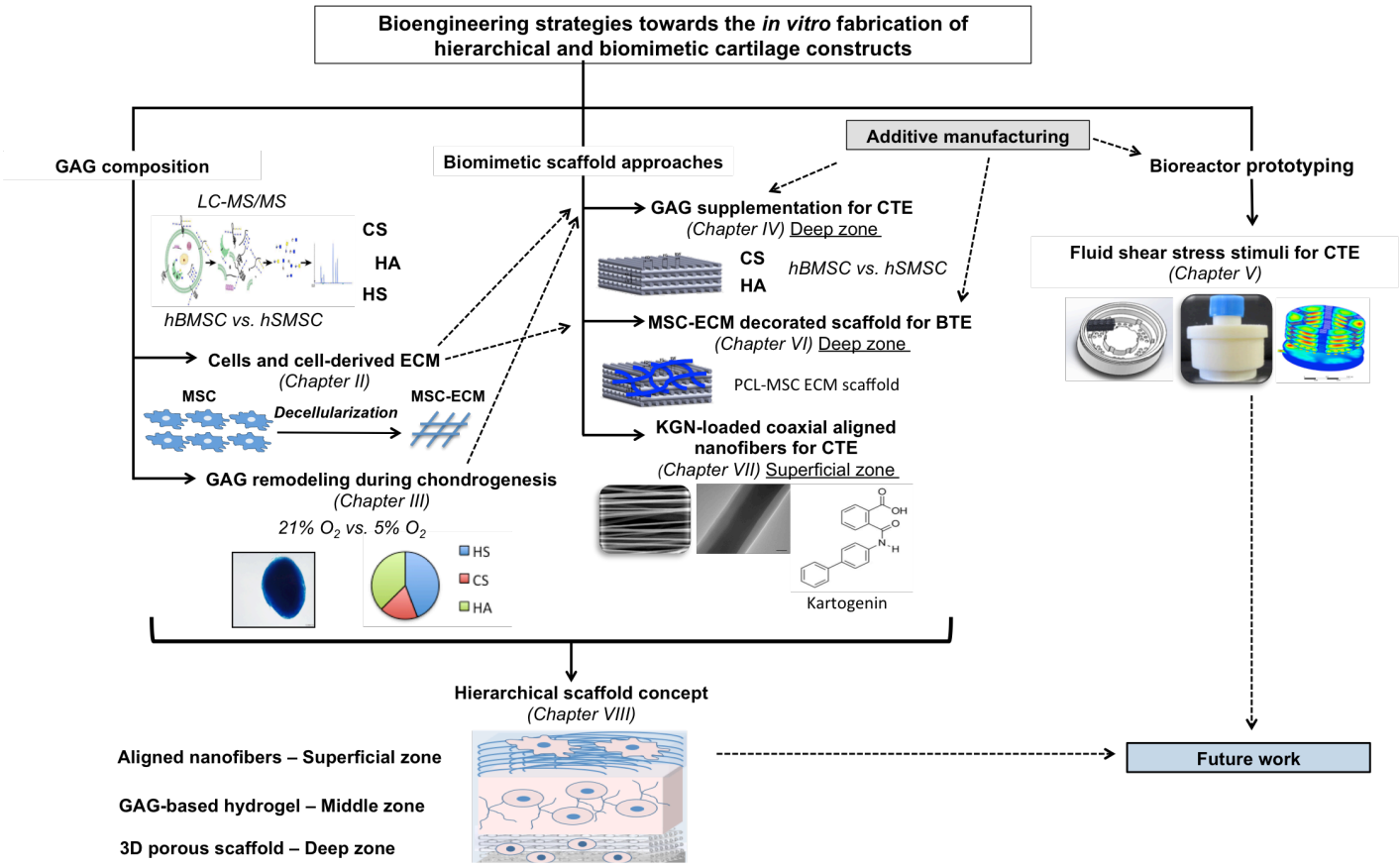

Figure I.1. Schematic representation of the strategies followed throughout this PhD thesis. The correspondent experimental chapters are also depicted in the figure.

References

Adesida, A.B., Mulet-Sierra, A., Jomha, N.M., (2012). Hypoxia mediated isolation and expansion enhances the chondrogenic capacity of bone marrow mesenchymal stromal cells. Stem Cell Res. Ther. 3, 9.

Agarwal, S., Wendorff, J.H., Greiner, A., (2009). Progress in the field of electrospinning for tissue engineering applications. Adv. Mater. 21, 3343–3351.

Aleksander-Konert, E., Paduszyński, P., Zajdel, A., Dzierzewicz, Z., Wilczok, A., (2016). In vitro chondrogenesis of Wharton's jelly mesenchymal stem cells in hyaluronic acid-based hydrogels. Cell. Mol. Biol. Lett. 21, 11.

Alves da Silva, M.L., Martins, A., Costa-Pinto, A.R., Correlo, V.M., Sol, P., Bhattacharya, M., Faria, S., Reis, R.L., Neves, N.M., (2011). Chondrogenic differentiation of human bone marrow mesenchymal stem cells in chitosan-based scaffolds using a flow-perfusion bioreactor. J. Tissue Eng. Regen. Med. 5, 722–732.

Ansari, S., Khorshidi, S., Karkhaneh, A., (2019). Engineering of gradient osteochondral tissue: From nature to lab. Acta Biomater. 87, 41–54.

Atesok, K., Doral, M.N., Karlsson, J., Egol, K.A., Jazrawi, L.M., Coelho, P.G., Martinez, A., Matsumoto, T., Owens, B.D., Ochi, M., Hurwitz, S.R., Atala, A., Fu, F.H., Lu, H.H., Rodeo, S.A., (2016). Multilayer scaffolds in orthopaedic tissue engineering. Knee Surgery, Sport. Traumatol. Arthrosc. 24, 2365–2373.

Bernhard, J.C., Vunjak-novakovic, G., (2016). Should we use cells , biomaterials , or tissue engineering for cartilage regeneration ? Stem Cell Res. Ther. 7, 56.

Bracaglia, L.G., Fisher, J.P., (2015). Extracellular Matrix-Based Biohybrid Materials for Engineering Compliant, Matrix-Dense Tissues. Adv. Healthc. Mater. 4, 2475–2487.

Cai, G., Liu, W., He, Y., Huang, J., Duan, L., Xiong, J., Liu, L., Wang, D., (2019). Recent advances in kartogenin for cartilage regeneration. J. Drug Target. 27, 28–32.

Camarero-Espinosa, S., Rothen-Rutishauser, B., Weder, C., Foster, E.J., (2016). Directed cell growth in multi-zonal scaffolds for cartilage tissue engineering. Biomaterials 74, 42–52.

Carter, D.R., Wong, M., (2003). Modelling cartilage mechanobiology. Philos. Trans. R. Soc. B Biol. Sci. 358, 1461–1471.

Chen, D., Shen, J., Zhao, W., Wang, T., Han, L., Hamilton, J.L., Im, H.-J., (2017). Osteoarthritis: toward a comprehensive understanding of pathological mechanism. Bone Res. 5, 16044.

Cheng, C.W., Solorio, L.D., Alsberg, E., (2014). Decellularized tissue and cell-derived extracellular matrices as scaffolds for orthopaedic tissue engineering. Biotechnol. Adv. 32, 462–484.

Choi, J.R., Yong, K.W., Choi, J.Y., (2018). Effects of mechanical loading on human mesenchymal stem cells for cartilage tissue engineering. J. Cell. Physiol. 233, 1913–1928.

Correia, C.R., Reis, R.L., Mano, J.F., (2015). Multiphasic, multistructured and hierarchical strategies for cartilage regeneration, in: Engineering Mineralized and Load Bearing Tissues, 143–160.

Costa, P.F., Vaquette, C., Baldwin, J., Chhaya, M., Gomes, M.E., Reis, R.L., Theodoropoulos, C., Hutmacher, D.W., (2014). Biofabrication of customized bone grafts by combination of additive manufacturing and bioreactor knowhow. Biofabrication 6, 035006.

Darling, E.M., Athanasiou, K.A., (2003). Articular Cartilage Bioreactors and Bioprocesses. Tissue Eng. 9, 9–23.

De Bari, C., Dell'Accio, F., Tylzanowski, P., Luyten, F.P., (2001). Multipotent mesenchymal stem cells from adult human synovial membrane. Arthritis Rheum. 44, 1928–1942.

Dominici, M., Le Blanc, K., Mueller, I., Slaper-Cortenbach, I., Marini, F., Krause, D., Deans, R., Keating, A., Prockop, D., Horwitz, E., (2006). Minimal criteria for defining multipotent mesenchymal stromal cells. The International Society for Cellular Therapy position statement. Cytotherapy 8, 315–317.

Fan, J., Varshney, R.R., Ren, L., Cai, D., Wang, D.A., (2009). Synovium-derived mesenchymal stem cells: a new cell source for musculoskeletal regeneration. Tissue Eng. Part B. Rev. 15, 75–86.

Fitzpatrick, L.E., McDevitt, T.C., (2015). Cell-derived matrices for tissue engineering and regenerative medicine applications. Biomater. Sci. 3, 12–24.

Fox, A.J.S., Bedi, A., Rodeo, S.A., (2009). The basic science of articular cartilage: structure, composition, and function. Sports Health 1, 461–468.

Gadjanski, I., (2018). Mimetic Hierarchical Approaches for Osteochondral Tissue Engineering, in: Osteochondral Tissue Engineering, Advances in Experimental Medicine and Biology.

Gasimli, L., Hickey, A.M., Yang, B., Li, G., Dela Rosa, M., Nairn, A. V., Kulik, M.J., Dordick, J.S., Moremen, K.W., Dalton, S., Linhardt, R.J., (2014). Changes in glycosaminoglycan structure on differentiation of human embryonic stem cells towards mesoderm and endoderm lineages. Biochim. Biophys. Acta - Gen. Subj. 1840, 1993–2003.

Gasimli, L., Linhardt, R.J., Dordick, J.S., (2012). Proteoglycans in stem cells. Biotechnol. Appl. Biochem. 59, 65–76.

Gonçalves, A., Costa, P., Rodrigues, M.T., Dias, I.R., Reis, R.L., Gomes, M.E., (2011). Effect of flow perfusion conditions in the chondrogenic differentiation of bone marrow stromal cells cultured onto starch based biodegradable scaffolds. Acta Biomater. 7, 1644–1652.

Hasehira, K., Hirabayashi, J., Tateno, H., (2017). Structural and quantitative evidence of α2–6-sialylated N-glycans as markers of the differentiation potential of human mesenchymal stem cells. Glycoconj. J. 34, 797–806.

Heathman, T.R., Nienow, A.W., McCall, M.J., Coopman, K., Kara, B., Hewitt, C.J., (2015). The translation of cell-based therapies: Clinical landscape and manufacturing challenges. Regen. Med. 10, 49–64.

Hootman, J.M., Helmick, C.G., (2006). Projections of US prevalence of arthritis and associated activity limitations. Arthritis Rheum. 54, 226–229.

Huang, B.J., Hu, J.C., Athanasiou, K.A., (2016). Cell-based tissue engineering strategies used in the clinical repair of articular cartilage. Biomaterials 98, 1–22.

Huey, D.J., Hu, J.C., Athanasiou, K.A., (2012). Unlike bone, cartilage regeneration remains elusive. Science 338, 917–921.

Hunziker, E.B., Quinn, T.M., Häuselmann, H.-J., (2002). Quantitative structural organization of normal adult human articular cartilage. Osteoarthr. Cartil. 10, 564–572.

Ji, W., Sun, Y., Yang, F., Van Den Beucken, J.J.J.P., Fan, M., Chen, Z., Jansen, J.A., (2011). Bioactive electrospun scaffolds delivering growth factors and genes for tissue engineering applications. Pharm. Res. 28, 1259–1272.

Jiang, H., Wang, L., Zhu, K., (2014). Coaxial electrospinning for encapsulation and controlled release of fragile water-soluble bioactive agents, J. Control. Release. 193, 296-303.

Johnson, K., Zhu, S., Tremblay, M.S., Payette, J.N., Wang, J., Bouchez, L.C., Meeusen, S., Althage, A., Cho, C.Y., Wu, X., Schultz, P.G., (2012). A stem cell-based approach to cartilage repair. Science. 336, 717–721.

Khorshidi, S., Solouk, A., Mirzadeh, H., Mazinani, S., Lagaron, J.M., Sharifi, S., Ramakrishna, S., (2016). A review of key challenges of electrospun scaffolds for tissue-engineering applications. J. Tissue Eng. Regen. Med. 10, 751–738.

Kim, J.E., Song, D.H., Kim, S.H., Jung, Y., Kim, S.J., (2018). Development and characterization of various osteoarthritis models for tissue engineering. PLoS One 13, e0194288.

Kock, L.M., Malda, J., Dhert, W.J.A., Ito, K., Gawlitta, D., (2014). Flow-perfusion interferes with chondrogenic and hypertrophic matrix production by mesenchymal stem cells. J. Biomech. 47, 2122–2129.

Langer, R., Vacanti, J.P., (1993). Tissue Engineering. Science. 260, 920–926.

Lawrence, R.C., Felson, D.T., Helmick, C.G., Arnold, L.M., Choi, H., Deyo, R.A., Gabriel, S., Hirsch, R., Hochberg, M.C., Hunder, G.G., Jordan, J.M., Katz, J.N., Kremers, H.M., Wolfe, F., (2008). Estimates of the prevalence of arthritis and other rheumatic conditions in the United States. Part II. Arthritis Rheum. 58, 26–35.

Le Blanc, K., (2003). Immunomodulatory effects of fetal and adult mesenchymal stem cells. Cytotherapy 5, 485–489.

Leijten, J., Georgi, N., Moreira Teixeira, L., van Blitterswijk, C.A., Post, J.N., Karperien, M., (2014). Metabolic programming of mesenchymal stromal cells by oxygen tension directs chondrogenic cell fate. Proc. Natl. Acad. Sci. 111, 13954–13959.

Li, G., Li, L., Tian, F., Zhang, L., Xue, C., Linhardt, R.J., (2015). Glycosaminoglycanomics of Cultured Cells using a Rapid and Sensitive LC-MS/MS Approach. ACS Chem. Biol. 10, 1303-1310.

Li, K., Zhang, C., Qiu, L., Gao, L., Zhang, X., (2017). Advances in Application of Mechanical Stimuli in Bioreactors for Cartilage Tissue Engineering. Tissue Eng. Part B Rev. 23, 399–411.

Linhardt, R.J., Toida, T., (2004). Role of glycosaminoglycans in cellular communication. Acc. Chem. Res. 37, 431–438.

Liu, X., Krishnamoorthy, D., Lin, L., Xue, P., Zhang, F., Chi, L., Linhardt, R.J., Iatridis, J.C., (2018). A method for characterising human intervertebral disc glycosaminoglycan disaccharides using liquid chromatography-mass spectrometry with multiple reaction monitoring. Eur. Cell. Mater. 35, 117–131.

Loh, X.J., Abdul Karim, A., Owh, C., (2015). Poly(glycerol sebacate) biomaterial: synthesis and biomedical applications. J. Mater. Chem. B 3, 7641–7651.

Low, S.W., Ng, Y.J., Yeo, T.T., Chou, N., (2009). Use of Osteoplug polycaprolactone implants as novel burr-hole covers. Singapore Med. J. 50, 777–780.

Mahmoudifar, N., Doran, P.M., (2010). Chondrogenic differentiation of human adipose-derived stem cells in polyglycolic acid mesh scaffolds under dynamic culture conditions. Biomaterials 31, 3858–3867.

Makris, E.A., Gomoll, A.H., Malizos, K.N., Hu, J.C., Athanasiou, K.A., (2015). Repair and tissue engineering techniques for articular cartilage. Nat. Rev. Rheumatol. 11, 21–34.

Man, Z., Yin, L., Shao, Z., Zhang, X., Hu, X., Zhu, J., Dai, L., Huang, H., Yuan, L., Zhou, C., Chen, H., Ao, Y., (2014). The effects of co-delivery of BMSC-affinity peptide and rhTGF-β1 from coaxial electrospun scaffolds on chondrogenic differentiation. Biomaterials 35, 5250–5260.

McCormick, F., Harris, J.D., Abrams, G.D., Frank, R., Gupta, A., Hussey, K., Wilson, H., Bach, B., Cole, B., (2014). Trends in the surgical treatment of articular cartilage lesions in the United States: An analysis of a large private-payer database over a period of 8 years. Arthrosc. - J. Arthrosc. Relat. Surg. 30, 222–226.

McCullen, S.D., Autefage, H., Callanan, A., Gentleman, E., Stevens, M.M., (2012). Anisotropic Fibrous Scaffolds for Articular Cartilage Regeneration. Tissue Eng. Part A 18, 2073–2083.

Melchels, F.P.W., Domingos, M.A.N., Klein, T.J., Malda, J., Bartolo, P.J., Hutmacher, D.W., (2012). Additive manufacturing of tissues and organs. Prog. Polym. Sci. 37, 1079–1104.

Mikael, P.E., Kim, H.S., Nukavarapu, S.P., (2017). Hybrid extracellular matrix design for cartilage-mediated bone regeneration. J. Biomed. Mater. Res. - Part B Appl. Biomater. 106, 300–309.

Mouw, J.K., Case, N.D., Guldberg, R.E., Plaas, A.H.K., Levenston, M.E., (2005). Variations in matrix composition and GAG fine structure among scaffolds for cartilage tissue engineering. Osteoarthr. Cartil. 13, 828–836.

Ng, K.W., Ateshian, G.A., Hung, C.T., (2009). Zonal Chondrocytes Seeded in a Layered Agarose Hydrogel Create Engineered Cartilage with Depth-Dependent Cellular and Mechanical Inhomogeneity. Tissue Eng. Part A 15, 2315–2324.

Nguyen, L.H., Kudva, A.K., Guckert, N.L., Linse, K.D., Roy, K., (2011). Unique biomaterial compositions direct bone marrow stem cells into specific chondrocytic phenotypes corresponding to the various zones of articular cartilage. Biomaterials 32, 1327–1338.

Ogata, Y., Mabuchi, Y., Yoshida, M., Suto, E.G., Suzuki, N., Muneta, T., Sekiya, I., Akazawa, C., (2015). Purified human synovium mesenchymal stem cells as a good resource for cartilage regeneration. PLoS One 10, e0129096.

Oliveira, J.T., Reis, R.L., (2011). Polysaccharide-based materials for cartilage tissue engineering applications. J. Tissue Eng. Regen. Med. 5, 421–436.

Panadero, J.A., Lanceros-Mendez, S., Ribelles, J.L.G., (2016). Differentiation of mesenchymal stem cells for cartilage tissue engineering: Individual and synergetic effects of three-dimensional environment and mechanical loading. Acta Biomater. 33, 1–12.

Pattappa, G., Johnstone, B., Zellner, J., Docheva, D., Angele, P., (2019). The Importance of Physioxia in Mesenchymal Stem Cell Chondrogenesis and the Mechanisms Controlling Its Response. Int. J. Mol. Sci. 20, 1–28.

Pittenger, M.F., Mackay, A.M., Beck, S.C., Jaiswal, R.K., Douglas, R., Mosca, J.D., Moorman, M.A., Simonetti, D.W., Craig, S., Marshak, D.R., (1999). Multilineage potential of adult human mesenchymal stem cells. Science. 284, 143–147.

Plaas, A.H.K., West, L.A., Wong-Palms, S., Nelson, F.R.T., (1998). Glycosaminoglycan sulfation in human osteoarthritis: Disease-related alterations at the non-reducing termini of chondroitin and dermatan sulfate. J. Biol. Chem. 273, 12642–12649.

Rai, R., Tallawi, M., Grigore, A., Boccaccini, A.R., (2012). Synthesis, properties and biomedical applications of poly(glycerol sebacate) (PGS): A review. Prog. Polym. Sci. 37, 1051–1078.

Ren, X., Wang, F., Chen, C., Gong, X., Yin, L., Yang, L., (2016). Engineering zonal cartilage through bioprinting collagen type II hydrogel constructs with biomimetic chondrocyte density gradient. BMC Musculoskelet. Disord. 17, 1–10.

Sakaguchi, Y., Sekiya, I., Yagishita, K., Muneta, T., (2005). Comparison of human stem cells derived from various mesenchymal tissues: Superiority of synovium as a cell source. Arthritis Rheum. 52, 2521–2529.

Salinas, E.Y., Hu, J.C., Athanasiou, K.A., (2018). A Guide for Using Mechanical Stimulation to Enhance Tissue-Engineered Articular Cartilage Properties. Tissue Eng. Part B Rev. 24, 345–358.

Schmidt, E.P., Overdier, K.H., Sun, X., Lin, L., Liu, X., Yang, Y., Ammons, L.A., Hiller, T.D., Suflita, M.A., Yu, Y., Chen, Y., Zhang, F., Burlew, C.C., Edelstein, C.L., Douglas, I.S., Linhardt, R.J., (2016). Urinary glycosaminoglycans predict outcomes in septic shock and acute respiratory distress syndrome. Am. J. Respir. Crit. Care Med. 194, 439–449.

Sharma, A., Rees, D., Roberts, S., Kuiper, N.J., (2017). A case study: Glycosaminoglycan profiles of autologous chondrocyte implantation (ACI) tissue improve as the tissue matures. Knee 24, 149–157.

Sperling, L.E., Reis, K.P., Pranke, P., Wendorff, J.H., (2016). Advantages and challenges offered by biofunctional core-shell fiber systems for tissue engineering and drug delivery. Drug Discov. Today 21, 1243–1256.

Steele, J.A.M., McCullen, S.D., Callanan, A., Autefage, H., Accardi, M. a., Dini, D., Stevens, M.M., (2014). Combinatorial scaffold morphologies for zonal articular cartilage engineering. Acta Biomater. 10, 2065–2075.

Steward, A.J., Kelly, D.J., (2015). Mechanical regulation of mesenchymal stem cell differentiation. J. Anat. 227, 717–731.

Sun, X., Li, L., Overdier, K.H., Ammons, L.A., Douglas, I.S., Burlew, C.C., Zhang, F., Schmidt, E.P., Chi, L., Linhardt, R.J., (2015). Analysis of Total Human Urinary Glycosaminoglycan Disaccharides by Liquid Chromatography-Tandem Mass Spectrometry. Anal. Chem. 87, 6220–6227.

Tan, A.R., Hung, C.T., (2017). Concise review: Mesenchymal stem cells for functional cartilage tissue engineering: Taking cues from chondrocyte-based constructs. Stem Cells Transl. Med. 6, 1295–1303.

Vinatier, C., Guicheux, J., (2016). Cartilage tissue engineering: From biomaterials and stem cells to osteoarthritis treatments. Ann. Phys. Rehabil. Med. 59, 139–144.

Vinatier, C., Mrugala, D., Jorgensen, C., Guicheux, J., Noël, D., (2009). Cartilage engineering: a crucial combination of cells, biomaterials and biofactors. Trends Biotechnol. 27, 307–314.

Wan, S., Borland, S., Richardson, S.M., Merry, C.L.R., Saiani, A., Gough, J.E., (2016). Self-assembling peptide hydrogel for intervertebral disc tissue engineering. Acta Biomater. 46, 29–40.

Wang, C., Hou, W., Guo, X., Li, J., Hu, T., Qiu, M., Liu, S., Mo, X., Liu, X., (2017). Two-phase electrospinning to incorporate growth factors loaded chitosan nanoparticles into electrospun fibrous scaffolds for bioactivity retention and cartilage regeneration. Mater. Sci. Eng. C 79, 507–515.

Wang, M., Liu, X., Lyu, Z., Gu, H., Li, D., Chen, H., (2017). Glycosaminoglycans (GAGs) and GAG mimetics regulate the behavior of stem cell differentiation. Colloids Surfaces B Biointerfaces 150, 175–182.

Weyers, A., Yang, B., Yoon, D.S., Park, J.-H., Zhang, F., Lee, K.B., Linhardt, R.J., (2012). A Structural Analysis of Glycosaminoglycans from Lethal and Nonlethal Breast Cancer Tissues: Toward a Novel Class of Theragnostics for Personalized Medicine in Oncology? Omi. A J. Integr. Biol. 16, 79–89.

Wise, J.K., Yarin, A.L., Megaridis, C.M., Cho, M., (2009). Chondrogenic differentiation of human mesenchymal stem cells on oriented nanofibrous scaffolds: engineering the superficial zone of articular cartilage. Tissue Eng. Part A 15, 913–21.

Woodfield, T.B.F., Blitterswijk, C.A. Van, Wijn, J. De, Sims, T.J., Hollander, A.P., Riesle, J., (2005). Polymer Scaffolds Fabricated with Pore-Size Gradients as a Model for Studying the Zonal Organization within Tissue-Engineered Cartilage Constructs. Tissue Eng. 11, 1297–1311.

Woodruff, M.A., Hutmacher, D.W., (2010). The return of a forgotten polymer - Polycaprolactone in the 21st century. Prog. Polym. Sci. 35, 1217–1256.

Zarembinski, T.I., Doty, N.J., Erickson, I.E., Srinivas, R., Wirostko, B.M., Tew, W.P., (2014). Thiolated hyaluronan-based hydrogels crosslinked using oxidized glutathione: An injectable matrix designed for ophthalmic applications. Acta Biomater. 10, 94–103.

Zhang, Q., Lu, H., Kawazoe, N., Chen, G., (2013). Preparation of collagen porous scaffolds with a gradient pore size structure using ice particulates. Mater. Lett. 107, 280–283.

Zhou, S., Cui, Z., Urban, J.P.G., (2004). Factors influencing the oxygen concentration gradient from the synovial surface of articular cartilage to the cartilage-bone interface: A modeling study. Arthritis Rheum. 50, 3915–3924.

Zhu, D., Tong, X., Trinh, P., Yang, F., (2017). Mimicking Cartilage Tissue Zonal Organization by Engineering Tissue-Scale Gradient Hydrogels as 3D Cell Niche. Tissue Eng. Part A 24, 1–10.

Chapter II

COMPOSITIONAL AND STRUCTURAL ANALYSIS OF GLYCOSAMINOGLYCANS IN CELL-DERIVED EXTRACELLULAR MATRICES

CHAPTER II – Compositional and structural analysis of glycosaminoglycans in cell-derived extracellular matrices

Outline

The extracellular matrix (ECM) is a highly dynamic and complex meshwork of proteins and glycosaminoglycans (GAGs) with a crucial role in tissue homeostasis and organization not only by defining tissue architecture and mechanical properties, but also by providing chemical cues that regulate major biological processes. GAGs are associated with important physiological functions, acting as modulators of signaling pathways that regulate several cellular processes such as cell growth and differentiation. Recently, *in vitro* fabricated cell-derived ECM have emerged as promising materials for regenerative medicine due to their ability of better recapitulate the native ECM-like composition and structure, overcoming the limitations of availability and pathogen transfer risks of tissue-derived ECM scaffolds. However, little is known about the molecular and more specifically, GAG composition of these cell-derived ECM.

In this study, three different cell-derived ECM were produced *in vitro* and characterized in terms of their GAG content, composition and sulfation patterns using a highly sensitive liquid chromatography-tandem mass spectrometry technique. Distinct GAG compositions and disaccharide sulfation patterns were verified for the different cell-derived ECM. Additionally, the effect of decellularization method on the GAG and disaccharide relative composition was also assessed.

In summary, the method presented here offers a novel approach to determine the GAG composition of cell-derived ECM, which we believe is critical for a better understanding of ECM role in directing cellular responses and has the potential for generating important knowledge to use in the development of novel ECM-like biomaterials for tissue engineering applications.

II.1. Introduction

The ECM is a complex and highly specialized three-dimensional meshwork of biomolecules including proteins (e.g., collagen, fibronectin, laminin and others) and proteoglycans. The ECM plays a pivotal role in tissue homeostasis not only by defining tissue architecture and mechanical properties, but also as a modulator of signaling pathways regulating major cellular functions, such as cell proliferation, migration and differentiation (Lu et al., 2011b; Naba et al., 2016). Dysregulation of the ECM composition and structure is known to contribute to several pathological conditions, such as fibrosis, cancer and osteoarthritis (Bonnans et al., 2014).

Due to the importance of its functions and the versatility of its native tissue-like properties, ECM obtained from the decellularization of tissues has been widely used as bioactive scaffolds for several tissue engineering and regenerative medicine applications (Badylak et al., 2010; Gilbert et al., 2006). However, the scarcity of autologous organs/tissues and the occurrence of immunogenic responses and pathogen transfer when allogeneic/xenogeneic sources were used limited the clinical use of whole organ/tissue-derived decellularized ECM (Wong and Griffiths, 2014). An alternative approach to overcome these limitations, the use of cultured cells to generate ECM decellularized scaffolds *in vitro* has been recently explored. Cell-derived ECM present additional advantages over tissue-derived ECM as they can mimic the composition of specific native ECM that is hard to isolate from tissues (e.g., stem cell niche) and they can be used to modify the surface of synthetic/natural biomaterial scaffolds, generating constructs with improved bioactivity and appropriate mechanical support (Hoshiba et al., 2010; Kang et al., 2012; Lu et al., 2011b, 2011a). Additionally, as ECM compositions vary considerably with cell type and tissue location, cell source selection is a crucial factor for the success of the tissue engineering strategy.

Mesenchymal stem/stromal cells (MSC) have been employed as one of the major sources to generate cell-derived ECM scaffolds for regenerative medicine applications, mainly targeting bone and cartilage repair (Lu et al., 2011b; Yang et al., 2018; Zeitouni et al., 2012; Zhang et al., 2016). Regarding cartilage repair strategies, chondrocytes, the unique cell type present in cartilage tissue, have also been successfully used to generate cell-derived ECM scaffolds (Jin et al., 2010; Park et al., 2015). However, despite all these studies, little is currently known about the molecular composition of *in vitro* produced cell-derived ECM, namely in terms of the specific types and amounts of proteins and proteoglycans retained after the decellularization process.

Proteoglycans are major structural components of ECM and consist of a core protein with one or more covalently attached glycosaminoglycan (GAG) chains. Proteoglycans are able to

bind to many growth factors, cytokines and chemokines, which make them key modulators of cellular functions and tissue development (Gasimli et al., 2012; Linhardt and Toida, 2004). GAGs are a family of linear, negatively charged carbohydrates with a repeating disaccharide unit. Based on the structure and sulfation level of the repeating disaccharide, GAGs can be generally classified into four families that include heparan sulfate (HS), chondroitin sulfate (CS), keratan sulfate (KS) and hyaluronic acid (HA) (Gasimli et al., 2012; Weyers and Linhardt, 2013). Proteoglycans and respective GAGs localize mainly in cell membranes and reside within the ECM, acting as molecular co-receptors in cell signaling for cell-cell and cell-ECM interactions important for cell survival and differentiation (Gasimli et al., 2012). The negatively charged GAGs are also associated with the maintenance of the biomechanical properties of tissues through controlling of hydration and swelling pressure, allowing tissues to absorb compressional forces. Additionally, the sulfation patterns in the GAG chains play crucial roles by allowing interactions, mainly of an ionic nature, with growth factors, cell surface receptors, enzymes, cytokines, chemokines and proteins that are associated with several biological processes, such as development, disease, cell growth and differentiation and microbial pathogenesis (Gasimli et al., 2014; Kjellén and Lindahl, 2018; Papy-Garcia and Albanese, 2017; Wang et al., 2017). In fact, GAGs role in controlling stem cell fate through modulation of important signaling pathways such as FGF signaling was previously suggested (Gasimli et al., 2012; Ibrahimi et al., 2004; Papy-Garcia and Albanese, 2017). Additionally, the effects of different GAGs in MSC proliferation and differentiation through mediation of growth factor activity have also been reported in the literature (Cool and Nurcombe, 2005; Dombrowski et al., 2009; Manton et al., 2007; Uygun et al., 2009). Therefore, the structural and growth factor sequestering/activation properties of GAGs make these biomolecules promising materials for a broad range of tissue engineering applications (Celikkin et al., 2017; Wang et al., 2017; Weyers and Linhardt, 2013). As major components of cartilage, GAGs, mainly CS and HA, have been incorporated in tissue engineering scaffolds to more effectively mimic the natural ECM and improve the quality of the generated tissue (Amann et al., 2017; Christiansen-Weber et al., 2018; Pfeifer et al., 2016).

As a result of the critical importance of GAGs in regulating many physiological processes in all organisms, accurately determining their composition, structure and sulfation patterns as well as their changes in normal versus diseased states in different organs, tissues, and cells is necessary to better understand the underlying mechanisms involved in normal development and several pathologies. Recently, studies have been conducted to elucidate the “GAGome” and glycome changes related to specific cellular functions and diseases. Linhardt group has previously reported differences in GAG sulfation patterns between cancerous and normal tissues, as well as between lethal and nonlethal breast cancer tissues (Weyers et al., 2012). Glycomics of MSC was previously suggested as a valuable tool to

evaluate their differentiation stage (Heiskanen et al., 2009). Moreover, high performance liquid chromatography (HPLC) analysis combined with mass spectrometry has been used to study GAGs as possible markers of MSC differentiation potential (Hasehira et al., 2017). Despite the availability of many different qualitative and quantitative techniques for analyzing GAGs, liquid chromatography-tandem mass spectrometry (LC-MS/MS) method using multiple reaction monitoring (MRM) detection represents a major advancement in the field of glycosaminoglycanomics due to its high sensitivity and specificity for detecting all GAG subtypes in complex biological samples (Kubaski et al., 2017; Sun et al., 2015). This method has been successfully applied, by our group and others, to analyze GAG disaccharides in various types of samples including biological fluids (e.g., plasma and urine) (Oguma et al., 2007; Sun et al., 2015), human milk at different lactation stages (Wang et al., 2018), cultured cells (Li et al., 2015) and different regions of human intervertebral disc (Liu et al., 2018). Interestingly, despite the great promise and attention received by tissue engineering and regenerative medicine research, only few studies have employed proteomics and glycomics methods to provide a more complete molecular characterization of decellularized ECM scaffolds or final engineered tissues.

In the present study, cell-derived ECM from different cell sources were generated and characterized qualitatively in terms of the efficacy of the decellularization process, their morphology and presence of relevant ECM proteins. Additionally, after GAG extraction, purification and enzymatic digestion, we used LC-MS/MS with MRM detection mode to perform GAG disaccharide compositional analysis of *in vitro* produced cell-derived ECM and respective cell sources (Figure II.1). This analysis can contribute with relevant knowledge about the GAG content and composition of the ECM secreted by these cells, which may provide new insights for the design of novel ECM biomimetic biomaterial scaffolds for regenerative medicine applications, especially for cartilage repair. Additionally, these results can also provide some understanding of how GAG composition, structure and sulfation levels are affected by the decellularization method used.

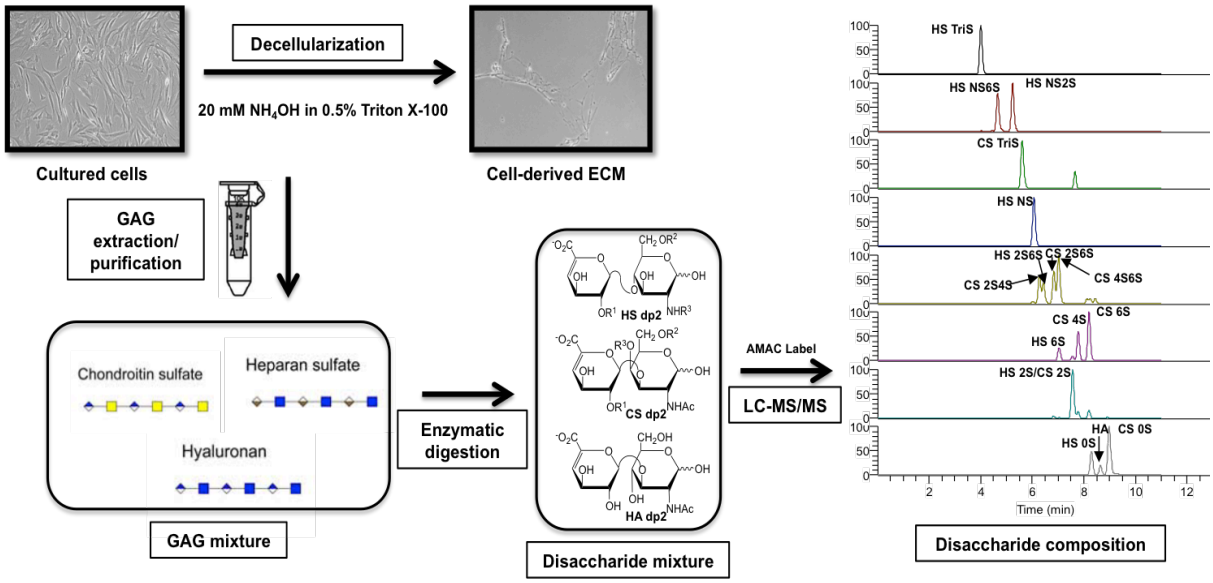

Figure II.1. Flow chart for cell-derived ECM and respective cultured cell sources sample treatment for GAG disaccharide compositional analysis by LC-MS/MS. GAG were purified from the different cell-derived ECM and respective monolayer cultures (before decellularization) and digested by heparinases and chondroitinase ABC, originating a disaccharide mixture. The disaccharide samples were then AMAC-labeled (structures in Supplementary Figure II.2) and analyzed by LC-MS/MS MRM to obtain the cell-derived ECM GAG disaccharide composition.

II.2. Material & Methods

II.2.1. Cell culture

Human chondrocytes purchased from CELL Applications, Inc. were cultured using high-glucose Dulbecco's Modified Eagle's Medium (DMEM: Gibco, Grand Island, NY USA) supplemented with 10% fetal bovine serum (FBS: Gibco, USA), 1X MEM non-essential aminoacids (Sigma, St. Louis, MO USA), 0.2 mM L-Ascorbic acid (Sigma), 0.4 mM L-Proline (Sigma) and 1% penicillin-streptomycin (Pen-strep: Gibco). Human bone marrow-derived MSC (BMSC, male 36 years) and human synovial-derived MSC (SMSC, male 28 years) were isolated according to protocols previously established (Dos Santos et al., 2010; Santhagunam et al., 2013). Bone marrow aspirates were obtained from Instituto Português de Oncologia Francisco Gentil, Lisboa-Potugal while synovium aspirates were obtained from Centro Hospitalar de Lisboa Ocidental, E.P.E, Hospital São Francisco Xavier, Lisboa, Portugal. All human samples were obtained from donors after written informed consent and with approval of the Ethics Committee of the respective clinical institution. Isolated BMSC and SMSC were cultured using DMEM supplemented with 10% FBS and 1% Pen-strep and cryopreserved in liquid/vapour nitrogen tanks until further use. All cultures were kept at 37ºC

and 5% CO_2 in a humidified atmosphere and only cells between passages 3 and 5 were used in this study.

II.2.2. Materials

Unsaturated disaccharide standards of CS, HS and HA were purchased from Iduron (Manchester, UK, see Table II.1 for structures). Sodium cyanoborohydrade ($NaCNBH_4$), 2-aminoacridone (AMAC) and acetic acid were obtained from Sigma-Aldrich (St. Louis, MO USA). Methanol (HPLC grade), water (HPLC grade), ammonium acetate (HPLC grade) and dimethyl sulfoxide (DMSO) were purchased from Fisher Scientific (Springfield, NJ USA). Enzymes chondroitin lyase ABC from *Proteus vulgaris* and recombinant *Flavobacterial* heparinase I, II and III were expressed in *E. coli* strains in our laboratory.

Table II.1. Heparan sulfate, chondroitin sulfate and hyaluronic acid disaccharide structures. The disaccharide structures on the left result from different "R" groups of the structures presented (right). These structures correspond to unsaturated uronic acids (ΔUA's), which were AMAC-labeled (AMAC-derivatized disaccharide structures are provided in Supplementary Figure II.2), analyzed by LC-MS/MS and used as standards.

HS disaccharides	
$TriS_{HS}$	ΔUA2S(1,4)GlcNS6S
$NS6S_{HS}$	ΔUA (1,4)GlcNS6S
$NS2S_{HS}$	ΔUA2S(1,4)GlcNS
NS_{HS}	ΔUA (1,4)GlcNS
$2S6S_{HS}$	ΔUA2S(1,4)GlcNAc6S
$6S_{HS}$	ΔUA (1,4)GlcNAc6S
$2S_{HS}$	ΔUA2S(1,4)GlcNAc
$0S_{HS}$	ΔUA(1,4)GlcNAc
CS disaccharides	
$TriS_{CS}$	ΔUA2S(1,3)GalNAc4S6S
$2S4S_{CS}$	ΔUA2S(1,3)GalNAc4S
$2S6S_{CS}$	ΔUA2S(1,3)GalNAc6S
$4S6S_{CS}$	ΔUA (1,3)GalNAc4S6S
$2S_{CS}$	ΔUA2S(1,3)GalNAc
$4S_{CS}$	ΔUA (1,3)GalNAc4S
$6S_{CS}$	ΔUA (1,3)GalNAc6S
$0S_{CS}$	ΔUA(1,3)GalNAc
HA disaccharide	
$0S_{HA}$	ΔUA(1,3)GlcNAc

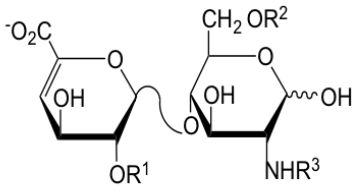

HS disaccharide unit

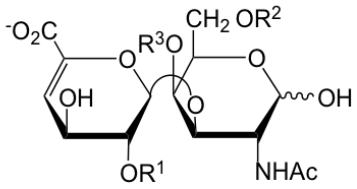

CS disaccharide unit

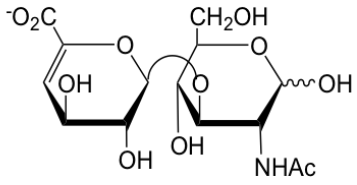

HA disaccharide unit

II.2.3. Decellularized cell-derived ECM preparation

Human chondrocytes, BMSC and SMSC were seeded in tissue culture-treated plates at 5000 cells/cm^2 and expanded in their respective media for 10-12 days with complete medium renewal twice a week. After reaching confluence, medium was discarded and cells were washed in Dulbecco's phosphate buffered saline (PBS, no calcium, no magnesium - catalog# 14190144, Gibco). ECM isolation was performed by a decellularization protocol using a 20 mM ammonium hydroxide (NH_4OH, Sigma) + 0.5% Triton X-100 (Sigma) solution in PBS according to previously reported methods (Kang et al., 2012; Yang et al., 2018). The solution was added to the culture and incubated for 5 min at room temperature. After confirmation of complete cell lysis and presence of intact ECM on the surface of the wells under a microscope, ECM was gently washed 3 times with distilled water. Then, the different cell-derived ECM layers were detached from the plates using a cell scrapper, collected in falcon tubes and freeze-dried. Cell culture monolayers before decellularization were washed twice with PBS to remove any media remnants, harvested and the pellets were collected by centrifugation. Afterwards, the cell pellets were rinsed twice with PBS, centrifuged and collected for GAG disaccharide analysis.

II.2.4. Immunofluorescence analysis

The success of the decellularization protocol for the different cell sources was confirmed by immunocytochemistry and phase/fluorescence microscopy. Therefore, cultures before and after decellularization were washed twice with PBS, fixed with 4% paraformaldehyde (PFA; Santa Cruz Biotechnology, Dallas, TX USA) for 30 min and then permeabilized with 0.1% Triton X-100 for 10 min. After permeabilization, samples were incubated with Phalloidin-TRITC (Sigma-Aldrich) (dilution 1:250, 2 µg/mL) for 45 min in the dark. Then, cells were washed twice with PBS and counterstained with DAPI (Sigma-Aldrich) (1.5 µg/mL) for 5 min and then washed with PBS. Cell cultures before and after decellularization were imaged in phase contrast mode and fluorescent mode under a microscope (Olympus IX51 Inverted Microscope: Olympus America Inc., Melville, NY USA).

The presence and distribution of the ECM proteins collagen I, fibronectin and laminin in the different cell-derived ECM was assessed by immunofluorescence staining. After decellularization, samples were washed with PBS and fixed with 4% PFA for 30 min at room temperature. Afterwards, cell-derived ECM were washed three times with 1% bovine serum albumin (BSA, Sigma) in PBS for 5 min. Cell-derived ECM were then blocked with a solution of 1% BSA and 10% donkey serum (Sigma) in PBS at room temperature for 45 min. Primary antibodies including mouse anti-human collagen I, fibronectin and laminin (10 µg/ml in 1%

BSA, 10% donkey serum in PBS) (R&D systems, Minneapolis, MN) were added into the samples, followed by an overnight incubation at 4ºC. After washing with 1% BSA in PBS, a NorthernLights™ 557-conjugated anti-mouse IgG secondary antibody (dilution 1:200 in 1%BSA PBS solution) (R&D systems) was added into the samples and incubated in the dark for 1 h at room temperature. Finally, the samples were washed with PBS and immunofluorescence staining was confirmed by microscopy (Olympus IX51 Inverted Microscope).

II.2.5. Scanning electron microscopy analysis

The morphological analysis of the different cell-derived ECM was performed using a field emission scanning electron microscope (FE-SEM, FEI-Versa 3D Dual Beam, Hillsboro). Before imaging, cell-derived ECM samples obtained in glass cover slips were mounted on a holder and sputter-coated with a thin layer of 60% gold-40% palladium. SEM imaging was performed at different magnifications using an accelerating voltage of 2 kV.

II.2.6. GAG disaccharide sample preparation: isolation, digestion and AMAC-labeling

Cell confluent monolayers and respective lyophilized cell-derived ECM samples collected from one culture dish were treated with 100 µL of BugBuster 10X Protein Extraction Reagent (Millipore Sigma, MA USA) and sonicated for 1 h. The samples were then desalted by passing through a 3 KDa molecular weight cut off (MWCO) spin column (Millipore, MA USA), and washed three times with distilled water. The casing tubes were replaced and 300 µL of digestion buffer (50 mM ammonium acetate containing 2 mM calcium chloride adjusted to pH 7.0) was added to the filter unit. Afterwards, recombinant heparin lyases I, II, III (10 mU each, pH optima 7.0−7.5) and recombinant chondroitin lyase ABC (10 mU each, pH optimum 7.4) were added to each sample, mixed well by pipetting and GAG enzymatic digestion was conducted by incubation overnight at 37°C. The enzymatic reaction was terminated by centrifugal ultrafiltration, the disaccharides were recovered in the filtrate and the filter unit was washed twice with 200 µL of distilled water. The final filtrates containing the disaccharide products were lyophilised and kept at -20°C until labeling.

Dried cell and cell-derived ECM disaccharide samples were AMAC-labelled by adding 10 µL of 0.1M AMAC in DMSO/acetic acid (17/3, V/V) solution and by incubating at room temperature for 10 min, followed by addition of 10 µL of 1M aqueous $NaCNBH_4$ solution and incubation for 1 h at 45°C. A mixture containing all 17 CS, HS and HA disaccharide standards (derivatives of the structures shown in Figure II.1 are summarized in Table II.1) prepared at a concentration of 0.5 ng/µL was similarly AMAC-labeled (structures in

Supplementary Figure II.2) and used for each run as an external standard. After the AMAC-labeling reaction, the samples were centrifuged and respective supernatants were recovered.

II.2.7. Compositional analysis of GAG disaccharides by LC-MS/MS

Disaccharide analysis was performed according to a previously reported method (Sun et al., 2015). LC was performed on an Agilent 1200 LC system at 45 °C using an Agilent Poroshell 120 ECC18 (2.7 µm, 3.0 × 50 mm) column. Mobile phase A (MPA) was 50 mM ammonium acetate aqueous solution, and the mobile phase B (MPB) was methanol. The mobile phase passed through the column at a flow rate of 300 µL/min. The gradient used was the following: 0-10 min, 5-45% B; 10-10.2 min, 45-100% B; 10.2-14 min, 100% B; 14-22 min, 100-5% B. The injection volume used for all the samples was 5 µL. A triple quadrupole mass spectrometry system equipped with an ESI source (Thermo Fisher Scientific, San Jose, CA USA) was used as a detector. The online MS analysis was performed at the MRM mode with the MS parameters: negative ionization mode with a spray voltage of 3000 V, a vaporizer temperature of 300 °C, and a capillary temperature of 270 °C. Data analysis was performed using Thermo Xcalibur™ software (Thermo Fisher Scientific, San Jose, CA USA). The disaccharides in different cell and cell-derived ECM samples were quantified by comparison of the sample peak area to that of an external standard.

II.2.8. Statistical analysis

All values were represented as the mean ± standard deviation (SD) of three (n=3) independent samples. Statistical analysis of the data was performed using the software GraphPad Prism version 7. One-way analysis of variance (ANOVA) was performed to determine significant differences among the multiple groups of data of cell-derived ECM and cell culture monolayers. Tukey's post-hoc test was used to determine the difference between any two groups. Student's t-test was used to determine significant differences in each GAG disaccharide composition between cell-derived ECM and respective cell culture before decellularization. Data were considered statistically significant if $p < 0.05$.

II.3. Results

II.3.1. Cell-derived ECM characterization

Decellularized cultured cell-derived ECM were obtained from three different human cell types (chondrocytes, BMSC and SMSC). Cultures were fully confluent before decellularization and presented a spindle-like morphology, characteristic of these cell types, with a well defined cell nuclei and cytoskeleton, as it is possible to observe in the fluorescent micrographs obtained after DAPI/Phalloidin staining (Figure II.2). After the decellularization treatment with a solution of 20 mM NH_4OH and 0.5% Triton X-100 in PBS for 5 min, it is possible to confirm the presence of a fibrillary network of ECM in all the different conditions. The residual DAPI staining after decellularization indicated that the cellular nuclei were disrupted and only the ECM secreted by cells remained, therefore confirming the success of the decellularization method used (Figure II.2).

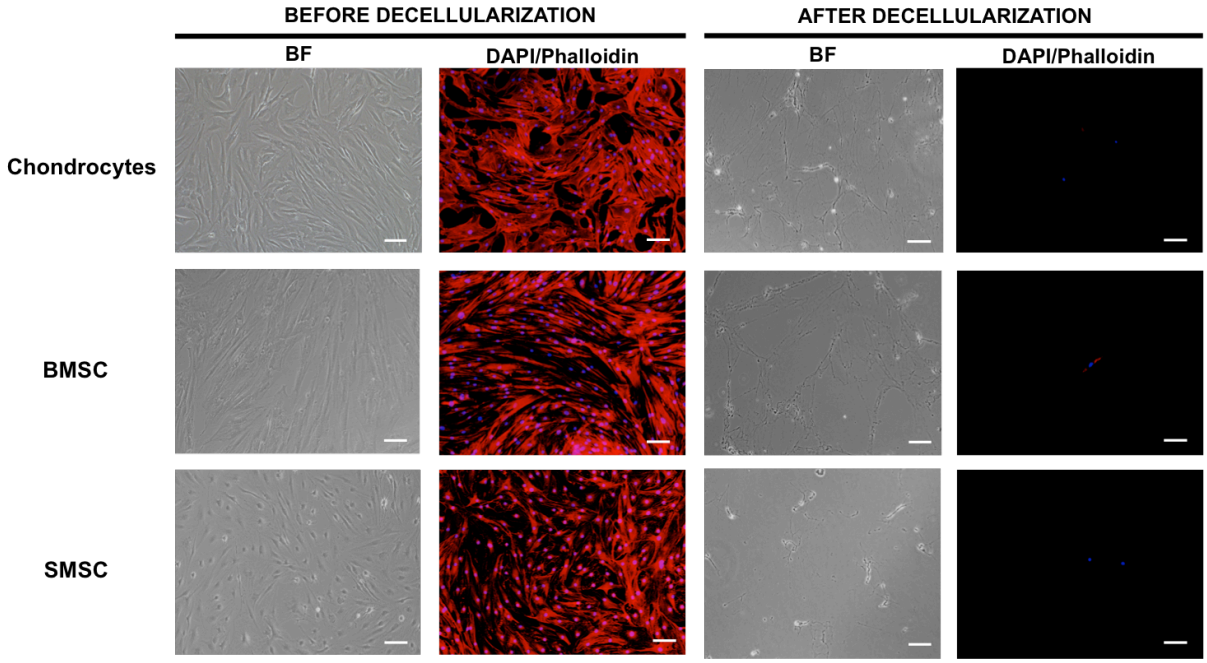

Figure II.2. Production of decellularized cell-derived ECM from cultures of human chondrocytes, BMSC and SMSC. Images of phase contrast microscopy and fluorescent microscopy DAPI/Phalloidin staining taken before and after the treatment with 20 mM NH_4OH, 0.5% Triton X-100 in PBS solution to confirm the success of the decellularization process. DAPI stains cell nuclei blue and Phalloidin stains actin-rich cell cytoskeleton red. Scale bar: 100 µm.

The different cell-derived ECM were assessed by immunostaining for the presence of known relevant ECM proteins, namely collagen type I, fibronectin and laminin. After decellularization, all the conditions stained positively for ECM proteins collagen type I, fibronectin and laminin. However, some differences in ECM proteins relative abundance

were observed between the different cell-derived ECM. Accordingly, Figure II.3 shows that SMSC-ECM presented a considerably lower level of fluorescent staining for all the proteins when compared with BMSC-ECM. Additionally, BMSC-ECM apparently expressed higher levels of collagen I, fibronectin and laminin than the other two types of cell-derived ECM studied.

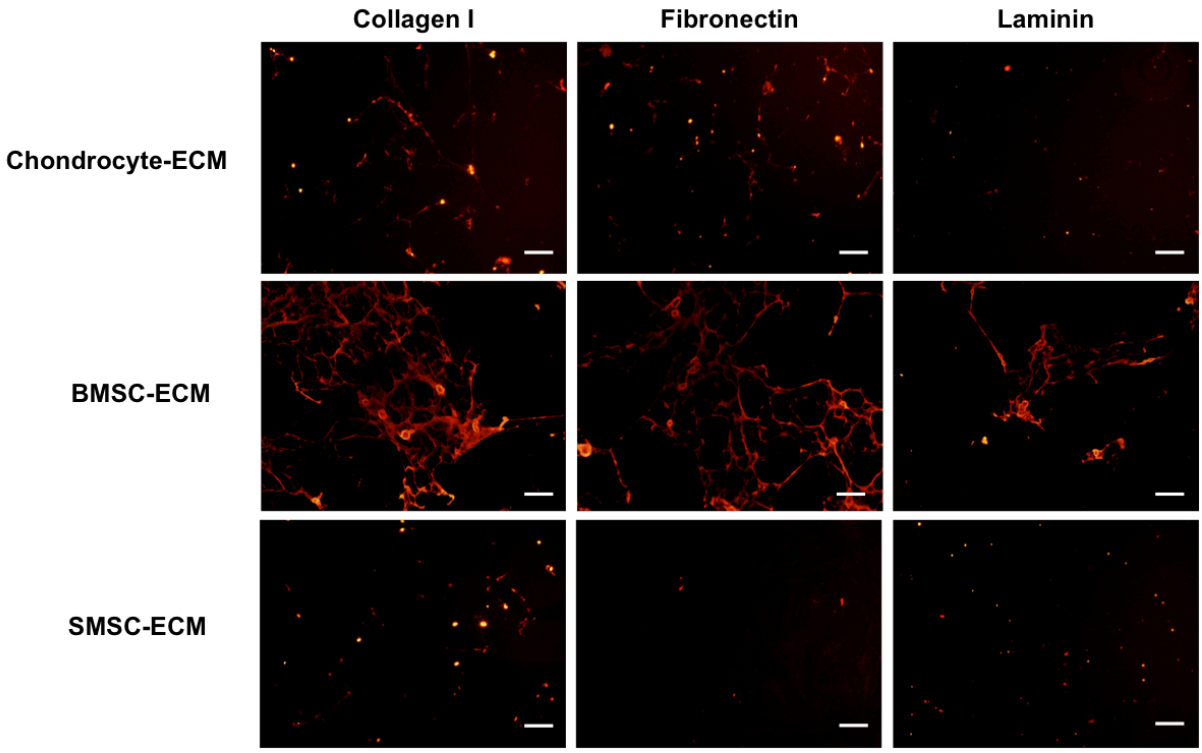

Figure II.3. Expression of relevant ECM proteins in cell-derived ECM produced from human chondrocytes, BMSC and SMSC. Immunofluorescent staining images of collagen I, fibronectin and laminin showed differences in the abundance and distribution of these proteins in the different types of cell-derived ECM. Scale bar: 100 μm.

The morphology and micro/nano scale features of the different cell-derived ECM were assessed by SEM analysis (Figure II.4). All the cell-derived ECM types presented a similar architecture composed by fibrillar networks. However, for the case of SMSC-ECM, as we can observe in Figure II.4, it was also possible to identify some globular-like structures together with fibrillar ones.

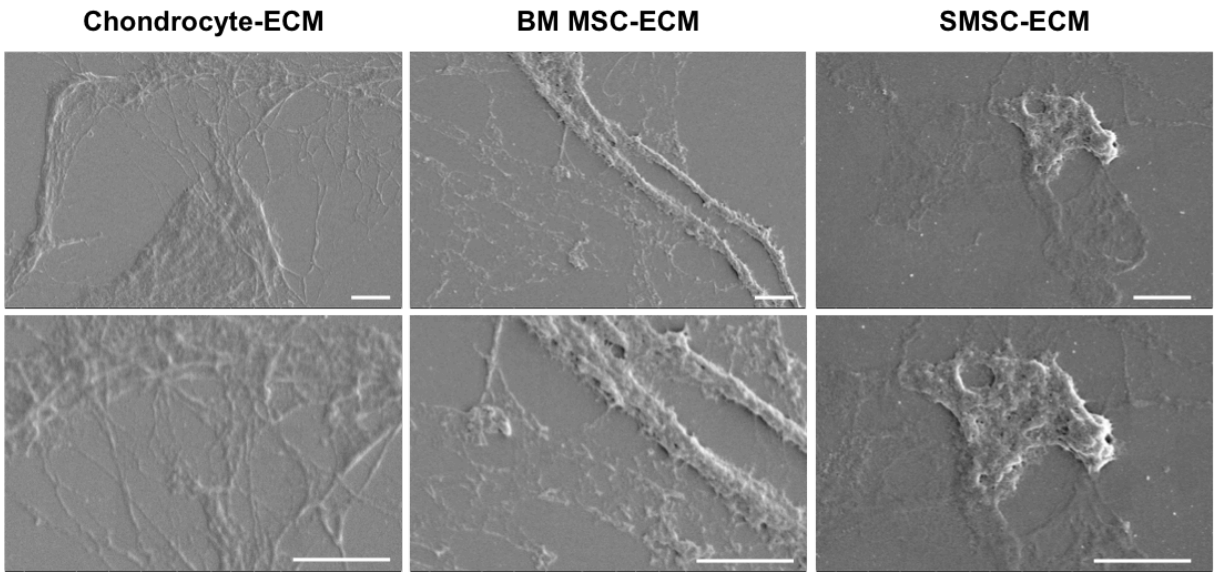

Figure II.4. SEM micrographs of ECM derived from human chondrocytes, BMSC and SMSC after the decellularization protocol. Scale bar: 2 μm.

II.3.2. Disaccharide composition of cell-derived ECM

The total amount of GAG (Figure II.5 A and Supplementary Table II.1) as well as the respective HS, CS and HA GAG amounts (Figure II.5 B and Supplementary Table II.1) for each cell-derived ECM were obtained after LC-MS/MS analysis and normalized to the dry weight of each sample. As it is possible to observe in Figure II.5 A, BMSC-ECM contained significant higher amounts of total GAG than Chondrocyte-ECM and SMSC-ECM. Regarding HS, CS and HA total composition (expressed as ng of GAG/mg of dry cell-derived ECM), there were evident differences in the GAG compositions of the cell-derived ECM obtained from different cell sources (Figure II.5 B). Chondrocyte-ECM was composed mainly by CS (86 ± 36 ng/mg), followed by lower average amounts of HS (16 ± 4 ng/mg) and HA (10 ± 6 ng/mg). Both BMSC-ECM (HA: 88 ± 20 ng/mg; CS: 79 ± 23 ng/mg; HS: 39 ± 16 ng/mg) and SMSC-ECM (CS: 35 ± 2 ng/mg; HA: 32 ± 8 ng/mg; HS: 8 ± 1 ng/mg) were more evenly composed by CS and HA, with lower amounts of HS. Interestingly, BMSC-ECM presented significantly higher amounts of HA when compared to ECM secreted by the other cell types.

The compositional analysis of the GAG disaccharides of the different cell-derived ECM was performed after enzymatic digestion of isolated GAG samples with heparin lyase I, II, III and chondroitin lyase ABC. The disaccharides were then AMAC-labeled by reductive amination and analyzed by LC-MS/MS using MRM. The HS and CS disaccharide composition for the different cell-derived ECM normalized to dry ECM weight is presented in Figure II.6 and Supplementary Table II.2. For all the cell-derived ECM, HS was comprised primarily of 0S, followed by NS and N2S (Figure II.6 A). However, some differences were noticed in the HS disaccharide amounts present in the different types of ECM. BMSC-ECM

presented a significantly higher amount of 0S and NS when compared to SMSC-ECM and Chondrocyte-ECM. Additionally, Chondrocyte-ECM presented a statistically significant higher amount of NS2S than the ECM derived from both MSC sources. In terms of CS disaccharides, all the cell-derived ECM conditions were primarily composed by 4S and 6S (Figure II.6 B). The amounts of 4S were significantly higher in BMSC-ECM comparing to other conditions of cell-derived ECM. Moreover, Chondrocyte-ECM presented higher amounts of 6S, however the difference was only statistically significant when compared to SMSC-ECM.

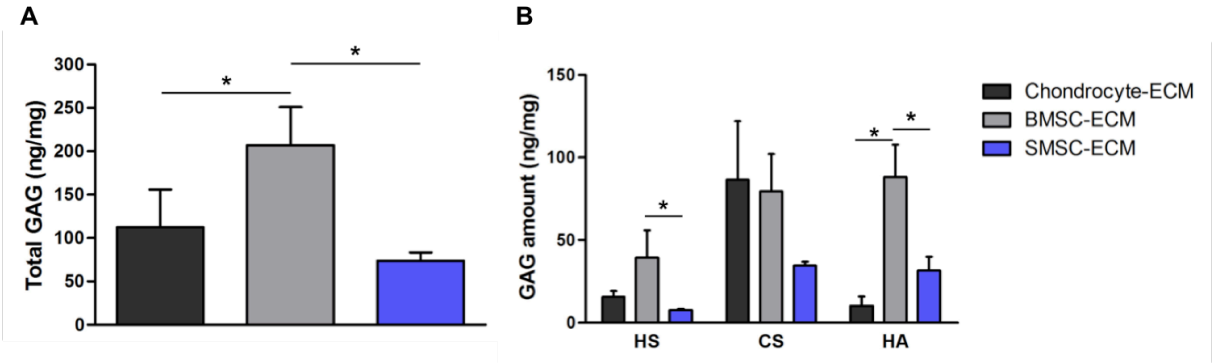

Figure II.5. GAG composition of the different cell-derived ECM produced from human chondrocytes, BMSC and SMSC. Total GAG (A) and HS, CS, HA total amounts (B) quantified as ng of GAG/mg of dry ECM. Results are presented as mean ± SD of three independent samples (n=3); * $p < 0.05$.

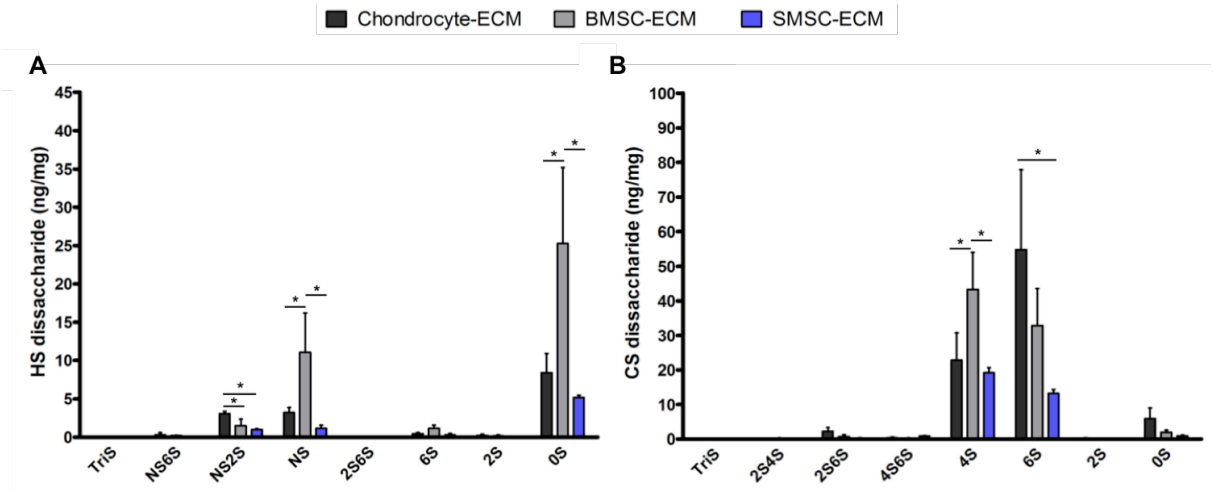

Figure II.6. HS (A) and CS (B) disaccharide composition of the different cell-derived ECM produced from human chondrocytes, BMSC and SMSC, quantified as ng of GAG/mg of dry ECM. Results are presented as mean ± SD of three independent samples (n=3); * $p < 0.05$.

II.3.3. Effects of the decellularization process on GAG amount and disaccharide percentage composition

The effect of the decellularization protocol on the total GAG amount of the different cell types tested was evaluated by quantifying the mass of GAG recovered from each culture dish before and after the treatment (Figure II.7 A-B, Supplementary Table II.3). BMSC presented a significantly higher total GAG amount compared to the other cell types. Additionally, as expected, the amounts of total GAG per dish were considerably lower in the cell-derived ECM samples comparing to the cell monolayers. However, the amounts of total GAG retained for the different types of cell-derived ECM were moderately close (Chondrocyte-ECM: 200 ± 78 ng/dish; BMSC-ECM: 223 ± 48 ng/dish; SMSC-ECM: 134 ± 17 ng/dish), with percentages of GAG retention varying between 20-30%. In Figure II.7 B and Supplementary Table II.3, it is possible to observe the amounts of HS, CS and HA recovered from each culture dish for the different cell-derived ECM and respective monolayer cultures. The decellularization process differentially affected HS, CS and HA GAG amounts among the different cultures. For example, CS was significantly lost during the generation of Chondrocyte-ECM and SMSC-ECM, which was not verified for BMSC-ECM. Contrarily, percentage-wise, HA was greatly diminished during BMSC decellularization, while approximately maintained during the generation of SMSC-ECM. This differential response was also observed for the HS and CS disaccharide amounts before and after decellularization, which are summarized in the Supplementary Table II.4.

The average GAG disaccharide percentage compositions of the various cell-derived ECM were determined and compared to the respective culture monolayers to further assess the effect of the decellularization method on GAG amount, sulfation level and disaccharide composition. The average HS, CS and HA percentage composition of the different cell-derived ECM and respective cell sources before decellularization is presented in Figure II.7 C and Supplementary Table II.5. All the cell-derived ECM presented significantly different HS, CS and HA percentage compositions when compared to its respective cell source, with the exception of HS percentage composition of SMSC-ECM and SMSC. Cultured chondrocytes were mainly composed by CS (50%), followed by HS (31%) and HA (19%). After decellularization, the generated Chondrocyte-ECM contained a higher relative average percentage of CS (77%) and lower relative average percentages of HS (15%) and HA (9%) when compared to chondrocyte cells. BMSC GAGs are mainly composed of HA (80%) with relatively low average percentages of HS (10%) and CS (10%). However, the ECM generated from BMSC consisted of a completely different GAG composition, with similar percentages of HA (43%) and CS (38%), but a lower percentage of HS (18%). SMSC cultures GAG mixtures were mainly composed of CS (68%), and lower relative percentages

of HA (19%) and HS (13%). SMSC-ECM showed a lower percentage of CS (47%), a higher percentage of HA (42%) and a slightly lower percentage of HS (10%). Despite the differences verified for the cell monolayers, the average percentage compositions of matrices generated from two different MSC sources, BMSC-ECM and SMSC-ECM, were fairly similar (HS: 18% *vs.* 10%; CS: 38% *vs.* 47% and HA: 43% *vs.* 42%, respectively).

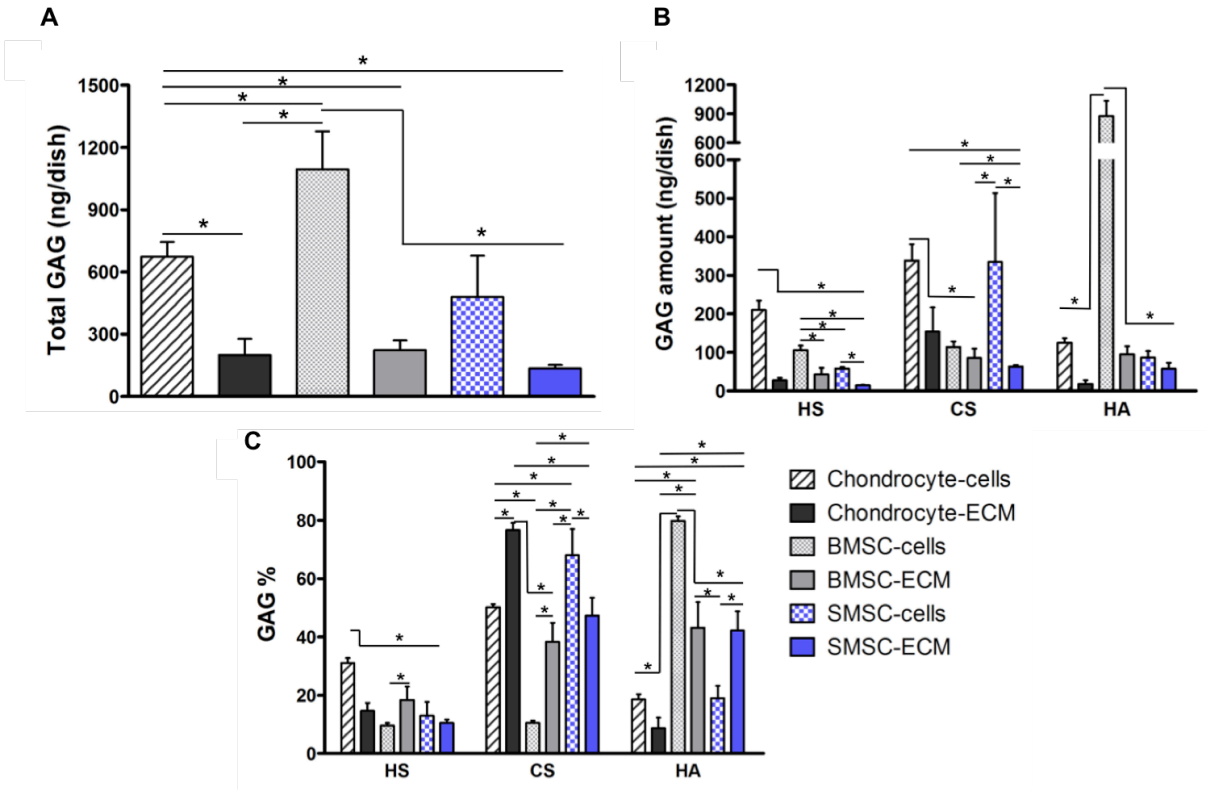

Figure II.7. Effect of the decellularization protocol on total GAG (A) and HS, CS and HA amounts (B) presented as ng obtained in each culture dish before and after the treatment. Average percentage GAG composition of the different cell-derived ECM and cell culture monolayers (C). Results are presented as mean ± SD of three independent samples (n=3); * $p < 0.05$.

The differences in average percentage HS and CS disaccharide composition between cultured cells and *in vitro* generated cell-derived ECM were also assessed and are presented in Figure II.8 and Supplementary Table II.6. Chondrocytes and Chondrocyte-ECM HS were mainly composed by 0S, NS and NS2S with significant differences observed after decellularization, namely a relatively lower average percentage of 0S and relatively higher average percentages of NS2S and NS in Chondrocyte-ECM when compared to chondrocyte cells (Figure II.8 A). In terms of CS disaccharides, Chondrocyte-ECM was mainly composed of 6S (63%), 4S (27%) and 0S (7%), and these values are significantly different from the observed values for CS composition of chondrocyte cells, which were composed of 4S (76%), and a lower percentage of 6S (17%) and a very small percentage of 0S (1%) (Figure II.8 B). BMSC-ECM HS was primarily composed of 0S (65%) and NS (28%) with low

percentage of NS2S (4%), whereas the HS composition observed for BMSC cell cultures was 0S (57%) and NS (27%) and NS2S (16%) (Figure II.8 C). Both BMSC cultured cells and BMSC-ECM showed CS disaccharide compositions predominantly composed of 4S and 6S (Figure II.8 D). However, significant differences were observed, with BMSC-ECM having a lower average percentage of 4S (55% *vs.* 75%) and a higher average percentage of 6S (41% versus 18%), compared to cultured cells. HS from both SMSC cultured cells and SMSC-ECM was mainly composed of 0S (72% and 68%, respectively) with lower average percentages of NS and NS2S (Figure II.8 E). Interestingly, significant differences in HS disaccharide composition between SMSC-ECM and their respective cell source were observed only for NS2S and a low percentage of 2S (6%) was detected in the cultured cells. The CS disaccharide compositions were similar to the observed for the other cell types, with both SMSC cultures and SMSC-ECM mainly composed of 4S and 6S. Additionally, the same trend was observed with SMSC-ECM, which showed a significantly lower percentage of 4S (56% versus 71%) and a significantly higher percentage of 6S (38% versus 21%) when compared to SMSC cell cultures before decellularization treatment (Figure II.8 F).

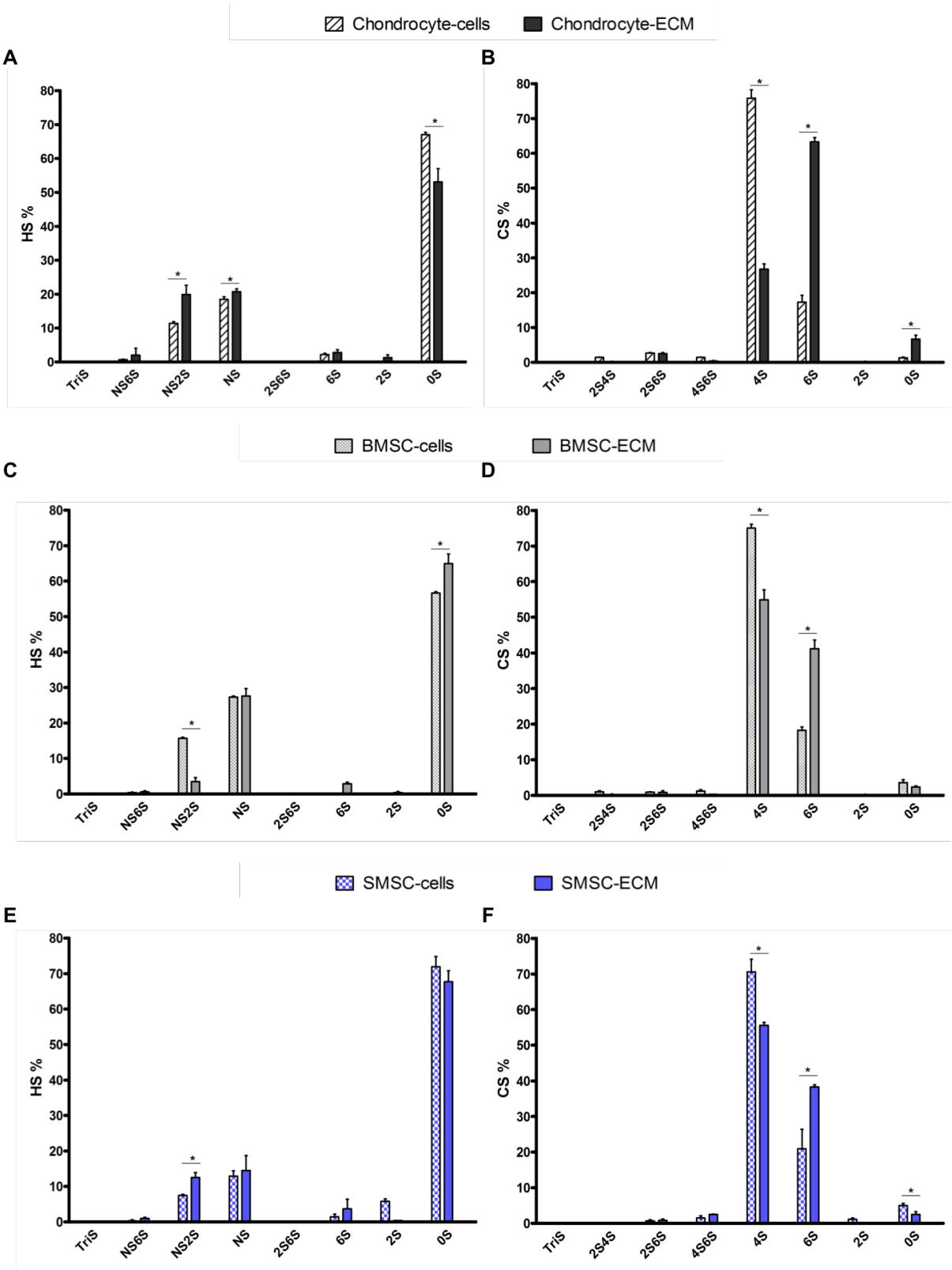

Figure II.8. Average relative percentage HS (A, C and E) and CS (B, D and F) composition of the different cell sources and respective cell-derived ECM: chondrocytes (A, B), BMSC (C, D) and SMSC (E, F). Results are presented as mean ± SD of three independent samples (n=3); * $p < 0.05$, denotes significant differences in each HS, CS disaccharide average relative percentage between cell-derived ECM and respective cell source.

II.4. Discussion

In this study, we produced different cell-derived ECM secreted from human chondrocytes, BMSC and SMSC based on previously reported methods (Kang et al., 2012; Yang et al., 2018). Fluorescent microscopy and DAPI/Phalloidin staining were used to observe cell cultures before and after decellularization and confirm the efficiency of the method. All cells were removed and a fibrillary network of ECM was observed for all conditions. Moreover, the different cell-derived ECM samples produced were also characterized for the presence of ECM proteins (collagen I, fibronectin and laminin). After removal of cellular components, these ECM proteins were still present as constituents of the cell-derived ECM. However, differences in the protein abundance and distribution were observed among the ECM-derived from different cell sources. Despite evidences of the presence of ECM proteins, a lower level of fluorescent staining was observed for all proteins in SMSC-ECM. However, this is accordance with the phase microscopy images from Figure II.2, in which a considerably lower amount of ECM network was obtained for SMSC-ECM when compared to Chondrocyte-ECM and BMSC-ECM. BMSC-ECM produced in this work stained positive for all the 3 ECM proteins, with lower staining area verified for laminin, which is in accordance to a previously published study (Lu et al., 2011a). These BMSC-ECM characterization results were consistent with a previous study that has shown the retention of ECM proteins after complete decellularization of adipose tissue derived-MSC *in vitro* cultures (Guneta et al., 2018). Concerning Chondrocyte-ECM, both fibronectin and collagen I presented higher levels of positive fluorescent staining than laminin. The presence of collagen I in the ECM was expected due to fact that chondrocytes tend to increase the expression of this protein when cultured as monolayer plastic adherent cultures. Previous literature also obtained similar results after immunofluorescence analysis of ECM secreted by human articular chondrocytes (Hoshiba et al., 2013). The morphology of the different cell-derived ECM was also characterized using SEM and a fibrillar structure was mainly observed, which was consistent with recently published reports (Kaukonen et al., 2017; Ragelle et al., 2017).

Proteoglycans and their major constituents, GAGs, are among the most important components of the ECM of multiple tissues. Despite the great relevance of GAGs within the ECM and the increasing number of studies targeting tissues and cells, few studies have focused on the GAGome profile of only ECM. However, recently, authors have been focused on studying the ECM components, or as recently defined as “matrisome” of healthy and disease tissues, aiming to identify novel prognostic/diagnostic markers and discover novel therapeutic opportunities (Naba et al., 2016). Additionally, other groups have applied proteomic tools to perform a comprehensive characterization of the protein composition of

cell-derived ECM produced *in vitro* by BMSC, adipose-derived MSC and neonatal fibroblasts (Ragelle et al., 2017). We assert that the characterization of the GAG content, composition and sulfation patterns of *in vitro* produced cell-derived ECM is critical for a better comprehension of ECM role in directing cellular responses, with the potential of generating useful information to improve the design of novel biomaterials that better recapitulate ECM signaling for tissue engineering and regenerative medicine applications.

In this work, we used a previously developed method of LC-MS/MS with MRM (Sun et al., 2015) to characterize *in vitro* cell-derived ECM obtained from human chondrocytes, BMSC and SMSC in terms of their GAG content, composition and sulfation pattern. By comparative analysis with the respective cell culture monolayers it was also possible to assess the effects of the decellularization protocol on total GAG and GAG disaccharide amounts. About 20-30% of the total GAG amount verified in the cell monolayers cultures was maintained after generation of the different cell-derived ECM. A higher percentage of GAG retention after decellularization (approximately 50%) was obtained in a previous study with adipose stem cell-derived ECM (Guneta et al., 2018). However, the method used for total GAG quantification was considerably less sensitive than the LC-MS/MS MRM used in this work. Importantly, HS, CS and HA and their disaccharides in the different conditions of cell-derived ECM were differently affected by the decellularization treatment. However, a statistically significant loss of HS was verified for all the groups during the decellularization, which might be explained by the depletion of cell surface HS proteoglycans during cell membrane disruption.

Chondrocyte-ECM was mainly consisted of CS and showed higher amounts and relative percentages of this GAG than both BMSC-ECM and SMSC-ECM. Chondrocytes are a unique native cell population within articular cartilage tissue and are responsible for secreting articular cartilage ECM. In articular cartilage, the predominant proteoglycan is aggrecan that consists of a core protein mainly with attached CS chains, but also KS chains and small amount of dermatan sulfate (DS) chains (Knudson and Knudson, 2001; Roughle, 2006). Since the main function of chondrocyte is to secrete cartilage ECM, it is expected that they would synthesize a matrix richer in CS when compared to other cell types, which is consistent with our results. Interestingly, it was previously reported that the chondrocyte proteoglycan metabolism can be directly or indirectly influenced by the scaffold material, as different synthetic and natural materials seeded with chondrocytes resulted in differences in GAG composition and CS sulfation (Mouw et al., 2005). Moreover, ECM composition and therefore also GAG composition is known to be dependent on the cell source (Ragelle et al., 2017). Each cell type secretes unique and specific ECM to fulfil the biological requirements of its native tissue. Considering cultured cells, higher similarities in average GAG composition were observed between chondrocytes and SMSC, which might be related to

these cells being more prone to undergo chondrogenesis when compared to BMSC. However, we observed a similarity in GAG composition and HS, CS disaccharide compositions between BMSC-ECM and SMSC-ECM than when these are compared to Chondrocyte-ECM. This suggests that despite being isolated from different tissues, both BMSC and SMSC secrete a more similar ECM in terms of GAG composition when compared to chondrocytes. The HS of cell-derived ECM were mainly composed of 0S with low amounts of NS and NS2S, whereas the CS of cell-derived ECM consisted of 4S and 6S. Different trends in CS 4S and 6S were observed for MSC- derived ECM and Chondrocyte-ECM. BMSC-ECM and SMSC-ECM showed slightly higher average relative percentages of 4S than 6S, while Chondrocyte-ECM showed a considerably higher average relative percentage of 6S than 4S. It is well established that the disaccharide composition of CS varies with age and degeneration of articular cartilage (Lauder et al., 2001). Accordingly, during embryogenesis CS chains are exclusively 6S, from fetal development to adolescence CS chains tend to be equally 4S and 6S, and during adulthood CS chains tend to have more 6S than 4S (Mouw et al., 2005; Sharma et al., 2017). We speculate that the more "immature" state of BMSC and SMSC and their known involvement in cartilage development, might prime them to secrete a more "juvenile-like" ECM with higher CS4S relative percentages when compared to the ECM secreted by adult chondrocytes. However, additional and more comprehensive studies are required to understand if the known relation of 4S and 6S in articular cartilage tissue can be expanded to cultured cells and cell-derived ECM.

After comparison between the different cell-derived ECM and their respective cultured cells before decellularization, we observed significant differences on the relative average percentages of total GAG and HS and CS disaccharides. Despite the differences in the relative average percentages, the trends observed in the CS disaccharides changes after the decellularization process were similar among the different samples, more specifically, all the cell-derived ECM samples showed lower relative average percentages of 4S and higher relative average of percentages of 6S when compared to the cultured cells before decellularization. Such similarities among the different conditions were not so clearly observed for HS disaccharides.

In summary, we successfully produced cell-derived ECM from different cell sources and characterized them in terms of their morphology and presence of relevant ECM proteins. Moreover, a highly sensitive and specific LC-MS/MS analytical method was used for the first time to determine the GAG content, composition and sulfation patterns of *in vitro* generated cell-derived ECM. Significant differences in GAG composition were observed between the cell-derived ECM secreted by different cell sources, confirming the expected tissue-ECM specificity. Finally, the analytical method presented in this first report of GAG composition of cell-derived ECM, together with further studies combining proteomic tools, might provide

important knowledge to better understand ECM molecular composition and function in regulating cellular responses. The structure-function studies should further the development of improved ECM-like biomimetic scaffolds for tissue engineering applications.

II.5. References

Amann, E., Wolff, P., Breel, E., van Griensven, M., Balmayor, E.R., (2017). Hyaluronic acid facilitates chondrogenesis and matrix deposition of human adipose derived mesenchymal stem cells and human chondrocytes co-cultures. Acta Biomater. 52, 130–144.

Badylak, S.F., Taylor, D., Uygun, K., (2010). Whole Organ Tissue Engineering: Decellularization and Recellularization of Three-Dimensional Matrix Scaffolds. Annu. Rev. Biomed. Eng. 13, 27–53.

Bonnans, C., Chou, J., Werb, Z., (2014). Remodelling the extracellular matrix in development and disease. Nat. Rev. Mol. Cell Biol. 15, 786–801.

Celikkin, N., Rinoldi, C., Costantini, M., Trombetta, M., Rainer, A., Święszkowski, W., (2017). Naturally derived proteins and glycosaminoglycan scaffolds for tissue engineering applications. Mater. Sci. Eng. C 78, 1277–1299.

Christiansen-Weber, T., Noskov, A., Cardiff, D., Garitaonandia, I., Dillberger, A., Semechkin, A., Gonzalez, R., Kern, R., (2018). Supplementation of specific carbohydrates results in enhanced deposition of chondrogenic-specific matrix during mesenchymal stem cell differentiation. J. Tissue Eng. Regen. Med. 12, 1261–1272.

Cool, S.M., Nurcombe, V., (2005). The osteoblast-heparan sulfate axis: Control of the bone cell lineage. Int. J. Biochem. Cell Biol. 37, 1739–1745.

Dombrowski, C., Song, S.J., Chuan, P., Lim, X., Susanto, E., Sawyer, A.A., Woodruff, M.A., Hutmacher, D.W., Nurcombe, V., Cool, S.M., (2009). Heparan Sulfate Mediates the Proliferation and Differentiation of Rat Mesenchymal Stem Cells. Stem Cells Dev. 18, 661–670.

Dos Santos, F., Andrade, P.Z., Boura, J.S., Abecasis, M.M., da Silva, C.L., Cabral, J.M.S., (2010). Ex vivo expansion of human mesenchymal stem cells: a more effective cell proliferation kinetics and metabolism under hypoxia. J. Cell. Physiol. 223, 27–35.

Gasimli, L., Hickey, A.M., Yang, B., Li, G., Dela Rosa, M., Nairn, A. V., Kulik, M.J., Dordick, J.S., Moremen, K.W., Dalton, S., Linhardt, R.J., (2014). Changes in glycosaminoglycan structure on differentiation of human embryonic stem cells towards mesoderm and endoderm lineages. Biochim. Biophys. Acta - Gen. Subj. 1840, 1993–2003.

Gasimli, L., Linhardt, R.J., Dordick, J.S., (2012). Proteoglycans in stem cells. Biotechnol. Appl. Biochem. 59, 65–76.

Gilbert, T.W., Sellaro, T.L., Badylak, S.F., (2006). Decellularization of tissues and organs. Biomaterials 27, 3675–3683.

Guneta, V., Zhou, Z., Tan, N.S., Sugii, S., Wong, M.T.C., Choong, C., (2018). Recellularization of decellularized adipose tissue-derived stem cells: Role of the cell-secreted extracellular matrix in cellular differentiation. Biomater. Sci. 6, 168–178.

Hasehira, K., Hirabayashi, J., Tateno, H., (2017). Structural and quantitative evidence of α2–6-sialylated N-glycans as markers of the differentiation potential of human mesenchymal stem cells. Glycoconj. J. 34, 797–806.

Heiskanen, A., Hirvonen, T., Salo, H., Impola, U., Olonen, A., Laitinen, A., Tiitinen, S., Natunen, S., Aitio, O., Miller-Podraza, H., Wuhrer, M., Deelder, A.M., Natunen, J., Laine, J., Lehenkari, P., Saarinen, J., Satomaa, T., Valmu, L., (2009). Glycomics of bone marrow-derived mesenchymal stem cells can be used to evaluate their cellular differentiation stage. Glycoconj. J. 26, 367–384.

Hoshiba, T., Lu, H., Kawazoe, N., Chen, G., (2010). Decellularized matrices for tissue engineering. Expert Opin. Biol. Ther. 10, 1717–1728.

Hoshiba, T., Lu, H., Kawazoe, N., Yamada, T., Chen, G., (2013). Effects of extracellular matrix proteins in chondrocyte-derived matrices on chondrocyte functions. Biotechnol. Prog. 29, 1331–1336.

Ibrahimi, O.A., Zhang, F., Hrstka, S.C.L., Mohammadi, M., Linhardt, R.J., (2004). Kinetic Model for FGF, FGFR, and Proteoglycan Signal Transduction Complex Assembly. Biochemistry 43, 4724–4730.

Jin, C.Z., Choi, B.H., Park, S.R., Min, B.H., (2010). Cartilage engineering using cell-derived extracellular matrix scaffold in vitro. J. Biomed. Mater. Res. - Part A 92, 1567–1577.

Kang, Y., Kim, S., Bishop, J., Khademhosseini, A., Yang, Y., (2012). The osteogenic differentiation of human bone marrow MSCs on HUVEC-derived ECM and β-TCP scaffold. Biomaterials 33, 6998–7007.

Kaukonen, R., Jacquemet, G., Hamidi, H., Ivaska, J., (2017). Cell-derived matrices for studying cell proliferation and directional migration in a complex 3D microenvironment. Nat. Protoc. 12, 2376–2390.

Kjellén, L., Lindahl, U., (2018). Specificity of glycosaminoglycan–protein interactions. Curr. Opin. Struct. Biol. 50, 101–108.

Knudson, C.B., Knudson, W., (2001). Cartilage proteoglycans. Semin. Cell Dev. Biol. 12, 69–78.

Kubaski, F., Osago, H., Mason, R.W., Yamaguchi, S., Kobayashi, H., Tsuchiya, M., Orii, T., Tomatsu, S., (2017). Glycosaminoglycans detection methods : Applications of mass spectrometry. Mol. Genet. Metab. 120, 67–77.

Lauder, R.M., Huckerby, T.N., Brown, G.M., Bayliss, M.T., Nieduszynski, I. A., (2001). Age-related changes in the sulphation of the chondroitin sulphate linkage region from human articular cartilage aggrecan. Biochem. J. 358, 523–528.

Li, G., Li, L., Tian, F., Zhang, L., Xue, C., Linhardt, R.J., (2015). Glycosaminoglycanomics of Cultured Cells Using a Rapid and Sensitive LC-MS/MS Approach. ACS Chem. Biol. 10, 1303–1310.

Linhardt, R.J., Toida, T., (2004). Role of glycosaminoglycans in cellular communication. Acc. Chem. Res. 37, 431–438.

Liu, X., Krishnamoorthy, D., Lin, L., Xue, P., Zhang, F., Chi, L., Linhardt, R.J., Iatridis, J.C., (2018). A method for characterising human intervertebral disc glycosaminoglycan disaccharides using liquid chromatography-mass spectrometry with multiple reaction monitoring. Eur. Cell. Mater. 35, 117–131.

Lu, H., Hoshiba, T., Kawazoe, N., Chen, G., (2011)a. Autologous extracellular matrix scaffolds for tissue engineering. Biomaterials 32, 2489–2499.

Lu, H., Hoshiba, T., Kawazoe, N., Koda, I., Song, M., Chen, G., (2011)b. Cultured cell-derived extracellular matrix scaffolds for tissue engineering. Biomaterials 32, 9658–9666.

Manton, K.J., Leong, D.F.M., Cool, S.M., Nurcombe, V., (2007). Disruption of heparan and chondroitin sulfate signaling enhances mesenchymal stem cell-derived osteogenic differentiation via bone morphogenetic protein signaling pathways. Stem Cells 25, 2845–2854.

Mouw, J.K., Case, N.D., Guldberg, R.E., Plaas, A.H.K., Levenston, M.E., (2005). Variations in matrix composition and GAG fine structure among scaffolds for cartilage tissue engineering. Osteoarthr. Cartil. 13, 828–836.

Naba, A., Clauser, K.R., Ding, H., Whittaker, C.A., Carr, S.A., Hynes, R.O., (2016). The extracellular matrix: Tools and insights for the “omics” era. Matrix Biol. 49, 10–24.

Oguma, T., Tomatsu, S., Montano, A.M., Okazaki, O., (2007). Analytical method for the determination of disaccharides derived from keratan, heparan, and dermatan sulfates in human serum and plasma by high-performance liquid chromatography/turbo ionspray ionization tandem mass spectrometry. Anal. Biochem. 368, 79–86.

Papy-Garcia, D., Albanese, P., (2017). Heparan sulfate proteoglycans as key regulators of the mesenchymal niche of hematopoietic stem cells. Glycoconj. J. 34, 377–391.

Park, Y.B., Seo, S., Kim, J.A., Heo, J.C., Lim, Y.C., Ha, C.W., (2015). Effect of chondrocyte-derived early extracellular matrix on chondrogenesis of placenta-derived mesenchymal stem cells. Biomed. Mater. 10, 035014.

Pfeifer, C.G., Berner, A., Koch, M., Krutsch, W., Kujat, R., Angele, P., Nerlich, M., Zellner, J., (2016). Higher ratios of hyaluronic acid enhance chondrogenic differentiation of human MSCs in a hyaluronic acid-gelatin composite scaffold. Materials (Basel). 9, 381.

Ragelle, H., Naba, A., Larson, B.L., Zhou, F., Prijić, M., Whittaker, C.A., Del Rosario, A., Langer, R., Hynes, R.O., Anderson, D.G., (2017). Comprehensive proteomic characterization of stem cell-derived extracellular matrices. Biomaterials 128, 147–159.

Roughle, P.J., (2006). The Structure and Function of Cartilage Proteoglicans. Eur. Cells Mater. 12, 92–101.

Santhagunam, A., Dos Santos, F., Madeira, C., Salgueiro, J.B., Cabral, J.M.S., (2013). Isolation and ex vivo expansion of synovial mesenchymal stromal cells for cartilage repair. Cytotherapy 16, 440–453.

Sharma, A., Rees, D., Roberts, S., Kuiper, N.J., (2017). A case study: Glycosaminoglycan profiles of autologous chondrocyte implantation (ACI) tissue improve as the tissue matures. Knee 24, 149–157.

Sun, X., Li, L., Overdier, K.H., Ammons, L.A., Douglas, I.S., Burlew, C.C., Zhang, F., Schmidt, E.P., Chi, L., Linhardt, R.J., (2015). Analysis of Total Human Urinary Glycosaminoglycan Disaccharides by Liquid Chromatography-Tandem Mass Spectrometry. Anal. Chem. 87, 6220–6227.

Uygun, B.E., Stojsih, S.E., Matthew, H.W.T., (2009). Effects of immobilized glycosaminoglycans on the proliferation and differentiation of mesenchymal stem cells. Tissue Eng. Part A 15, 3499–3512.

Wang, C., Lang, Y., Li, Q., Jin, X., Li, G., Yu, G., (2018). Glycosaminoglycanomic profiling of human milk in different stages of lactation by liquid chromatography-tandem mass spectrometry. Food Chem. 258, 231–236.

Wang, M., Liu, X., Lyu, Z., Gu, H., Li, D., Chen, H., (2017). Glycosaminoglycans (GAGs) and GAG mimetics regulate the behavior of stem cell differentiation. Colloids Surfaces B Biointerfaces 150, 175–182.

Weyers, A., Linhardt, R.J., (2013). Neoproteoglycans in tissue engineering. FEBS J. 280, 2511–2522.

Weyers, A., Yang, B., Yoon, D.S., Park, J.-H., Zhang, F., Lee, K.B., Linhardt, R.J., (2012). A Structural Analysis of Glycosaminoglycans from Lethal and Nonlethal Breast Cancer Tissues: Toward a Novel Class of Theragnostics for Personalized Medicine in Oncology? Omi. A J. Integr. Biol. 16, 79–89.

Wong, M.L., Griffiths, L.G., (2014). Immunogenicity in xenogeneic scaffold generation: Antigen removal vs. decellularization. Acta Biomater. 10, 1806–1816.

Yang, Y., Lin, H., Shen, H., Wang, B., Lei, G., Tuan, R.S., (2018). Mesenchymal stem cell-derived extracellular matrix enhances chondrogenic phenotype of and cartilage formation by encapsulated chondrocytes in vitro and in vivo. Acta Biomater. 69, 71–82.

Zeitouni, S., Krause, U., Clough, B.H., Halderman, H., Falster, A., Blalock, D.T., Chaput, C.D., Sampson, H.W., Gregory, C.A., (2012). Human mesenchymal stem cell-derived matrices for enhanced osteoregeneration. Sci. Transl. Med. 4, 132–155.

Zhang, W., Zhu, Y., Li, J., Guo, Q., Peng, J., Liu, S., Yang, J., Wang, Y., (2016). Cell-Derived Extracellular Matrix: Basic Characteristics and Current Applications in Orthopedic Tissue Engineering. Tissue Eng. Part B Rev. 22, 193–207.

Supporting Information

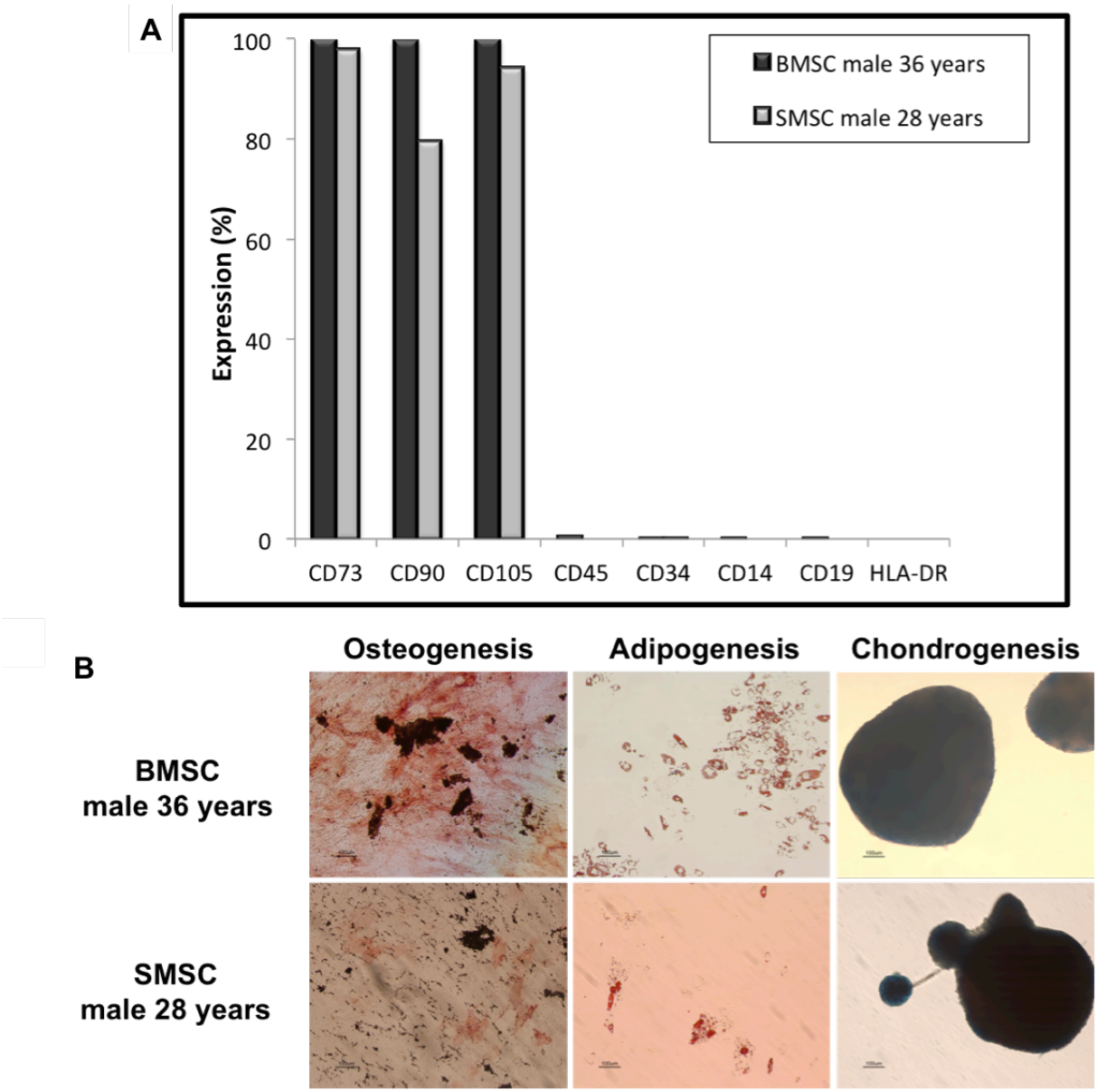

Supplementary Figure II.1. Characterization of MSC isolated from bone marrow aspirates (BMSC) collected from a male donor (36 years) and of MSC isolated from synovium aspirates obtained from a male donor (28 years). Immunophenotypic characterization of BMSC and SMSC assessed by flow cytometry (A). Multilineage differentiation potential of BMSC and SMSC (B). Osteogenic, adipogenic and chondrogenic differentiation was confirmed after 14 days induction by ALP/von Kossa, Oil Red-O and Alcian Blue stainings, respectively. Scale bar: 100 µm.

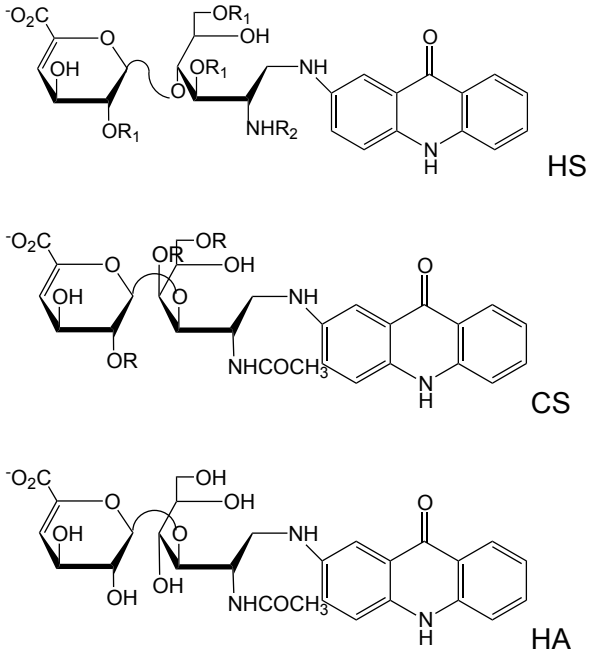

Supplementary Figure II.2. Structures of AMAC derivatized disaccharides used in LC-MS/MS analysis.

Supplementary Table II.1. Total GAG amounts obtained for the different cell-derived ECM produced from chondrocytes, BMSC and SMSC presented as ng of GAG/mg of dry ECM. Results are presented as mean ± SD of three independent samples (n=3).

	Total GAG (ng/mg)			
	HS	**CS**	**HA**	**Total**
Chondrocyte-ECM	15.7 ± 3.5	86.4 ± 35.5	10.3 ± 5.6	112.4 ± 43.6
BMSC-ECM	39.4 ± 16.4	79.4 ± 22.6	88.0 ± 19.6	206.8 ± 44.0
SMSC-ECM	7.7 ± 0.8	34.6 ± 2.3	31.5 ± 8.4	73.8 ± 9.5

Supplementary Table II.2. HS and CS disaccharides amounts obtained for the different cell-derived ECM produced from chondrocytes, BMSC and SMSC presented as ng of GAG/mg of dry ECM. Results are presented as mean ± SD of three independent samples (n=3).

HS disaccharide (ng/mg)								
	TriS	**NS6S**	**NS2S**	**NS**	**2S6S**	**6S**	**2S**	**0S**
Chondrocyte -ECM	0.0±0.0	0.3±0.3	3.1±0.3	3.2±0.6	0.0±0.0	0.4±0.1	0.2±0.2	8.4±2.5
BMSC-ECM	0.0±0.0	0.2±0.0	1.5±0.9	11.1±5.1	0.0±0.0	1.1±0.5	0.2±0.2	25.3±9.9
SMSC-ECM	0.0±0.0	0.1±0.0	1.0±0.1	1.1±0.4	0.0±0.0	0.3±0.2	0.0±0.0	5.2±0.3
CS disaccharide (ng/mg)								
	TriS	**2S4S**	**2S6S**	**4S6S**	**4S**	**6S**	**2S**	**0S**
Chondrocyte -ECM	0.0±0.0	0.1±0.0	2.2±1.1	0.3±0.2	22.8±8.0	54.8±23.1	0.2±0.2	6.0±3.0
BMSC-ECM	0.0±0.0	0.2±0.2	0.7±0.6	0.3±0.1	43.3±10.7	32.9±10.7	0.2±0.2	1.9±0.6
SMSC-ECM	0.0±0.0	0.0±0.0	0.3±0.1	0.9±0.1	19.2±1.5	13.3±1.1	0.0±0.0	0.9±0.2

Supplementary Table II.3. Total GAG amounts presented as ng/dish for the different cell-derived ECM and respective cell culture monolayers prior to decellularization treatment. Results are presented as mean ± SD of three independent samples (n=3).

	Total GAG (ng/dish)			
	HS	**CS**	**HA**	**Total**
Chondrocyte	209.5 ± 24.6	338.2 ± 42.2	125.0 ± 11.8	672.7 ± 70.9
Chondrocyte-ECM	27.9 ± 6.3	153.6 ± 63.1	18.3 ± 10.0	199.8 ± 77.5
BMSC	105.7 ± 11.5	113.9 ± 14.3	873.8 ± 160.3	1093.4 ± 184.4
BMSC-ECM	42.4 ± 17.7	85.6 ± 24.3	94.9 ± 21.2	222.9 ± 47.5
SMSC	57.8 ± 3.5	334.8 ± 178.7	86.5 ± 17.1	479.1 ± 199.3
SMSC-ECM	14.0 ± 1.4	63.0 ± 4.2	57.5 ± 15.4	134.4 ± 17.3

Supplementary Table II.4. HS and CS disaccharide amounts presented as ng/dish for the different cell-derived ECM and respective cell culture monolayers prior to decellularization treatment. Results are presented as mean ± SD of three independent samples (n=3).

HS disaccharide (ng/dish)								
	TriS	**NS6S**	**NS2S**	**NS**	**2S6S**	**6S**	**2S**	**0S**
Chondrocyte	0.0±0.0	1.5±0.0	23.8±2.3	38.8±5.4	0.1±0.1	4.6±1.0	0.3±0.0	140.4±16.9
Chondrocyte-ECM	0.0±0.0	0.5±0.5	5.4±0.5	5.7±1.1	0.0±0.0	0.8±0.3	0.4±0.3	14.9±4.5
BMSC	0.0±0.0	0.4±0.0	16.6±2.1	28.8±3.2	0.1±0.1	0.0±0.0	0.0±0.0	59.8±6.1
BMSC-ECM	0.0±0.0	0.2±0.0	1.6±1.0	11.9±5.5	0.0±0.0	1.2±0.5	0.2±0.2	27.2±10.7
SMSC	0.1±0.0	0.2±0.2	4.3±0.4	7.5±1.3	0.0±0.0	0.8±0.5	3.4±0.6	41.5±0.9
SMSC-ECM	0.0±0.0	0.1±0.1	1.7±0.2	2.1±0.8	0.0±0.0	0.5±0.4	0.1±0.0	9.4±0.5

CS disaccharide (ng/dish)								
	TriS	**2S4S**	**2S6S**	**4S6S**	**4S**	**6S**	**2S**	**0S**
Chondrocyte	0.0±0.0	4.8±0.3	9.0±1.0	4.5±0.2	257.0±40.0	58.0±1.8	0.3±0.0	4.5±0.5
Chondrocyte-ECM	0.0±0.0	0.2±0.1	3.9±2.0	0.6±0.4	40.5±14.1	97.4±41.1	0.4±0.3	10.6±5.4
BMSC	0.0±0.0	1.1±0.3	1.0±0.1	1.3±0.4	85.5±11.7	20.9±3.4	0.0±0.0	4.1±0.5
BMSC-ECM	0.0±0.0	0.2±0.2	0.7±0.6	0.3±0.1	46.7±11.5	35.5±11.5	0.2±0.2	2.0±0.7
SMSC	0.1±0.0	0.2±0.0	2.0±0.3	4.6±0.7	233.3±114.4	74.9±55.8	3.4±0.6	16.3±7.0
SMSC-ECM	0.0±0.0	0.1±0.0	0.5±0.2	1.6±0.1	35.0±2.7	24.1±2.0	0.1±0.0	1.6±0.4

Supplementary Table II.5. Average percentage GAG composition for the different cell-derived ECM and respective cell culture monolayers prior to decellularization treatment. Results are presented as mean ± SD of three independent samples (n=3).

	Total GAG relative %		
	HS	**CS**	**HA**
Chondrocyte	31 ± 2	50 ± 1	19 ± 2
Chondrocyte-ECM	15 ± 3	77 ± 2	9 ± 4
BMSC	10 ± 1	10 ± 1	80 ± 2
BMSC-ECM	18 ± 5	38 ± 6	43 ± 9
SMSC	13 ± 5	68 ± 9	19 ± 4
SMSC-ECM	10 ± 1	47 ± 6	42 ± 7

Supplementary Table II.6. Average percentage HS and CS disaccharide composition for the different cell-derived ECM and respective cell culture monolayers prior to decellularization treatment. Results are presented as mean ± SD of three independent samples (n=3).

HS disaccharide relative %								
	TriS	**NS6S**	**NS2S**	**NS**	**2S6S**	**6S**	**2S**	**0S**
Chondrocyte	0 ± 0	1 ± 0	11 ± 0	18 ± 1	0 ± 0	2 ± 0	0 ± 0	67 ± 1
Chondrocyte-ECM	0 ± 0	2 ± 2	20 ± 3	21 ± 1	0 ± 0	3 ± 1	1 ± 1	53 ± 4
BMSC	0 ± 0	0 ± 0	16 ± 0	27 ± 0	0 ± 0	0 ± 0	0 ± 0	57 ± 0
BMSC-ECM	0 ± 0	1 ± 0	4 ± 1	28 ± 2	0 ± 0	3 ± 0	0 ± 0	65 ± 3
SMSC	0 ± 0	0 ± 0	7 ± 0	13 ± 1	0 ± 0	1 ± 1	6 ± 1	72 ± 3
SMSC-ECM	0 ± 0	0 ± 0	12 ± 1	15 ± 4	0 ± 0	4 ± 3	0 ± 0	68 ± 3
CS disaccharide relative %								
	TriS	**2S4S**	**2S6S**	**4S6S**	**4S**	**6S**	**2S**	**0S**
Chondrocyte	0 ± 0	1 ± 0	3 ± 0	1 ± 0	76 ± 2	17 ± 2	0 ± 0	1 ± 0
Chondrocyte-ECM	0 ± 0	0 ± 0	2 ± 0	0 ± 0	27 ± 2	63 ± 1	0 ± 0	7 ± 1
BMSC	0 ± 0	1 ± 0	1 ± 0	1 ± 0	75 ± 1	18 ± 1	0 ± 0	4 ± 1
BMSC-ECM	0 ± 0	0 ± 0	1 ± 0	0 ± 0	55 ± 3	41 ± 2	0 ± 0	2 ± 0
SMSC	0 ± 0	0 ± 0	1 ± 0	2 ± 1	71 ± 4	21 ± 6	1 ± 0	5 ± 1
SMSC-ECM	0 ± 0	0 ± 0	1 ± 0	3 ± 0	56 ± 1	38 ± 1	0 ± 0	3 ± 1

Chapter III

GLYCOSAMINOGLYCAN REMODELING DURING CHONDROGENIC DIFFERENTIATION OF HUMAN BONE MARROW/SYNOVIAL-DERIVED MESENCHYMAL STEM/STROMAL CELLS UNDER NORMOXIA/HYPOXIA

CHAPTER III – Glycosaminoglycan remodeling during chondrogenic differentiation of human bone marrow/synovial-derived mesenchymal stem/stromal cells under normoxia/hypoxia

Outline

Glycosaminoglycans (GAGs) are major components of cartilage extracellular matrix (ECM), which play an important role in tissue homeostasis not only in providing mechanical load resistance, but also as signaling mediators of cell adhesion, migration, proliferation and differentiation. GAGs are linear, highly charged, acidic carbohydrates with a repeating disaccharide unit. Specific GAG types as well as their disaccharide sulfation patterns can be predictive of the tissue maturation level but also of disease and degeneration states.

In this work, we used a highly sensitive liquid chromatography-tandem mass spectrometry (LC-MS/MS) method to perform a comparative study in terms of GAG type, disaccharide composition and sulfation patterns between tissues generated from human bone marrow- and synovial-derived mesenchymal stem/stromal cells (hBMSC/hSMSC) after 7, 14 and 21 days of chondrogenic differentiation under normoxic (21% O_2) and hypoxic (5% O_2) micromass cultures. GAG and respective disaccharide profiles obtained from the LC-MS/MS analysis were compared with undifferentiated cells (day 0) and differentiated human chondrocytes (day 21). Prior to LC-MS/MS analysis, the chondrogenic differentiation of hBMSC/hSMSC cultured under different oxygen tensions was assessed through the aggregate diameter, chondrogenic gene expression and by histological/immunofluorescence stainings.

In all the studied conditions, our results demonstrated a notable increase in the average relative percentage of CS, the main GAG in cartilage composition, throughout MSC chondrogenic differentiation. Additionally, hypoxic culture conditions resulted in significantly different average GAG and CS disaccharide percentage compositions compared to the normoxic ones. Nevertheless, such effect was considerably more evident in hBMSC-derived chondrogenic aggregates.

In summary, the GAG profiles described here may provide new insights to predict cartilage tissue differentiation/disease states and to characterize the quality of MSC-derived cartilage tissues obtained under different oxygen tension culture conditions.

III.1. Introduction

Articular cartilage defects do not heal spontaneously due to the avascular nature of the tissue combined with the scarcity of resident stem cells. Current surgical methods such as microfracture and mosaicplasty can relieve pain to some extent but fail to generate functional and phenotypically stable hyaline-like cartilage tissue (Richter et al., 2016). Autologous chondrocyte implantation (ACI), a cell-based strategy, in which the chondrocytes are isolated form non-weight bearing areas of the articular cartilage, expanded *in vitro* and then implanted into the cartilage defect site, have failed to generate stable hyaline cartilage with long-term functionality. The limited clinical outcomes of ACI result from the fact that chondrocytes gradually lose their phenotype and undergo dedifferentiation during *in vitro* expansion (Darling and Athanasiou, 2005; Rackwitz et al., 2014).

Mesenchymal stem/stromal cells (MSCs) are a promising alternative to chondrocytes for cartilage regeneration due to their ease of isolation, higher *in vitro* expansion rates, multilineage differentiation capacity and low immunogenicity (Huang et al., 2017). MSCs have been successfully isolated from different tissues including bone marrow, adipose tissue, umbilical cord, periosteum and synovium. However, MSCs from different sources have been shown to differ considerably in chondrogenic potential. Indeed, considering cartilage regeneration, MSCs obtained from bone marrow, synovium and periosteum have been reported as superior sources for chondrogenesis (Bernardo et al., 2007; C. Y. Li et al., 2015; Tan and Hung, 2017; Yoshimura et al., 2007). Additionally, several studies have reported a superior chondrogenic ability of cells derived form human synovial joint tissues when compared with MSC derived form bone marrow or adipose tissue (Fan et al., 2009; Ogata et al., 2015; Sakaguchi et al., 2005; Shirasawa et al., 2006).

MSC chondrogenic differentiation is usually performed in high-density pellet or micromass cell culture systems to provide a 3D environment attempting to recapitulate the condensation step of endochondral bone formation during embryonic development. Previous work has suggested that micromass culture systems generate MSC-based cartilage tissues more hyaline-like and less hypertrophic when compared to pellet cultures (Zhang et al., 2010).

In vivo, articular cartilage tissue is under hypoxic conditions (1%-6% O_2 tension, compared to atmospheric air) (Zhou et al., 2004). Therefore, aiming to provide a closer mimicry of native articular cartilage niche, researchers have explored low oxygen tension conditions as a strategy to enhance MSC chondrogenic differentiation (Adesida et al., 2012; Leijten et al., 2014; Bae et al., 2018).

Glycosaminoglycans (GAGs) are linear, highly charged carbohydrates with a repeating disaccharide unit and are among the principal constituents of articular cartilage. According to

the structure and sulfation level of the repeating disaccharide, GAGs can be generally divided into four classes: heparan sulfate (HS), chondroitin sulfate (CS), keratan sulfate (KS) and hyaluronic acid (HA). GAGs play a crucial role in articular cartilage homeostasis not only by providing mechanical load resistance, but also due to their involvement in several signaling pathways regulating important biological processes such as cell adhesion, growth and differentiation (Gasimli et al., 2012; Uygun et al., 2009; Weyers and Linhardt, 2013). Indeed, changes in GAG composition and structure have been associated with different cell differentiation stages and with cartilage diseases such as osteoarthritis (Hasehira et al., 2017; Plaas et al., 1998). Therefore, due to their biological importance, GAG production is one the main outcomes evaluated to confirm chondrogenic differentiation and assess the quality of the engineered cartilage tissues produced. Nevertheless, the great majority of the GAG measurements reported were obtained using the dimethylmethylene blue (DMMB) assay and correspond to total sulfated GAG content, being unable to discriminate among the different GAG types. Moreover, only few studies have reported GAG disaccharide composition of engineered cartilage tissues using electrophoresis or high-performance liquid chromatography (HPLC) methods (Mouw et al., 2005; Wan et al., 2016). These methods lack the sensitivity and accuracy of liquid chromatography tandem mass spectrometry (LC-MS/MS), which might be critical when evaluating the low amounts usually generated in microscale culture strategies. In fact, Linhardt research group previously developed a highly sensitive and selective LC-MS/MS approach which was able to provide the GAG disaccharide composition of different types of tissues and biological samples, including urine, cell cultures, cell-derived extracellular matrices and intervertebral disc (G. Li et al., 2015; Liu et al., 2018; Silva et al., 2019; Sun et al., 2015). In addition, such method was also successfully used to identify changes in GAG and disaccharide composition after early mesoderm and endoderm lineage commitment of human embryonic stem cells (ESC) (Gasimli et al., 2014) and to study temporal changes in GAG composition during MSC differentiation towards the hepatic lineage (Mikael et al., 2019).

In this work, the chondrogenic differentiation of human bone marrow-derived MSC (hBMSC) and human synovial-derived MSC (hSMSC) under different oxygen tensions (normoxia (21% O_2) and hypoxia (5% O_2)) was evaluated by aggregate diameter measurements, RT-qPCR analysis and by histological/immunofluorescence stainings. LC-MS/MS analysis was used to identify temporal changes in GAG type and disaccharide composition during hBMSC/hSMSC chondrogenic differentiation under normoxic/hypoxic culture conditions. An overview of the general steps required for the GAG compositional analysis of the different chondrogenic aggregate samples is provided in Figure III.1.

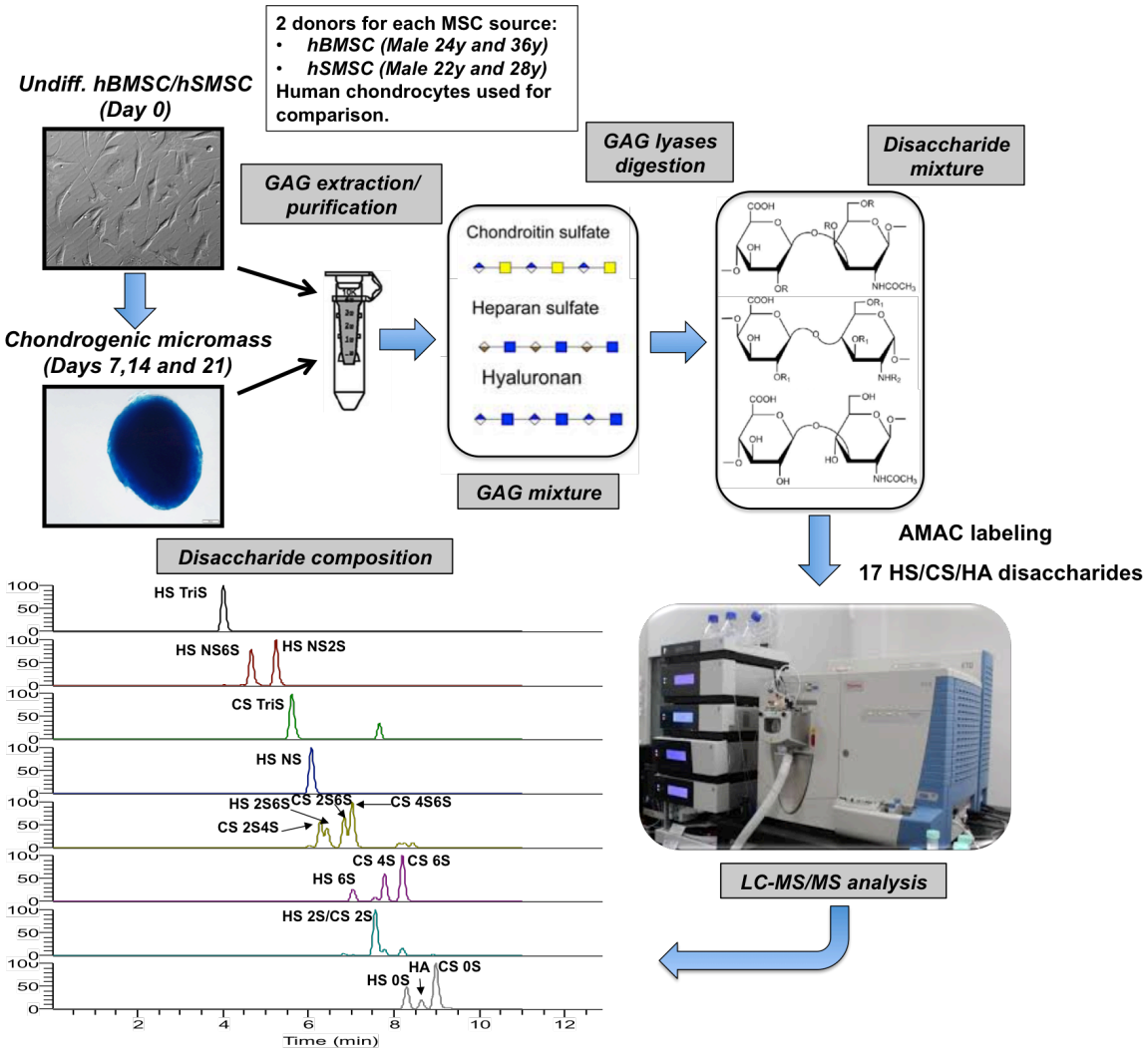

Figure III.1. Experimental scheme of the steps for sample preparation for GAG disaccharide compositional analysis. GAGs from undifferentiated cells (hBMSC, hSMSC and chondrocytes) and respective derived aggregates undergoing chondrogenic differentiation in normoxic (21% O_2) / hypoxic (5% O_2) conditions were purified and digested by enzymes (heparinases and chondroitinase ABC), originating disaccharide mixtures. The disaccharide samples were then AMAC-labeled, analyzed by LC-MS/MS and the obtained spectra were compared with the ones of external disaccharide standards.

III.2. Materials & Methods

III.2.1. Materials

Sodium cyanoborohydrade ($NaCNBH_4$), 2-aminoacridone (AMAC) and acetic acid were obtained from Sigma-Aldrich (St. Louis, MO USA). Methanol (HPLC grade), water (HPLC grade), ammonium acetate (HPLC grade) and dimethyl sulfoxide (DMSO) were purchased from Fisher Scientific (Springfield, NJ USA). Enzymes chondroitin lyase ABC from *Proteus vulgaris* and recombinant *Flavobacterial* heparinase I, II and III were expressed in *E. coli* strains in our laboratory. Unsaturated disaccharide standards of CS, HS and HA were purchased from Iduron (Manchester, UK, structures available in Table II.1 – Chapter II).

III.2.2. Human cell samples

Bone marrow aspirates (Male 36 years) were obtained from Instituto Português de Oncologia Francisco Gentil, Lisboa-Potugal and an additional sample of fresh unprocessed bone marrow sample (Male 24 years) was purchased from Lonza (Basel, Switzerland). Synovium aspirates from donors undertaking routine arthroscopic surgery with no history of joint disease (Male 22 years and male 28 years) were obtained from Centro Hospitalar de Lisboa Ocidental, E.P.E, Hospital São Francisco Xavier, Lisboa, Portugal. All human samples were obtained from healthy donors after written informed consent and with the approval of the Ethics Committee of the respective clinical institution. Human bone marrow-derived MSC (hBMSC) and human synovial-derived MSC (hSMSC) were isolated according to previously established protocols (Dos Santos et al., 2010; Santhagunam et al., 2013). Isolated hBMSC and hSMSC were cultured using Dulbecco's Modified Eagle's Medium (DMEM, Gibco, Grand Island, NY USA) supplemented with 10% fetal bovine serum (FBS, Life Technologies) and 1% antibiotics (penicillin-streptomycin, Pen-strep, Gibco) and cryopreserved in liquid/vapour nitrogen tanks until further use. Human chondrocytes (HC) purchased from CELL Applications, Inc. were cultured using high-glucose DMEM supplemented with 10% FBS, 1X MEM non-essential aminoacids (Sigma, St. Louis, MO USA), 0.2 mM L-Ascorbic acid (Sigma), 0.4 mM L-Proline (Sigma) and 1% Pen-strep. All cultures were kept at 37ºC and 5%CO_2 in a humidified atmosphere. All the experiments were performed using cells between passages 3 and 5.

III.2.3. MSC characterization

III.2.3.1. Cell morphology

Undifferentiated hBMSC and hSMSC morphology was observed under a phase contrast/fluorescence microscope (Olympus IX51 Inverted Microscope: Olympus America Inc., Melville, NY USA). For fluorescence staining, culture medium was removed and cells were washed twice with PBS, fixed with 4% PFA (Santa Cruz Biotechnology, Dallas, TX USA) for 30 min and permeabilized with 0.1% Triton X-100 (Sigma-Aldrich) for 10 min. Upon permeabilization, cells were incubated with Phalloidin-TRITC (dilution 1:250, 2 µg/mL, Sigma-Aldrich) for 45 min in the dark. Then, cells were washed twice with PBS, stained with DAPI (1.5 µg/mL, Sigma-Aldrich) for 5 min, washed again with PBS and imaged under fluorescence microscopy.

III.2.3.2. Immunophenotypic analysis

hBMSC and hSMSC were tested for the expression of specific cell surface markers previously defined as minimal criteria to identify human MSC (Dominici et al., 2006), using a panel of phycoerythrin (PE)-conjugated mouse anti-human monoclonal antibodies CD14, CD19, CD34, CD45, CD73, CD90, CD105 and HLA-DR and appropriate isotype controls (Biolegend, San Diego, CA). Thus, cells were incubated with each antibody for 15 min protected from light at room temperature and fixed with 2% PFA. Samples were analyzed by flow cytometry in a FACSCalibur™ instrument (Becton Dickinson, NJ USA) for quantification of the expression of each cell surface marker. A minimum of 10000 events was collected for each sample and the CellQuest™ software (Becton Dickinson) was used for data acquisition and analysis.

III.2.3.3. Multilineage differentiation potential

hBMSC and hSMSC capacity to differentiate towards the osteogenic, adipogenic and chondrogenic lineage was evaluated. Cells were plated on 12-well plates at 6000 cells/cm^2 and cultured with DMEM+10%FBS. When 80% confluence was reached, osteogenic and adipogenic differentiation was induced using StemPro™ Osteogenesis Differentiation Kit (Gibco™, Thermo Fisher Scientific) and StemPro™ Adipogenesis Differentiation Kit (Gibco™, Thermo Fisher Scientific), respectively. For chondrogenic differentiation, cells were concentrated to a density of 10^7 cells/mL and plated as droplets of 10 µL on ultra-low attachment 24-well culture plates (Falcon BD Biosciences, Corning, NY USA) and incubated for 1.5 h under humidified atmosphere at 37ºC and 5%CO_2 to promote aggregation. Afterwards, excess fluid was removed and differentiation was induced using the StemPro™ Chondrogenesis Differentiation Kit (Gibco™, Thermo Fisher Scientific). The differentiation protocols were conducted for 14 days and the culture medium was changed twice a week.

After 14 days of multilineage differentiation, the culture medium was removed, cells were washed with PBS, fixed in 4% PFA for 20 min at room temperature and rinsed in miliQ ultrapure water. To confirm osteogenic differentiation, the cells were incubated with a 4% (v/v) Fast Violet solution (Sigma-Aldrich) and Naphtol AS-MX Phosphate Alkaline solution (Sigma-Aldrich) for 45 min in the dark at room temperature. Afterwards, cells were washed three times with miliQ ultrapure water and once with PBS, and Von Kossa staining was performed by incubation with a 2.5% silver nitrate solution (Sigma-Aldrich) for 30 min at room temperature protected from light to assess the presence of calcium deposits. Adipogenic differentiation was evaluated by incubating the cells with a 0.3% Oil-Red-O solution (Sigma-Aldrich, in isopropanol) for 1 h at room temperature to identify lipid accumulation.

Chondrogenic differentiation was assessed by incubation of the cellular aggregates with a 1% (w/v) Alcian Blue 8GX solution (Sigma-Aldrich, in 0.1N HCl) for 1 h at room temperature to detect sulfated proteoglycans deposition. Finally, upon completion of the different staining protocols, cells were washed twice with PBS, rinsed with distilled water and imaged with a light microscope (LEICA® DMI3000B).

III.2.4. Chondrogenic differentiation of human BMSC, SMSC and chondrocytes under different oxygen tensions (normoxia-21% O_2 and hypoxia-5% O_2)

Human BMSC, SMSC and chondrocytes were harvested, concentrated and droplets of 15 µL containing 1.5 x 10^5 cells were placed in each well of an ultra-low attachment 24-well culture plates, and incubated for 1.5 h at 37ºC and 5%CO_2 to promote initial cell aggregation. Afterwards, the aggregates were submersed with chondrogenic medium consisting of high glucose DMEM (Thermo Fisher Scientific) with 100nM dexamethasone (Sigma-Aldrich), 50 µg/mL ascorbic acid 2-phosphate (Sigma-Aldrich), 40 µg/mL L-Proline (Sigma-Aldrich), 1mM sodium pyruvate (Gibco), ITS™+ Premix supplement (6.25 µg/mL bovine insulin; 6.25 µg/mL transferrin; 6.25 µg/mL selenous acid; 5.33 µg/mL linoleic acid; 1.25 µg/mL BSA, Corning), Pen-strep (100 U/mL penicillin; 100 µg/mL streptomycin) and 10 ng/mL TGF-β3 (R&D Systems) and the cultures were placed in incubators under normoxia (21% O_2) or hypoxia (5% O_2) conditions. The chondrogenic differentiation protocol was performed for 21 days and culture medium was changed twice a week.

III.2.5. Chondrogenic aggregates size measurements

At the end of the 21 days of chondrogenic differentiation, the aggregates generated from different cell sources under normoxia/hypoxia were imaged in a phase contrast microscope (Olympus IX51 Inverted Microscope). The estimation of the chondrogenic aggregates diameters was performed by measuring 30 individual aggregates per condition (one per image) using the ImageJ software (ImageJ 1.51f, National Institutes of Health, USA).

III.2.6. Histological and immunofluorescence analysis

The final chondrogenic aggregates (day 21) derived from hBMSC, hSMSC and chondrocytes cultured under normoxia/hypoxia were fixed with 4% PFA for 20 min and washed with PBS. Afterwards, the aggregates were included in Tissue-Tek® O.C.T. Compound (VWR), frozen in liquid nitrogen and stored at -80ºC. The OCT blocks were sliced into 10 µm sections using a microtome cryostat (Microm HM 505E Cryostat, GMI, MN USA)

at -20ºC and mounted in glass slides. The slides were washed twice in PBS (5 min each wash) and then washed with 0.1 M glycine (Sigma-Aldrich) solution in PBS for 10 min at room temperature to remove PFA residues. Samples were permeabilized with 0.1% Triton solution in PBS for 10 min and incubated with a blocking solution (10% FBS in TBST – 20 mM Tris-HCl pH 8.0 (Sigma-Aldrich), 150 mM NaCl (Sigma-Aldrich), 0.05% (v/v) Tween-20 (Sigma-Aldrich)) for 30 min at room temperature and dried with a tissue.

For histological evaluation of the chondrogenic aggregates, the cross-sections were incubated with a 1% (w/v) Alcian Blue solution (in 0.1N HCl) for 1 h and with a 0.1% (w/v) aqueous Safranin-O (Sigma-Aldrich) solution for 30 min to assess for the presence of GAGs. Then, the slides were washed three times with PBS, rinsed with distilled water and mounted with Mowiol mounting medium (Sigma-Aldrich). Images of the histological stainings of the chondrogenic aggregates were obtained using a light microscope (LEICA® DMI3000B).

For immunofluorescence analysis of the chondrogenic aggregates, the slides were incubated with primary antibodies (in blocking solution) for collagen II (1:200, mouse collagen II monoclonal antibody 6B3, ThermoFisher Scientific), aggrecan (1:400, mouse aggrecan monoclonal antibody BC-3, ThermoFisher Scientific) and lubricin (1:200, rabbit lubricin polyclonal antibody, ThermoFisher Scientific) overnight at 4ºC. Afterwards, the slides were washed three times with TBST (5 min each wash) and incubated with respective secondary antibodies Goat anti-mouse IgG- AlexaFluor 546 (1:500, ThermoFisher Scientific) and Goat anti-rabbit IgG- AlexaFluor 546 (1:500, ThermoFisher Scientific) for 45 min in the dark at room temperature. The slides were then washed with TBST (3 washes, 5 min each) and counterstained with DAPI for 5 min at room temperature. After washing the slides again with TBST, samples were mounted with Mowiol. Chondrogenic aggregates were examined under a confocal microscope (Zeiss LSM 710).

III.2.7. Reverse transcription and real-time quantitative PCR (RT-qPCR) analysis

Total RNA was extracted from the final chondrogenic aggregates (day 21) derived from the different cell sources under normoxia/hypoxia as well as from the undifferentiated cells (day 0) using the RNeasy Mini kit (Quiagen, Hilden, Germany) according to the manufacturer's guidelines and quantified using a Nanodrop (ND-100 Spectrophotometer, Nanodrop Technologies). cDNA was synthesized from the purified RNA using iScript™ Reverse Transcription Supermix (Bio-Rad, Hercules, CA USA) following the manufacturer's guidelines. The reaction mixtures with a total volume of 20 µL were incubated in a thermal cycler (Veriti Thermal Cycler, Applied Biosystems, CA USA) for 5 min at 25ºC, 20 min at 46ºC and 1 min at 95ºC and then were maintained at 4ºC.

The real time quantitative PCR (RT-qPCR) analysis was performed using the TaqMan® Fast Advanced Master Mix (Applied Biosystems) and StepOnePlus real-time PCR system (Applied Biosystems) according to the manufacturer's guidelines. Reactions were run in triplicate using TaqMan® Gene Expression Assays (20X) (Thermo Fisher Scientific) for human *Sox9* (Hs00165814_m1), human *ACAN* (Hs00153936_m1) and human *GAPDH* (Hs02758991_g1). The obtained CT values were normalized against the expression of housekeeping gene *GAPDH* and the analysis was performed using the $2^{-\Delta\Delta Ct}$ method. Results for *Sox9* and *ACAN* expressions in the hBMSC/hSMSC/chondrocyte-based chondrogenic aggregates cultured under normoxia/hypoxia are presented as fold-change expression levels relative to hBMSC/hSMSC/chondrocyte at day 0.

III.2.8. Compositional GAG disaccharide analysis

III.2.8.1. Sample preparation: GAG isolation, digestion and AMAC-labeling

Undifferentiated cells (day 0) and chondrogenic aggregates at different culture timepoints (days 7, 14 and 21 for hBMSC/hSMSC and day 21 for chondrocytes) for both normoxia/hypoxia were collected, treated with the BugBuster 10X Protein Extraction Reagent (Millipore Sigma, MA USA) and sonicated in a bath containing ice for aggregate dissociation. Then, samples were desalted by passing through a 3KDa molecular weight cut off (MWCO) spin column (Millipore, MA USA), and washed three times with distilled water. The casing tubes were replaced and 300 µL of digestion buffer (50 mM ammonium acetate containing 2 mM calcium chloride adjusted to pH 7.0) was added to the filter unit. Afterwards, recombinant heparin lyases I, II, III (pH optima 7.0−7.5) and recombinant chondroitin lyase ABC (10 mU each, pH optimum 7.4) were added to each sample, mixed well by pipetting and samples GAG enzymatic digestion was conducted by incubation overnight at 37°C. The enzymatic reaction was terminated by centrifugation to remove the enzymes and the filter unit was washed twice with 200 µL of distilled water. The final filtrates containing the disaccharide products were lyophilized and kept at -20°C until labeling. Samples were AMAC-labeled by adding 10 µL of 0.1M AMAC in DMSO/acetic acid (17/3, V/V) solution and by incubating at room temperature for 10 min, followed by addition of 10 µL of 1M aqueous $NaCNBH_4$ solution and incubation for 1 hour at 45°C. A mixture containing all 17 CS, HS and HA disaccharide standards prepared at a concentration of 0.5 ng/µL was similarly AMAC-labelled and used for each run as an external standard. After the AMAC-labeling reaction, the samples were centrifuged and the respective supernatants were recovered.

III.2.8.2. LC-MS/MS analysis

Disaccharide analysis was performed according to a previously published method (Sun et al., 2015). LC was performed on an Agilent 1200 LC system at 45 °C using an Agilent Poroshell 120 ECC18 (2.7 µm, 3.0 × 50 mm) column. Mobile phase A (MPA) was 50 mM ammonium acetate aqueous solution, and the mobile phase B (MPB) was methanol. The mobile phase passed through the column at a flow rate of 300 µL/min and the gradient used was the following: 0-10 min, 5-45% B; 10-10.2min, 45-100%B; 10.2-14min, 100%B; 14-22min, 100-5%B. The injection volume used for all the samples was 5 µL. A triple quadrupole mass spectrometry system equipped with an ESI source (Thermo Fisher Scientific, San Jose CA, USA) was used as a detector. The online MS analysis was performed at the Multiple Reaction Monitoring (MRM) mode with the MS parameters: negative ionization mode with a spray voltage of 3000 V, a vaporizer temperature of 300°C, and a capillary temperature of 270°C. Data analysis was performed using Thermo Xcalibur™ software (Thermo Fisher Scientific, San Jose, CA USA). The disaccharides amounts in the samples were quantified via comparison of the sample peak area to that of an external standard.

III.2.9. Statistical analysis

Results are presented as mean values ± SD from two independent donors (n=3 for each donor), unless specified differently. The statistical analysis of the LC-MS/MS data was performed using one-way ANOVA for multiple comparisons, followed by Tukey post-hoc test. Comparisons between gene expressions of the chondrogenic aggregates (from the same cell source) generated under 5% O_2 and 21% O_2 tensions were performed using the unpaired student *t* test. GraphPad Prism version 7 was used in the analysis and data was considered to be significant when p-values were less than 0.05 (95% confidence intervals, *p < 0.05).

III.3. Results

III.3.1. hBMSC and hSMSC characterization

The cell sources used in this study were characterized in terms of their morphology (Figure III.2 A), immunophenotype (Figure III.2 B) and multilineage differentiation capacity (Figure III.2 C). Both hBMSC and hSMSC presented a standard morphological MSC phenotype with a long, fibroblastic appearance with defined nuclei and cytoskeleton. Regarding the immunophenotypical characterization, for both sources, less than 2% of the

population expressed hematopoietic lineage markers CD14, CD19, CD34, CD45 and HLA-DR. Considering the positive markers (CD73, CD90 and CD105), the expression of CD73 and CD105 was above to 95% for both hBMSC and hSMSC. In the case of CD90, while more than 98% of hBMSC expressed this marker, hSMSC presented a expression of approximately 82%. In terms of the *in vitro* multilineage differentiation potential, after 2 weeks induction, both hBMSC and hSMSC were able to differentiate towards the osteogenic, adipogenic and chondrogenic lineages as confirmed by ALP/Von Kossa, Oil Red-O and Alcian Blue staining, respectively.

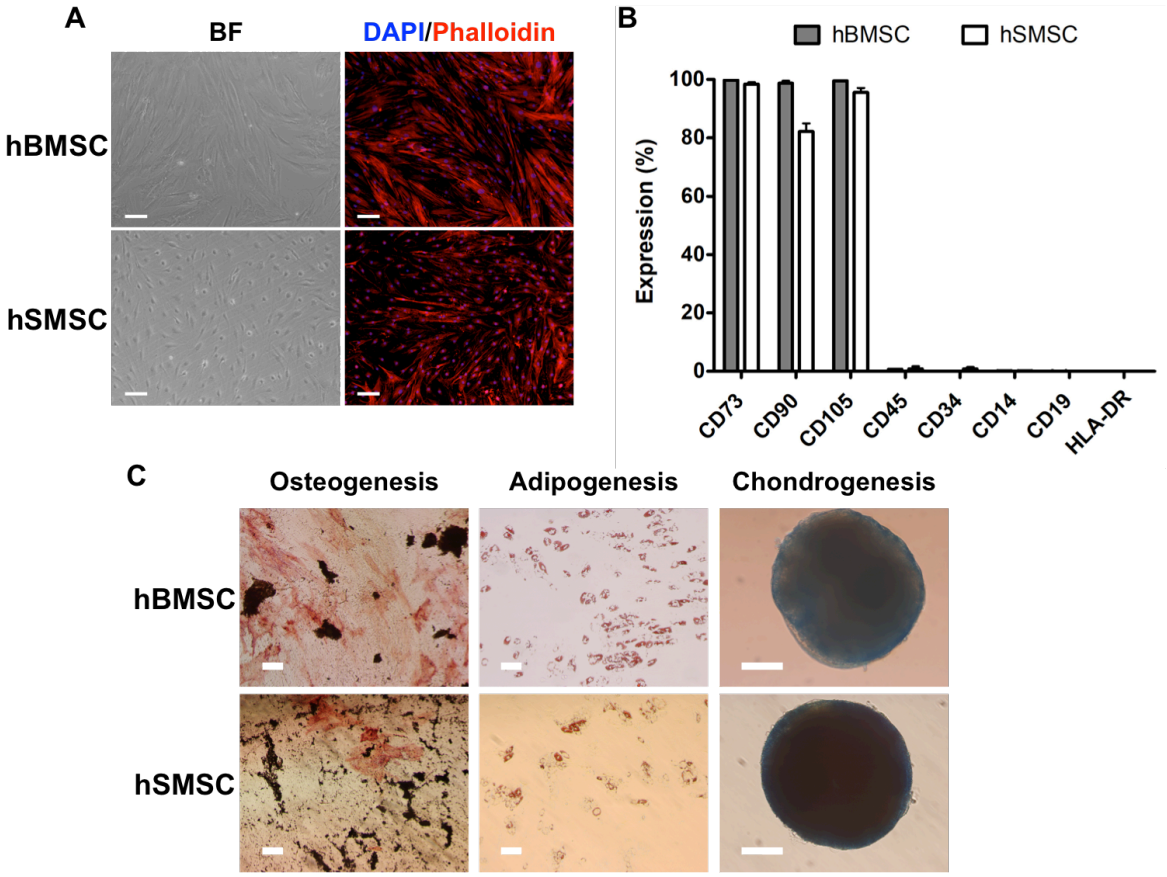

Figure III.2. Characterization of hBMSC and hSMSC used in this study. The morphology of hBMSC and hSMSC was observed by light and fluorescence microscopy after DAPI/Phalloidin staining (DAPI stains nuclei blue and Phalloidin stains actin-rich cell cytoskeleton red) (A). Immunophenotypical analysis of hBMSC and hSMSC (B). Multilineage differentiation potential of hBMSC and hSMSC assessed after 14 days under osteogenic, adipogenic and chondrogenic induction. Osteogenic differentiation was confirmed by ALP/Von Kossa staining. Adipogenesis was evaluated by staining the cells with Oil Red-O. Chondrogenic differentiation was assessed by Alcian Blue staining. Values are represented as mean ± SEM of two independent donors for each cell source. Scale bars: 100 µm.

III.3.2. Evaluation of the chondrogenic differentiation of human BMSC, SMSC and chondrocytes under normoxia (21% O_2) / hypoxia (5% O_2)

At the end of the chondrogenic differentiation protocol (day 21), the final hBMSC/hSMSC/HC-based chondrogenic aggregates generated under normoxia (21% O_2) and hypoxia (5% O_2) were evaluated in terms of typical cartilage ECM proteins/proteoglycans expression (Figure III.3), aggregate diameter (Figure III.4) and chondrogenic marker genes expression (Figure III.5).

Regardless of the cell source and the oxygen tension used, all the conditions stained positively for the presence of GAGs after Alcian Blue and Safranin-O stainings. Additionally, immunofluorescence analysis showed that all the final chondrogenic aggregates stained positive for the presence of typical cartilage ECM components collagen II, aggrecan and lubricin (Figure III.3).

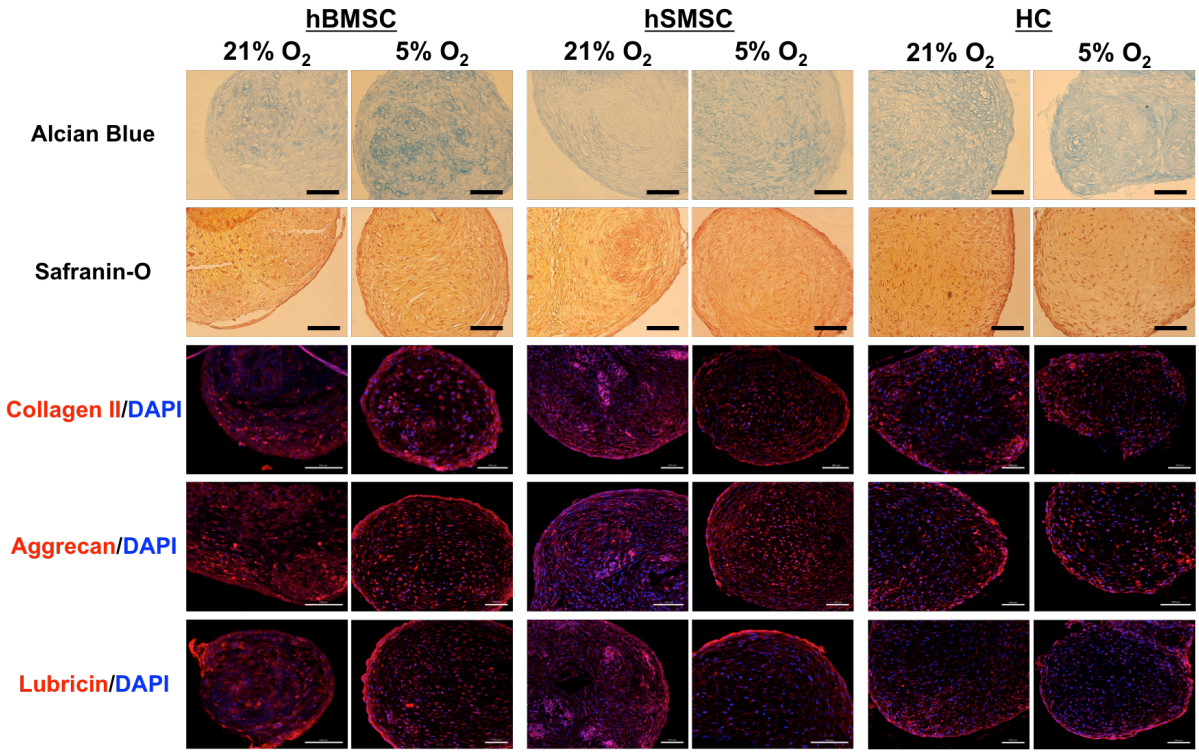

Figure III.3. Histological (Alcian Blue and Safranin-O stainings) and immunofluorescence (Collagen II, Aggrecan and Lubricin) analysis of the final (day 21) chondrogenic aggregates generated by hBMSC, hSMSC and HC under normoxia (21% O_2)/hypoxia (5% O_2). For immunofluorescence analysis, samples were counterstained with DAPI. Scale bars: 100 µm.

As it is possible to observe in Figure III.4, for all the cell sources, hypoxic cultures lead to the formation of aggregates with higher average diameters than the ones obtained under normoxia. Considering the MSC sources, within the same oxygen tension, hSMSC-derived chondrogenic aggregates showed higher average diameters that hBMSC-derived ones.

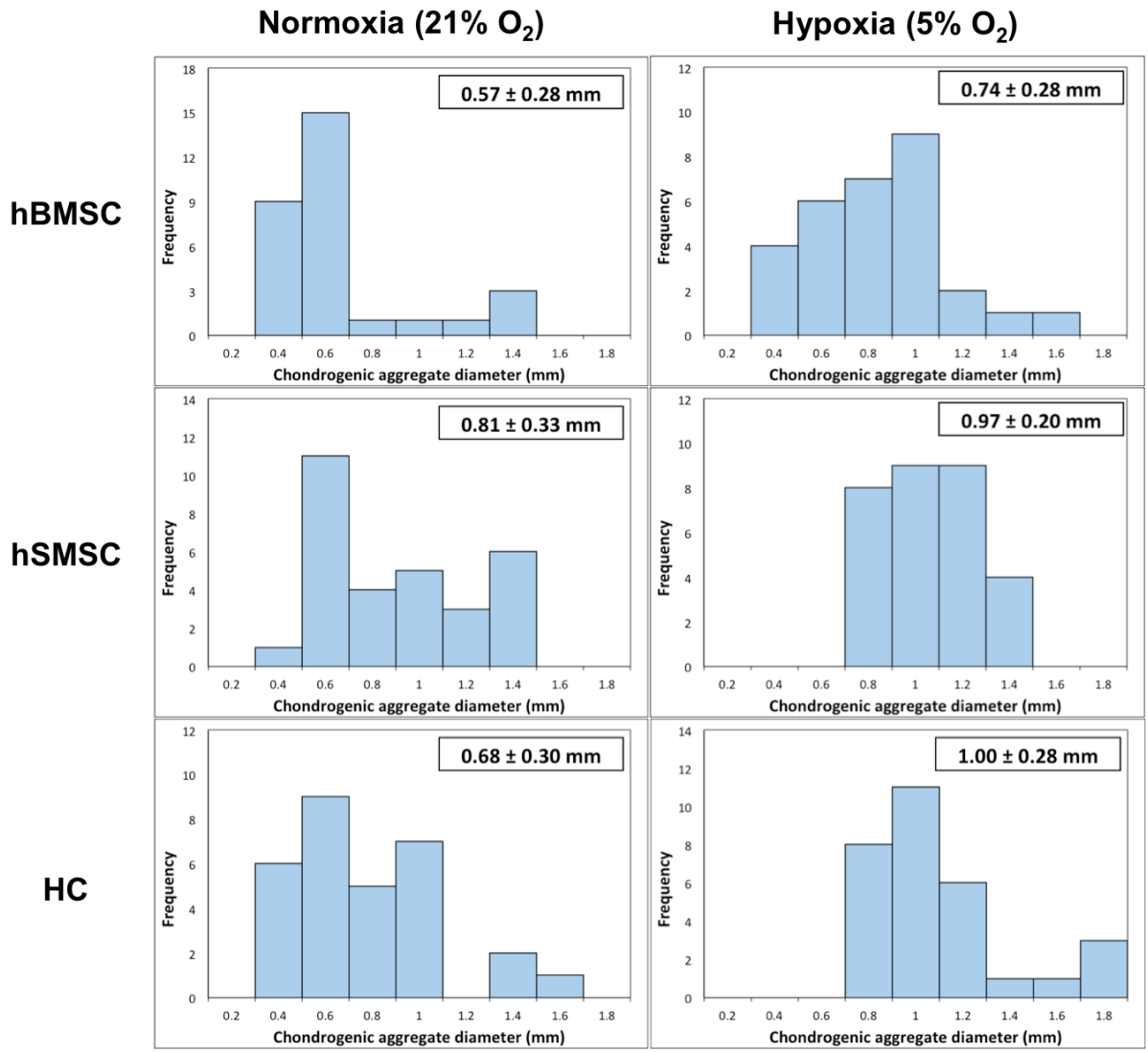

Figure III.4. Average diameter and respective distribution of the aggregates generated by hBMSC, hSMSC and HC after 21 days micromass chondrogenic cultures under normoxia (21% O_2)/hypoxia (5% O_2). Data are presented as mean ± SD, n=30 individual aggregates.

Figure III.5 shows the RT-qPCR analysis performed in the final cartilage engineered tissues generated from hBMSC, hSMSC and HC under normoxia (21% O_2) and hypoxia (5% O_2). Although all the conditions showed upregulation of *Sox9* and *ACAN* chondrogenic marker genes, tissues obtained from different MSC sources showed different responses to low oxygen tensions. While for hBMSC-derived chondrogenic aggregates, hypoxic cultures presented significantly higher *Sox9* and *ACAN* expressions than normoxic ones, an opposite trend was observed for hSMSC-derived chondrogenic aggregates. HC-derived aggregates cultured under hypoxia also showed higher gene expressions than normoxic cultures, however significant differences were only observed for *ACAN*.

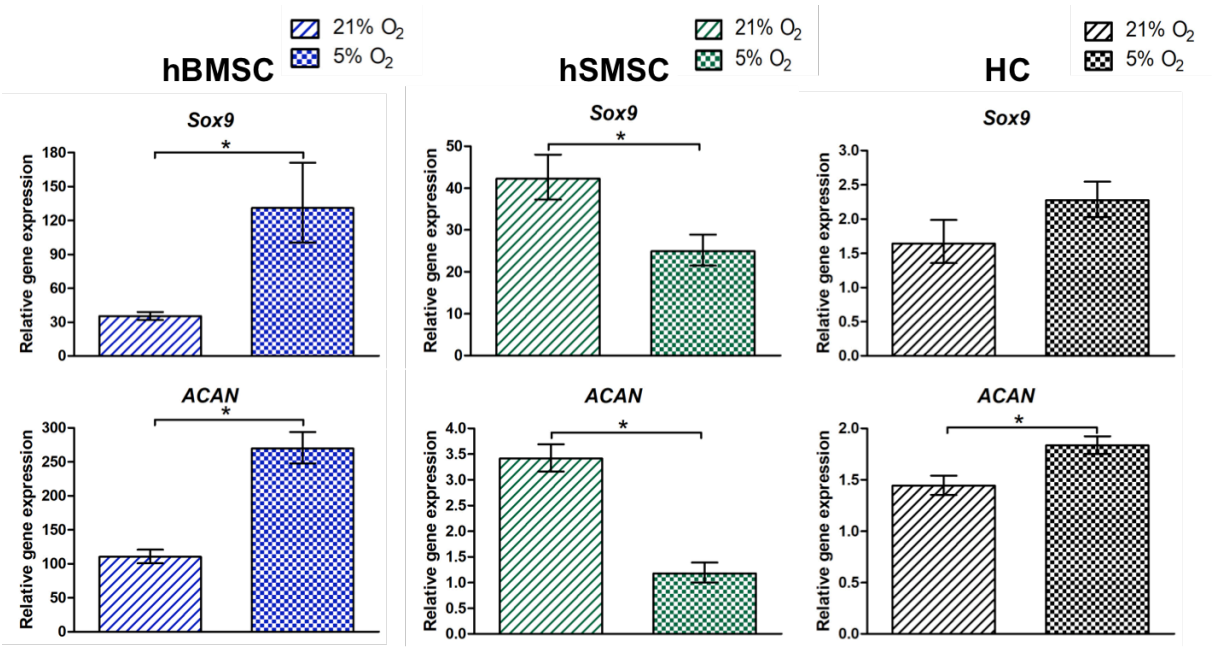

Figure III.5. RT-qPCR analysis of the final (day 21) chondrogenic aggregates generated by hBMSC, hSMSC and HC under normoxia (21% O_2)/hypoxia (5% O_2). *Sox 9* and *ACAN* gene expressions are normalized against the housekeeping gene *GAPDH* and presented as fold-change levels relative to the respective cell source (hBMSC, hSMSC and HC) at day 0. Data are presented as mean ± SD, n=3. *$p < 0.05$.

III.3.3. GAG and respective disaccharide changes during human BMSC, SMSC and chondrocyte chondrogenic differentiation under normoxia (21% O_2) / hypoxia (5% O_2)

GAG remodeling during the chondrogenic differentiation of hBMSC and hSMSC under hypoxic/normoxic culture conditions was studied using LC-MS/MS analysis. For that, samples were harvested at different timepoints during the differentiation (days 0, 7, 14 and 21) and GAGs were purified, enzymatically digested and labeled for compositional disaccharide analysis. HC-aggregates differentiated under the same conditions were used as controls. In Figure III.6 it is shown the temporal changes in the average percentage GAG composition in hBMSC/hSMSC-derived chondrogenic aggregates during the differentiation. Significantly distinct GAG average compositions were observed among the different cell sources. In their undifferentiated state (day 0), hBMSC were mainly composed by HA (74%, of total GAG content) with lower percentages of CS (14%) and HS (12%). In contrast, the main GAG component in undifferentiated hSMSC was CS (55%) with lower average percentages of HA (23%) and HS (22%), which was more similar to HC average GAG composition (CS: 58%, HS: 33% and HA: 9%) than hBMSC. During chondrogenic differentiation, for all the conditions tested, it is possible to observe an increase in CS average percentages and corresponding decrease in average percentages of HS and HA overtime. Hypoxia conditions appeared to favor significantly increased CS average

percentages compared to normoxia in hBMSC-derived chondrogenic aggregates. However, the same trend was not observed for the cartilage tissues derived from other cell sources. In fact, at the end of the differentiation protocol (day 21), hBMSC-derived chondrogenic aggregates obtained under hypoxic conditions showed significantly higher CS and reduced HA, HS average percentages than the ones generated at normoxic conditions (CS: 91%, HA: 8% and HS: 1% at hypoxia *vs.* CS: 59%, HA: 30% and HS: 11% at normoxia). In contrast, while the GAG composition for hSMSC-derived cartilage tissues obtained under hypoxia was 71% CS, 25% HA and 4% HS, tissues generated under normoxia showed a GAG composition of 86% CS, 9% HA and 5% HS. In addition, HC-derived cartilage tissues were mainly composed by CS with higher average percentages than the ones observed for the other cell sources (CS: 95% at hypoxia and 94% at normoxia) and no significant differences in GAG composition were noticed between HC-aggregates generated under hypoxia/normoxia.

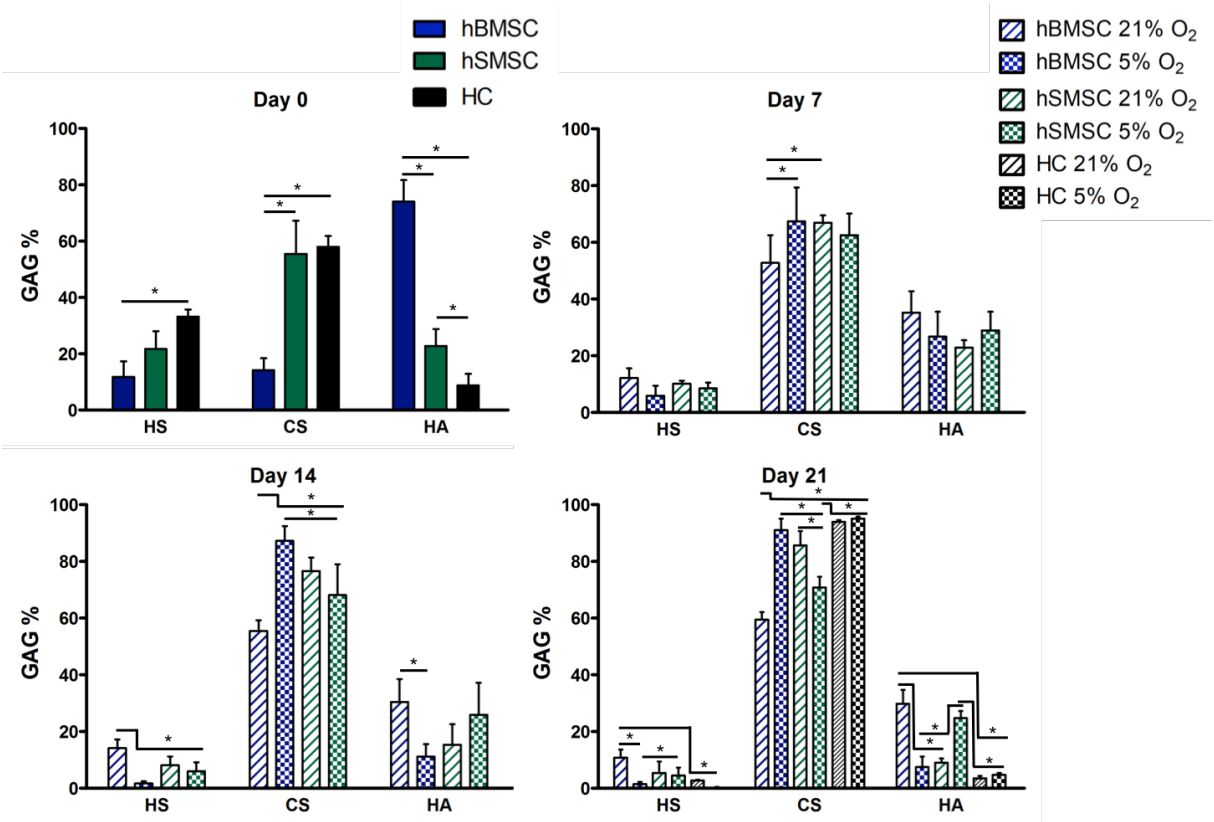

Figure III.6. Average percentage GAG composition of undifferentiated cells (day 0) and during chondrogenic differentiation (days 7, 14 and 21) of hBMSC and hSMSC under normoxic (21% O_2)/hypoxic (5% O_2) conditions. HC were used for comparison at days 0 and 21. Data are presented as mean ± SD of three replicates for each donor (n=6) for hBMSC and hSMSC and n=3 for HC. *p < 0.05.

The average percentage HS and CS disaccharide compositional changes during the chondrogenic differentiation of hBMSC, hSMSC and HC under hypoxia/normoxia are presented in Figure III.7 and Figure III.8, respectively. Regarding HS disaccharides, all the samples were mainly composed by 0S, with lower percentages of NS and NS2S. Generally, during chondrogenic differentiation, the average percentages for the different HS disaccharides were nearly maintained and changes resulting from culture under different oxygen tensions were not noticed. However, some significant differences were observed in the HS composition of the different cell sources, mainly at the end of the protocol (day 21). At day 21, HC-derived aggregates showed significantly higher average percentages of 0S than the hSMSC-derived ones, contrarily to what was observed for cells in the undifferentiated state (day 0).

In Figure III.8 it is possible to observe that, for all the conditions, CS was mainly composed by 4S and 6S with lower percentages of 0S. Significant differences in 4S and 6S average percentages were observed between the tissues generated from different cell sources and also as a result of culture under different oxygen tensions. While in their undifferentiated state (day 0), all cell types presented higher average percentages for 4S than 6S, after 21 days of chondrogenic differentiation, the obtained tissues (with the exception of hBMSC-derived cartilage) showed higher amounts of 6S than 4S. Moreover, for tissues derived from all cell sources, this increase in 6S average percentages (and subsequent decrease in 4S) was clearly favored by hypoxia. Noteworthy, HC-derived cartilage tissues presented significantly higher 6S (and lower 4S) average percentages than the tissues obtained from both MSC sources.

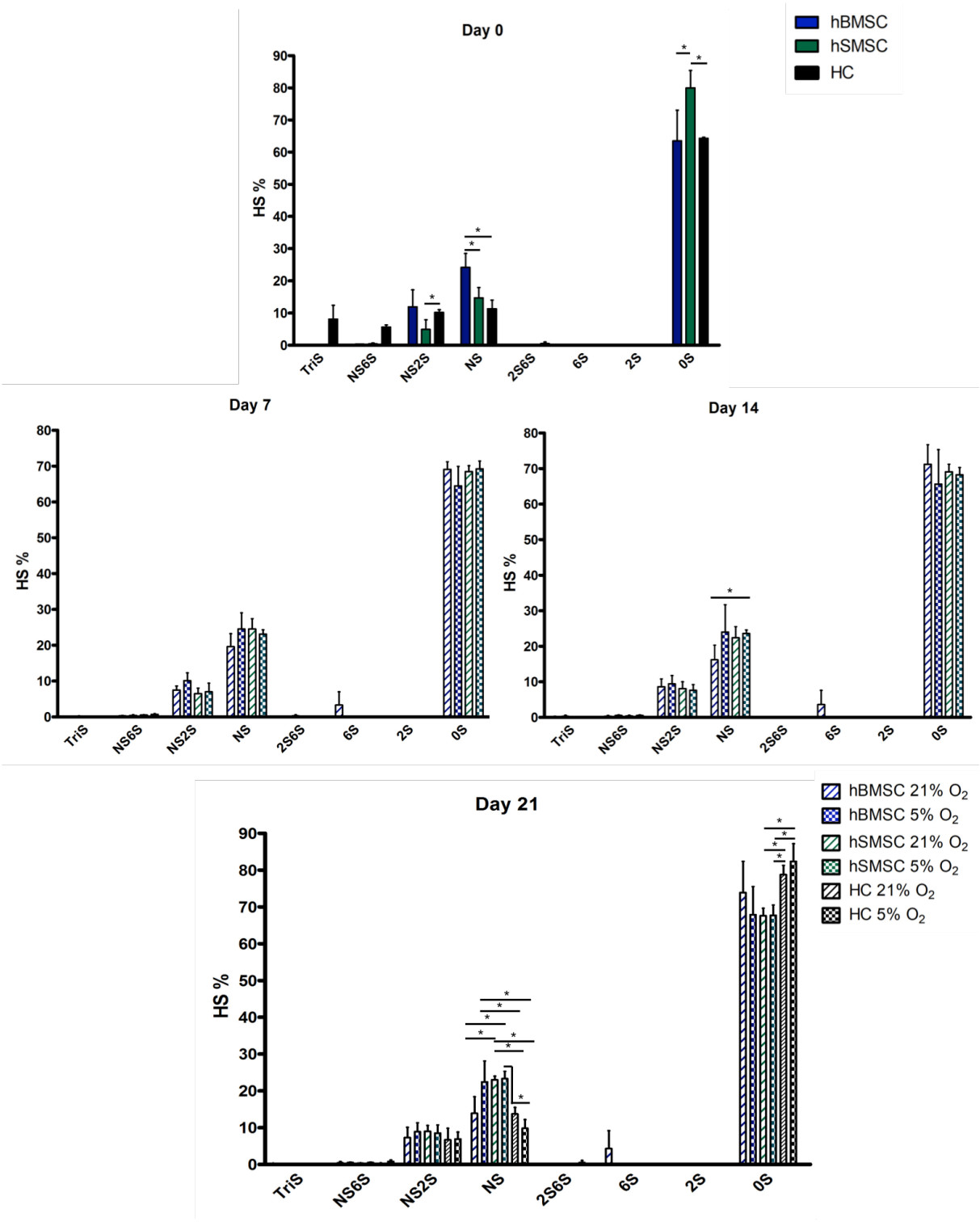

Figure III.7. Average percentage HS disaccharide composition of undifferentiated cells (day 0) and during chondrogenic differentiation (days 7, 14 and 21) of hBMSC and hSMSC under normoxic (21% O_2)/hypoxic (5% O_2) conditions. HC were used for comparison at days 0 and 21. Data are presented as mean ± SD of three replicates for each donor (n=6) for hBMSC and hSMSC and n=3 for HC. *p < 0.05.

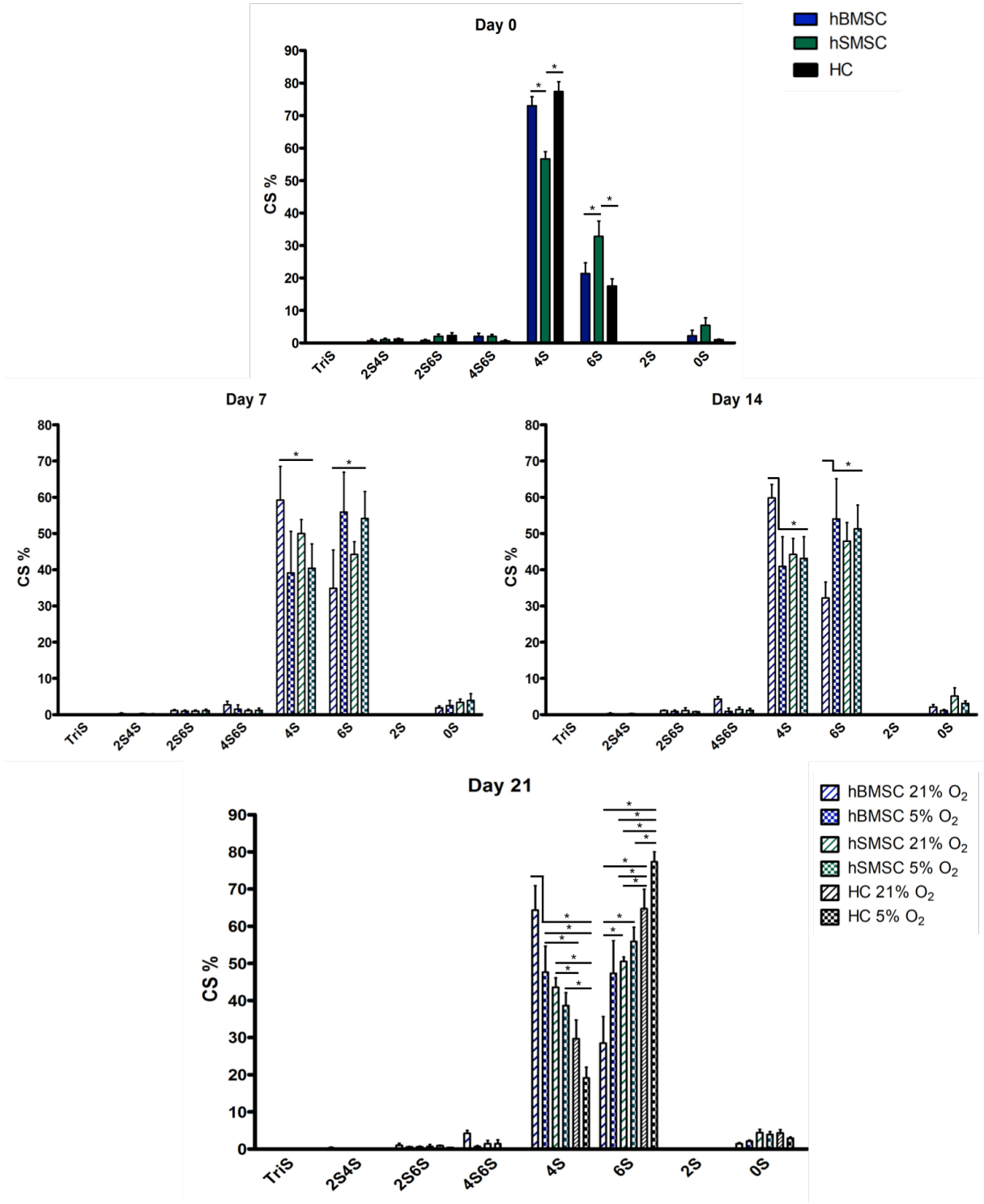

Figure III.8. Average percentage CS disaccharide composition of undifferentiated cells (day 0) and during chondrogenic differentiation (days 7, 14 and 21) of hBMSC and hSMSC under normoxic (21% O_2)/hypoxic (5% O_2) conditions. HC were used for comparison at days 0 and 21. Data are presented as mean ± SD of three replicates for each donor (n=6) for hBMSC and hSMSC and n=3 for HC. *p < 0.05.

III.4. Discussion

To the best of our knowledge, this study represents one of the first reports of the use of highly sensitive and selective LC-MS/MS methods to evaluate the GAG remodeling during MSC chondrogenic differentiation. Herein, we compared the GAG composition of the tissues generated from two different human MSC sources (hBMSC and hSMSC) when cultured under different oxygen tension conditions (normoxia-21% O_2 and hypoxia-5% O_2). HC were cultured under the same conditions as the other cell sources and used throughout this study as control samples. Both sources used in this work were characterized and proved to be compliant with the criteria defined by Dominici *et al* for MSC identification (Dominici et al., 2006). Regarding the immunophenotypic analysis, hSMSC showed slightly decreased expression of CD90 (<95%). However, since the panel of markers proposed by Dominici *et al* focused on the identification of hBMSC, there are no specific defined sets of markers to identify MSC isolated from other sources, which might have its own intrinsic levels of markers expression. Moreover, a decreased CD90 expression in hSMSC analyzed by flow cytometry was previously described in other studies (Ferro et al., 2019; Nagase et al., 2008).

The chondrogenic aggregates derived from hSMSC presented higher average diameters that the ones derived from hBMSC, regardless of the oxygen tension used (1.4-fold in 21% O_2 and 1.3-fold in 5% O_2). In accordance with our results, Ogata and colleagues obtained MSC-derived tissues with the same range of millimeter scale diameters and showed that hSMSC-derived tissues presented diameters 1.2-fold larger than hBMSC-derived tissues (Ogata et al., 2015). For all the cell sources, the chondrogenic aggregates produced under hypoxia showed higher diameters (1.3-fold for hBMSC, 1.1-fold for hSMSC and 1.5-fold for HC) than the ones generated at atmospheric oxygen tension. This hypoxia-induced increase in aggregate size was also reported for hBMSC-derived micropellet tissues produced under 2% O_2 (Markway et al., 2010). However, in contrast to what we showed, Bae and colleagues did not observed any considerable differences between the diameter of the hSMSC-derived pellets obtained under 21% O_2 and 5% O_2 (Bae et al., 2018).

RT-qPCR results showed increased *ACAN* and *Sox9* expressions for hBMSC- and HC-derived cartilage tissues when cultured under hypoxia, which is concordant with previous studies (Lafont et al., 2008; Leijten et al., 2014; Markway et al., 2010). In contrast with the other cell sources and with the reported by Bae and colleagues for hSMSC-derived pellets, the final hSMSC-derived cartilage tissues obtained under hypoxia showed lower expressions of *ACAN* and *Sox9* than the ones generated at normoxic conditions (Bae et al., 2018). Nevertheless, contrarily to hBMSC and HC, the effect of low oxygen-cultures in hSMSC chondrogenesis is not fully characterized yet as only very few studies have addressed this issue.

LC-MS/MS analysis revealed significant changes in GAG and disaccharide composition during hBMSC, hSMSC and HC chondrogenic differentiation under normoxic/hypoxic conditions. Undifferentiated hSMSC presented a GAG composition profile much more similar to HC than hBMSC. This might be related with the fact that hSMSC are described as more prone for chondrocyte differentiation than hBMSC. In fact, it was previously shown that the gene expression profiles of hSMSC and chondrocytes are closer to each other than those of extra-articular tissue-derived MSC including hBMSC (Segawa et al., 2009). As the most predominant GAG in articular cartilage is CS, variations in CS relative amounts might provide insights about the differentiation state of the MSC-derived tissues produced. In our analysis, we observed an increase in the CS average percentages during the chondrogenic differentiation of both hBMSC and hSMSC. Additionally, we observed that hypoxia affected differently the GAG remodeling of hBMSC and hSMSC. While for hBMSC-derived cartilage tissues, hypoxia resulted in higher average percentages of CS than normoxia, an opposite trend was observed for hSMSC-derived cartilage tissues. In fact, these different hypoxia-induced changes in CS composition of the tissues generated by hBMSC and hSMSC are coherent and might be related with the trends observed for *ACAN* gene expression.

The GAG content of HC-derived cartilage tissues was mainly composed by CS (95% at 5% O_2 and 94% at 21% O_2) and was not significantly affected by oxygen tension. These percentages are similar to the values reported by Osago *et al* (ranging from 95.2 - 96.3%, depending on the tissue digestion method used) for the total CS composition of porcine articular cartilage analyzed by LC-MS/MS (Osago et al., 2018). The lower CS average percentages observed for the MSC-derived cartilage tissues might suggest early differentiation states. However, with proper precautions in the comparison resulting from the species difference, the CS percentage values observed for hBMSC-derived cartilage tissues at 5% O_2 (91%) and hSMSC-derived cartilage tissues at 21% O_2 (86%) are relatively close to the ones verified for HC-derived cartilage tissues.

The disaccharide composition of CS in articular cartilage, particularly the 6S/4S ratio is known to vary with age and degeneration of the tissue (Lauder et al., 2001). In fact, while during embryonic development CS chains are exclusively 6S, they change to be equally composed by 4S and 6S from fetal development to adolescence, and composed by more 6S than 4S in adult cartilage (Hitchcock et al., 2008; Sharma et al., 2017). Additionally, osteoarthritic cartilage has been shown to consist primarily of 6S (Hitchcock et al., 2007). Therefore, changes in the sulfation patterns, namely the relations between 6S and 4S percentages observed during hBMSC/hSMSC chondrogenic differentiation could provide valuable insights about the maturation level of the tissues generated. With the exception of hBMSC-derived cartilage tissue at 21% O_2, all the other samples showed higher 6S/lower 4S percentages (higher 6S/4S ratio) in relation to the respective cell source at day 0. HC-

derived cartilage tissues presented higher 6S/4S ratios than MSC-derived tissues, suggesting a higher tissue maturation level. Additionally, hypoxia demonstrated to have a significant effect in the sulfation pattern of the final tissues, as for all the cell sources, tissues produced under 5% O_2 presented higher 6S/4S ratios than the ones generated at 21% O_2. These findings are concordant with the studies reporting that hypoxia enhance MSC chondrogenesis towards more mature cartilage tissues (Leijten et al., 2014). Concerning cartilage regeneration strategies, besides oxygen tension and cell source, the scaffold material has also been shown to affect the disaccharide composition of the cartilage tissue produced (Mouw et al., 2005; Wang et al., 2010).

In summary, we used a highly sensitive LC-MS/MS method to provide a novel analysis of the GAG remodeling during MSC chondrogenesis and assess how it varies with the MSC source and oxygen tension culture conditions. However, some limitations are important to highlight. This method was based on disaccharide analysis through the use of chondroitinase ABC and heparinases, so, it could only detect CS, HS and HA. Therefore, additional methodological developments should be pursued in order to allow for the quantification of KS, which is known to be present in articular cartilage. As this method do not assess core proteins, it would be interesting to perform this analysis in combination with a proteomics approach in order to provide better information about the composition and functionality of the final *in vitro* produced tissues. A detailed analysis of the GAG remodeling during chondrogenesis is important not only to better understand the mechanisms of cartilage development and disease, but also to provide new insights for improved cartilage regeneration strategies and new methods to characterize the quality of the tissue substitutes produced.

III.5. References

Adesida, A.B., Mulet-Sierra, A., Jomha, N.M., (2012). Hypoxia mediated isolation and expansion enhances the chondrogenic capacity of bone marrow mesenchymal stromal cells. Stem Cell Res. Ther. 3, 9.

Bae, H.C., Park, H.J., Wang, S.Y., Yang, H.R., Lee, M.C., Han, H.-S., (2018). Hypoxic condition enhances chondrogenesis in synovium-derived mesenchymal stem cells. Biomater. Res. 22, 1–8.

Bernardo, M.E., Emons, J.A.M., Karperien, M., Nauta, A.J., Willemze, R., Roelofs, H., Romeo, S., Marchini, A., Rappold, G.A., Vukicevic, S., Locatelli, F., Fibbe, W.E., (2007). Human mesenchymal stem cells derived from bone marrow display a better chondrogenic differentiation compared with other sources. Connect. Tissue Res. 48, 132–140.

Darling, E.M., Athanasiou, K.A., (2005). Rapid phenotypic changes in passaged articular chondrocyte subpopulations. J. Orthop. Res. 23, 425–432.

Dominici, M., Le Blanc, K., Mueller, I., Slaper-Cortenbach, I., Marini, F., Krause, D., Deans, R., Keating, A., Prockop, D., Horwitz, E., (2006). Minimal criteria for defining multipotent mesenchymal stromal cells. The International Society for Cellular Therapy position statement. Cytotherapy 8, 315–317.

Dos Santos, F., Andrade, P.Z., Boura, J.S., Abecasis, M.M., da Silva, C.L., Cabral, J.M.S., (2010). Ex vivo expansion of human mesenchymal stem cells: a more effective cell proliferation kinetics and metabolism under hypoxia. J. Cell. Physiol. 223, 27–35.

Fan, J., Varshney, R.R., Ren, L., Cai, D., Wang, D.A., (2009). Synovium-derived mesenchymal stem cells: a new cell source for musculoskeletal regeneration. Tissue Eng. Part B. Rev. 15, 75–86.

Ferro, T., Santhagunam, A., Madeira, C., Salgueiro, J.B., da Silva, C.L., Cabral, J.M.S., (2019). Successful isolation and ex vivo expansion of human mesenchymal stem/stromal cells obtained from different synovial tissue-derived (biopsy) samples. J. Cell. Physiol. 234, 3973–3984.

Gasimli, L., Hickey, A.M., Yang, B., Li, G., Dela Rosa, M., Nairn, A. V., Kulik, M.J., Dordick, J.S., Moremen, K.W., Dalton, S., Linhardt, R.J., (2014). Changes in glycosaminoglycan structure on differentiation of human embryonic stem cells towards mesoderm and endoderm lineages. Biochim. Biophys. Acta - Gen. Subj. 1840, 1993–2003.

Gasimli, L., Linhardt, R.J., Dordick, J.S., (2012). Proteoglycans in stem cells. Biotechnol. Appl. Biochem. 59, 65–76.

Hasehira, K., Hirabayashi, J., Tateno, H., (2017). Structural and quantitative evidence of α2–6-sialylated N-glycans as markers of the differentiation potential of human mesenchymal stem cells. Glycoconj. J. 34, 797–806.

Hitchcock, A.M., Yates, K.E., Costello, C.E., Zaia, J., (2008). Comparative glycomics of connective tissue glycosaminoglycans. Proteomics 8, 1384–1397.

Hitchcock, A.M., Yates, K.E., Shortkroff, S., Costello, C.E., Zaia, J., (2007). Optimized extraction of glycosaminoglycans from normal and osteoarthritic cartilage for glycomics profiling. Glycobiology 17, 25–35.

Huang, Y.Z., Xie, H.Q., Silini, A., Parolini, O., Zhang, Y., Deng, L., Huang, Y.C., (2017). Mesenchymal Stem/Progenitor Cells Derived from Articular Cartilage, Synovial Membrane and Synovial Fluid for Cartilage Regeneration: Current Status and Future Perspectives. Stem Cell Rev. Reports 13, 575–586.

Lafont, J.E., Talma, S., Hopfgarten, C., Murphy, C.L., (2008). Hypoxia promotes the differentiated human articular chondrocyte phenotype through SOX9-dependent and -independent pathways. J. Biol. Chem. 283, 4778–4786.

Lauder, R.M., Huckerby, T.N., Brown, G.M., Bayliss, M.T., Nieduszynski, I.A., (2001). Age-related changes in the sulphation of the chondroitin sulphate linkage region from human articular cartilage aggrecan. Biochem. J. 358, 523–528.

Leijten, J., Georgi, N., Moreira Teixeira, L., van Blitterswijk, C.A., Post, J.N., Karperien, M., (2014). Metabolic programming of mesenchymal stromal cells by oxygen tension directs chondrogenic cell fate. Proc. Natl. Acad. Sci. 111, 13954–13959.

Li, C.Y., Wu, X.Y., Tong, J.B., Yang, X.X., Zhao, J.L., Zheng, Q.F., Zhao, G. Bin, Ma, Z.J., (2015). Comparative analysis of human mesenchymal stem cells from bone marrow and adipose tissue under xeno-free conditions for cell therapy. Stem Cell Res. Ther. 6, 55.

Li, G., Li, L., Tian, F., Zhang, L., Xue, C., Linhardt, R.J., (2015). Glycosaminoglycanomics of Cultured Cells using a Rapid and Sensitive LC-MS/MS Approach. ACS Chem. Biol. 10, 1303–1310.

Liu, X., Krishnamoorthy, D., Lin, L., Xue, P., Zhang, F., Chi, L., Linhardt, R.J., Iatridis, J.C., (2018). A method for characterising human intervertebral disc glycosaminoglycan disaccharides using liquid chromatography-mass spectrometry with multiple reaction monitoring. Eur. Cell. Mater. 35, 117–131.

Markway, B.D., Tan, G.K., Brooke, G., Hudson, J.E., Cooper-White, J.J., Doran, M.R., (2010). Enhanced chondrogenic differentiation of human bone marrow-derived mesenchymal stem cells in low oxygen environment micropellet cultures. Cell Transplant. 19, 29–42.

Mikael, P.E., Willard, C., Koyee, A., Barlao, C.-G., Liu, X., Han, X., Ouyang, Y., Xia, K., Linhardt, R.J., Dordick, J.S., (2019). Remodeling of Glycosaminoglycans During Differentiation of Adult Human Bone Mesenchymal Stromal Cells Toward Hepatocytes. Stem Cells Dev. 28, 278–289.

Mouw, J.K., Case, N.D., Guldberg, R.E., Plaas, A.H.K., Levenston, M.E., (2005). Variations in matrix composition and GAG fine structure among scaffolds for cartilage tissue engineering. Osteoarthr. Cartil. 13, 828–836.

Nagase, T., Muneta, T., Ju, Y.J., Hara, K., Morito, T., Koga, H., Nimura, A., Mochizuki, T., Sekiya, I., (2008). Analysis of the chondrogenic potential of human synovial stem cells according to harvest site and culture parameters in knees with medial compartment osteoarthritis. Arthritis Rheum. 58, 1389–1398.

Ogata, Y., Mabuchi, Y., Yoshida, M., Suto, E.G., Suzuki, N., Muneta, T., Sekiya, I., Akazawa, C., (2015). Purified human synovium mesenchymal stem cells as a good resource for cartilage regeneration. PLoS One 10, e0129096.

Osago, H., Kobayashi-Miura, M., Hamasaki, Y., Hara, N., Hiyoshi, M., Tsuchiya, M., (2018). Complete solubilization of cartilage using the heat-stable protease thermolysin for comprehensive GAG analysis. Anal. Biochem. 548, 115–118.

Plaas, A.H.K., West, L.A., Wong-Palms, S., Nelson, F.R.T., (1998). Glycosaminoglycan sulfation in human osteoarthritis: Disease-related alterations at the non-reducing termini of chondroitin and dermatan sulfate. J. Biol. Chem. 273, 12642–12649.

Rackwitz, L., Djouad, F., Janjanin, S., Nöth, U., Tuan, R.S., (2014). Functional cartilage repair capacity of de-differentiated, chondrocyte- and mesenchymal stem cell-laden hydrogels in vitro. Osteoarthr. Cartil. 22, 1148–1157.

Richter, D.L., Schenck, R.C., Wascher, D.C., Treme, G., (2016). Knee Articular Cartilage Repair and Restoration Techniques: A Review of the Literature. Sports Health 8, 153–160.

Sakaguchi, Y., Sekiya, I., Yagishita, K., Muneta, T., (2005). Comparison of human stem cells derived from various mesenchymal tissues: Superiority of synovium as a cell source. Arthritis Rheum. 52, 2521–2529.

Santhagunam, A., Dos Santos, F., Madeira, C., Salgueiro, J.B., Cabral, J.M.S.,(2013). Isolation and ex vivo expansion of synovial mesenchymal stromal cells for cartilage repair. Cytotherapy 16, 440–453.

Segawa, Y., Muneta, T., Makino, H., Nimura, A., Mochizuki, T., Ju, Y.J., Ezura, Y., Umezawa, A., Sekiya, I., (2009). Mesenchymal stem cells derived from synovium, meniscus, anterior cruciate ligament, and articular chondrocytes share similar gene expression profiles. J. Orthop. Res. 27, 435–441.

Sharma, A., Rees, D., Roberts, S., Kuiper, N.J., (2017). A case study: Glycosaminoglycan profiles of autologous chondrocyte implantation (ACI) tissue improve as the tissue matures. Knee 24, 149–157.

Shirasawa, S., Sekiya, I., Sakaguchi, Y., Yagishita, K., Ichinose, S., Muneta, T., (2006). In vitro chondrogenesis of human synovium-derived mesenchymal stem cells: Optimal condition and comparison with bone marrow-derived cells. J. Cell. Biochem. 97, 84–97.

Silva, J.C., Carvalho, M.S., Han, X., Xia, K., Mikael, P.E., Cabral, J.M.S., Ferreira, F.C., Linhardt, R.J., (2019). Compositional and structural analysis of glycosaminoglycans in cell-derived extracellular matrices. Glycoconj. J. 36, 141–154.

Sun, X., Li, L., Overdier, K.H., Ammons, L.A., Douglas, I.S., Burlew, C.C., Zhang, F., Schmidt, E.P., Chi, L., Linhardt, R.J., (2015). Analysis of Total Human Urinary Glycosaminoglycan Disaccharides by Liquid Chromatography-Tandem Mass Spectrometry. Anal. Chem. 87, 6220–6227.

Tan, A.R., Hung, C.T., (2017). Concise review: Mesenchymal stem cells for functional cartilage tissue engineering: Taking cues from chondrocyte-based constructs. Stem Cells Transl. Med. 6, 1295–1303.

Uygun, B.E., Stojsih, S.E., Matthew, H.W.T., (2009). Effects of immobilized glycosaminoglycans on the proliferation and differentiation of mesenchymal stem cells. Tissue Eng. Part A 15, 3499–3512.

Wan, S., Borland, S., Richardson, S.M., Merry, C.L.R., Saiani, A., Gough, J.E., (2016). Self-assembling peptide hydrogel for intervertebral disc tissue engineering. Acta Biomater. 46, 29–40.

Wang, Q.G., Hughes, N., Cartmell, S.H., Kuiper, N.J., (2010). The composition of hydrogels for cartilage tissue engineering can influence glycosaminoglycan profiles. Eur. Cells Mater. 19, 86–95.

Weyers, A., Linhardt, R.J., (2013). Neoproteoglycans in tissue engineering. FEBS J. 280, 2511–2522.

Yoshimura, H., Muneta, T., Nimura, A., Yokoyama, A., Koga, H., Sekiya, I., (2007). Comparison of rat mesenchymal stem cells derived from bone marrow, synovium, periosteum, adipose tissue, and muscle. Cell Tissue Res. 327, 449–462.

Zhang, L., Su, P., Xu, C., Yang, J., Yu, W., Huang, D., (2010). Chondrogenic differentiation of human mesenchymal stem cells: A comparison between micromass and pellet culture systems. Biotechnol. Lett. 32, 1339–1346.

Zhou, S., Cui, Z., Urban, J.P.G., (2004). Factors influencing the oxygen concentration gradient from the synovial surface of articular cartilage to the cartilage-bone interface: A modeling study. Arthritis Rheum. 50, 3915–3924.

Chapter IV

EFFECTS OF GAG SUPPLEMENTATION IN THE CHONDROGENIC DIFFERENTIATION OF HUMAN BONE MARROW/SYNOVIAL-DERIVED MSC ON 3D POLY (ε-CAPROLACTONE) SCAFFOLDS

CHAPTER IV – Effects of GAG supplementation in the chondrogenic differentiation of human bone marrow/synovial-derived MSC on poly (ε-caprolactone) scaffolds

Outline

The lack of effective and long-term treatments for articular cartilage defects, resulting from injury or highly prevalent and debilitating diseases (such as osteoarthritis), has increased the interest for tissue engineering strategies as a potential alternative to address this unmet clinical need. Such approaches, combining cells, 3D biomaterial matrices, and external biochemical/physical cues, hold the promise for generating fully functional cartilage tissue.

Herein, this study aims at evaluating the use of the major cartilage GAGs, chondroitin sulfate (CS) and hyaluronic acid (HA), as external biochemical cues to promote the chondrogenic differentiation of human bone marrow- and synovium-derived mesenchymal stem/stromal cells (hBMSC and hSMSC) on poly (ε-caprolactone) (PCL) scaffolds. Custom-made 3D porous and highly interconnected PCL scaffolds were fabricated by 3D-extrusion. Culture conditions including chondrogenic medium and oxygen tension, were selected based on the cell metabolic activity and GAG production on such scaffolds. hBMSC/hSMSC were cultured on PCL scaffolds with non-/CS-/HA-supplemented chondrogenic medium for 21 days and no significant effects in cellularity resulting from GAG supplementation were observed. All conditions stained positively for cartilage ECM production, however, significantly higher secreted GAG amounts were obtained in both hBMSC-/hSMSC-derived constructs when cultured under HA-supplementation. RT-qPCR analysis suggests that both CS and HA supplementation favored the chondrogenic differentiation of hBMSC and hSMSC in PCL scaffolds, as demonstrated by the upregulation of chondrogenic markers. Remarkably, in contrast to tissues generated using hBMSCs, the hSMSC-based constructs showed decreased expression of hypertrophic marker *COL X*. Histology/immunohistochemical analysis confirmed the presence of typical hyaline cartilage components (GAGs, collagen II and aggrecan) under all the conditions. Additionally, transmission electron microscopy (TEM) analysis of the final tissue constructs revealed the ultrastructure of differentiated MSC and of a dense extracellular matrix (ECM) containing collagen fibers.

Overall, these results highlight the potential of integrating GAG supplementation in tissue engineering strategies to promote MSC chondrogenic differentiation towards the fabrication of improved bioengineered cartilage substitutes.

IV.1. Introduction

Articular cartilage is a thin specialized tissue that covers the bone surfaces of synovial joints, enabling mobility with reduced friction and mechanical load dissipation. Due to its avascular constitution and low cellularity, articular cartilage has a limited self-healing capacity upon injury in physical trauma or in degenerative diseases such as osteoarthritis. Osteoarthritis is a progressive chronic joint disease and the leading cause of pain and disability in adults worldwide, comprising nearly $100 billion of annual healthcare and socioeconomic costs in US (Chen et al., 2017; Tan and Hung, 2017). The growing relevance of joint diseases, together with the inability of traditional surgical treatments in generating tissue with native-like features and functionality, has increased the interest in exploring cartilage tissue engineering (CTE) strategies. The success of such CTE strategies rely on a proper combination of cells capable of undergoing chondrogenic differentiation upon induction with adequate biochemical/physical factors, and biomaterial scaffolds providing a favorable environment for cell growth and cartilage-specific ECM production (Tan and Hung, 2017).

Mesenchymal stem/stromal cells (MSCs) have been widely explored in CTE as an alternative cell source to chondrocytes, mainly due to their easier accessibility, higher proliferative capacity, and advantageous immunomodulatory/trophic properties (Chamberlain et al., 2007; Tan and Hung, 2017). MSCs can be obtained from a wide variety of tissues including bone marrow, adipose tissue, periosteum, muscle, umbilical cord matrix and synovium, however, chondrogenic differentiation potential has been described as cell source dependent (Koga et al., 2008; Sakaguchi et al., 2005; Yoshimura et al., 2007). Bone marrow-derived MSC (BMSC) are the most used cell source and are considered the gold-standard cells for cell-based therapeutic strategies. However, several CTE studies have suggested that synovium-derived MSC (SMSC) are a superior cell source for cartilage repair due to their higher chondrogenic potential compared to MSCs derived from non-joint tissues (Fan et al., 2009; Futami et al., 2012; Huang et al., 2017; Sakaguchi et al., 2005; Shirasawa et al., 2006; Yoshimura et al., 2007).

Additive manufacturing technologies, such as 3D extrusion, have been widely employed in CTE, exploring their capacity to fabricate scaffolds with the shape and geometry that perfectly match patient's cartilage defect in a fast and reproducible manner (Hoque et al., 2012; Mota et al., 2015). Synthetic biodegradable poly (ε-caprolactone) (PCL), which was previously approved by the FDA for clinical use, has been used to produce extruded scaffolds in different MSC-based CTE strategies mainly due to its easy processing and advantageous chemical, thermal and mechanical properties (Kim et al., 2010; Theodoridis et al., 2019; Woodruff and Hutmacher, 2010).

MSC chondrogenic potential can be enhanced through exposure to specific biochemical (e.g., growth and differentiation modulators such as TGF-β superfamily), physical (e.g., mechanical stimulation) and environmental cues (e.g., oxygen tension) (Vinatier et al., 2009). Considering the hypoxic (compared to atmospheric air) nature of articular cartilage *in vivo*, which varies from 1% O_2 tension in the deep zone to 6% O_2 in the superficial zone, as well as of synovial fluid (6.5-9% O_2) and most MSC niches *in vivo* (1-5% O_2), different CTE approaches have exploited the use of low oxygen tensions to promote MSC chondrogenesis (Lund‐Olesen, 1970; Pattappa et al., 2019; Zhou et al., 2004). Our group and others previously reported higher *in vitro* proliferative and chondrogenic potential of both BMSC and SMSC when cultured under hypoxic conditions (Adesida et al., 2012; Bae et al., 2018; Dos Santos et al., 2010; Ferro et al., 2019; Leijten et al., 2014). A different study also showed augmented chondrogenic differentiation when BMSC were cultured on porous scaffolds exposed to low oxygen tensions (3% O_2) (Bornes et al., 2015).

Glycosaminoglycans (GAGs) are linear, anionic polysaccharides consisting of repeating disaccharide units and either exists as constituents of ECM or on the cell surface covalently attached to core proteins, turning into proteoglycans. Aggrecan is the most predominant proteoglycan in cartilage ECM and consists in a core protein with many GAG chains mainly composed of chondroitin sulfate (CS) (Gasimli et al., 2012; Knudson and Knudson, 2001). The highly negatively charged sulfate groups of CS generate electrostatic repulsion and high water uptake, which is crucial for cartilage resistance to compressive forces and shock-absorbing capacity (Oliveira and Reis, 2011). Although present at lower concentrations than CS, hyaluronic acid (HA), a non-sulfated GAG, plays a pivotal role in regulating cartilage ECM structural organization and signaling (Oliveira and Reis, 2011; Wang et al., 2017). Both CS and HA are known to participate in several signaling pathways, regulating cellular processes such as cell adhesion, migration, proliferation and differentiation through interaction with a wide variety of GAG-binding proteins within the ECM (Gasimli et al., 2012; Wang et al., 2017). Thus, CS and HA have been incorporated in CTE scaffolds aiming to improve MSC chondrogenic differentiation (Bornes et al., 2015; Pfeifer et al., 2016; Sawatjui et al., 2015; Varghese et al., 2008). Nevertheless, very few studies have been performed that explore the use of GAGs, CS and HA, as medium additives to enhance MSC chondrogenic differentiation in an integrated CTE approach, and, to the best of our knowledge, none has been conducted using SMSC or comparing different MSC sources.

The primary aim of this study was to assess the effects of CS and HA in the chondrogenic differentiation of MSC on 3D-extruded PCL scaffolds. We hypothesize that integrating predominant cartilage GAGs (CS and HA) as culture medium additives in our CTE strategy might enhance MSC chondrogenic differentiation through a more closely resemble of native tissue's biochemical microenvironment and ECM-cell signaling. Porous

PCL scaffolds capable of being tailored to meet patient cartilage defect specificities were fabricated by 3D-extrusion and their structural features were characterized. Upon optimization of culturing conditions, two different human MSC sources (hBMSC and hSMSC) were studied and their responses to GAG supplementation were compared, by assessing cellularity and cartilage ECM production throughout culture. The quality of the final tissue-engineered cartilage constructs generated by each MSC source under the different GAG supplementations was assessed by RT-qPCR, histological/immunohistochemical and transmission electron microscopy (TEM) analysis.

IV.2. Materials & Methods

IV.2.1. Isolation and culture of human MSCs from bone marrow and synovium aspirates

Human bone marrow-derived MSCs (hBMSCs) and human synovium-derived MSCs (hSMSCs) were isolated and characterized in terms of their immunophenotype and multilineage differentiation potential following protocols previously developed by our group (Dos Santos et al., 2010; Santhagunam et al., 2013) (Supplementary Table IV.1 and Supplementary Figure IV.1). Bone marrow aspirates were obtained from healthy donors (male 36 years and male 35 years) after informed consent, with the approval of the ethics committee of Instituto Português de Oncologia Francisco Gentil. Synovium aspirates were obtained from patients (male 28 years and male 22 years) undergoing arthroscopy who had no history of joint disease, after their informed consent at Centro Hospitalar de Lisboa Ocidental, E.P.E., Hospital São Franscisco Xavier, Lisboa, Portugal. Isolated hBMSCs and hSMSCs were cultured with Dulbecco's Modified Eagle's Medium (DMEM, Gibco) supplemented with 10% fetal bovine serum (FBS, MSC qualified, Life Technologies) and 1% antibiotic-antimycotic (Anti-Anti, Gibco) and cryopreserved in liquid/vapor-phase nitrogen tanks. All cultures were maintained at 37ºC and 5% CO_2 in a humidified atmosphere and cells between passages P3-P6 were used in the experimental assays.

IV.2.2. Fabrication and structural characterization of PCL scaffolds

PCL (MW 50000 Da, CAPA^{TM} 6500, Perstorp Caprolactones, UK) scaffolds were fabricated in a layer-by-layer manner using an in-house developed melt-extrusion machine, the Bioextruder (Figure IV.1), as previously described (Domingos et al., 2009; Silva et al., 2017). Briefly, 3D CAD models were designed in SolidWorks software (Dassault Systèmes, S.A.) and the scaffolds were extruded with a 0-90º lay-down fiber orientation with the desired

size, structure and architecture. The PCL filament material was heated at 80ºC (above PCL's melting temperature ~ 60ºC) and extruded in a built plate through a robot-guided nozzle with motion controlled by a computer. The scaffolds were fabricated with the following extrusion parameters: deposition velocity of 8 mm/sec; rotation velocity of 22.5 rpm; slice thickness of 280 µm and a nozzle diameter of 300 µm, which corresponds to the diameter of a single fiber of the scaffold. The structure of the generated scaffolds was characterized using scanning electron microscopy (SEM, Hitachi S-2400, Japan) and micro-computed tomography (µ-CT, Scansky 1174v2, Brucker version 1.1, MA USA) (Silva et al., 2017).

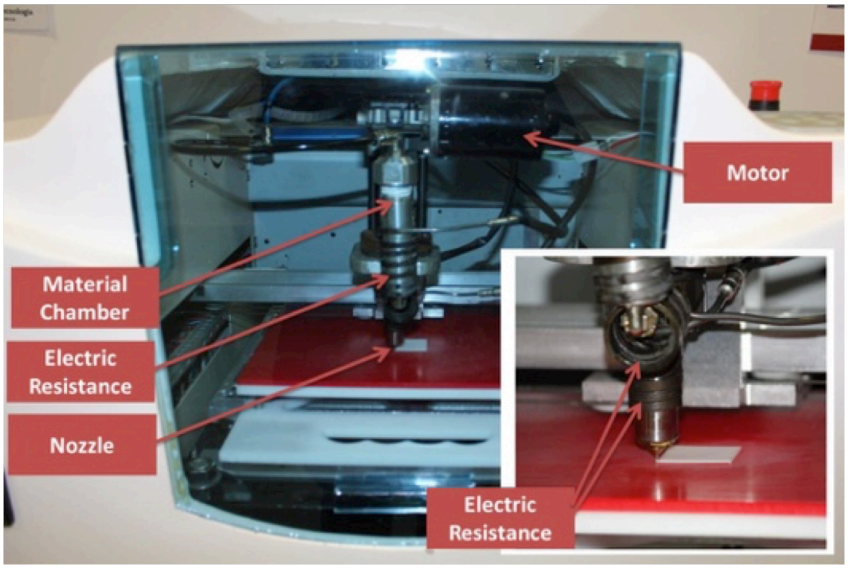

Figure IV.1. Bioextruder equipment used to fabricate the PCL scaffolds studied in this thesis. The Bioextruder machine was developed at the Centre for Rapid and Sustainable Product Development – Polytechnic Institute of Leiria. Adapted from (Moura et al., 2015).

IV.2.3. Optimization of MSC culture conditions on PCL scaffolds: culture medium and oxygen tension

Previous to GAG supplementation *in vitro* cell culture assays, an experiment comparing two different commercially available culture mediums for MSC chondrogenic differentiation (Hyclone™ AdvanceSTEM™ Chondrogenic Differentiation Medium (Thermo Fisher Scientific, Rockford, IL USA) + 1% Anti-Anti *vs.* StemPro™ Chondrogenesis Differentiation Kit (StemPro Chondro, Gibco™, Thermo Fisher Scientific) + 1% Anti-Anti, with standard expansion medium DMEM + 10% FBS + 1% Anti-Anti used as control) was performed at normoxia conditions. Afterwards, the culture medium with the best performance was used in an additional experiment comparing the effects of three different oxygen tensions (Normoxia: 21% O_2 / Hypoxia: 2% O_2 and 5% O_2) in the chondrogenic differentiation of MSC on PCL scaffolds. The effect of the different oxygen tensions in the proliferative potential of hBMSC

in PCL scaffolds was also assessed under standard expansion culture medium (DMEM + 10% FBS).

Before cell seeding, PCL scaffolds (dimensions: 7mm x 7mm x 3mm) were sterilized by UV exposure (2 h each side of the scaffold) and through washing with 70% ethanol for 3 h. Afterwards, the scaffolds were rinsed three times with a phosphate buffered saline (PBS, Gibco) + 1% Anti-Anti solution and moistened with culture medium for 1 h. To perform the optimization experiments, 1 x 10^5 hBMSCs were seeded in each scaffold and incubated without culture medium for 1.5 h to promote initial cell adhesion. Then, the scaffolds were cultured for 21 days under the different culture mediums or oxygen tensions at 37ºC/5% CO_2 and the culture medium was fully replaced twice a week. The selection of the culture medium and oxygen tension that resulted in the highest hBMSC chondrogenic potential on PCL scaffolds was performed based on the equivalent cell numbers and sGAG amounts (day 21) evaluated as specified in following sections IV.2.5 and IV.2.6, respectively.

IV.2.4. hBMSCs and hSMSCs seeding on PCL scaffolds and culture under different GAG supplementation conditions

hBMSCs or hSMSCs were seeded on PCL scaffolds at a density of 1 x 10^5 cells/scaffold and incubated for 1.5 h at 37ºC/5%CO_2 in the absence of culture medium to favour initial cell attachment. Then, Hyclone™ AdvanceSTEM ™Chondrogenic Differentiation medium + 1% Anti-Anti supplemented with different main cartilage GAG constituents (CS and HA) was added to the scaffolds. For that, based on previously reported values of GAG concentration in healthy human knee and synovial joint fluid (Bollet and Nance, 1966; Mazzucco et al., 2004; Nakayama et al., 2002), sterile CS (#C6737, Sigma-Aldrich, UK) and high molecular-weight HA (#53747, MW ~ 1.5-1.8 x 10^6 Da, Sigma-Aldrich) were dissolved in culture medium to generate 2% CS and 0.4% HA (w/v) medium supplemented solutions. Thus, three different experimental groups were considered for each cell source according to the GAG-supplemented medium used: (i) non-supplemented control (PCL), (ii) CS-supplemented (PCL-CS) and (iii) HA-supplemented (PCL-HA). All cultures were maintained in a hypoxic environment (5% O_2 tension) to provide a closer mimic of the native cartilage niche and promote MSC chondrogenesis. The experiment was conducted for 21 days and culture medium was renewed twice a week.

IV.2.5. Cell viability and proliferation assay

The metabolic activity of hBMSCs/hSMSCs in the different GAG supplementation experimental groups was evaluated throughout the culture (days 1, 7, 14, and 21) using

AlamarBlue® cell viability reagent (ThermoFischer Scientific, USA) following the manufacturer's guidelines. Briefly, a 10% v/v AlamarBlue® solution in culture medium was added to the scaffolds and incubated at 37 ºC in 5% CO_2 chamber for 2.5 h. Fluorescence intensity was measured in a plate reader (Infinite® M200 PRO, TECAN, Switzerland) at an excitation/emission wavelength of 560/590 nm and compared to a calibration curve (specific for each donor and culture medium used) to access the equivalent number of cells in each scaffold. Acellular scaffolds (for each experimental group) were used as blank controls in the fluorescence intensity measurements. In each experiment, three different scaffolds were considered for each experimental group and fluorescence intensity values of each sample were measured in triplicate.

IV.2.6. Alcian Blue staining and sGAG quantification assay

At days 14 and 21 of the differentiation protocol, scaffold samples were harvested, washed thoroughly with PBS to remove all medium remnants, and fixed with 2% w/v paraformaldehyde (PFA, Sigma-Aldrich) solution for 20 min. Afterwards, samples were washed with PBS and incubated with 1% w/v Alcian Blue 8GX (Sigma-Aldrich) solution (in 0.1N hydrochloric acid, Sigma-Aldrich) for 1 h to assess for the presence of sulfated GAG (sGAG). The samples were rinsed twice with PBS, washed once with distilled water and imaged using a LEICA® DMI3000B (Leica Microsystems, Germany) microscope equipped with a digital camera (Nikon DXM1200F, Nikon Instruments Inc., Japan). sGAG content in the scaffolds of the different experimental groups was quantified by Alcian Blue dye precipitation following previously reported protocols (Dingle et al., 1975; Nam et al., 2011). For that, Alcian Blue stained samples were treated with a 2% w/v sodium dodecyl sulfate (SDS, Sigma-Aldrich) solution with constant shaking overnight. The absorbance of the resultant solutions was measured in a plate reader (Infinite® M200 PRO, TECAN) at 620 nm, compared to a calibration curve (generated using CS standards sodium salt from shark cartilage, #C4384, Sigma-Aldrich, UK) to estimate the sGAG content, and normalized to the equivalent cell numbers of the respective scaffold. For an independent experiment, three scaffolds were considered for each experimental group and the absorbance values of each sample were measured in triplicate.

IV.2.7. RNA isolation and gene expression analysis by real time quantitative PCR

At day 21, scaffolds cultured with hBMSCs and hSMSCs under the different GAG stimulation conditions were collected for gene expression analysis by real time quantitative PCR (RT-qPCR). Total RNA was extracted using the RNeasy Mini Kit (QIAGEN, Hilden,

Germany) according to the manufacturer's protocol and quantified by UV spectrophotometry using a Nanodrop (NanoVue Plus, GE Healthcare, Chicago, IL USA). cDNA was synthesized from the isolated RNA using iScript™ Reverse Transcription Supermix (Bio-Rad, Hercules, CA USA) according to the manufacturer's guidelines. Reaction mixtures (20 µl) were incubated in a T100™ thermal cycler (Bio-Rad) with the following temperature protocol: 5 min at 25ºC, 20 min at 46ºC and 1 min at 95ºC. RT-qPCR was performed using Fast SYBR™ Green Master Mix (Applied Biosystems, CA USA) and the StepOnePlus real-time PCR equipment (Applied Biosystems). All reaction mixtures (20 µl) containing the specific primer sequences for the target genes and cDNA template were carried out in accordance with the manufacturer's guidelines and using the following temperature protocol: denaturation step at 95ºC for 20 sec, followed by 40 cycles of 95ºC for 3 sec and 60ºC for 30 sec. All samples were assayed in triplicate and the results were analyzed using the $2^{-\Delta\Delta Ct}$ method. Target genes (collagen type I (*COL I*), collagen type II (*COL II*), Aggrecan (*ACAN*), collagen type X (*COL X*) and runt-related transcription factor 2 (*Runx2*)) expression was primarily normalized to the housekeeping gene glyceraldehyde 3-phosphate dehydrogenase (*GAPDH*) and then determined as a fold-change relative to the baseline expression of hBMSCs/hSMSCs at day 0. The specific primer sequences used in the RT-qPCR analysis are presented in Table IV.1.

Table IV.1 Primer sequences used in this study for RT- qPCR analysis.

Gene	Fwd primer sequence	Rev primer sequence
GAPDH	5'-GGTCACCAGGGCTGCTTTTA -3'	5'-CCTGGAAGATGGTGATGGGA-3'
COL I	5'-CATCTCCCCTTCGTTTTTGA-3'	5'-CCAAATCCGATGTTTCTGCT-3'
COL II	5'-GGAATTCCTGGAGCCAAAGG-3'	5'-AGGACCAGTTCTTGAG-3'
ACAN	5'-CACTGGCGAGCACTGTAACAT-3'	5'-TCCACTGGTAGTCTTGGGCAT-3'
COL X	5'-CCAGGTCTGGATGGTCCTA-3'	5'-GTCCTCCAACTCCAGGATCA-3'
Runx2	5'-TGTGAGGTGATGTCCTCGTCTGTAG-3'	5'-ACACATATGATGGCCGAGGTGA-3'

IV.2.8. Histological/Immunohistochemical analysis

The final hBMSCs/hSMSCs-PCL constructs generated under different GAG stimulations were fixed in 4% w/v PFA and embedded in Bio-Agar (Bio-Optica, Italy). Afterwards, the samples were dehydrated with progressive graded ethanol series (70%, 90% and 96% (v/v)), cleared with xylene and embedded in paraffin. The paraffin blocks were sliced into 5 µm sections using a microtome Leica RM2235 (Leica Biosystems) and mounted in glass slides. Afterwards, upon deparaffinization and rehydration of the slides, endogenous peroxidase activity was blocked with 3% hydrogen peroxidase treatment (H_2O_2, Sigma-Aldrich) for 10 min. For histological assessment of the constructs, slides were stained with haematoxylin-

eosin (H&E, Sigma-Aldrich) for 5 min to visualize cells/cell nuclei, Toluidine Blue (0.1% w/v aqueous solution, Sigma-Aldrich) for 5 min to identify proteoglycans and with safranin-O (1% w/v aqueous solution, Sigma-Aldrich) for 15 min to observe secreted GAG. Regarding the immunohistochemical analysis, sections were incubated overnight at room temperature with rabbit polyclonal antibodies to collagen II (1:800 dilution, Anti-Collagen II antibody ab34712, Abcam, UK) and aggrecan (1:250 dilution, Anti-Aggrecan II antibody ab140707, Abcam, UK); and visualized after incubation for 30 min with anti-rabbit Dako EnVision^{+} System-HRP Labelled Polymer (Agilent Dako, CA USA). The slides were finally counterstained with haematoxylin, dehydrated and mounted. The histological/immunohistological analysis images were obtained at 200x magnification using a Leica DMLB optical microscope equipped with a Leica DFC290 HD camera (Leica Microsystems).

IV.2.9. Transmission electron microscopy (TEM) analysis

At the end of the experiment, culture medium was removed; samples were washed with PBS and fixed with a 3% glutaraldehyde (Sigma-Aldrich) in 0.1 M sodium cacodylate buffer (Sigma-Aldrich) solution overnight at 4ºC. Samples were kept in 0.1 M sodium cacodylate buffer at 4ºC until further processing. The fixed samples were embedded in agar, rinsed with cacodylate buffer and post-fixed with a 1% v/v osmium tetroxide (Sigma-Aldrich) in 0.1 M cacodylate buffer for 1 h at room temperature. Afterwards, the constructs were fixed with 1% v/v uranyl acetate (Sigma-Aldrich) in acetate acetic acid buffer 0.1 M (pH 5) for 1 h and dehydrated by exposure to gradually increasing ethanol concentrations (70%, 95% and 100% in distilled water; 3 x 10 min each). Additionally, the constructs were treated twice with propylene oxide (Sigma-Aldrich) for 15 mim, incubated with epoxypropane for 1 h and embedded in epoxy resin (Epon^{TM}, Hexion Inc., Columbus, OH USA). Finally, samples were cut with a diamond knife (0.5 µm slices) in a Reichert Ultracut E ultramicrotome (Leica Microsystems) and the ultrastructure of cells/ECM of the different constructs was imaged using a JEOL 1200EX TEM equipment (JEOL USA, Inc., MA USA).

IV.2.10. Mechanical compressive testing

The final tissue constructs were assessed in terms of their mechanical properties under compressive testing (Supplementary Figure IV.3) using an Instron machine (Instron® Model 5544) equipped with a 2 kN load cell and a 50 mm diameter cylindrical compression plate, operating with an extension rate of 1 mm/min. Acellular PCL scaffolds were used as control. For each experimental group, four (n=4) independent scaffold samples were tested. The experimental data obtained from the measurements was processed using Bluehill® 3

software and the Young's/compressive modulus was calculated by the slope of the initial linear region (0-15%) of the stress-strain curve.

IV.2.11. Statistical analysis

Results are presented as mean values ± standard error of mean (SEM) of the values obtained for three (n=3) independent experiments, unless otherwise specified. Statistical analysis of the data was performed using one-way ANOVA, followed by Tukey post-hoc test. GraphPad Prism version 7 software was used in the analysis and data was considered to be significant when *p*-values obtained were less than 0.05 (95% confidence intervals) (*$p < 0.05$).

IV.3. Results

IV.3.1. Fabrication and characterization of 3D-extruded porous PCL scaffolds

Custom-made porous PCL scaffolds with a 0-90º fiber orientation pattern and a pore size of 390 µm (Figure IV.2 A) were fabricated using an in-house developed 3D-extrusion equipment and their structure/morphological properties were assessed by SEM (Figure IV.2 B) and µ-CT (Figure IV.2 C) as previously described (Silva et al., 2017). µ-CT analysis of the PCL scaffolds estimated high porosity of approximately 56.6% and high interconnectivity of 99.7%, which is beneficial for cell infiltration and also favors efficient nutrient supply, gas diffusion and waste removal.

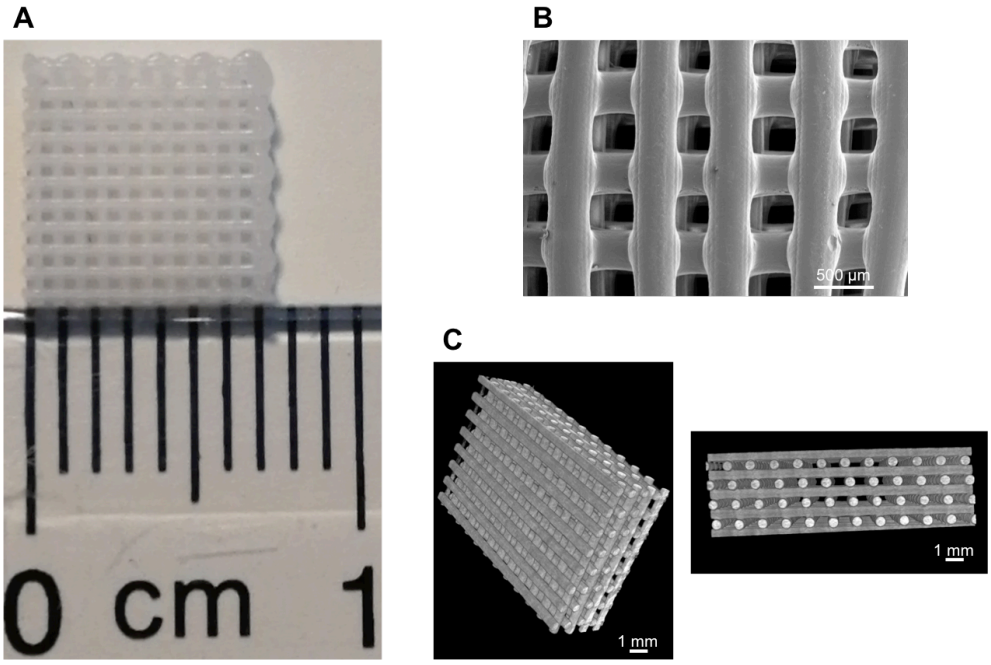

Figure IV.2. Characterization of 3D-extruded PCL scaffold: macroscopic view (A), SEM micrograph image (B) and 3D reconstruction images obtained after µ-CT analysis (C). Scale bars are depicted in the figure.

IV.3.2. Optimization of MSC culture on PCL scaffolds: chondrogenic culture medium and oxygen tension selection

Before studying the effects of CS and HA supplementation on hBMSC and hSMSC chondrogenic differentiation in PCL scaffolds, preliminary experimental assays were performed using only hBMSC to select the chondrogenic medium (between two commercially available formulations) and oxygen tension (2% O_2, 5% O_2 and 21% O_2) with improved results concerning the equivalent number of cells and sGAG production in this specific 3D culture system.

Regarding the chondrogenic medium selection (Figure IV.3), hBMSC-PCL constructs cultured under Hyclone Chondro medium presented significantly higher ($p < 0.05$) equivalent cells numbers at days 14 and 21 than the ones cultured under StemPro Chondro medium (Figure IV.3 A). As shown in Figure IV.3 B, PCL-hBMSC constructs cultured for 21 days with Hyclone Chondro medium presented sGAG amounts (14.1 ± 3.6 µg/10^5 cells) higher than the ones cultured in StemPro Chondro (11.6 ± 1.8 µg/10^5 cells) and control DMEM + 10% FBS (7.2 ± 1.4 µg/10^5 cells). Alcian Blue staining images (Figure IV.3 C) demonstrate that hBMSC-PCL constructs cultured under both chondrogenic mediums stained positively for sGAG deposition, however the staining appeared more predominant and uniformely distributed along the scaffold when Hyclone Chondro was used. Although at a lower intensity, it was also possible to observe positive staining for sGAG when constructs were

maintained in standard expansion medium (DMEM + 10% FBS) without addition of any chondroinductive supplements, suggesting that PCL scaffold alone supports some level of sGAG secretion by MSCs.

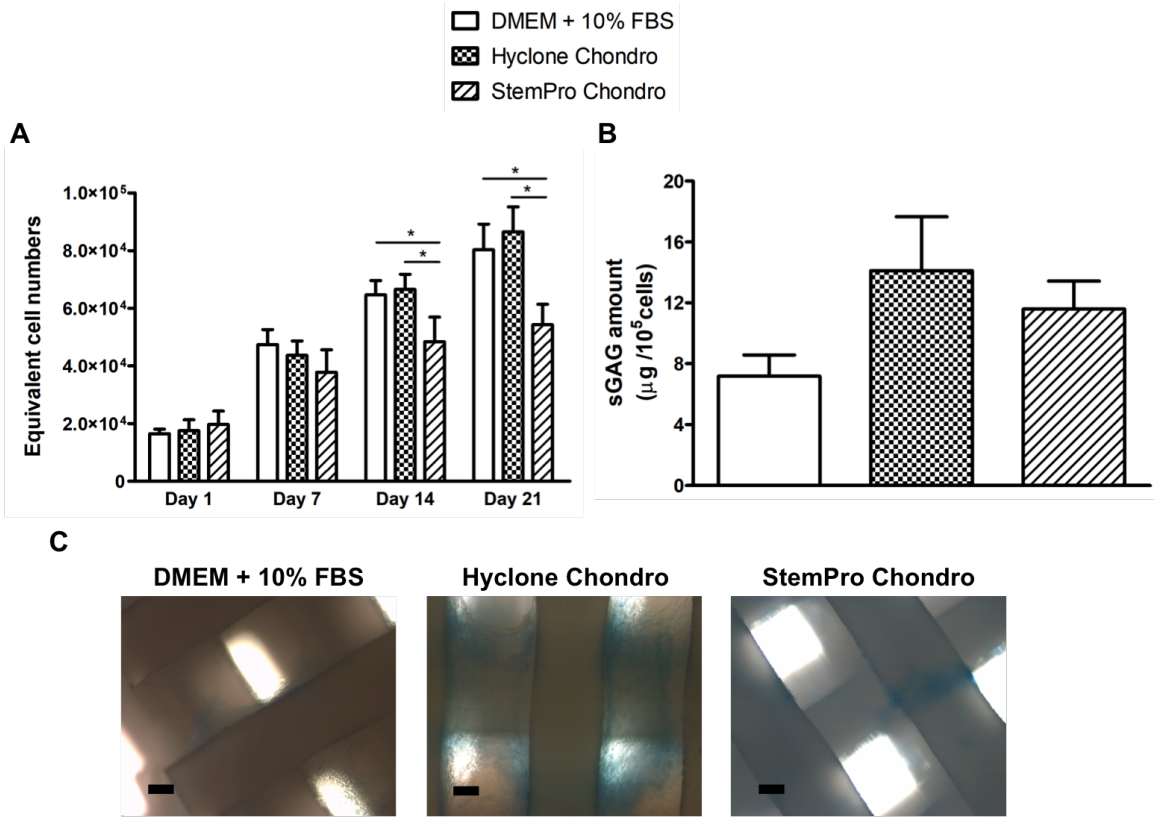

Figure IV.3. Comparison of different commercially available culture medium for the chondrogenic differentiation of hBMSC on PCL scaffolds. Equivalent cell numbers assessed by Alamar Blue assay throughout the culture period (A) and sGAG amounts at the end of the experiment (B) for the different culture medium tested. Alcian Blue staining (C) to identify the presence of sGAG deposition in the final tissue constructs (day 21). Results are presented as average ± SEM of three (n=3) independent experiments. *$p < 0.05$. Scale bar: 100 µm.

The effect of oxygen tension in the hBMSC proliferation on PCL scaffolds was assessed using expansion medium (DMEM + 10% FBS). Scaffolds cultured under both low oxygen tensions (2% O_2 and 5% O_2) showed increased cell proliferation comparing to normoxia condition, presenting significantly ($p < 0.05$) higher equivalent cell numbers (Figure IV.4 A) and fold increases (Figure IV.4 B) from day 14 onwards. At day 21, hBMSC scaffold culture under the different oxygen tensions reached equivalent cell numbers and fold increases in cell number (relative to day 1) of 1.21 ± 0.04 × 10^5 cells and 5.17 ± 0.16 for 2% O_2, 1.23 ± 0.08 × 10^5 cells and 4.78 ± 0.30 for 5% O_2 and 1.02 ± 0.11 × 10^5 cells and 3.67 ± 0.39 for 21% O_2. hBMSC chondrogenic differentiation under the three different oxygen tensions was also performed culturing the cell-scaffold constructs with Hyclone Chondro medium. Figure IV.4 C shows that cultures under both hypoxia conditions resulted in significantly ($p < 0.05$)

higher equivalent cell numbers (from day 7 onwards) when compared to the ones at 21% O_2. At day 21, the hBMSC-PCL constructs cultured under the different oxygen tensions showed sGAG deposition upon Alcian Blue staining (Figure IV.4 E) and resulted in sGAG amounts of 12.3 ± 0.5 µg/10^5 cells, 18.3 ± 0.9 µg/10^5 cells (p < 0.05 relative to 2% O_2) and 16.1 ± 2.0 µg/10^5 cells for 2% O_2, 5% O_2 and 21% O_2, respectively (Figure IV.4 D).

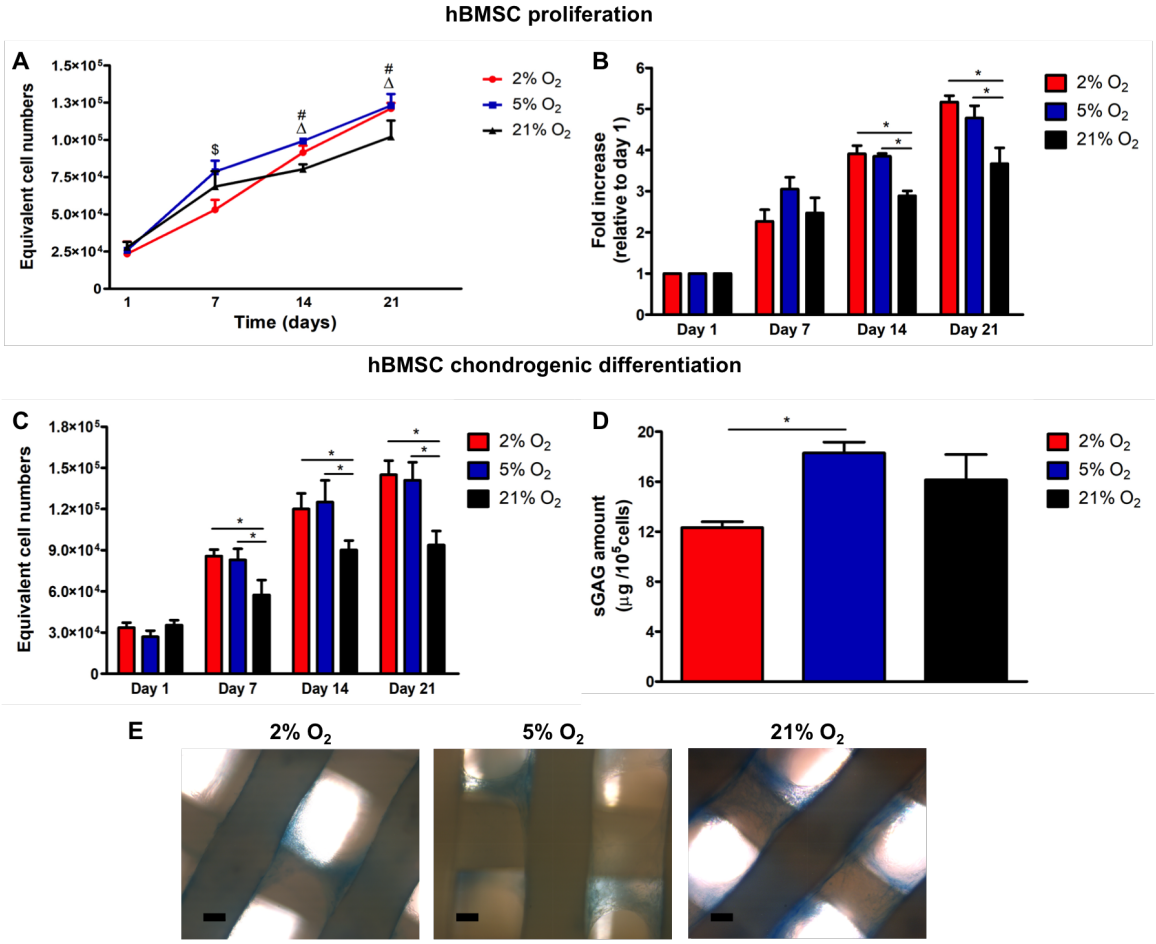

Figure IV.4. Effects of oxygen tension in hBMSC culture on PCL scaffolds. Cell proliferation evaluated by Alamar Blue assay (A) throughout culture (#, Δ and $ correspond to statistical difference of 2% O_2 *vs.* 21% O_2, 5% O_2 *vs.* 21% O_2 and 2% O_2 *vs.* 5% O_2, respectively) and fold increase in cell numbers relative to day 1 (B). hBMSC chondrogenic differentiation under different oxygen tensions was evaluated by assessment of equivalent cell numbers throughout culture (C), and sGAG amounts (D), Alcian Blue staining (E) at the end of the experiment day 21. Results are presented as average ± SEM of three (n=3) independent experiments. *p < 0.05. Scale bar: 100 µm.

IV.3.3. Effects of CS and HA supplementation on hBMSC/hSMSC chondrogenic differentiation

Based on the results of the previous section, the effects of CS and HA supplementation on the chondrogenic differentiation of hBMSC and hSMSC on PCL scaffolds (Figure IV.5) were studied using Hyclone Chondro medium and 5% O_2 tension.

For both hBMSC (Figure IV.5 A) and hSMSC (Figure IV.5 B), GAG supplementation did not show any significant effect on the equivalent cell numbers throughout all the 21 days of culture. Regarding sGAG amounts in hBMSC-based constructs (Figure IV.5 C), no significant differences were observed among the different conditions at day 14. It was noteworthy that at day 21, the PCL-HA group generated sGAG amounts (30.6 ± 4.7 μg/10^5 cells) significantly higher ($p < 0.05$) than the PCL-CS (15.6 ± 1.5 μg/10^5 cells) and PCL (18.1 ± 1.0 μg/10^5 cells) groups. In the case of hSMSC-based constructs (Figure IV.5 D), HA-supplementation originated constructs with significantly increased ($p < 0.05$) sGAG amounts than the ones cultured under CS-supplementation both at day 14 and 21. After 21 days of chondrogenic differentiation, the amounts of sGAG produced by hSMSC in PCL, PCL-CS and PCL-HA were 11.1 ± 4.5 μg/10^5 cells cells, 9.4 ± 0.4 μg/10^5 cells and 22.4 ± 4.9 μg/10^5 cells, respectively. Figure IV.5 E shows Alcian Blue staining images (at day 21) of both hBMSC-PCL and hSMSC-PCL constructs cultured under the different GAG-supplemented mediums. All constructs stained positively for Alcian Blue, therefore confirming the presence of secreted sGAGs.

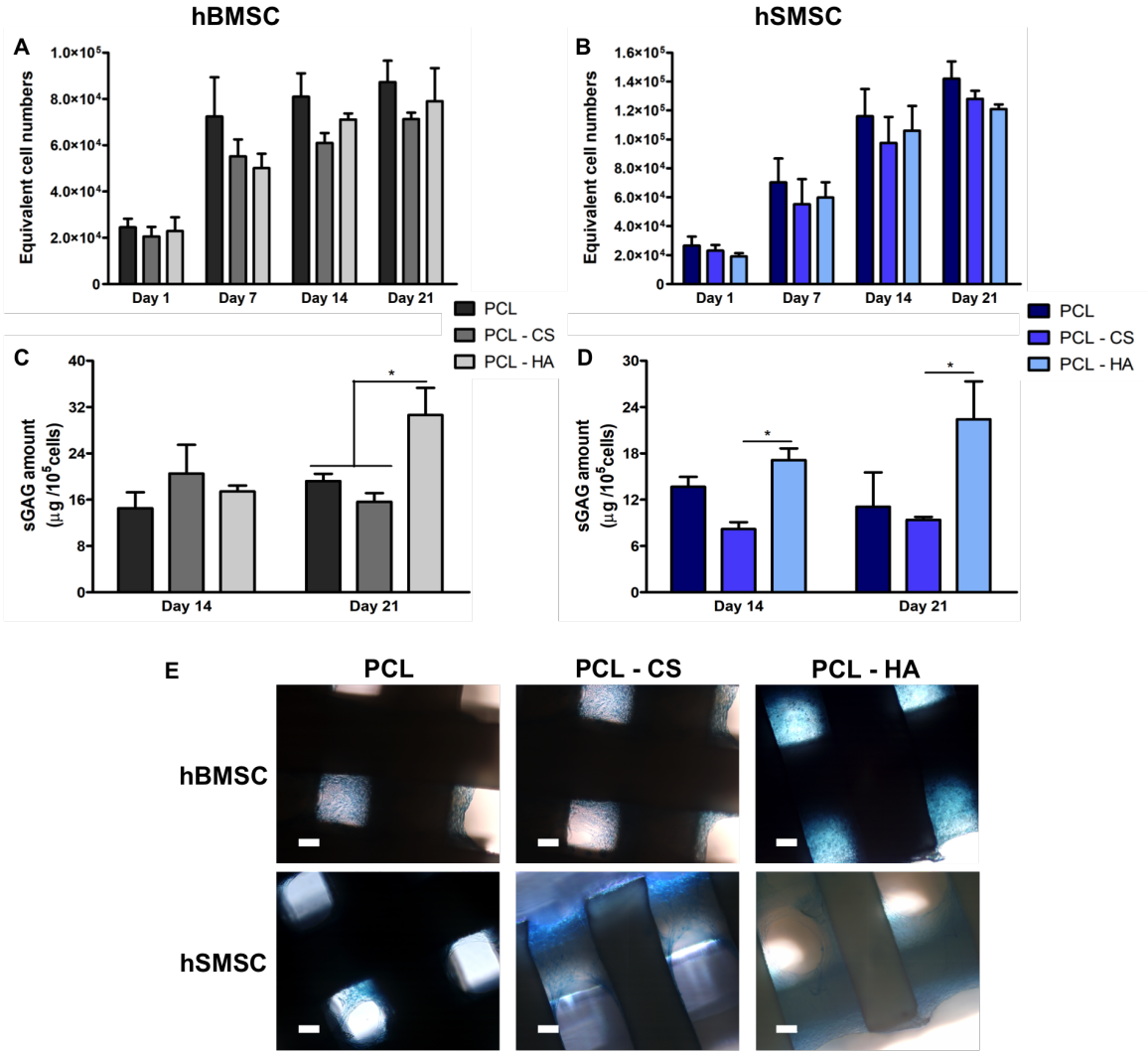

Figure IV.5. Effects of CS and HA supplementation on the chondrogenic differentiation of hBMSC/hSMSC in PCL scaffolds. Equivalent cell numbers estimated using the Alamar Blue assay for hBMSC-PCL (A) and hSMSC-PCL (B) constructs throughout all culture time. sGAG amounts analyzed at day 14 and 21 in hBMSC-PCL (C) and hSMSC-PCL (D) constructs. Alcian Blue staining (E) to identify sGAGs presence at day 21. Results are presented as average ± SEM of three (n=3) independent experiments. *$p < 0.05$. Scale bar: 100 µm.

IV.3.4. Gene expression analysis

The expression of genes associated with chondrogenesis and tissue hypertrophy in the final hBMSC/hSMSC-PCL constructs (day 21) cultured under different GAG supplementation was evaluated by RT-qPCR analysis (Figure IV.6). Both hBMSC-PCL (Figure IV.6 A) and hSMSC-PCL (Figure IV.6 B) tissue engineered constructs showed a significant downregulation ($p < 0.05$) of *COL I* expression compared to the respective cell source before scaffold seeding (day 0). Regarding the hBMSC-PCL constructs, both CS and HA supplementation resulted in a significantly higher ($p < 0.05$) *COL II* expression when compared with non-supplemented PCL group. However, PCL-CS and PCL-HA groups *COL II* expressions were not statistically different ($p > 0.05$) between them (Figure IV.6 C). Interestingly, in the hSMSC-derived constructs, PCL-HA group presented significantly higher ($p < 0.05$) *COL II* expression levels than both PCL and PCL-CS groups, which were not significantly different among them (Figure IV.6 D). Concerning *ACAN* expression, while significant upregulation (relative to hBMSCs at day 0) was observed for all hBMSC-PCL groups, without significant differences among these (Figure IV.6 E), in hSMSC-PCL constructs, only PCL-HA showed increased *ACAN* expression with significantly higher ($p < 0.05$) levels than both PCL and PCL-CS groups (Figure IV.6 F). All hBMSC-PCL constructs presented a significant upregulation of cartilage hypertrophic marker *COL X* (Figure IV.6 G). In contrast, the hSMSC-PCL constructs showed significant *COL X* downregulation compared to hSMSC at day 0, regardless of the GAG-supplementation protocol used. Additionally, the PCL-HA group presented significantly reduced ($p < 0.05$) *COL X* expressions compared to the other two groups (Figure IV.6 H). Regarding osteogenic marker *Runx2* expression, all hBMSC-PCL (Figure IV.6 I) constructs showed significant upregulation, while for hSMSC-PCL (Figure IV.6 J), only the non-supplemented group presented significantly increased expression levels when compared to the respective MSC source before scaffold seeding (day 0). It was noteworthy that for both MSC sources, HA supplementation resulted in final tissue engineered constructs with significantly decreased ($p < 0.05$) *Runx2* expressions compared to the respective non-supplemented PCL group. Moreover, a similar effect was also observed in hSMSC-PCL constructs when cultured under CS supplementation.

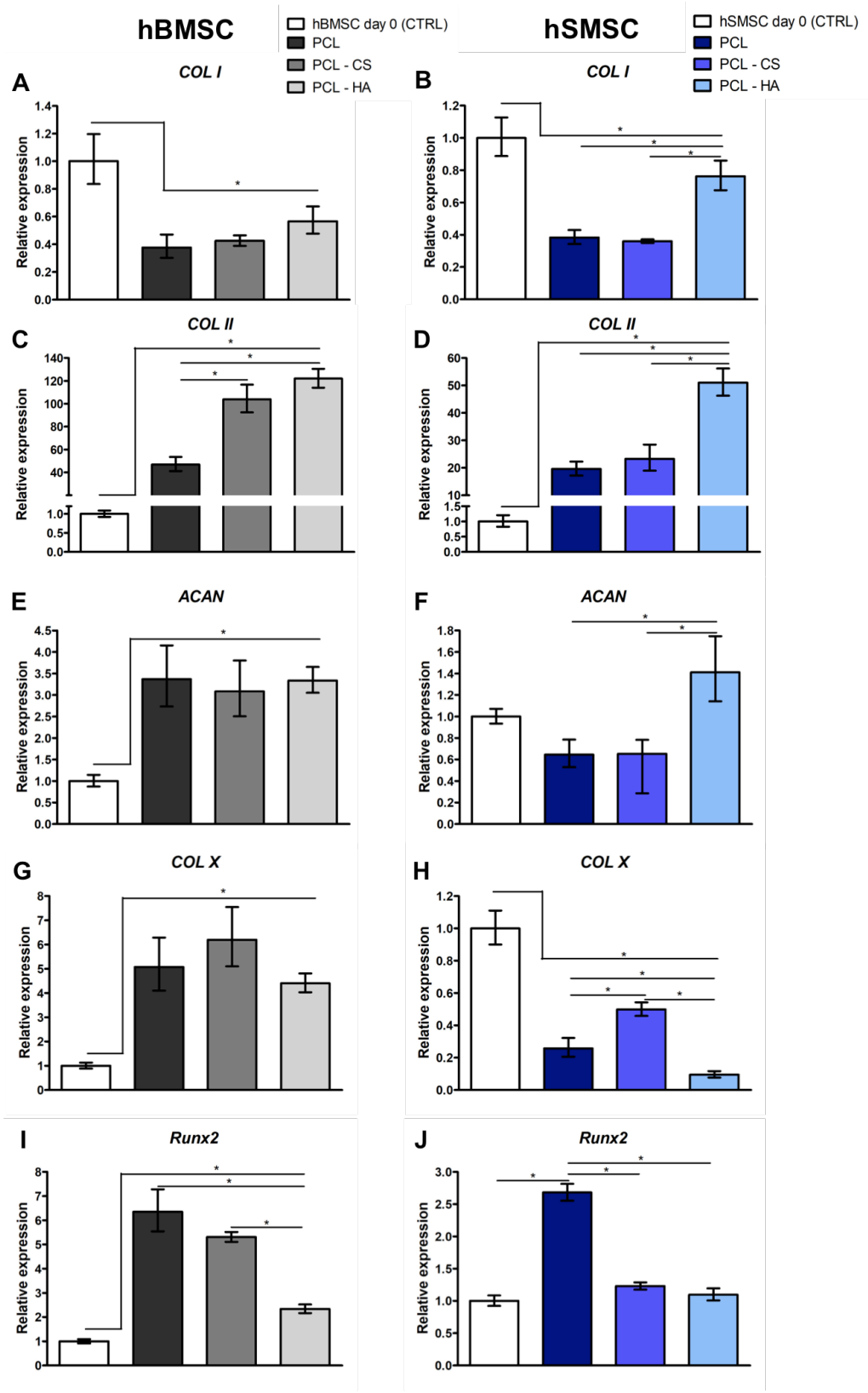

Figure IV.6. RT-qPCR analysis of the final hBMSC/hSMSC-PCL constructs generated under the different GAG supplementations (day 21). *COL I* (A, B), *COL II* (C, D), *ACAN* (E, F), *COL X* (G, H) and *Runx2* (I, J) gene expressions are normalized against the housekeeping gene *GAPDH* and presented as fold-change levels relative to hBMSC/hSMSC at day 0 prior to scaffold seeding. *$p < 0.05$.

IV.3.5. Histological, immunohistochemical and TEM analysis

The final hBMSC-PCL and hSMSC-PCL engineered constructs generated after 21 days of culture under the different GAG-supplemented mediums were processed and evaluated by histological (Figure IV.7), immunohistochemical (Figure IV.8) and TEM (Figure IV.9) analysis.

Representative histological images after H&E staining, confirmed the presence and distribution of cells with defined nuclei in all hBMSC-PCL (Figure IV.7 A) and hSMSC-PCL (Figure IV.7 B) tissue constructs cultured under different GAG supplementations. Additionally, Toluidine Blue and Safranin-O positive staining in all the experimental groups of hBMSC-PCL and hSMSC-PCL engineered tissues confirmed the presence proteoglycans and GAGs, respectively.

Figure IV.8 shows the representative images resultant from the immunodetection analysis performed on the final hBMSC-PCL (Figure IV.8 A) and hSMSC-PCL (Figure IV.8 B) constructs to assess for the presence of cartilage ECM components, collagen II and aggrecan (brown stain). Collagen II protein expression was clearly observed in all the experimental groups tested, regardless of the GAG supplementation and MSC source. Nevertheless, the immunohistochemical images suggested a more intense and spread collagen II protein expression in the hBMSC-PCL tissue constructs. All hBMSC-PCL and hSMSC-PCL constructs stained positively for the presence of major cartilage proteoglycan aggrecan. However, for both cell sources, PCL-CS and PCL-HA experimental groups exhibited a more abundant and distributed positive staining for aggrecan presence than PCL.

The ultrastructure of the cells and ECM present in the final hBMSC-PCL/hSMSC-PCL tissue constructs obtained after 21 days of chondrogenic differentiation under different GAG supplementations was analyzed by TEM and can be observed in Figure IV.9. TEM images of all experimental groups showed cells embedded in a dense ECM, however the presence of collagen fibers characteristic of cartilage ECM, was more evident, for both MSC sources, when tissue constructs were generated under CS and HA supplementation.

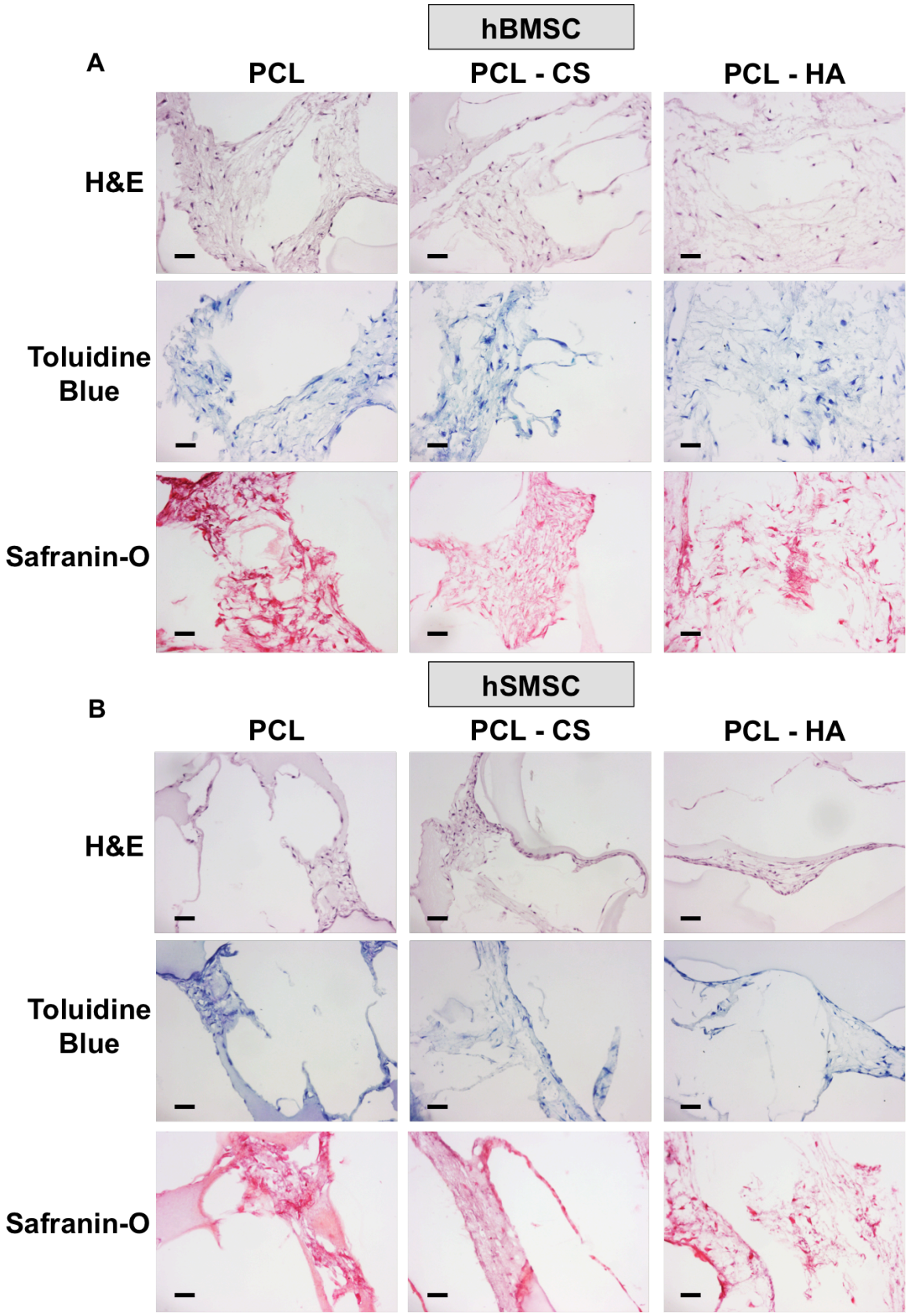

Figure IV.7. Histological analysis of the final hBMSC-PCL (A) and hSMSC-PCL (B) tissue constructs obtained under the different GAG supplementations (day 21). H&E staining to identify cell nuclei, Toluidine Blue staining to assess the presence of proteoglycans and Safranin-O staining for sulfated GAGs identification. Scale bar: 50 μm.

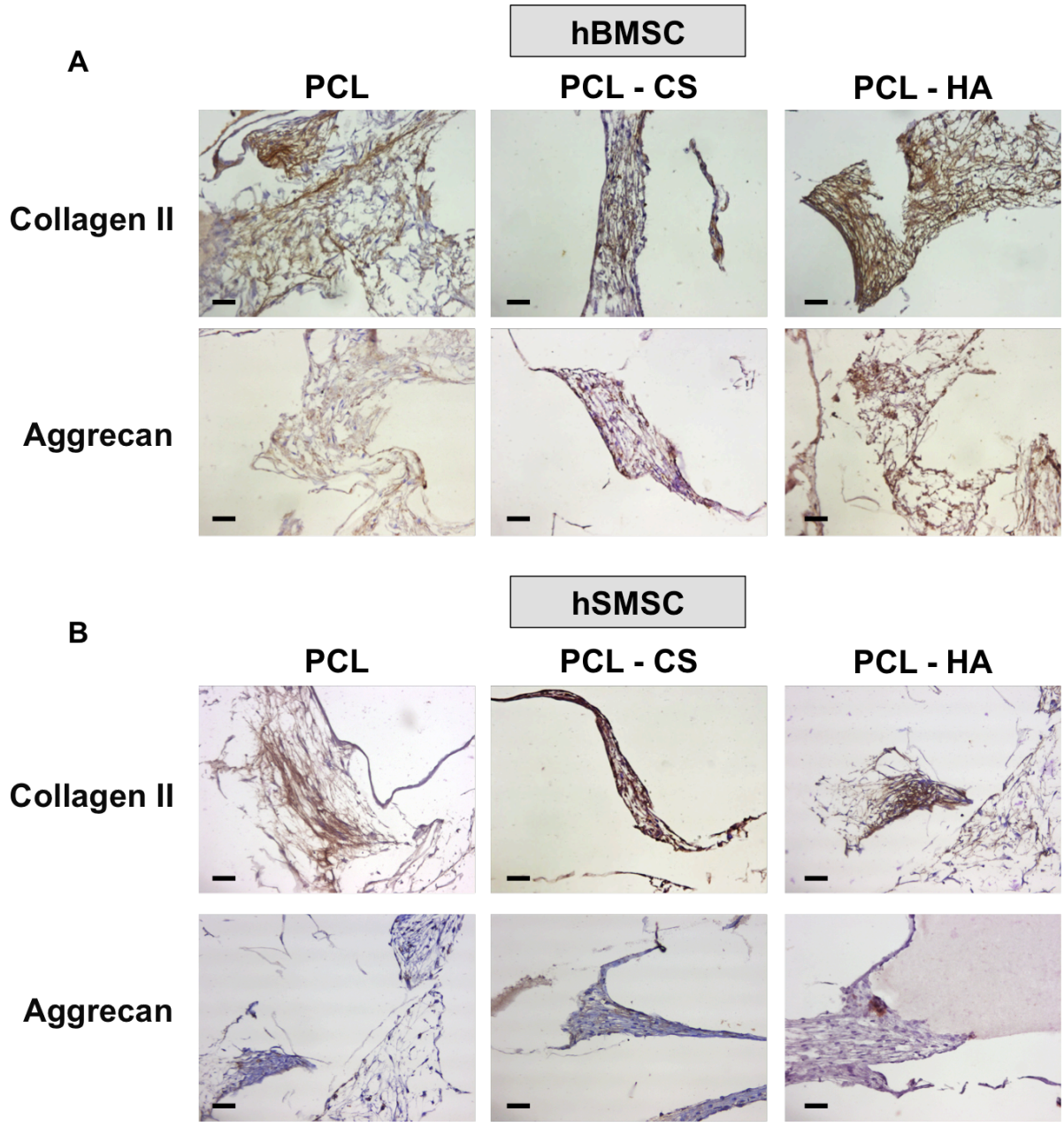

Figure IV.8. Immunohistochemical analysis of the final hBMSC-PCL (A) and hSMSC-PCL (B) tissue constructs obtained under the different GAG supplementations (day 21). Positive staining for collagen II and aggrecan is observed in brown and samples were counterstained with haematoxylin. Scale bar: 50 μm.

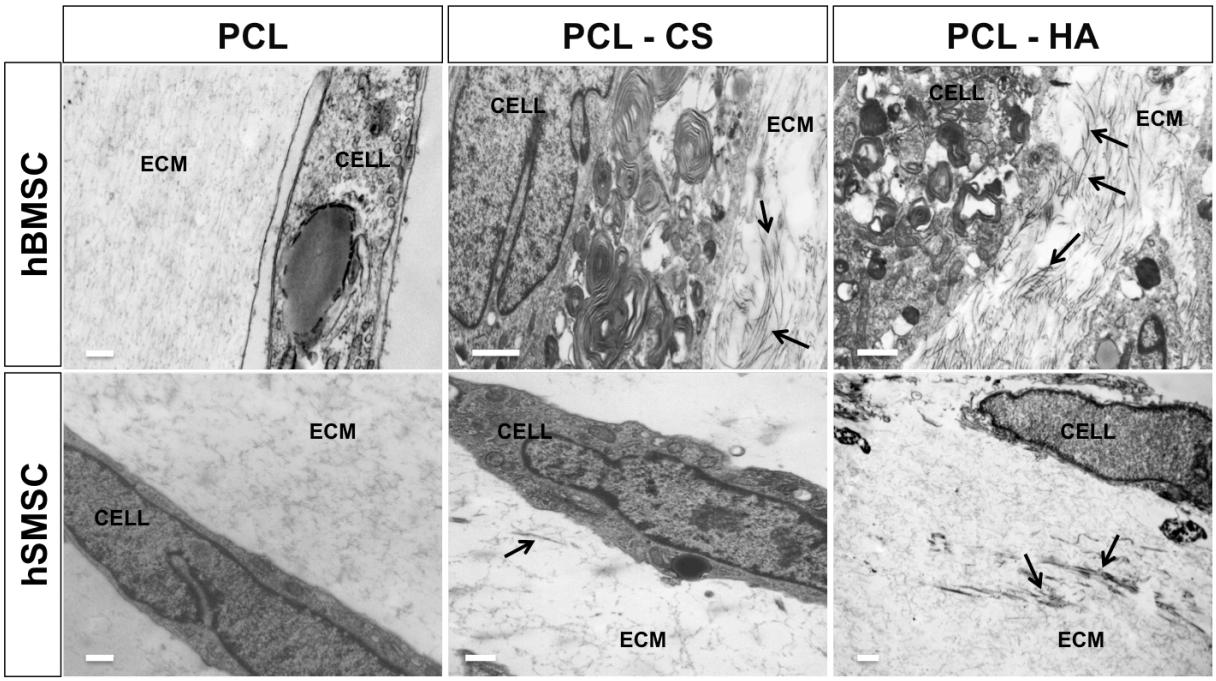

Figure IV.9. TEM images of cells and ECM present in the final hBMSC-PCL and hSMSC-PCL tissue constructs generated under the different GAG supplementations (day 21). Black arrows highlight the presence of collagen fibers. Scale bar: 1 μm.

IV.4. Discussion

The objective of this work was to evaluate the effects of CS and HA supplementation as medium additives in the chondrogenic differentiation of MSCs on 3D porous PCL scaffolds. In this study, two different sources of MSC (hBMSC and hSMSC) were considered and their responses to GAG supplementation were compared. These sources were selected due to their reported superior chondrogenic ability in CTE strategies (Koga et al., 2008; Sakaguchi et al., 2005). The PCL scaffolds fabricated in this study presented high porosity and high interconnectivity, and a pore size of 390 μm, which falls within the range of pore sizes (300-450 μm) previously reported to favor MSC chondrogenic differentiation in 3D PCL scaffolds (Im et al., 2012; Zhao et al., 2016).

As gold-standard cells for cellular therapy and most used cell source in CTE strategies, hBMSC were used in the optimization studies to select the culture medium and oxygen tension with highest chondrogenic potential. Hyclone Chondro, the chondrogenic medium that generated higher cell metabolic activities and sGAG production, has also been successfully employed in other CTE approaches using MSC isolated from different sources (Jeon and Alsberg, 2013; Nieto et al., 2015). Regarding the oxygen tension study, both 2% and 5% O_2 hypoxia conditions promoted a significantly higher hBMSC proliferation in PCL scaffolds than the normoxia (21% O_2) condition. Accordingly, different studies have

previously reported enhanced proliferation of both hBMSC and hSMSC in 2D tissue culture plates when cultured under hypoxic conditions (Dos Santos et al., 2010; Ferro et al., 2019; Park et al., 2018). Additionally, in agreement with our observations, Grayson *et al* showed improved hBMSC proliferation in 3D poly (ethylene terephthalate) scaffolds when exposed to hypoxia (2% O_2) (Grayson et al., 2006). In the present study, chondrogenic differentiation of hBMSC in PCL scaffolds under hypoxia (5% O_2) resulted in higher GAG production than the other oxygen tensions tested. Over the past few years, several studies have reported a positive effect of hypoxic cultures in increasing the GAG amounts produced by BMSC under chondrogenic induction, either cultured as 3D micromasses/pellets or seeded in 3D biomaterial scaffolds (Adesida et al., 2012; X. Huang et al., 2017; Leijten et al., 2014; Rodenas-Rochina et al., 2017). Rodenas-Rochina *et al* reported considerable higher amounts of sGAGs secreted by BMSCs differentiated in PCL scaffolds under hypoxia (5% O_2) than the ones cultured at normoxia (21% O_2) (Rodenas-Rochina et al., 2017). Interestingly, we observed a significantly decreased sGAG amount in the constructs cultured under 2% O_2 compared to the ones at 5% O_2. Nevertheless, it is important to note that the oxygen tension values reported are the ones controlled in the incubator, which differ than those experienced by cells that are hard to determine due to technological limitations. Accordingly, Fink *et al* demonstrated that monolayer cultures of human MSCs showed a considerably lower O_2 tension at the cell surface than the one defined by the incubator due to the fact that oxygen has to diffuse through the culture medium before reaching the cells. Such phenomenon is aggravated in 3D scaffolds culture systems, in which the diffusion limitations are more pronounced, especially when ECM production increases the tissue construct's density (Das et al., 2010; Fink et al., 2004). Therefore, in this study, the lower sGAG amounts observed in tissue constructs cultured under 2% O_2 tension might be related with diffusional limitations reached in this condition that are hampering sGAG production without affecting cell viability, which were not reached in the 5% O_2 cultures. In fact, a study performed by Malladi and colleagues reported impaired sGAG production by adipose-derived MSC micromass differentiated cultures at 2% O_2 when compared to normoxia (Malladi et al., 2006). It is extremely difficult to make direct comparisons of hypoxia studies due to dissimilarities in cell sources, culture conditions, scaffold materials and duration of low-oxygen exposure among the different protocols. Further efforts in developing standardized protocols for hypoxic cultures might lead to a broader consensus on the effects of hypoxia in MSC chondrogenesis. Nevertheless, the majority of research supports the use of low-oxygen culture conditions around 3-5% O_2 tensions to promote *in vitro* MSC chondrogenesis in CTE scaffolds (Das et al., 2010; Gaut and Sugaya, 2015).

GAGs are main constituents of cartilage and crucial for the maintenance of the structural organization and mechanical properties of the tissue. Decreased GAG (particularly CS and

HA) amounts in cartilage tissue have been associated with ageing and pathologies such as osteoarthritis and rheumatoid arthritis (Bollet and Nance, 1966; Nakayama et al., 2002; Temple-Wong et al., 2016). The GAG amounts in human cartilage tissues have been previously reported as a CS concentration of 18.4 ± 1.3 mg/mL in normal adult cartilage, with values ranging from 2 to 4 mg/mL for HA concentration in the synovial fluid from healthy human knee joints (Balazs, 1974; Bollet and Nance, 1966; Mazzucco et al., 2004; Nakayama et al., 2002; Temple-Wong et al., 2016). Thus, based on the reported values, we used upper limit values of 2% CS (20mg/mL) and 0.4% HA (4mg/mL) (w/v) medium solutions to experimentally assess the effects of GAG supplementation on MSC chondrogenic differentiation in 3D PCL scaffolds.

For both MSC sources, CS and HA supplementation did not cause any significant enhancement or detrimental effects on the equivalent cell numbers present in the PCL scaffolds. These results are in accordance with Schwartz *et al,* who also reported no significant differences in equivalent cell numbers in BMSCs-seeded chitosan sponges cultured under different HA-supplemented chondrogenic medium concentrations (Schwartz et al., 2011). In the present work, CS and HA supplementation showed beneficial effects on hBMSC and hSMSC chondrogenic differentiation in PCL scaffolds. After 21 days of chondrogenic differentiation, only the HA-supplemented group resulted in a significant increase in sGAG amounts in both hBMSC-PCL and hSMSC-PCL constructs. Additionally, in hSMSC-PCL constructs, a significant enhancement in sGAG amounts was also observed at an earlier stage (day 14) for the HA-supplemented group when compared to CS-supplemented group. Based on the average values at the end of the experiment, HA-supplementation of hBMSC-PCL constructs resulted in approximately 1.59- and 1.96- fold increase in sGAG amounts relative to non-supplemented and CS-supplemented conditions, respectively. In hSMSC-PCL constructs, the HA-supplemented group resulted in GAG amounts 2.02- and 2.39-fold higher than the PCL and PCL-CS groups, respectively. Therefore, our results suggest an improved and faster sGAG production by hSMSCs in PCL scaffolds when cultured with HA-supplementation. In accordance with our results, other studies using HA-supplemented medium to promote MSC chondrogenesis in 3D culture systems reported significantly enhanced sGAG amounts relative to the non-supplemented condition (Christiansen-Weber et al., 2018; Schwartz et al., 2011). The addition of CS to chondrogenic medium has also been shown by Chen *et al* to stimulate cartilage ECM accumulation during the chondrogenic differentiation of human umbilical cord blood (UCB)–derived MSCs in collagen scaffolds (Chen et al., 2011). However, their study used chondroitin sulfate C type, which is different from the chondroitin sulfate A sodium salt employed in our study.

Gene expression analysis of the final hBMSC-PCL and hSMSC-PCL constructs showed that GAG supplementation, particularly with HA, promotes the upregulation of chondrogenic marker genes *COL II* and *ACAN* while downregulating the expression of fibrocartilage marker *COL I*. Additionally, hBMSC-PCL constructs showed upregulation of hypertrophic marker *COL X* and osteogenic marker *Runx2*, while the hSMSC-PCL constructs exhibited downregulation of *COL X* and upregulation of *Runx2*, which was only significant for cells in the PCL group. However, for both MSC sources, HA and CS supplementation resulted in a significant decrease in *Runx2* expression when compared to the non-supplemented group. The observed chondrogenic genes expression and reduced expression of osteogenic/hypertrophic markers by hSMSC-PCL constructs when supplemented with GAGs may also be related with the hypothesis that hSMSCs are possibly a more "cartilage-committed" stem cell population and therefore more prone for chondrogenesis than hBMSCs (Fan et al., 2009). In their undifferentiated state before cell seeding (day 0), hSMSCs showed significant upregulation of chondrogenic markers and downregulation of hypertrophy and osteogenic markers when compared to hBMSCs (Supplementary Figure IV.2), which is accordance with previously published literature (Ogata et al., 2015). Our results also agree with previous studies reporting that supplementation with HA and CS in MSC-based CTE approaches resulted in enhancement of chondrogenic markers expression and suppression of hypertrophic markers (Chen et al., 2011; Christiansen-Weber et al., 2018).

All the final hBMSC-PCL and hSMSC-PCL tissue constructs showed presence of defined cell nuclei and cartilage-like ECM composed of proteoglycans and consequently GAGs. Immunohistological analysis suggests collagen II protein expression with similar intensity among all the constructs, but a more intense staining for aggrecan in the constructs cultured with GAG-supplemented medium compared to non-supplemented group, regardless of MSC source. Such observation was in agreement with a previous study highlighting the beneficial effect of HA supplementation in aggrecan deposition by BMSCs (Schwartz et al., 2011). TEM analysis revealed the presence of cells embedded in ECM in all experimental groups. Nevertheless, the presence of collagen fibers characteristic of cartilage ECM was more clearly observed in the hBMSC-PCL and hSMSC-PCL constructs obtained after culture with CS- and HA- supplemented chondrogenic mediums. Moreover, the cell/ECM structures obtained in our study were consistent with the ones reported in a previous TEM analysis of ECM secreted by hBMSCs differentiated in alginate beads for 21 days in chondrogenic medium (Dashtdar et al., 2016).

In this study, we hypothesized that GAG supplementation could result in improved MSC chondrogenesis through a closer mimicry of the native tissue biochemistry and ECM-cell signaling. However, the addition of GAGs to the culture medium, mainly of high MW HA used in this work, can also result in a closer resemble of synovial fluid viscosity and possibly, in

the recapitulation at some extent of the native tissue mechanical cues that can influence differentiation. In fact, Wu *et al* demonstrated the benefits of using HA supplementation to simulate synovial fluid properties in the preservation of chondrocyte phenotype when cultured in porous polyurethane scaffolds under mechanical stimulation (Wu et al., 2017). Therefore, we believe this closer mimicking of the native tissue synovial fluid properties might have also played a role in enhancing MSC chondrogenesis in PCL scaffolds, especially in the case of hSMSC.

In summary, custom-made 3D porous PCL scaffolds were produced and used as platform to study the effects of CS and HA supplementation in the chondrogenic differentiation of hBMSC and hSMSC under hypoxic conditions. GAG supplementation did not promote any significant effect on cell equivalent numbers present in the scaffolds. All experimental groups stained positively for secreted GAGs, however, for both MSC sources, significantly increased GAG amounts were only obtained when constructs were cultured with HA-supplemented medium. RT-qPCR analysis showed the upregulation of *COL II* and *ACAN* marker genes, suggesting that GAG supplementation (particularly with HA) supported the MSC chondrogenic differentiation in PCL scaffolds, however differences between the two MSC sources were observed. All hBMSC-PCL constructs presented upregulation of *COL X*, indicating some degree of tissue hypertrophy, which was not observed for the final tissue constructs obtained with hSMSC. Histological, immunohistochemical and TEM analysis confirmed the presence of cartilage-like ECM in all the experimental groups. Overall, this study highlights the use of GAG supplementation integrated with hSMSCs and customizable 3D scaffolds as a promising strategy to promote MSC chondrogenic differentiation towards the fabrication of improved bioengineered cartilage tissue substitutes.

IV.5. References

Adesida, A.B., Mulet-Sierra, A., Jomha, N.M., (2012). Hypoxia mediated isolation and expansion enhances the chondrogenic capacity of bone marrow mesenchymal stromal cells. Stem Cell Res. Ther. 3, 9.

Bae, H.C., Park, H.J., Wang, S.Y., Yang, H.R., Lee, M.C., Han, H.-S., (2018). Hypoxic condition enhances chondrogenesis in synovium-derived mesenchymal stem cells. Biomater. Res. 22, 1–8.

Balazs, E.A., (1974). The Physical Properties of Synovial Fluid and the Special Role of Hyaluronic Acid. Disord. Knee 61–74.

Bollet, A.J., Nance, J.L., (1966). Biochemical findings in normal and osteoarthritic articular cartilage. II. Chondroitin sulfate concentration and chain length, water, and ash content. J. Clin. Invest. 45, 1170–1177.

Bornes, T.D., Jomha, N.M., Mulet-Sierra, A., Adesida, A.B., (2015). Hypoxic culture of bone marrow-derived mesenchymal stromal stem cells differentially enhances in vitro chondrogenesis within cell-seeded collagen and hyaluronic acid porous scaffolds. Stem Cell Res. Ther. 6, 84.

Chamberlain, G., Fox, J., Ashton, B., Middleton, J., (2007). Concise review: Mesenchymal stem cells: Their phenotype, differentiation capacity, immunological features, and potential for homing. Stem Cells 25, 2739–2749.

Chen, D., Shen, J., Zhao, W., Wang, T., Han, L., Hamilton, J.L., Im, H.-J., (2017). Osteoarthritis: toward a comprehensive understanding of pathological mechanism. Bone Res. 5, 16044.

Chen, W.C., Yao, C.L., Chu, I.M., Wei, Y.H., (2011). Compare the effects of chondrogenesis by culture of human mesenchymal stem cells with various type of the chondroitin sulfate C. J. Biosci. Bioeng. 111, 226–231.

Christiansen-Weber, T., Noskov, A., Cardiff, D., Garitaonandia, I., Dillberger, A., Semechkin, A., Gonzalez, R., Kern, R., (2018). Supplementation of specific carbohydrates results in enhanced deposition of chondrogenic-specific matrix during mesenchymal stem cell differentiation. J. Tissue Eng. Regen. Med. 12, 1261–1272.

Das, R., Jahr, H., Osch, G.J.V.M. Van, Farrell, E., (2010). The Role of Hypoxia in Bone Marrow – Derived Mesenchymal Stem Cells : Considerations for Regenerative Medicine Approaches. Tissue Eng. Part B. Rev. 16, 159–168.

Dashtdar, H., Murali, M.R., Selvaratnam, L., Balaji Raghavendran, H., Suhaeb, A.M., Ahmad, T.S., Kamarul, T., (2016). Ultra-structural changes and expression of chondrogenic and hypertrophic genes during chondrogenic differentiation of mesenchymal stromal cells in alginate beads. PeerJ 4, e1650.

Dingle, J.T., Horsfield, P., Fell, H.B., Barratt, M.E.J., (1975). Breakdown of proteoglycan and collagen induced in pig articular cartilage in organ culture. Ann. Rheum. Dis. 34, 303–311.

Domingos, M., Dinucci, D., Cometa, S., Alderighi, M., Bártolo, P.J., Chiellini, F., (2009). Polycaprolactone Scaffolds Fabricated via Bioextrusion for Tissue Engineering Applications. Int. J. Biomater. 2009, 239643.

Dos Santos, F., Andrade, P.Z., Boura, J.S., Abecasis, M.M., da Silva, C.L., Cabral, J.M.S., (2010). Ex vivo expansion of human mesenchymal stem cells: a more effective cell proliferation kinetics and metabolism under hypoxia. J. Cell. Physiol. 223, 27–35.

Fan, J., Varshney, R.R., Ren, L., Cai, D., Wang, D.A., (2009). Synovium-derived mesenchymal stem cells: a new cell source for musculoskeletal regeneration. Tissue Eng. Part B. Rev. 15, 75–86.

Ferro, T., Santhagunam, A., Madeira, C., Salgueiro, J.B., da Silva, C.L., Cabral, J.M.S., (2019). Successful isolation and ex vivo expansion of human mesenchymal stem/stromal cells obtained from different synovial tissue-derived (biopsy) samples. J. Cell. Physiol. 234, 3973–3984.

Fink, T., Abildtrup, L., Fogd, K., Abdallah, B.M., Kassem, M., Ebbesen, P., Zachar, V., (2004). Induction of Adipocyte-Like Phenotype in Human Mesenchymal Stem Cells by Hypoxia. Stem Cells 22, 1346–1355.

Futami, I., Ishijima, M., Kaneko, H., Tsuji, K., Ichikawa-Tomikawa, N., Sadatsuki, R., Muneta, T., Arikawa-Hirasawa, E., Sekiya, I., Kaneko, K., (2012). Isolation and Characterization of Multipotential Mesenchymal Cells from the Mouse Synovium. PLoS One 7, e45517.

Gasimli, L., Linhardt, R.J., Dordick, J.S., (2012). Proteoglycans in stem cells. Biotechnol. Appl. Biochem. 59, 65–76.

Gaut, C., Sugaya, K., (2015). Critical review on the physical and mechanical factors involved in tissue engineering of cartilage. Regen. Med. 10, 665–679.

Grayson, W.L., Zhao, F., Izadpanah, R., Bunnell, B., Ma, T., (2006). Effects of hypoxia on human mesenchymal stem cell expansion and plasticity in 3D constructs. J. Cell. Physiol. 207, 331–339.

Hoque, M.E., Chuan, Y.L., Pashby, I., (2012). Extrusion based rapid prototyping technique: An advanced platform for tissue engineering scaffold fabrication. Biopolymers 97, 83–93.

Huang, X., Hou, Y., Zhong, L., Huang, D., Qian, H., Karperien, M., Chen, W., (2017). Promoted Chondrogenesis of Cocultured Chondrocytes and Mesenchymal Stem Cells under Hypoxia Using In-situ Forming Degradable Hydrogel Scaffolds. Biomacromolecules 19, 94–102.

Huang, Y.-Z., Silini, A., Parolini, O., Xie, H.-Q., Huang, Y.-C., Zhang, Y., Deng, L., (2017). Mesenchymal Stem/Progenitor Cells Derived from Articular Cartilage, Synovial Membrane and Synovial Fluid for Cartilage Regeneration: Current Status and Future Perspectives. Stem Cell Rev. Reports 13, 575–586.

Im, G.I., Ko, J.Y., Lee, J.H., (2012). Chondrogenesis of adipose stem cells in a porous polymer scaffold: Influence of the pore size. Cell Transplant. 21, 2397–2405.

Jeon, O., Alsberg, E., (2013). Regulation of stem cell fate in a three-dimensional micropatterned dual-crosslinked hydrogel system. Adv. Funct. Mater. 23, 4765–4775.

Kim, H.J., Lee, J.H., Im, G. Il, (2010). Chondrogenesis using mesenchymal stem cells and PCL scaffolds. J. Biomed. Mater. Res. - Part A 92, 659–666.

Knudson, C.B., Knudson, W., (2001). Cartilage proteoglycans. Semin. Cell Dev. Biol. 12, 69–78.

Koga, H., Muneta, T., Nagase, T., Nimura, A., Ju, Y.J., Mochizuki, T., Sekiya, I., (2008). Comparison of mesenchymal tissues-derived stem cells for in vivo chondrogenesis: Suitable conditions for cell therapy of cartilage defects in rabbit. Cell Tissue Res. 333, 207–215.

Leijten, J., Georgi, N., Moreira Teixeira, L., van Blitterswijk, C.A., Post, J.N., Karperien, M., (2014). Metabolic programming of mesenchymal stromal cells by oxygen tension directs chondrogenic cell fate. Proc. Natl. Acad. Sci. 111, 13954–13959.

Lund-Olesen, K., (1970). Oxygen tension in synovial fluids. Arthritis Rheum. 13, 769–776.

Malladi, P., Xu, Y., Chiou, M., Giaccia, A.J., Longaker, M.T., (2006). Effect of reduced oxygen tension on chondrogenesis and osteogenesis in adipose-derived mesenchymal cells. Am. J. Physiol. Physiol. 290, 1139–1146.

Mazzucco, D., Scott, R., Spector, M., (2004). Composition of joint fluid in patients undergoing total knee replacement and revision arthroplasty: Correlation with flow properties. Biomaterials 25, 4433–4445.

Mota, C., Puppi, D., Chiellini, F., Chiellini, E., (2015). Additive manufacturing techniques for the production of tissue engineering constructs. J. Tissue Eng. Regen. Med. 9, 174–190.

Moura, C.S., Da Silva, C.L., Bártolo, P.J., Ferreira, F.C., (2015). Combination of 3D extruded-based poly (ε-caprolactone) scaffolds with mesenchymal stem/stromal cells: Strategy optimization. Procedia Eng. 110, 122–127.

Nakayama, Y., Narita, T., Mori, A., Uesaka, S., Miyazaki, K., Ito, H., (2002). The effects of age and sex on chondroitin sulfates in normal synovial fluid. Arthritis Rheum. 46, 2105–2108.

Nam, J., Johnson, J., Lannutti, J.J., Agarwal, S., (2011). Modulation of embryonic mesenchymal progenitor cell differentiation via control over pure mechanical modulus in electrospun nanofibers. Acta Biomater. 7, 1516–1524.

Nieto, A., Dua, R., Zhang, C., Boesl, B., Ramaswamy, S., Agarwal, A., (2015). Three Dimensional Graphene Foam/Polymer Hybrid as a High Strength Biocompatible Scaffold. Adv. Funct. Mater. 25, 3916–3924.

Ogata, Y., Mabuchi, Y., Yoshida, M., Suto, E.G., Suzuki, N., Muneta, T., Sekiya, I., Akazawa, C., (2015). Purified human synovium mesenchymal stem cells as a good resource for cartilage regeneration. PLoS One 10, e0129096.

Oliveira, J.T., Reis, R.L., (2011). Polysaccharide-based materials for cartilage tissue engineering applications. J. Tissue Eng. Regen. Med. 5, 421–436.

Pattappa, G., Johnstone, B., Zellner, J., Docheva, D., Angele, P., (2019). The Importance of Physioxia in Mesenchymal Stem Cell Chondrogenesis and the Mechanisms Controlling Its Response. Int. J. Mol. Sci. 20, 1–28.

Pfeifer, C.G., Berner, A., Koch, M., Krutsch, W., Kujat, R., Angele, P., Nerlich, M., Zellner, J., (2016). Higher ratios of hyaluronic acid enhance chondrogenic differentiation of human MSCs in a hyaluronic acid-gelatin composite scaffold. Materials (Basel). 9.

Rodenas-Rochina, J., Kelly, D.J., Gómez Ribelles, J.L., Lebourg, M., (2017). Influence of oxygen levels on chondrogenesis of porcine mesenchymal stem cells cultured in polycaprolactone scaffolds. J. Biomed. Mater. Res. A 105, 1684–1691.

Sakaguchi, Y., Sekiya, I., Yagishita, K., Muneta, T., (2005). Comparison of human stem cells derived from various mesenchymal tissues: Superiority of synovium as a cell source. Arthritis Rheum. 52, 2521–2529.

Santhagunam, A., Dos Santos, F., Madeira, C., Salgueiro, J.B., Cabral, J.M.S., (2013). Isolation and ex vivo expansion of synovial mesenchymal stromal cells for cartilage repair. Cytotherapy 16, 440–453.

Sawatjui, N., Damrongrungruang, T., Leeanansaksiri, W., Jearanaikoon, P., Hongeng, S., Limpaiboon, T., (2015). Silk fibroin/gelatin-chondroitin sulfate-hyaluronic acid effectively enhances in vitro chondrogenesis of bone marrow mesenchymal stem cells. Mater. Sci. Eng. C 52, 90–96.

Schwartz, Z., Griffon, D.J., Fredericks, L.P., Lee, H.-B., Weng, H.-Y., (2011). Hyaluronic acid and chondrogenesis of murine bone marrow mesenchymal stem cells in chitosan sponges. Am. J. Vet. Res. 72, 42–50.

Shirasawa, S., Sekiya, I., Sakaguchi, Y., Yagishita, K., Ichinose, S., Muneta, T., (2006). In vitro chondrogenesis of human synovium-derived mesenchymal stem cells: Optimal condition and comparison with bone marrow-derived cells. J. Cell. Biochem. 97, 84–97.

Silva, J.C., Moura, C.S., Alves, N., Cabral, J.M.S., Ferreira, F.C., (2017). Effects of different fibre alignments and bioactive coatings on mesenchymal stem/stromal cell adhesion and proliferation in poly (ε-caprolactone) scaffolds towards cartilage repair. Procedia Manuf. 12, 132–140.

Tan, A.R., Hung, C.T., (2017). Concise review: Mesenchymal stem cells for functional cartilage tissue engineering: Taking cues from chondrocyte-based constructs. Stem Cells Transl. Med. 6, 1295–1303.

Temple-Wong, M.M., Ren, S., Quach, P., Hansen, B.C., Chen, A.C., Hasegawa, A., D'Lima, D.D., Koziol, J., Masuda, K., Lotz, M.K., Sah, R.L., (2016). Hyaluronan concentration and size distribution in human knee synovial fluid: variations with age and cartilage degeneration. Arthritis Res. Ther. 18, 18.

Theodoridis, K., Aggelidou, E., Vavilis, T., Manthou, M.E., Tsimponis, A., Demiri, E.C., Boukla, A., Salpistis, C., Bakopoulou, A., Mihailidis, A., Kritis, A., (2019). Hyaline cartilage next generation implants from Adipose Tissue Derived Mesenchymal Stem Cells: Comparative study on 3D-Printed Polycaprolactone scaffold patterns. J. Tissue Eng. Regen. Med. 13, 342–355.

Varghese, S., Hwang, N.S., Canver, A.C., Theprungsirikul, P., Lin, D.W., Elisseeff, J., (2008). Chondroitin sulfate based niches for chondrogenic differentiation of mesenchymal stem cells. Matrix Biol. 27, 12–21.

Vinatier, C., Mrugala, D., Jorgensen, C., Guicheux, J., Noël, D., (2009). Cartilage engineering: a crucial combination of cells, biomaterials and biofactors. Trends Biotechnol. 27, 307–314.

Wang, M., Liu, X., Lyu, Z., Gu, H., Li, D., Chen, H., (2017). Glycosaminoglycans (GAGs) and GAG mimetics regulate the behavior of stem cell differentiation. Colloids Surfaces B Biointerfaces 150, 175–182.

Woodruff, M.A., Hutmacher, D.W., (2010). The return of a forgotten polymer - Polycaprolactone in the 21st century. Prog. Polym. Sci. 35, 1217–1256.

Wu, Y., Stoddart, M.J., Wuertz-Kozak, K., Grad, S., Alini, M., Ferguson, S.J., (2017). Hyaluronan supplementation as a mechanical regulator of cartilage tissue development under joint-kinematicmimicking loading. J. R. Soc. Interface 14, 20170255.

Yoshimura, H., Muneta, T., Nimura, A., Yokoyama, A., Koga, H., Sekiya, I., (2007). Comparison of rat mesenchymal stem cells derived from bone marrow, synovium, periosteum, adipose tissue, and muscle. Cell Tissue Res. 327, 449–462.

Zhao, Y., Tan, K., Zhou, Y., Ye, Z., Tan, W.S., (2016). A combinatorial variation in surface chemistry and pore size of three-dimensional porous poly(ε-caprolactone) scaffolds modulates the behaviors of mesenchymal stem cells. Mater. Sci. Eng. C 59, 193–202.

Zhou, S., Cui, Z., Urban, J.P.G., (2004). Factors influencing the oxygen concentration gradient from the synovial surface of articular cartilage to the cartilage-bone interface: A modeling study. Arthritis Rheum. 50, 3915–3924.

Supporting Information

Supplementary Table IV.1. Immunophenotypic characterization of human MSC derived from bone marrow (hBMSC) or synovium (hSMSC) using fluorescence activated cell-sorting (FACS) analysis. Expressions of typical markers for human MSC are presented as average ± standard error of mean (SEM) of two different donors for each cell source.

	Positive expression (%)	
Surface Marker	**hBMSC**	**hSMSC**
CD73	99.76 ± 0.02	98.13 ± 0.50
CD90	98.69 ± 0.80	79.51 ± 3.79
CD105	99.56 ± 0.13	95.60 ± 1.48
CD45	0.74 ± 0.11	0.66 ± 0.64
CD34	0.05 ± 0.03	1.09 ± 0.57
CD14	0.23 ± 0.04	0.64 ± 0.61
CD19	0.13 ± 0.01	0.01 ± 0.02
HLA-DR	0.00 ± 0.00	0.01 ± 0.00

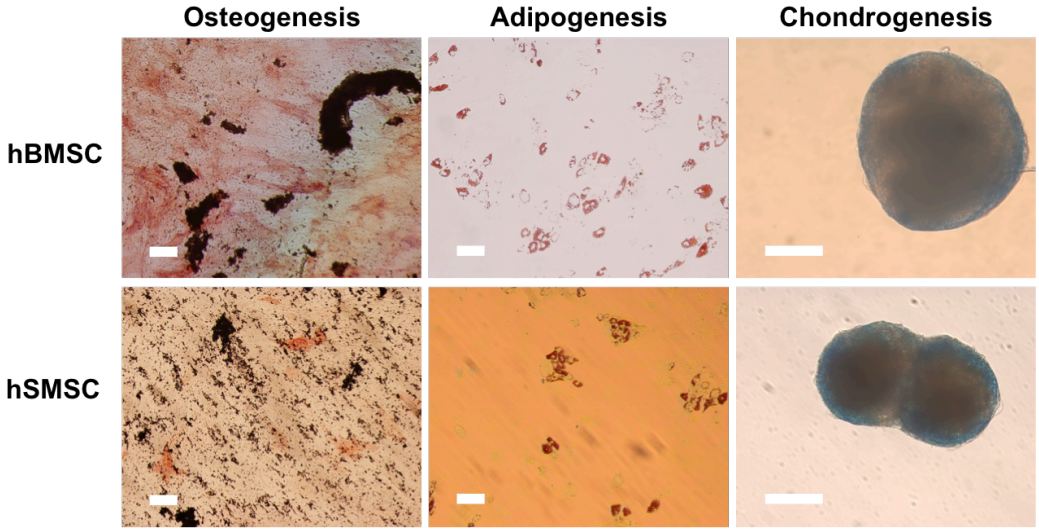

Supplementary Figure IV.1. Multilineage differentiation potential of human MSC isolated from bone marrow (BMSC) or synovium (SMSC) aspirates. After 14 days of specific induction, osteogenic, adipogenic and chondrogenic differentiation were confirmed by ALP/Von-Kossa, Oil-Red-O and Alcian Blue stainings, respectively. Scale bar: 100 µm.

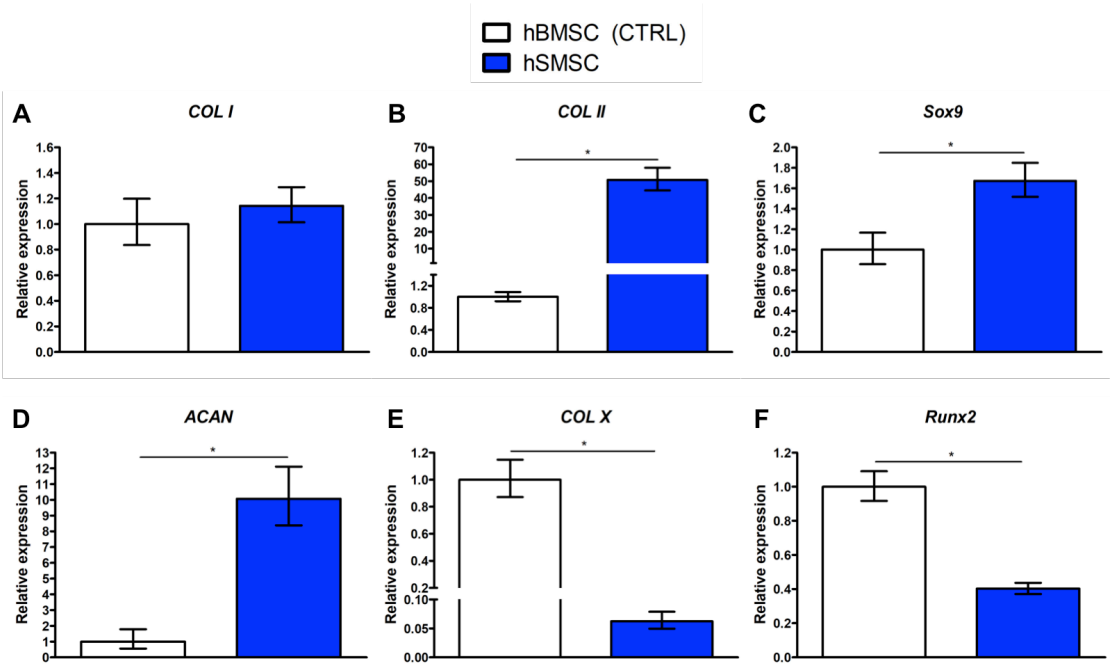

Supplementary Figure IV.2. Gene expression analysis by RT-qPCR of hBMSC and hSMSC before seeding of PCL scaffolds (day 0). *COL I* (A), *COL II* (B), *Sox9* (C), *ACAN* (D), *COL X* (E) and *Runx2* (F) gene expressions are normalized against the housekeeping gene *GAPDH* and presented as fold change levels relative to hBMSC (day 0). Results are presented as average ± standard deviation (SD). *$p < 0.05$ denotes statistical significant differences between hSMSC and hBMSC target gene expressions.

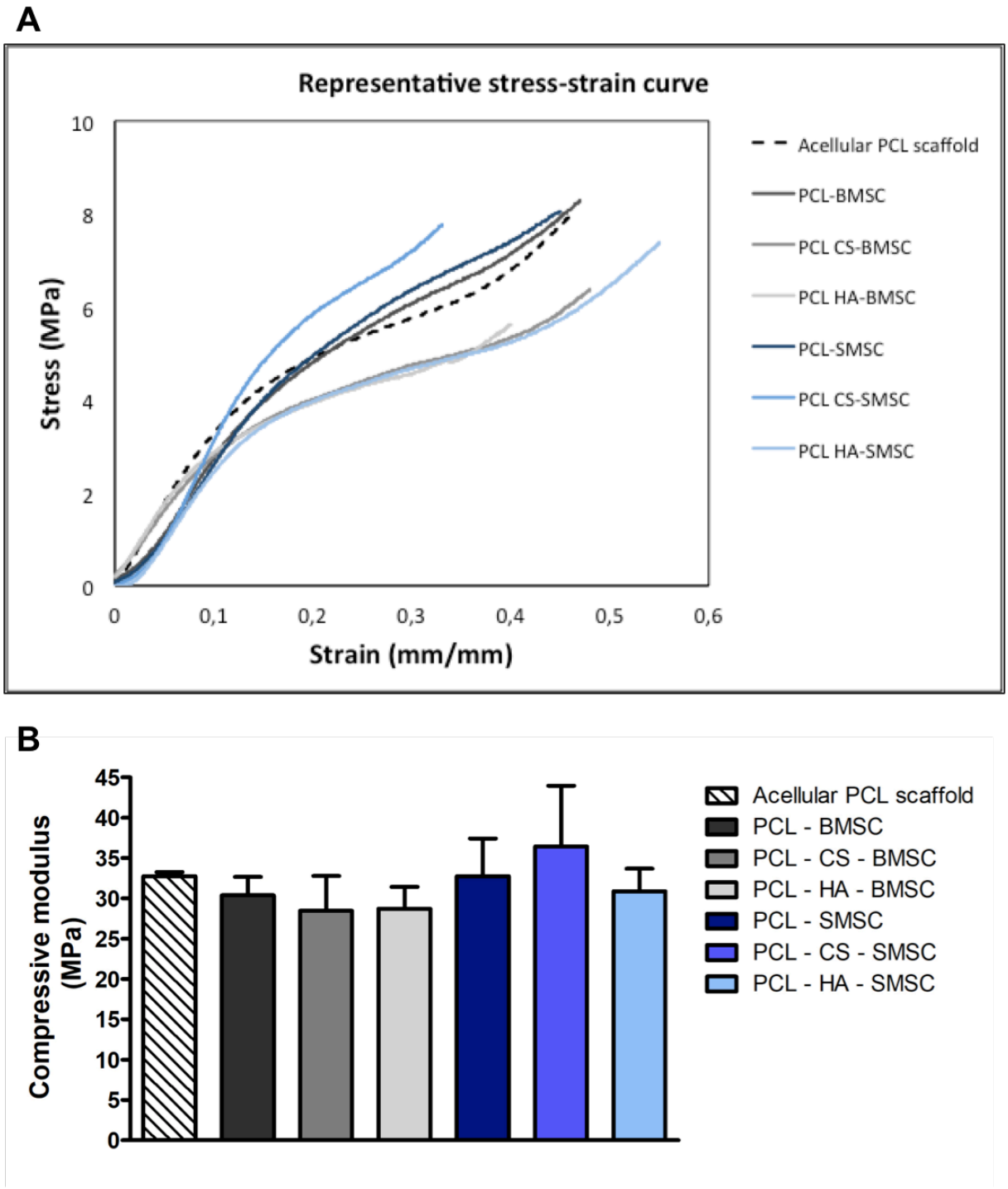

Supplementary Figure IV.3. Compressive mechanical testing of the final hBMSC-PCL/hSMSC-PCL tissue constructs (at day 21) cultured under the different GAG supplementations: Representative stress-strain curves (A) and compressive modulus (B). Results are presented as average ± standard deviation (SD) of four independent samples (n=4).

Chapter V

EXTRUDED PERFUSION BIOREACTOR PROMOTES THE CHONDROGENIC DIFFERENTIATION OF HUMAN MSC IN 3D POROUS PCL SCAFFOLDS

CHAPTER V – Extruded perfusion bioreactor promotes the chondrogenic differentiation of human mesenchymal stem/stromal cells in 3D porous poly (ε-caprolactone) scaffolds

Outline

Novel bioengineering strategies for the *ex vivo* fabrication of native-like tissue-engineered cartilage are crucial for the translation of these approaches to clinically manage highly prevalent and debilitating joint diseases. Bioreactors that provide different biophysical stimuli have been used in tissue engineering approaches aimed at enhancing the quality of the cartilage tissue generated. However, such systems are often highly complex, costly and not very versatile.

In the current study, we propose a novel, cost-effective and customizable perfusion bioreactor fabricated by additive manufacturing (AM) for the study of the effect of fluid flow on the chondrogenic differentiation of human bone-marrow mesenchymal stem/stromal cells (hBMSCs) in 3D porous poly (ε-caprolactone) (PCL) scaffolds. Human bone marrow mesenchymal stem/stromal cells (hBMSCs) were firstly seeded and grown in PCL scaffolds and hBMSCs-PCL constructs were transferred to 3D extrusion bioreactors for continuous perfusion culture under chondrogenic inductive conditions. Perfused constructs showed similar cell proliferation and significantly higher sulfated glycosaminoglycan production (≈1.8-fold) in comparison to non-perfused counterparts. Importantly, perfusion bioreactor culture promoted significantly higher expression of the chondrogenic marker genes while downregulating hypertrophy.

Overall, our results show that the chondrogenic differentiation of hBMSCs was improved in cell-scaffold construct perfusion culture and highlight the potential of customizable AM platforms for developing personalized repair strategies and for more reliable *in vitro* models with a wide range of applications.

V.1. Introduction

Cartilage tissue engineering (CTE) approaches, aiming at fabricating tissue substitutes that recapitulate the biochemical, structural and mechanical properties of native cartilage, have been introduced as promising alternatives to the current clinical surgical methods (Madeira et al., 2015). CTE strategies often comprise a combination of cells (chondrocytes or mesenchymal stem/stromal cells (MSCs)), biomaterial scaffolds and external stimuli through the modulation of biological and/or physical factors (Bernhard and Vunjak-Novakovic, 2016; Madeira et al., 2015; Vinatier et al., 2009).

MSCs have been used in CTE as an attractive alternative to chondrocytes due to their high availability from a wide variety of tissue sources, their high *in vitro* proliferative potential and immunomodulatory/trophic properties, and their ability to differentiate towards cartilage upon induction with proper external cues (Chamberlain et al., 2007; Pittenger et al., 1999; Tan and Hung, 2017).

Biodegradable scaffold matrices based either in naturally occurring or synthetic materials have been widely used in combination with MSCs for CTE strategies (Camarero-Espinosa et al., 2016). Among synthetic materials, poly (ε-caprolactone) (PCL), which was previously approved by the FDA for various medical applications, has been used as scaffold material with MSCs in different cartilage regeneration strategies (Kim et al., 2010; Li et al., 2005; Theodoridis et al., 2019).

Integrated CTE approaches have also employed the use of external cues to augment MSC chondrogenic potential. Such signaling cues can be biochemical (e.g., growth factors – TGF-β superfamily, fibroblast growth factor (FGF)-2 (Mariani et al., 2014; Mauck et al., 2003) or small molecules such as kartogenin (Cai et al., 2019)), environmental (e.g. low oxygen tension to recapitulate the hypoxic environment of articular cartilage *in vivo*) (Leijten et al., 2014) or physical factors (e.g., mechanical/electrical stimulation) (Li et al., 2017; Vaca-González et al., 2017). Low oxygen tension culture conditions have been shown to enhance MSC chondrogenesis in porous scaffolds (Bornes et al., 2015). Bioreactor technology has been successfully employed for the expansion of MSC (Dos Santos et al., 2014) and/or for chondrogenic priming (Gupta et al., 2018), prior to tissue substitute fabrication. In CTE strategies, commercially and tailor-made bioreactor devices have been developed to apply controlled and dynamic mechanical stimuli to cell-seeded scaffolds, aiming to generate cartilage-like tissue *in vitro* through a closer mimicking of the articular motion forces (Hansmann et al., 2013; Li et al., 2017). Examples of mechanical loading applied using bioreactor platforms to regulate MSC chondrogenic differentiation in CTE settings include direct compression (Bian et al., 2011; Huang et al., 2010), hydrostatic pressure (Correia et al., 2012), direct shear stress (Li et al., 2010), fluid-induced shear stress (Gonçalves et al.,

2011; Kock et al., 2014; Mahmoudifar and Doran, 2010), or multimodal biaxial combining different stimuli (Meinert et al., 2017; Schatti et al., 2011). Such bioreactor platforms are often complex systems designed to meet specific requirements for a standardized scaffold structure and biophysical stimuli. A lack of versatility represents a major drawback for the generalized use of bioreactors in personalized CTE strategies, as any modification of the standardized bioreactor often require costly and laborious manufacturing steps (Costa et al., 2014; Martin et al., 2009). Additive manufacturing (AM) technology, such as 3D melt-extrusion, offers a promising alternative to overcome these limitations as it allows versatile and cost-effective fabrication of both scaffold and bioreactor with the desired size, shape and architecture complexity (Mota et al., 2015). Notably, this highly reproducible and versatile approach is fully compliant with a personalized CTE approach as the “patient-tailored” scaffold can be produced to perfectly fit the defect site. Moreover, bioreactor prototypes can be easily customized to provide the specific physical stimuli required for each case.

Fluid perfusion within the constructs allows an efficient nutrient/metabolite transfer and gas exchange beneficial for cartilage extracellular matrix (ECM) synthesis. Additionally, previously published literature suggest that shear stress, resulting from fluid perfusion, favors the chondrogenic differentiation of MSCs (Gonçalves et al., 2011; Mahmoudifar and Doran, 2010). Nevertheless, reports on hypertrophy observed in MSC-based engineered cartilage tissues under perfused culture (Kock et al., 2014) highlight the need for further studies to better understand the effects of fluid-induced shear stress in MSC chondrogenesis and thus optimize its application in CTE approaches.

In this study, we propose a new concept of a cost-effective and customizable perfusion bioreactor, readily fabricated by AM 3D-extrusion, to study the effect of fluid-induced shear stress in the chondrogenic differentiation of human bone marrow MSCs (hBMSCs) in porous PCL scaffolds. Unlike the majority of previous designs, the bioreactor presented here is totally produced by extrusion using standard and commercially available 3D printer and low-cost materials, without the need for additional complex metallic pieces, which allows its widespread use in clinical applications or for academic research purposes. Extruded bioreactor dimensions and perfusion system were conceptualized to allow for the use of several bioreactors in parallel, easily fitted on standard incubator chambers and perfused using a multichannel peristaltic pump. Moreover, this bioreactor platform can easily accommodate multiple scaffolds receiving uniform fluid-flow induced shear stress stimuli simultaneously and allows the simple collection of the engineered tissue constructs, in contrast to other designs requiring a more time-consuming and cumbersome handling Importantly, these devices can be easily modified to receive as many scaffolds as required, with different sizes and shapes according to the patient lesion site. This extruded bioreactor system explores the use of fluid-flow induced shear stress as a single mechanical stimuli to

improve the quality of MSC-based cartilage tissue-engineered constructs. Herein, computer-aided design (CAD) models of the bioreactor prototypes were used for fluid-flow modeling. The perfusion system introduced here significantly enhanced the chondrogenic potential of hBMSC, while preventing tissue hypertrophy, as demonstrated by the results of sulfated glycosaminoglycan (sGAG) production, immunohistochemical and gene expression analysis when compared with cells cultured under static culture conditions.

V.2. Material & Methods

V.2.1. Cell isolation and culture

hBMSCs were isolated from bone marrow (BM) aspirates (two male donors: 35 and 36 years old) and characterized according to a previously established protocol (Dos Santos et al., 2010). BM samples were obtained from healthy donors upon informed consent, with the approval of the Ethics Committee of Instituto Português de Oncologia Francisco Gentil (Laws n° 97/95, n° 46/2004). Isolated hBMSCs were cultured using low-glucose Dulbecco's Modified Eagle's Medium (DMEM, Gibco, Thermo Fisher Scientific, MA USA) supplemented with 10% v/v fetal bovine serum MSC-qualified (FBS, Life Technologies, CA USA) and 1% v/v antibiotic-antimycotic (Anti-Anti, Gibco), kept at 37°C and 5% CO_2 in humidified atmosphere and cryopreserved in a liquid/vapor-phase nitrogen container until further use. All the experiments were performed using cells between passages P3-P5 and culture medium was fully replaced every 3-4 days.

V.2.2. Fabrication and characterization of PCL scaffolds

PCL (MW 50000 Da, CAPA™ 6500, Perstorp Caprolactones, UK) scaffolds were fabricated using in-house developed melt-extrusion equipment, the Bioextruder, and characterized as previously described (Domingos et al., 2009; Silva et al., 2017). Scaffolds were fabricated with the desired size (dimensions: 10mm x 10mm x 3mm) and structure, and with a selected 0-90° lay-down pattern according to previously designed three-dimensional (3D) CAD models (*SolidWorks*® software, Dassault Systèmes, S.A.). The produced scaffolds were characterized in terms of their structure and architectural features by scanning electron microscopy (SEM, Hitachi S-2400, Japan) and micro-computed tomography (μ-CT, Scansky 1174v2, Bruker version 1.1, MA USA).

V.2.3. Design and fabrication of extruded perfusion bioreactors

The bioreactor prototype parts were generated employing CAD (*SolidWorks*® software) and fabricated by melt-extrusion using a commercially available 3D printer (MakerBot® Replicator™ 2X, MakerBot Industries, NY USA). The parts of the cylindrical shape bioreactor were produced in acrylonitrile butadiene styrene (ABS, MakerBot) using the fabrication parameters described in Figure V.1 Biii. Three individual parts composing the bioreactor were extruded: an external vase, an internal part able to perfectly fit the PCL scaffolds and a lid that can assemble a 25 cm^2 t-flask lid with a filter (Corning Inc., NY USA) to allow oxygenation (Figure V.1 Bi-ii). The bioreactor vessel was designed to fit six PCL scaffolds and with a working volume of 25 mL of culture medium. The outer bioreactor surfaces were coated with a thin layer of poly (dimethylsiloxane) (PDMS, SYLGARD™ 184 Silicone Elastomer Kit, Corning Inc., NY USA) to seal any porosity and prevent medium leakage. Additionally, the bioreactor vessel was connected to a peristaltic pump (Ismatec REGLO digital peristaltic pump, Ismatec®, Germany) through Tygon® tubes (Ismatec®) to allow for controlled perfusion with culture medium. The fluid flows in a closed system from the bottom left (inlet) of the bioreactor and leaves the reactor vessel by the top right (outlet), as it is possible to observe in Figure V.3 B.

V.2.4. Computational fluid dynamic analysis

A computational fluid dynamics (CFD) simulation was performed using the *ANSYS*®*Workbench* 2.0 Framework software (version R19.1, ANSYS Inc., PA USA) to predict the fluid velocities in different regions within the bioreactor vessel. The conditions for the computational simulations were defined as: bioreactor working volume = 25 mL; flow rate = 0.2 mL/min (as used in the *in vitro* culture experiments); temperature = 37°C; pressure of 1 atm; flow regime defined as subsonic and turbulence model as laminar. The pressure at the bioreactor vessel outlet was assumed to be zero and the bioreactor chamber was considered as rigid and impermeable.

V.2.5. *In vitro* cytotoxicity testing of the materials comprising the bioreactor platform

The biocompatibility of the ABS material used in the bioreactor (discs with 10 mm diameter and 2 mm thickness produced with different printing infill – 25%, 50%, 75% and 100%) as well as the PCL scaffold was tested following the ISO 10993-5 guidelines ("Biological evaluation of medical devices - Part 5: Tests for cytotoxicity: in vitro methods," 2009) using L929 mouse fibroblasts (ATCC number CCL-1). All materials were evaluated by

the indirect extract test and direct contact test. Cells cultured on tissue culture polystyrene (TCPS) plates with DMEM + 10%FBS + 1%Anti-Anti culture medium under standard conditions were used as negative control and latex was used as positive control for cell death. Extracts were prepared by incubating the materials in culture medium (0.2 g material/mL medium) for 72 h at 37°C and 5% CO_2 under agitation. To perform both tests, L929 fibroblasts were seeded on TCPS plates at a cell density of 1.5×10^5 cells/well and cultured for 24 h at 37°C and 5% CO_2 to obtain a confluent monolayer. Culture medium was removed and cells were exposed to the extract´s conditioned medium for 24 h at 37°C and 5% CO_2 for the indirect extract test. Afterwards, extract conditioned medium was removed and the MTT assay (*In Vitro* Toxicology Assay Kit, MTT based, Sigma-Aldrich, MO USA) was performed according to the manufacturer's guidelines. Briefly, cells were incubated with MTT solution (yellow, 1 mg/mL) for 2 h at 37°C; and the violet formazan product (resultant from the MTT metabolic reduction by metabolically active cells) was dissolved using a 0.1 N HCl solution in anhydrous isopropanol (Sigma-Aldrich). The absorbance of the resultant solution was measured in a plate reader (Infinite® M200 PRO, TECAN, Switzerland) at 570 nm, and the percentage of viable cells for the different samples was calculated by comparison with the values obtained for the negative control cultures. Three samples of each condition were assayed and the absorbance of each sample was measured in triplicate. In the direct contact test, the different materials were placed in contact with a confluent monolayer of L929 fibroblasts and incubated for 24 h at 37°C and 5% CO_2. Cell viability and morphology were qualitatively assessed under an inverted optical microscope (LEICA® DMI3000B, Leica Microsystems, Germany) equipped with a digital camera (Nikon DXM1200F, Nikon Instruments Inc., Japan).

V.2.6. Bioreactor culture of hBMSCs-PCL constructs

PCL scaffolds were sterilized by UV exposure (2 h each side of the scaffold) and by incubation in 70% v/v ethanol for 3 h. The scaffolds were washed three times with a 1% v/v Anti-Anti solution in phosphate buffered saline (PBS, Gibco) for 3 h (1 h each wash) and conditioned with culture medium for 1 h at 37°C. Each PCL scaffold placed on ultra-low attachment plate (VWR) was seeded with 1.5×10^5 hBMSC and incubated for 1.5 h at 37°C and 5% CO_2, before being completely immersed with culture medium, to promote initial cell attachment. hBMSCs were expanded in PCL scaffolds for 14 days in DMEM + 10% FBS + 1% Anti-Anti at 37°C/5% CO_2/21% O_2 and the culture medium was fully renewed twice a week. Prior to dynamic/static culture of hBMSCs-PCL constructs, the bioreactors and tubes were sterilized thoroughly by 70% ethanol and 1% Anti-Anti (in PBS) washing. At day 14, hBMSCs-PCL constructs were transferred to the bioreactor prototypes and cultured under

perfusion (volumetric flow rate of 0.2 mL/min, based in previously reported studies (Mahmoudifar and Doran, 2010, 2005)) or static (non-perfused) conditions with 25 mL of chondrogenic medium (Hyclone™ AdvanceSTEM™ Chondrogenic Differentiation medium, Thermo Scientific, Rockford, IL USA) + 1% Anti-Anti for additional 21 days. All bioreactor cultures were performed at 37°C/5% CO_2 under hypoxic conditions (5% O_2 tension) to generate closer mimicry of the *in vivo* articular cartilage microenvironment and to promote MSC chondrogenic differentiation. For a single experiment, each bioreactor harbored six different hBMSCs-PCL constructs and 50% of culture medium was replaced weekly.

V.2.7. hBMSC viability and proliferation assay

The viability and proliferation of hBMSC in PCL scaffolds were evaluated throughout the 5 weeks of culture (days 1, 7, 14, 21, 28 and 35) by assessing cell metabolic activity using AlamarBlue® cell viability reagent (ThermoFisher Scientific, USA) according to the manufacturer's protocol. In this assay, the scaffolds were removed from the bioreactors and placed in a multi-well plate. AlamarBlue® cell viability reagent was diluted in culture medium (1:10 dilution, v/v), added to the scaffolds and incubated at 37°C in a 5% CO_2 chamber for 2.5 h. Fluorescence intensity values were quantified in triplicate using a plate reader (Infinite® M200 PRO, TECAN) at 560/590 nm excitation/emission wavelengths and compared to a calibration curve (specific for each donor) to estimate the equivalent number of cells in the scaffolds. Acellular PCL scaffolds were used as blank control for the fluorescence intensity measurements.

V.2.8. Metabolite analysis

The concentrations of glucose and lactate were analyzed before and after each medium change during the culture of hBMSC under static conditions in PCL scaffolds and hBMSCs-PCL constructs in the bioreactor. The collected medium samples were centrifuged for 10 min to remove dead cells and debris. Metabolite concentrations were determined using an automatic multi-parameter analyzer (YSI 7100MBS, Yellow Springs Instruments, OH USA). Specific glucose consumption rate, specific lactate production rate and the apparent yield of lactate from glucose ($Y_{Lac/Gluc}$) for defined culture time intervals during hBMSC expansion and chondrogenic differentiation were calculated according to a previously published method (Dos Santos et al., 2010).

V.2.9. Assessment of hBMSC chondrogenic differentiation

V.2.9.1. sGAG detection and quantification assay

At the end of the bioreactor culture (day 35), scaffold samples were harvested, washed thoroughly with PBS to remove all medium remnants, and fixed with 2% paraformaldehyde (PFA, Sigma-Aldrich) solution for 20 min. Samples were incubated with 1% Alcian Blue 8GX (Sigma-Aldrich) solution (in 0.1 N hydrochloric acid) for 1 h to assess for the presence of sGAG. Scaffold constructs were rinsed twice with PBS, washed once with distilled water and imaged using an inverted microscope (LEICA® DMI3000B, Leica Microsystems) equipped with a digital camera (Nikon DXM1200F, Nikon Instruments Inc.). sGAG content of the final tissue constructs was quantified by Alcian Blue dye precipitation following previously reported protocols (Dingle et al., 1975; Nam et al., 2011). In this assay, Alcian Blue stained samples were re-dissolved with a 2% sodium dodecyl sulfate (SDS, Sigma-Aldrich) solution with constant agitation overnight. Absorbance values of the resultant solutions were quantified in a plate reader (Infinite® M200 PRO, TECAN) at 620 nm and compared to a calibration curve to estimate the sGAG content in each construct. The sGAG content was also normalized to the equivalent number of cells previously determined for the respective scaffold. In each independent experiment, three scaffolds per experimental group were considered and the absorbance of each sample was measured in triplicate. Acellular PCL scaffolds submitted to the same protocol were used as blank control for the absorbance measurements.

V.2.9.2. Histological and immunohistochemical analysis

The final tissue constructs obtained after the bioreactor culture were harvested, rinsed with PBS and fixed in 2% PFA. The samples were dehydrated with a progressive graded ethanol series (70%, 90% and 96% (v/v)), cleared with xylene (Sigma-Aldrich) and embedded in paraffin. The paraffin blocks were sliced into 5 μm sections using a microtome Leica RM2235 (Leica Biosystems) and mounted in glass slides. Upon deparaffinization and rehydration of the slides, endogenous peroxidase activity was blocked with 3% v/v hydrogen peroxide (H_2O_2, Sigma-Aldrich) treatment for 10 min. For histological evaluation of the constructs, the cross-sections were stained with haematoxylin-eosin (H&E, Sigma-Aldrich) for 5 min to visualize cells/cell nuclei; 0.1% w/v Toluidine Blue (Sigma-Aldrich) for 5 min to identify proteoglycans; and with 1% w/v Safranin-O (Sigma-Aldrich) for 15 min to observe secreted GAG. In the immunohistochemical analysis, cross-sections were incubated overnight at room temperature with rabbit polyclonal antibodies to collagen II (1:800 dilution,

Anti-Collagen II antibody ab34712, Abcam, UK) and aggrecan (1:250 dilution, Anti-Aggrecan II antibody ab140707, Abcam, UK), followed by incubation for 30 min with anti-rabbit Dako EnVision^{+} System-HRP Labeled Polymer (Agilent Dako, CA USA). Slides were counterstained with haematoxylin, dehydrated and mounted. Images of the histological and immunohistochemical stainings were obtained at 200× magnification using a Leica DMLB optical microscope equipped with a Leica DFC290 HD camera (Leica Microsystems).

V.2.9.3. RNA extraction and real time quantitative PCR (RT-qPCR) analysis

Scaffolds were collected and kept at -80°C until further analysis to quantify the expression of chondrogenic gene markers by cells at the end of perfusion/non-perfusion bioreactor culture. Total RNA was isolated using RNeasy Mini Kit (Quiagen, Hilden, Germany). The scaffolds were first incubated in lysis buffer with agitation for 20 min at 4°C, followed by the total RNA extraction protocol according to the manufacturer's guidelines. RNA was quantified by UV spectrophotometry (NanoVue Plus, GE Healthcare, Chicago, IL USA). cDNA was synthesized from the purified RNA using iScript^{TM} cDNA Synthesis Kit (Bio-Rad, Hercules, CA USA) and the T100^{TM} Thermal Cycler (Bio-Rad) following manufacturer's supplied protocol. The RT-qPCR analysis was performed using Fast SYBR^{TM} Green Master Mix (Applied Biosystems, CA USA) and a StepOne Real-Time PCR System (Applied Biosystems) according with the manufacturer's guidelines. The primer sequences (Stabvida, Portugal) used in the RT-qPCR analysis are specified in Table V.1. All samples were assayed in triplicate and the CT values obtained were normalized against the expression of the housekeeping gene glyceraldehyde-3-phosphate dehydrogenase (*GAPDH*). The analysis was performed using the $2^{-\Delta\Delta CT}$ method, and data was presented as fold-change expression levels relative to hBMSCs at day 0.

Table V.1. Primer sequences used for RT-qPCR analysis.

Gene	Fwd primer sequence	Rev primer sequence
GAPDH	5'-GGTCACCAGGGCTGCTTTTA -3'	5'-CCTGGAAGATGGTGATGGGA-3'
COL I	5'-CATCTCCCCTTCGTTTTTGA-3'	5'-CCAAATCCGATGTTTCTGCT-3'
COL II	5'-GGAATTCCTGGAGCCAAAGG-3'	5'-AGGACCAGTTCTTGAG-3'
Sox9	5'-TACGACTACACCGACCACCA-3'	5'-TTAGCATCATCTCGGCCATC-3'
ACAN	5'-CACTGGCGAGCACTGTAACAT-3'	5'-TCCACTGGTAGTCTTGGGCAT-3'
COL X	5'-CCAGGTCTGGATGGTCCTA-3'	5'-GTCCTCCAACTCCAGGATCA-3'
Runx2	5'-TGTGAGGTGATGTCCTCGTCTGTAG-3'	5'-ACACATATGATGGCCGAGGTGA-3'

V.2.10. Statistical analysis

Results are presented as mean ± standard error of mean (SEM) of the values obtained for three (n=3) independent experiments, unless otherwise specified. Statistical analysis was performed using GraphPad Prism version 7 software (GraphPad Software Inc., La Jolla, USA). Comparisons between independent samples (perfusion bioreactor *vs.* non-perfusion bioreactor) were determined by unpaired student *t* test and data was considered to be statistically significant when *p*-values obtained were less than 5% (*$p < 0.05$).

V.3. Results

V.3.1. Design and fabrication of the perfusion bioreactor system

PCL scaffolds (Figure V.1 Ai) were produced in a controlled layer-by-layer process using an in-house developed AM 3D-extrusion system, and with the desired shape, size and architecture (Silva et al., 2017). The morphological features of the fabricated scaffolds were assessed by μ-CT (Figure V.1 Aii) and SEM (Figure V.1 Aiii) analysis. Scaffolds with a 0-90° fiber orientation and a pore size of 390 μm were generated to achieve high porosity (56.6%) and high interconnectivity (99.7%), which favor efficient gas exchange, nutrient supply and waste removal.

Bioreactor prototypes were fabricated from in-house designed CAD models (Figure V.1 Bi) using a commercially available 3D extrusion system. As demonstrated in Figure V.1 B, three parts extruded independently were assembled to compose the whole bioreactor (Figure V.1 Bii): an external vase, an inner part customized to perfectly accommodate the PCL scaffolds and a lid that can harbour a vented t-flask cap. The prototype was developed to allow fluid perfusion of the scaffolds inside the bioreactor by connection through tubing to a peristaltic pump. Culture medium enters the bioreactor vessel from the bottom left part (inlet), flows through a thin chamber on the bottom of the reactor and then upstream, through a porous disperser in the bottom surface of the bioreactor into the scaffolds chamber. Then, the culture medium exits the system from the top right (outlet). Additionally, based on this concept, the bioreactor was custom-made to accommodate six PCL scaffolds with a working volume of 25 mL using the extrusion parameters summarized in Figure V.1 Biii.

Prior to cell culture experiments, the materials (ABS disks with different printing infill and PCL scaffolds) were tested for cytotoxicity using L929 fibroblasts following ISO 10993-5 guidelines (Supplementary Figure V.1). The MTT extract indirect test (Supplementary Figure V.1 A) showed that cells cultured with the extracts obtained from culture incubation of the different materials presented high cell viabilities over 86%, while cells cultured in direct

contact with the same materials presented regular fibroblast morphology with no evidence of any inhibition halo effect or cell death (Supplementary Figure V.1 B).

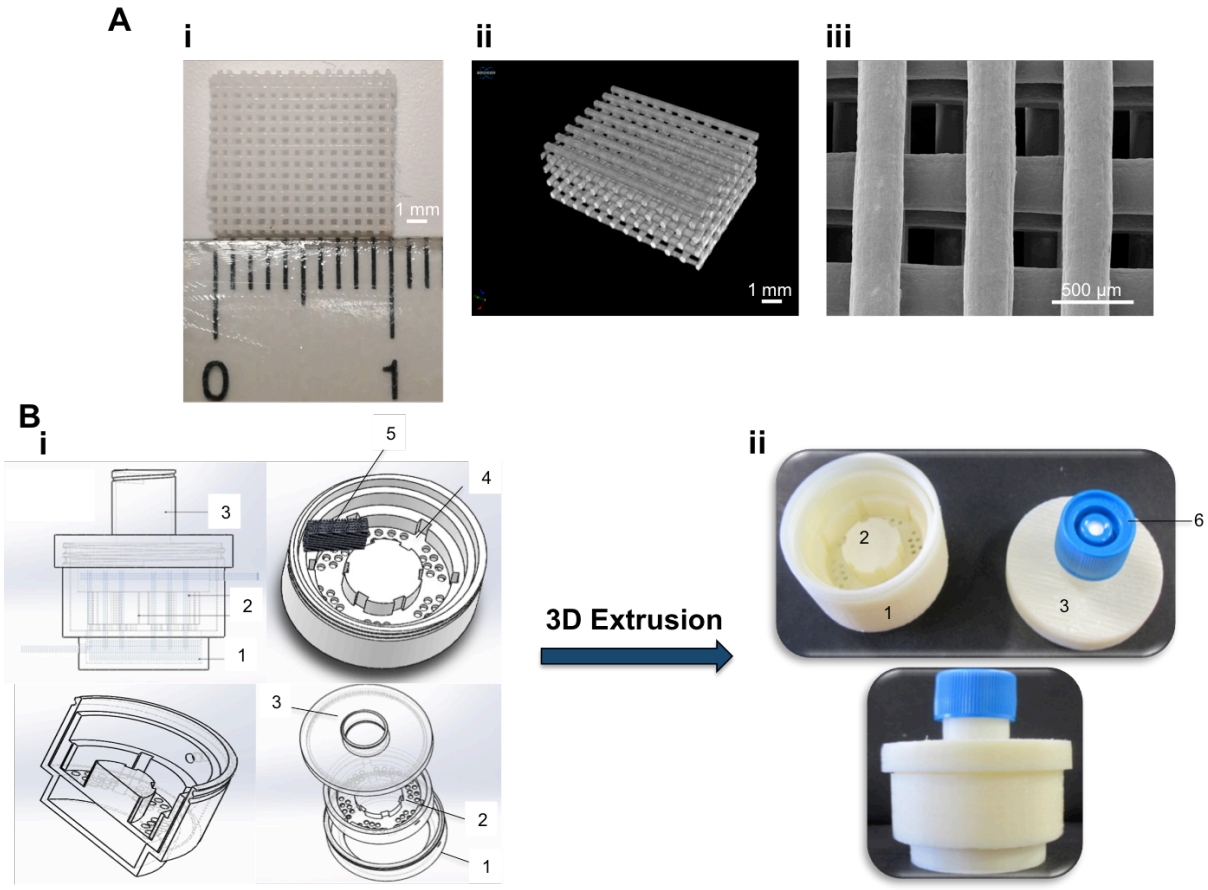

iii Bioreactor fabrication parameters:

Material	Acrylonitrile butadiene styrene (ABS)
Printing infill	100%
Layer height	0.2 mm
Extrusion head temperature	230°C
Build plate temperature	110°C
Speed while extruding	50 mm/s
Bioreactor mass	39.4 g
Working volume	25 mL
# scaffold compartments	6

Figure V.1. Fabrication of PCL scaffold (A) and extruded bioreactor platform (B). Characterization of 3D extruded PCL scaffolds structure: photograph of a PCL scaffold with 10 mm × 10 mm × 3 mm dimensions (Ai), respective 3D reconstruction image obtained after µ-CT analysis (Aii) and SEM micrograph (Aiii). Scale bar: 1 mm for (i), (ii) and 500 µm for (iii). CAD models of the parts composing the bioreactor prototype were developed using *SolidWorks*® software (Bi). The bioreactor consists of an external vase (1), an internal part (2) with a bottom porous disperser and a scaffold chamber including compartments (4) to perfectly fit six PCL scaffolds (5), and a lid (3) designed to assemble a filter t-flask cap (6) to allow oxygenation. Fluid flows in a closed system (through tubing and a peristaltic pump), entering the bioreactor from the bottom left (inlet) and leaves the vessel by the top right (outlet). Prior to whole bioreactor assembly, the parts were fabricated in ABS material by 3D melt-extrusion (Bii) using defined printing parameters (Biii).

V.3.2. CFD analysis predicts fluid velocities distribution within the bioreactor

CFD modelling was used to simulate the flow pattern of the culture medium within the extruded perfusion bioreactor vessel (Figure V.2 and Supplementary Figure V.2). Prior to CFD analysis, a CAD model of the volume geometry of the bioreactor was imported from *SolidWorks*® and a respective mesh was created in *ANSYS*®. For the perfusion flow rate defined for the *in vitro* culture assays (0.2 mL/min), it was estimated a residential time (time needed for the total replacement of the working volume in the bioreactor vessel) of 125 min (≈ 2.08 h). Figure V.2 C shows the predicted fluid velocity distributions and values along six different horizontal planes inside the bioreactor vessel: a top plane near the outlet right above the scaffolds (1), three planes intersecting the scaffolds (2-4), a plane at the top surface of the bottom porous fluid disperser below the scaffols (5) and a plane at the lower surface of the bottom porous fluid disperser (6). In this configuration, the maximum linear velocities were observed near the inlet and outlet of the bioreactor, with an estimated value of approximately 1.22×10^{-5} m/s. The observation of the three planes (2-4) intersecting the scaffold compartments suggests that the fluid velocity distributions are quite homogeneous along all the six scaffolds surface. Moreover, this analysis indicates that the tangential fluid velocity values experienced by the scaffolds are quite low, which were previously hypothesized to favour chondrogenic phenotype maintenance (Carter and Wong, 2003; Stevens et al., 1999). The fluid perfusion through the bottom fluid disperser pores (plane 6 to 5) increased fluid velocities in the parallel regions between two adjacent scaffold compartments. Importantly, as it is possible to observe in Figure V.2 A, B and Figure V.1 Bi, the disperser was designed with no pores in the regions bellow the scaffold compartments to avoid the occurrence of high fluid velocities which may induce harmful or unwanted mechanical effects on the cell-scaffold constructs. An additional CFD analysis, predicting the fluid-flow velocities patterns and intensities in three different horizontal (Supplementary Figure V.2 Ai-iv) and vertical (Supplementary Figure V.2 Bi-iv) planes, is also provided. Overall, our simulation results demonstrate homogeneous fluid perfusion in the regions tangential to the scaffolds, suggesting uniform hydrodynamic stress conditions at scaffold surface.

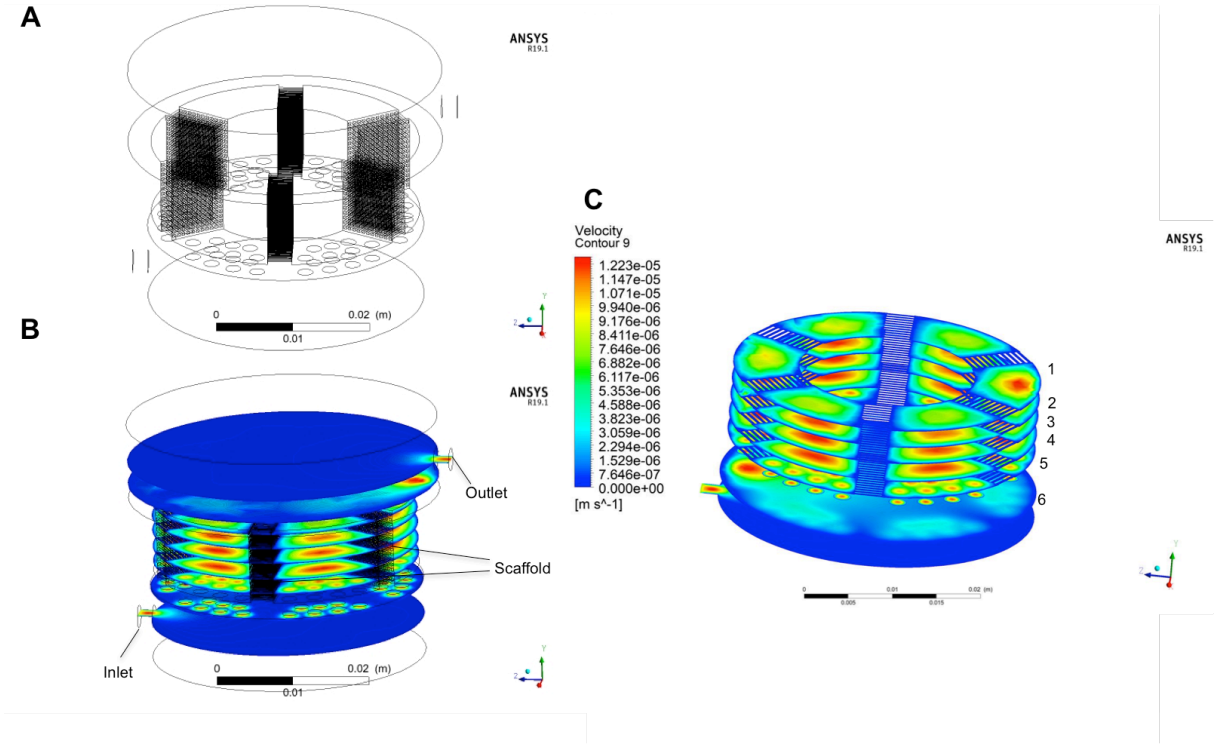

Figure V.2. Computational fluid flow modeling predicts linear velocities distribution within the bioreactor. Representative model of the bioreactor inner region considered in the CFD analysis, specifying the location of the PCL scaffolds (A). Contour plot with the linear fluid velocities distribution inside the bioreactor, highlighting the inlet and outlet regions of the system (B). Fluid velocity distributions and values for linear velocities (expressed in m/s) for different horizontal planes (corresponding to different regions – a top plane near the outlet right above the scaffolds (1), three planes intersecting the scaffolds (2-4), a plane at the top surface of the bottom porous fluid disperser, right below the scaffolds (5) and a plane at the lower surface of the bottom porous fluid disperser (6)) within the bioreactor vessel (C). CFD analysis was performed using *ANSYS*® software version R19.1 with the following parameters: 25 mL fluid volume in the bioreactor vessel; fluid perfusion rate of 0.2 mL/min; ambient conditions of 37°C and 1 atm; flow regime defined as subsonic and turbulence model as laminar. The pressure at the bioreactor vessel outlet was assumed to be zero and the bioreactor chamber was considered as rigid and impermeable.

V.3.3 Bioreactor culture of hBMSCs-PCL constructs

The *in vitro* assays for bioreactor culture were performed following the experimental scheme presented in Figure V.3 A. hBMSCs were expanded in PCL scaffolds for 2 weeks under static culture conditions in DMEM + 10% FBS + 1% Anti-Anti, and afterwards, the hBMSCs-PCL constructs were transferred to the ABS extruded perfusion bioreactors and cultured with a 0.2 mL/min flow rate of chondrogenic medium at 37°C/5% CO_2/5% O_2 (Figure V.3 A, B). A bioreactor culture operating without perfusion was used as a control. The number of cells present in the PCL scaffolds throughout all culture monitored by AlamarBlue® cell viability assay are presented in Figure V.3 C. As expected, cell numbers increased considerably during the first 14 days of culture in DMEM + 10% FBS + 1% Anti-Anti, and were maintained during the following 21 days under chondrogenic induction. Additionally,

cells remained viable without significant differences in equivalent cell numbers between non-perfusion and perfusion cultures in the bioreactor, reaching final equivalent cell number values per scaffold at day 35 of $(1.31 \pm 0.13) \times 10^5$ and $(1.32 \pm 0.17) \times 10^5$, respectively.

The concentrations of glucose (Figure V.3 Di) and lactate (Figure V.3 Dii) in the cell culture supernatants were measured to evaluate the cell metabolic profile throughout all culture (in static expansion and bioreactor differentiation stage). As expected, for both non-perfused/perfused bioreactors, glucose concentration decreased between each medium change while lactate concentration showed an opposite trend. Additionally, under both conditions tested and throughout all culture time, glucose was always available (never reaching values close to 0 mM), while lactate concentration never reached inhibitory values (over 35 mM previously defined for human MSC (Schop et al., 2009)), with maximum values of 10.45 ± 0.07 mM and 11.75 ± 0.21 mM, observed at day 35 for bioreactor culture under static conditions and perfusion, respectively. Glucose consumption, lactate production and apparent yield of lactate from glucose throughout all culture experiments were calculated and are presented in Supplementary Figure V.3. Under both conditions, a higher glucose specific consumption rate (Supplementary Figure V.3 A) and lactate specific production rate (Supplementary Figure V.3 B) were observed during the expansion phase under static conditions, in comparison to the differentiation stage. From day 14 onwards, the glucose specific consumption rate and lactate specific production rate values were considerably reduced, suggesting a lower cell metabolism during chondrogenic differentiation in bioreactor cultures under non-perfusion and perfusion conditions. Moreover, $Y_{Lac/Gluc}$ (Supplementary Figure V.3 C) during all culture stages (expansion and chondrogenic differentiation) were also calculated, ranging from 1.61 ± 0.07 to 3.19 ± 0.19 for non-perfused culture in the bioreactor (average $Y_{Lac/Gluc}$ = 2.37 during expansion; average $Y_{Lac/Gluc}$ = 2.51 during differentiation; and average $Y_{Lac/Gluc}$ = 2.45 for all culture) and 1.48 ± 0.04 to 2.94 ± 0.04 for perfusion bioreactor condition (average $Y_{Lac/Gluc}$ = 2.23 during expansion; average $Y_{Lac/Gluc}$ = 2.52 during differentiation; and average $Y_{Lac/Gluc}$ = 2.39 for all culture).

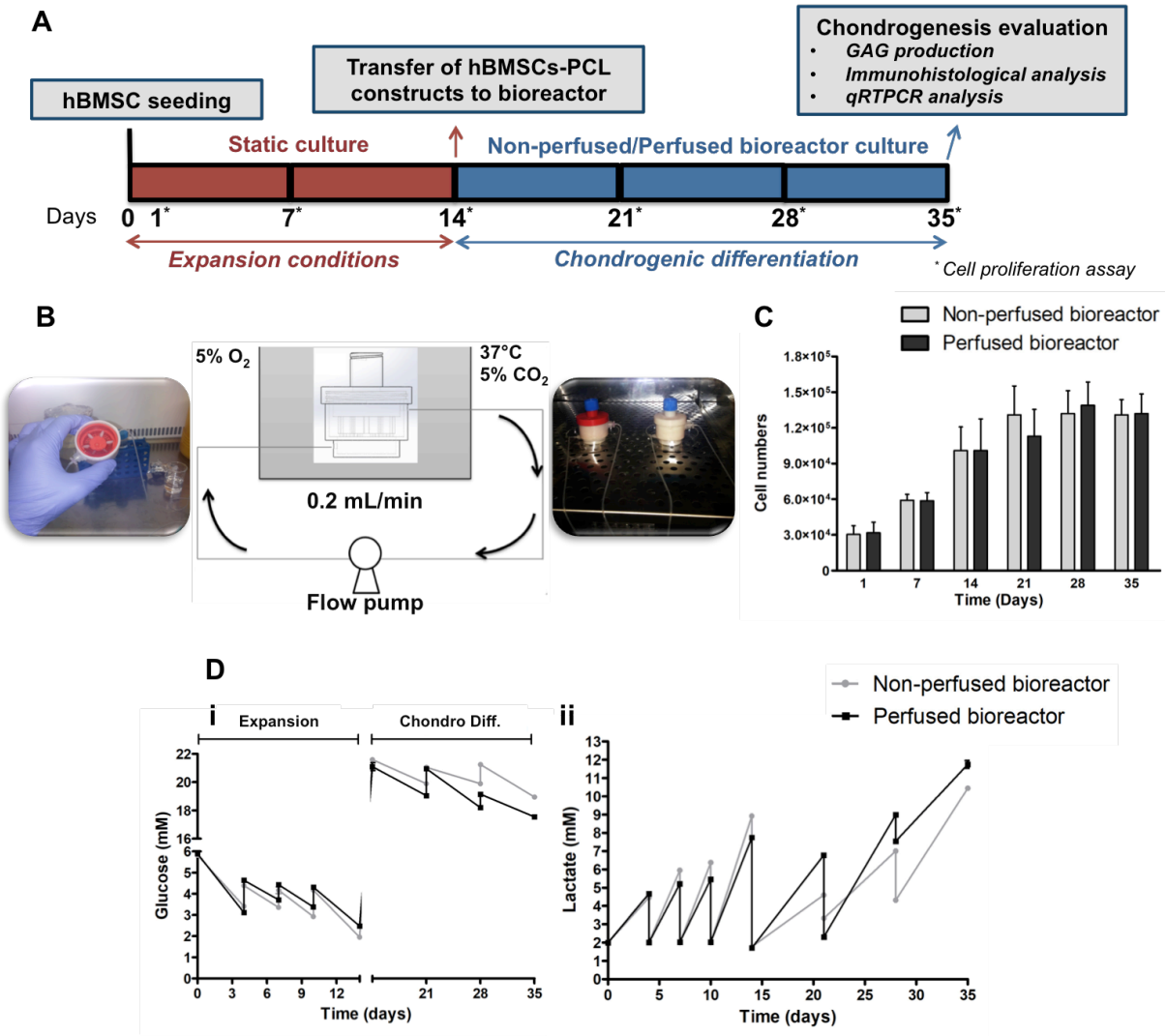

Figure V.3. Bioreactor culture of hBMSCs-PCL constructs. Scheme of the experimental plan followed (A). hBMSC were seeded on the PCL scaffolds and cultured under standard expansion conditions for 2 weeks; at day 14, hBMSCs-PCL constructs were transferred to non-perfused/perfused bioreactors and exposed to chondrogenic induction conditions for 3 weeks. Representative images and culture conditions scheme (hypoxic environment 5%O_2 / continuous flow rate of 0.2 mL/min) for the perfused culture of hBMSCs-PCL constructs (B). Cell proliferation throughout culture (C). Metabolic analyses throughout culture (D) expressed by the concentration profiles (in mM) for glucose (i) and lactate (ii). Note that the initial glucose concentration of expansion medium is 1.0 g/L while for the chondrogenic differentiation medium is ≈4.0 g/L. Results for cell numbers in non-perfused/perfused constructs are represented as mean ± SEM of three (n=3) independent experiments.

V.3.4 Perfusion culture enhances cartilage ECM production

At the end of bioreactor culture, the generated constructs were harvested and were assessed for the presence of typical cartilage ECM components. Both tissue constructs obtained after static or perfused bioreactor culture stained positively for Alcian Blue (Figure V.4 A), confirming the presence of sGAG. However, as it is shown in Figure V.4 B, perfused constructs presented a significantly higher ($p < 0.05$) amount of sGAG (15.88 ± 0.88 μg/10^5 cells) compared to constructs cultured without perfusion (9.05 ± 1.83 μg/10^5 cells). In fact, this observation suggests a beneficial effect of perfusion culture in promoting sGAG production by cells, resulting in an approximately 1.8-fold increase compared to non-perfused constructs.

The final constructs were also processed and evaluated by histological (Figure V.4 C) and immunohistochemical analysis (Figure V.4 D). Both non-perfused/perfused constructs showed the presence of cells with defined nuclei after H&E staining (Figure V.4 Ci-ii). Additionally, Toluidine Blue (Figure V.4 Ciii-iv) and Safranin-O (Figure V.4 Cv-vi) positive stainings for both conditions confirmed the presence of proteoglycans and GAG, respectively. Importantly, the apparently more intensive staining observed in Figure V.4 Civ and Figure V.4 Cvi is consistent with the higher sGAG content (Figure V.4 B) observed for constructs obtained after perfusion bioreactor culture. Figure V.4 D shows the images resultant from the immunodetection protocol performed on the final constructs to assess for the presence of main cartilage ECM components, collagen II (Figure V.4 D i-ii) and aggrecan (Figure V.4 Diii-iv). While bioreactor culture under static conditions (Figure V.4 Di) and perfusion bioreactor culture (Figure V.4 Dii) lead to constructs staining positive for the presence of collagen II, the same was not observed for aggrecan. Perfused constructs showed more abundant and distributed positive staining for aggrecan (Figure V.4 Div), in contrast to the small spots of lower aggrecan expression (highlighted by the black arrows) verified for the non-perfusion condition (Figure V.4 Diii). The higher aggrecan expression observed after perfusion culture is concordant with the results presented above for sGAG amounts and histological analysis.

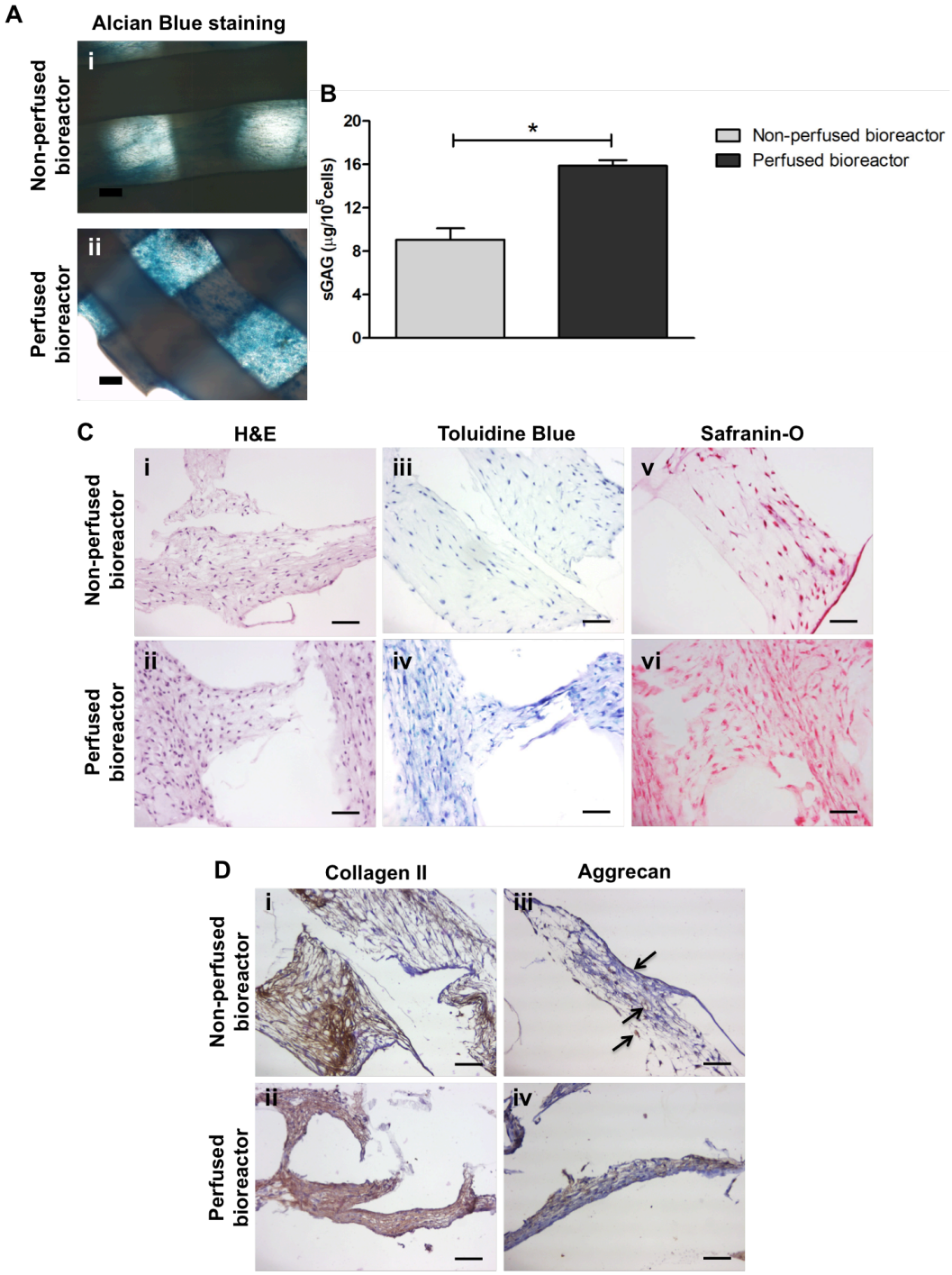

Figure V.4. Perfused bioreactor culture of hBMSCs-PCL constructs promotes cartilage ECM production. Alcian Blue staining (A) in the final hBMSCs-PCL constructs detects sGAG deposition after static (i) or perfusion (ii) bioreactor culture. Scale bar: 100 μm. Quantification of the amount of sGAG per number of cells present in the final constructs obtained after non-perfused/perfused bioreactor culture (B). Results are expressed as mean ± SEM of three (n=3) independent experiments. *p < 0.05. Histological analysis (C) of the final tissue constructs generated after static/perfused bioreactor culture: H&E (i, ii), Toluidine Blue (iii, iv), and Safranin-O (v, vi) staining. Scale bar: 50 μm. Immunohistochemical analysis (D) of the final tissue constructs to detect main cartilage ECM components collagen II (static bioreactor (i) and perfusion bioreactor (ii)) and aggrecan (static bioreactor (iii) and perfusion bioreactor (iv)). Positive staining is observed in brown and samples were counterstained with haematoxylin. Black arrows highlight small spots of aggrecan expression. Scale bar: 50 μm.

V.3.5. Flow-perfusion promotes the expression of chondrogenic genes while reducing hypertrophy

RT-qPCR analysis was performed to assess the effects of the perfusion culture in the chondrogenic gene expression profile of the final constructs. RNA was isolated prior to scaffold seeding (day 0) and from constructs harvested after bioreactor culture under non-perfusion/perfusion conditions (day 35). Figure V.5 shows the values for gene expression of chondrogenic markers *Sox9* (Figure V.5 A), *ACAN* (Figure V.5 C), *COL II* (Figure V.5 E), fibrocartilage marker *COL I* (Figure V.5 B), hypertrophy marker *COL X* (Figure V.5 D) and osteogenic marker *Runx2* (Figure V.5 E), normalized to the housekeeping gene *GAPDH* expression and presented as fold-change relative to the values obtained for hBMSC at day 0. Perfused constructs presented significantly higher ($p < 0.05$) expression of chondrogenic markers *Sox9*, *ACAN* and *COL II* compared to constructs cultured without perfusion. Such enhancement was considerably more pronounced for the expression of the main chondrocyte marker *COL II*. Regarding the expression of *COL I* and *Runx2*, both conditions showed downregulation relative to hBMSCs at day 0, however no statistical differences were observed. Notably, the perfusion bioreactor platform developed here operating with a flow rate of 0.2 ml/min resulted in a statistical significant decrease ($p < 0.05$) in the expression of the hypertrophic marker *COL X* when compared to bioreactor culture under static conditions.

Thus, our RT-qPCR results suggest that perfused bioreactor culture of hBMSCs-PCL constructs favored MSC chondrogenic differentiation while preventing tissue hypertrophy observed for non-perfused constructs.

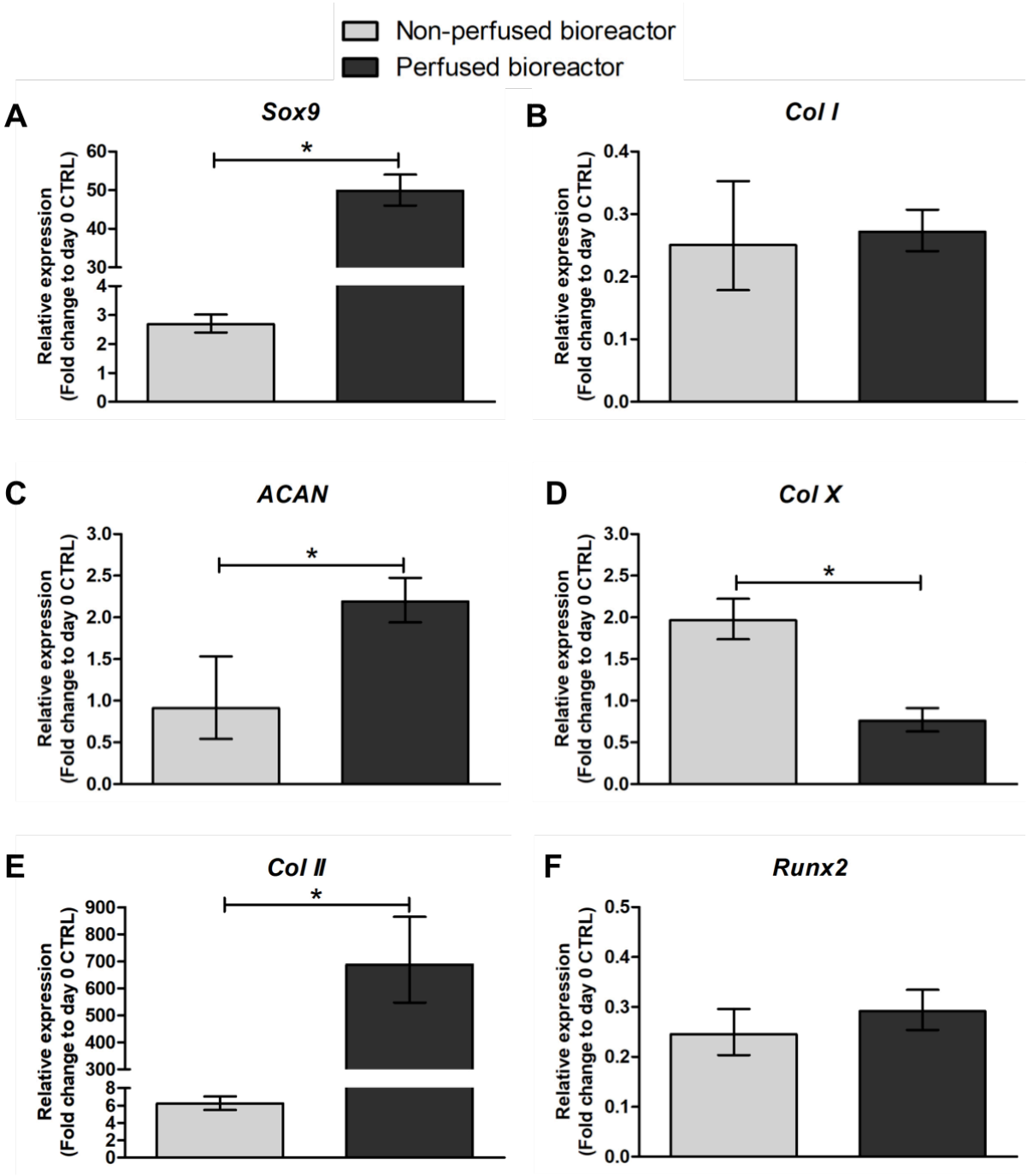

Figure V.5. Gene expression evaluation by RT-qPCR analysis of the final tissue constructs obtained after non-perfused/perfused bioreactor culture. *Sox9* (A), *Col I* (B), *ACAN* (C), *Col X* (D) *Col II* (E) and *Runx2* (F) *gene* expressions are normalized against the housekeeping gene *GAPDH* and presented as fold-change levels relative to hBMSC at day 0 prior to scaffold seeding. Values are represented as mean ± SEM of 3 independent experiments. *$p < 0.05$.

V.4. Discussion

The role of mechanical signals in the regulation of MSC fate has been demonstrated and explored for a broad range of tissue engineering strategies (Hao et al., 2015; Kelly and Jacobs, 2010). In CTE, mechanical stimuli such as fluid flow-induced shear stress, compression, tension and hydrostatic pressure have been applied alone or combined using bioreactor systems and demonstrated to promote the chondrogenic potential of MSC (Correia et al., 2012; Fahy et al., 2018; Huang et al., 2010; Kock et al., 2014; Li et al., 2017; Mahmoudifar and Doran, 2010; Meinert et al., 2017; Salinas et al., 2018; Schatti et al., 2011). However, the molecular mechanisms involved in the MSC mechanotransduction signaling are not fully understood (Panadero et al., 2016). Flow perfusion has been applied for the production of both MSC-based tissue engineered bone (Chen et al., 2017; Costa et al., 2014) and cartilage (Alves da Silva et al., 2011; Gonçalves et al., 2011; Mahmoudifar and Doran, 2010). It has been suggested that different magnitudes of shear stress generated by fluid perfusion result into distinct engineered cartilage phenotypes (Carter and Wong, 2003; Kock et al., 2014). Therefore, more studies on the effects of fluid perfusion on MSC chondrogenic differentiation are needed to deepen our understanding of the underlying molecular signaling involved and to define boundary stimulation conditions for magnitudes and regimes envisaging improved protocols for CTE approaches.

Bioreactors used to provide different mechanical stimuli in CTE are often complex systems designed to meet the requirements for a standardized scaffold size and architecture. Recently, AM technologies, which revolutionized the tissue engineering field by making possible the development of anatomically complex patient-customized implants, were also used for the manufacturing of versatile and cost-effective bioreactor platforms that can be easily modified according to the specificities of the target application (Costa et al., 2015, 2014; Mota et al., 2015). The possibility of fabricating both scaffold and bioreactor device with a high degree of customization and process automation is a critical step towards the efficient, fast and reproducible production of personalized high-quality tissue substitutes.

In the present work, we used CAD and 3D-extrusion to manufacture a custom-made bioreactor platform that allows study the effect of fluid perfusion on the chondrogenic differentiation of MSC in 3D porous PCL scaffolds, also fabricated by extrusion. CFD has been described as an invaluable tool to predict and visualize the distribution of fluidic velocities and forces within a bioreactor system, enabling a better understanding of the role of the hydrodynamic environment in tissue engineering strategies (Hutmacher and Singh, 2008). Herein, we performed a CFD analysis to predict fluid velocities distribution and intensity in different regions of the bioreactor in order to avoid any detrimental effects on the cells caused by shear stresses too high or by insufficient nutrient transfer. Additionally, our

analysis predicted a homogeneous fluid perfusion in the regions tangential to the scaffolds, suggesting that all six scaffolds within the bioreactor would be exposed to similar hydrodynamic conditions. Prior to *in vitro* cell culture experiments, ABS material used to fabricate the bioreactor was tested for different printing infill following the ISO 10993-5 guidelines and demonstrated high biocompatibility, which is in accordance with previously published literature on the use of ABS as scaffold for CTE (Rosenzweig et al., 2015).

Similar to other studies focusing chondrogenic differentiation (Kock et al., 2014; Tiğli et al., 2011), we promoted an expansion phase to allow hBMSC growth and spreading throughout the PCL scaffolds, and afterwards, hBMSC-PCL constructs were transferred to perfusion bioreactor for mechanical stimulation. No statistical differences were observed in equivalent cell numbers between perfused and non-perfused bioreactor culture, confirming that the flow rate selected did not cause any detrimental effect to cell viability and proliferation. Concordant results were reported by Tiğli et al. (Tiğli et al., 2011), who observed no significant differences in cell proliferation between non-perfusion and perfusion culture of human embryonic stem cells - derived MSC in porous silk scaffolds under chondrogenic induction. Additionally, Alves da Silva and colleagues (Alves Da Silva et al., 2010) reported no differences in cell proliferation between static and perfused culture of PCL nanofiber meshes seeded with hBMSCs, during 21 days under chondrogenic differentiation conditions.

Our metabolite analysis, performed both during hBMSCs static expansion in PCL scaffolds placed in TCPS plates and chondrogenic differentiation in the bioreactor under static conditions or perfusion, revealed that glucose exhaustion was never observed during the culture time. Moreover, inhibitory lactate concentrations for MSCs over 35 mM (Schop et al., 2009) were never reached throughout all culture period, indicating that the medium changes protocol used was sufficient. Our results for glucose consumption/lactate production rates indicate a higher MSC energy metabolism during expansion with a considerable reduction during chondrogenesis, which is in accordance with the described by Pattappa et al. for pellet chondrogenic cultures (Pattappa et al., 2011). Moreover, Gupta and colleagues also observed a decrease in glucose consumption and lactate production during chondrogenic differentiation of human periosteum derived progenitor cells in spinner flasks (Gupta et al., 2018). MSCs have a metabolic requirement dominated by aerobic glycolysis during self-renewal, while upon differentiation, the metabolism shifts to oxidative phosphorylation (Folmes et al., 2012; Liu et al., 2014). We observed apparent yields of lactate from glucose higher than 2 under both culture conditions, suggesting that lactate is being generated from alternative carbon sources, such as glutamine (Eibes et al., 2010).

Fluid perfusion in the bioreactor system produces shear stress that was previouly shown to influence MSC differentiation processes (Yeatts et al., 2013; Rodrigues et al., 2011). At

the end of the experiment, perfused constructs showed a statistically significant higher sGAG amounts than the values obtained in non-perfusion culture, suggesting a favorable effect of flow perfusion in the production of cartilage ECM. This was also suggested by histological and immunohistochemical analysis of the final tissue constructs, mainly by the evidence of considerable higher expression and distribution of main cartilage constituent aggrecan after perfusion bioreactor culture, which is in accordance with the increased sGAG amounts and the more intense Toluidine Blue and Safranin-O staining. Our histological/immunohistochemical analysis data is in agreement with previous studies on the effect of perfusion culture in MSC chondrogenesis in CTE scaffolds (Alves da Silva et al., 2011; Alves Da Silva et al., 2010). Despite some authors reporting detrimental effects in sGAG production after perfusion culture (Gonçalves et al., 2011; Kock et al., 2014), other studies also show significantly higher amounts in perfused constructs (Schatti et al., 2011; Tiğli et al., 2011), which is in agreement with our results.

Gene expression results, namely the significantly higher expression levels of *Sox9*, *ACAN* and *COL II* compared to non-perfused culture, as well as downregulation of *Runx2* and *COL I*, indicate that the flow perfusion culture protocol, using the bioreactor developed here, promotes MSC chondrogenic differentiation in 3D porous PCL scaffolds. Additionally, the perfused constructs presented significantly lower *COL X* expression than the non-perfused counterparts, suggesting a role of flow-induced shear stress in preventing tissue hypertrophy. MSC differentiation fate regulation through perfusion has also been predicted to be dependent on the flow rate magnitudes involved (Carter and Wong, 2003; Salinas et al., 2018). A previous study using a perfusion bioreactor with a flow rate of 1 mL/min to promote chondrogenesis, showed similar trends for cartilage marker genes, however data on *COL X* expression was not provided (Tiğli et al., 2011). Interestingly, despite evidence of tissue hypertrophy, Kock et al. (Kock et al., 2014) also reported a decrease in *COL X* expression upon 28 days of perfusion culture of MSC pellet-PCL scaffold constructs when compared to static culture. However, it was also observed a significant decrease in the secreted GAG amount in perfused constructs, suggesting an unwanted effect resulting from flow perfusion. In fact, the flow rate used in the present study (0.2 mL/min) is approximately 6-fold lower than the one used by Kock et al. (1.22 mL/min), which might be the reason for the different outcomes observed and is in agreement with the previous hypotheses that exposure of chondrocytes to low fluid-induced shear stress favors the maintenance of a chondrogenic phenotype, whereas high magnitudes promotes cartilage hypertrophy and fibrous tissue formation (Carter and Wong, 2003; Stevens et al., 1999; Tagil and Aspenberg, 1999). Moreover, another study also reported decreased expression of the hypertrophic marker *COL X* in chitosan-based scaffolds cultured with hBMSC in a perfusion bioreactor (0.1 mL/min), in comparison to the constructs maintained without perfusion (Alves da Silva et al.,

2011). Interestingly, two recent studies highlighted the rate of fluid shear stress as an effective regulator of the chondrogenic differentiation of MSC in 2D-culture conditions (Lu et al., 2016; Yue et al., 2018). Nevertheless, when making comparisons, it is important to consider the differences in bioreactor platform geometry and flow rate magnitudes/regimes used in each study and to note that distinct MSC chondrogenic differentiation outputs might arise not only from the perfusion effect, but also from the type of MSC-source (e.g. BMSC, synovium-derived MSC, adipose tissue-derived MSC, umbilical cord blood-derived MSC), the scaffold material/structure as well as from the culture protocol (e.g. monolayer or pellet, culture medium) used.

In conclusion, we present a new concept of a fully customizable, AM-based extrusion, perfusion bioreactor, capable of providing flow-induced shear stress stimuli to MSC-based tissue constructs for CTE applications. Our results demonstrate that a perfusion bioreactor culture enhances the chondrogenic differentiation of hBMSCs in PCL scaffolds, as suggested by increased cartilage-like ECM production and expression of chondrogenic marker genes when compared to non-perfusion culture conditions. In this first proof-of-concept study, we performed our *in vitro* culture experiments under a single flow rate. A study varying flow rate stimulation values and using a Design of Experiments strategy should be performed to determine the optimal perfusion bioreactor operating conditions required to maximize the chondrogenic potential of MSC, assessed *in vitro*. It would be also interesting to further use our perfusion bioreactor platform to investigate MSC fate in the absence of chondrogenic induction medium. Additionally, the versatility of the platform presented here allows tailoring scaffolds to different types of 3D culture systems such as cell pellets or micromasses. Therefore, the study of the effect of cell culture technique (i.e., a comparison between MSCs seeded on scaffolds and MSC pellets assembled in scaffolds) on MSC chondrogenic differentiation under perfusion conditions is particularly interesting and should be addressed in the future. As articular cartilage motion results from a combination of compressive, tensile and shear stresses (Schatti et al., 2011), future studies should focus on the development of novel AM-based bioreactor platforms enabling the application of multiple mechanical stimuli simultaneously to enhance MSC chondrogenesis by providing a closer mimicry of the native cartilage microenvironment. The work here described presents a promising bioreactor platform for personalized CTE strategies and *in* vitro disease modeling, while highlighting the advantages of AM-based bioreactor development for the automated fabrication of patient-tailored tissue engineering products targeting a wide range of regenerative medicine applications.

V.5. References

Alves da Silva, M.L., Martins, A., Costa-Pinto, A.R., Correlo, V.M., Sol, P., Bhattacharya, M., Faria, S., Reis, R.L., Neves, N.M., (2011). Chondrogenic differentiation of human bone marrow mesenchymal stem cells in chitosan-based scaffolds using a flow-perfusion bioreactor. J. Tissue Eng. Regen. Med. 5, 722–732.

Alves Da Silva, M.L., Martins, A., Costa-Pinto, A.R., Costa, P., Faria, S., Gomes, M., Reis, R.L., Neves, N.M., (2010). Cartilage tissue engineering using electrospun PCL nanofiber meshes and MSCs. Biomacromolecules 11, 3228–3236.

Bernhard, J.C., Vunjak-Novakovic, G., (2016). Should we use cells , biomaterials , or tissue engineering for cartilage regeneration ? Stem Cell Res. Ther. 7, 56.

Bian, L., Zhai, D.Y., Zhang, E.C., Mauck, R.L., Burdick, J.A., (2011). Dynamic Compressive Loading Enhances Cartilage Matrix Synthesis and Distribution and Suppresses Hypertrophy in hMSC-Laden Hyaluronic Acid Hydrogels. Tissue Eng. Part A 18, 715–724.

Biological evaluation of medical devices - Part 5: Tests for cytotoxicity: in vitro methods, (2009). ISO/EN 10993-5 Geneva, Switzerland.

Bornes, T.D., Jomha, N.M., Mulet-Sierra, A., Adesida, A.B., (2015). Hypoxic culture of bone marrow-derived mesenchymal stromal stem cells differentially enhances in vitro chondrogenesis within cell-seeded collagen and hyaluronic acid porous scaffolds. Stem Cell Res. Ther. 6, 84.

Cai, G., Liu, W., He, Y., Huang, J., Duan, L., Xiong, J., Liu, L., Wang, D., (2019). Recent advances in kartogenin for cartilage regeneration. J. Drug Target. 27, 28–32.

Camarero-Espinosa, S., Rothen-Rutishauser, B., Foster, E.J., Weder, C., (2016). Articular cartilage: From formation to tissue engineering. Biomater. Sci. 4, 734–767.

Carter, D.R., Wong, M., (2003). Modelling cartilage mechanobiology. Philos. Trans. R. Soc. B Biol. Sci. 358, 1461–1471.

Chamberlain, G., Fox, J., Ashton, B., Middleton, J., (2007). Concise review: Mesenchymal stem cells: Their phenotype, differentiation capacity, immunological features, and potential for homing. Stem Cells 25, 2739–2749.

Chen, G., Xu, R., Zhang, C., Lv, Y., (2017). Responses of MSCs to 3D scaffold matrix mechanical properties under oscillatory perfusion culture. ACS Appl. Mater. Interfaces 9, 1207–1218.

Correia, C., Pereira, A.L., Duarte, A.R.C., Frias, A.M., Pedro, A.J., Oliveira, J.T., Sousa, R.A., Reis, R.L., (2012). Dynamic Culturing of Cartilage Tissue: The Significance of Hydrostatic Pressure. Tissue Eng. Part A 18, 1979–1991.

Costa, P.F., Hutmacher, D.W., Theodoropoulos, C., Gomes, M.E., Reis, R.L., Vaquette, C., (2015). Additively manufactured device for dynamic culture of large arrays of 3D tissue engineered constructs. Adv. Healthc. Mater. 4, 864–873.

Costa, P.F., Vaquette, C., Baldwin, J., Chhaya, M., Gomes, M.E., Reis, R.L., Theodoropoulos, C., Hutmacher, D.W., (2014). Biofabrication of customized bone grafts by combination of additive manufacturing and bioreactor knowhow. Biofabrication 6, 035006.

Dingle, J.T., Horsfield, P., Fell, H.B., Barratt, M.E.J., (1975). Breakdown of proteoglycan and collagen induced in pig articular cartilage in organ culture. Ann. Rheum. Dis. 34, 303–311.

Domingos, M., Dinucci, D., Cometa, S., Alderighi, M., Bártolo, P.J., Chiellini, F., (2009). Polycaprolactone Scaffolds Fabricated via Bioextrusion for Tissue Engineering Applications. Int. J. Biomater. 2009, 239643.

Dos Santos, F., Andrade, P.Z., Boura, J.S., Abecasis, M.M., da Silva, C.L., Cabral, J.M.S., (2010). Ex vivo expansion of human mesenchymal stem cells: a more effective cell proliferation kinetics and metabolism under hypoxia. J. Cell. Physiol. 223, 27–35.

Dos Santos, F., Campbell, A., Fernandes-Platzgummer, A., Andrade, P.Z., Gimble, J.M., Wen, Y., Boucher, S., Vemuri, M.C., Da Silva, C.L., Cabral, J.M.S., (2014). A xenogeneic-free bioreactor system for the clinical-scale expansion of human mesenchymal stem/stromal cells. Biotechnol. Bioeng. 111, 1116–1127.

Eibes, G., dos Santos, F., Andrade, P.Z., Boura, J.S., Abecasis, M.M.A., da Silva, C.L., Cabral, J.M.S., (2010). Maximizing the ex vivo expansion of human mesenchymal stem cells using a microcarrier-based stirred culture system. J. Biotechnol. 146, 194–197.

Fahy, N., Alini, M., Stoddart, M.J., (2018). Mechanical stimulation of mesenchymal stem cells: Implications for cartilage tissue engineering. J. Orthop. Res. 36, 52–63.

Folmes, C.D.L., Dzeja, P.P., Nelson, T.J., Terzic, A., (2012). Metabolic plasticity in stem cell homeostasis and differentiation. Cell Stem Cell 11, 596–606.

Gonçalves, A., Costa, P., Rodrigues, M.T., Dias, I.R., Reis, R.L., Gomes, M.E., (2011). Effect of flow perfusion conditions in the chondrogenic differentiation of bone marrow stromal cells cultured onto starch based biodegradable scaffolds. Acta Biomater. 7, 1644–1652.

Gupta, P., Geris, L., Luyten, F.P., Papantoniou, I., (2018). An Integrated Bioprocess for the Expansion and Chondrogenic Priming of Human Periosteum-Derived Progenitor Cells in Suspension Bioreactors. Biotechnol. J. 13, 1700087.

Hansmann, J., Groeber, F., Kahlig, A., Kleinhans, C., Walles, H., (2013). Bioreactors in tissue engineering-principles, applications and commercial constraints. Biotechnol. J. 8, 298–307.

Hao, J., Zhang, Y., Jing, D., Shen, Y., Tang, G., Huang, S., Zhao, Z., (2015). Mechanobiology of mesenchymal stem cells: Perspective into mechanical induction of MSC fate. Acta Biomater. 20, 1–9.

Huang, A.H., Farrell, M.J., Kim, M., Mauck, R.L., (2010). Long-term dynamic loading improves the mechanical properties of chondrogenic mesenchymal stem cell-laden hydrogels. Eur. Cells Mater. 19, 72–85.

Hutmacher, D.W., Singh, H., (2008). Computational fluid dynamics for improved bioreactor design and 3D culture. Trends Biotechnol. 26, 166–172.

Kelly, D.J., Jacobs, C.R., (2010). The role of mechanical signals in regulating chondrogenesis and osteogenesis of mesenchymal stem cells. Birth Defects Res. Part C - Embryo Today Rev. 90, 75–85.

Kim, H.J., Lee, J.H., Im, G. Il, (2010). Chondrogenesis using mesenchymal stem cells and PCL scaffolds. J. Biomed. Mater. Res. - Part A 92, 659–666.

Kock, L.M., Malda, J., Dhert, W.J.A., Ito, K., Gawlitta, D., (2014). Flow-perfusion interferes with chondrogenic and hypertrophic matrix production by mesenchymal stem cells. J. Biomech. 47, 2122–2129.

Leijten, J., Georgi, N., Moreira Teixeira, L., van Blitterswijk, C.A., Post, J.N., Karperien, M., (2014). Metabolic programming of mesenchymal stromal cells by oxygen tension directs chondrogenic cell fate. Proc. Natl. Acad. Sci. 111, 13954–13959.

Li, K., Zhang, C., Qiu, L., Gao, L., Zhang, X., (2017). Advances in Application of Mechanical Stimuli in Bioreactors for Cartilage Tissue Engineering. Tissue Eng. Part B Rev. 23, 399–411.

Li, W.J., Tuli, R., Okafor, C., Derfoul, A., Danielson, K.G., Hall, D.J., Tuan, R.S., (2005). A three-dimensional nanofibrous scaffold for cartilage tissue engineering using human mesenchymal stem cells. Biomaterials 26, 599–609.

Li, Z., Yao, S.-J., Alini, M., Stoddart, M.J., (2010). Chondrogenesis of Human Bone Marrow Mesenchymal Stem Cells in Fibrin–Polyurethane Composites Is Modulated by Frequency and Amplitude of Dynamic Compression and Shear Stress. Tissue Eng. Part A 16, 575–584.

Liu, M., Li, Y., Yang, S.T., (2014). Expansion of human amniotic fluid stem cells in 3-dimensional fibrous scaffolds in a stirred bioreactor. Biochem. Eng. J. 82, 71–80.

Lu, J., Fan, Y., Gong, X., Zhou, X., Yi, C., Zhang, Y., Pan, J., (2016). The lineage specification of mesenchymal stem cells is directed by the rate of fluid shear stress. J. Cell. Physiol. 231, 1752–1760.

Madeira, C., Santhagunam, A., Salgueiro, J.B., Cabral, J.M.S., (2015). Advanced cell therapies for articular cartilage regeneration. Trends Biotechnol. 33, 35–42.

Mahmoudifar, N., Doran, P.M., (2010). Chondrogenic differentiation of human adipose-derived stem cells in polyglycolic acid mesh scaffolds under dynamic culture conditions. Biomaterials 31, 3858–3867.

Mahmoudifar, N., Doran, P.M., (2005). Tissue engineering of human cartilage in bioreactors using single and composite cell-seeded Scaffolds. Biotechnol. Bioeng. 91, 338–355.

Mariani, E., Pulsatelli, L., Facchini, A., (2014). Signaling pathways in cartilage repair. Int. J. Mol. Sci. 15, 8667–8698.

Martin, I., Smith, T., Wendt, D., (2009). Bioreactor-based roadmap for the translation of tissue engineering strategies into clinical products. Trends Biotechnol. 27, 495–502.

Mauck, R.L., Nicoll, S.B., Seyhan, S.L., Ateshian, G.A., Hung, C.T., (2003). Synergistic Action of Growth Factors and Dynamic Loading for Articular Cartilage Tissue Engineering. Tissue Eng. 9, 597–611.

Meinert, C., Schrobback, K., Hutmacher, D.W., Klein, T.J., (2017). A novel bioreactor system for biaxial mechanical loading enhances the properties of tissue-engineered human cartilage. Sci. Rep. 7, 16997.

Mota, C., Puppi, D., Chiellini, F., Chiellini, E., (2015). Additive manufacturing techniques for the production of tissue engineering constructs. J. Tissue Eng. Regen. Med. 9, 174–190.

Nam, J., Johnson, J., Lannutti, J.J., Agarwal, S., (2011). Modulation of embryonic mesenchymal progenitor cell differentiation via control over pure mechanical modulus in electrospun nanofibers. Acta Biomater. 7, 1516–1524.

Panadero, J.A., Lanceros-Mendez, S., Ribelles, J.L.G., (2016). Differentiation of mesenchymal stem cells for cartilage tissue engineering: Individual and synergetic effects of three-dimensional environment and mechanical loading. Acta Biomater. 33, 1–12.

Pattappa, G., Heywood, H.K., de Bruijn, J.D., Lee, D.A., (2011). The metabolism of human mesenchymal stem cells during proliferation and differentiation. J. Cell. Physiol. 226, 2562–2570.

Pittenger, M.F., Mackay, A.M., Beck, S.C., Jaiswal, R.K., Douglas, R., Mosca, J.D., Moorman, M.A., Simonetti, D.W., Craig, S., Marshak, D.R., (1999). Multilineage potential of adult human mesenchymal stem cells. Science. 284, 143–147.

Rodrigues, C.A.V., Fernandes, T.G., Diogo, M.M., da Silva, C.L., Cabral, J.M.S., (2011). Stem cell cultivation in bioreactors. Biotechnol. Adv. 29, 815–829.

Rosenzweig, D.H., Carelli, E., Steffen, T., Jarzem, P., Haglund, L., (2015). 3D-printed ABS and PLA scaffolds for cartilage and nucleus pulposustissue regeneration. Int. J. Mol. Sci. 16, 15118–15135.

Salinas, E.Y., Hu, J.C., Athanasiou, K.A., (2018). A Guide for Using Mechanical Stimulation to Enhance Tissue-Engineered Articular Cartilage Properties. Tissue Eng. Part B Rev. 24, 345–358.

Schatti, O., Grad, S., Goldhahn, J., Salzmann, G., Li, Z., Alini, M., Stoddart, M.J., Platz, D., (2011). A Combination of Shear and Dynamic Compression Leads To Mechanically Induced Chondrogenesis of Human Mesenchymal Stem Cells. Eur. Cells Mater. 22, 214–225.

Schop, D., Janssen, F.W., van Rijn, L.D.S., Fernandes, H., Bloem, R.M., de Bruijn, J.D., van Dijkhuizen-Radersma, R., (2009). Growth, Metabolism, and Growth Inhibitors of Mesenchymal Stem Cells. Tissue Eng. Part A 15, 1877–1886.

Silva, J.C., Moura, C.S., Alves, N., Cabral, J.M.S., Ferreira, F.C., (2017). Effects of different fibre alignments and bioactive coatings on mesenchymal stem/stromal cell adhesion and proliferation in poly (ε-caprolactone) scaffolds towards cartilage repair. Procedia Manuf. 12, 132–140.

Stevens, S.S., Beaupré, G.S., Carter, D.R., (1999). Computer model of endochondral growth and ossification in long bones: biological and mechanobiological influences. J. Orthop. Res. 17, 646–653.

Tagil, M., Aspenberg, P., (1999). Cartilage induction by controlled mechanical stimulation in vivo. J. Orthop. Res. 17, 200–204.

Tan, A.R., Hung, C.T., (2017). Concise review: Mesenchymal stem cells for functional cartilage tissue engineering: Taking cues from chondrocyte-based constructs. Stem Cells Transl. Med. 6, 1295–1303.

Theodoridis, K., Aggelidou, E., Vavilis, T., Manthou, M.E., Tsimponis, A., Demiri, E.C., Boukla, A., Salpistis, C., Bakopoulou, A., Mihailidis, A., Kritis, A., (2019). Hyaline cartilage next generation implants from Adipose Tissue Derived Mesenchymal Stem Cells: Comparative study on 3D-Printed Polycaprolactone scaffold patterns. J. Tissue Eng. Regen. Med. 13, 342–355.

Tiğli, R.S., Cannizaro, C., Gümüşderelioğlu, M., Kaplan, D.L., (2011). Chondrogenesis in perfusion bioreactors using porous silk scaffolds and hESC-derived MSCs. J. Biomed. Mater. Res. - Part A 96, 21–28.

Vaca-González, J.J., Guevara, J.M., Moncayo, M.A., Castro-Abril, H., Hata, Y., Garzón-Alvarado, D.A., (2017). Biophysical Stimuli: A Review of Electrical and Mechanical Stimulation in Hyaline Cartilage. Cartilage 194760351773063.

Vinatier, C., Mrugala, D., Jorgensen, C., Guicheux, J., Noël, D., (2009). Cartilage engineering: a crucial combination of cells, biomaterials and biofactors. Trends Biotechnol. 27, 307–314.

Yeatts, A.B., Choquette, D.T., Fisher, J.P., (2013). Bioreactors to influence stem cell fate: augmentation of mesenchymal stem cell signalling pathways via dynamic culture systems. Biochem. Biophys. Acta 1830, 2470–2480.

Yue, D., Zhang, M., Lu, J., Zhou, J., Bai, Y., Pan, J., (2019). The rate of fluid shear stress is a potent regulator for the differentiation of mesenchymal stem cells. J. Cell. Physiol. 234, 16312–116319.

Supporting Information

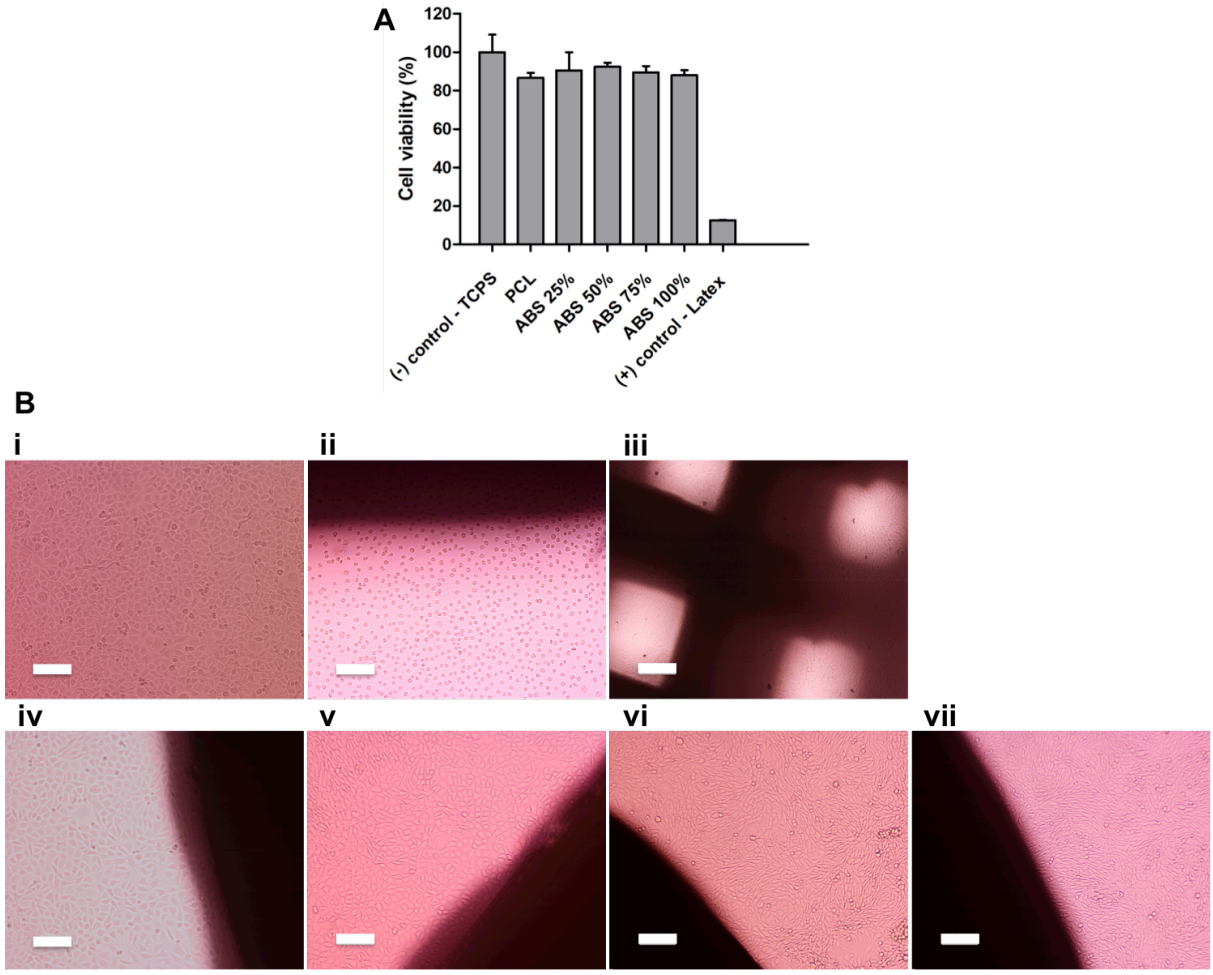

Supplementary Figure V.1. *In vitro* biocompatibility tests of the extruded-based bioreactor platform materials following the ISO 10993-5 guidelines. Percentage of viable cells after indirect extract test (MTT assay) of the different materials used in the bioreactor platform (ABS disks with different printing infill-25%, 50% 75% and 100% and PCL scaffold) as well as the negative control (L929 cells in TCPS under standard culture conditions) and positive control (Latex) for cell death (A). Results are presented as mean ± standard deviation (SD) of three (n=3) independent samples. Microscopic images after direct contact cytotoxicity test of the different materials of the bioreactor platform and controls (B): Negative control – cells in TCPS (i), positive control – Latex (ii), PCL scaffold (iii) and ABS disks extruded with 25% (iv), 50% (v), 75% (vi) and 100% (vii) printing infill. Scale bar: 100 µm.

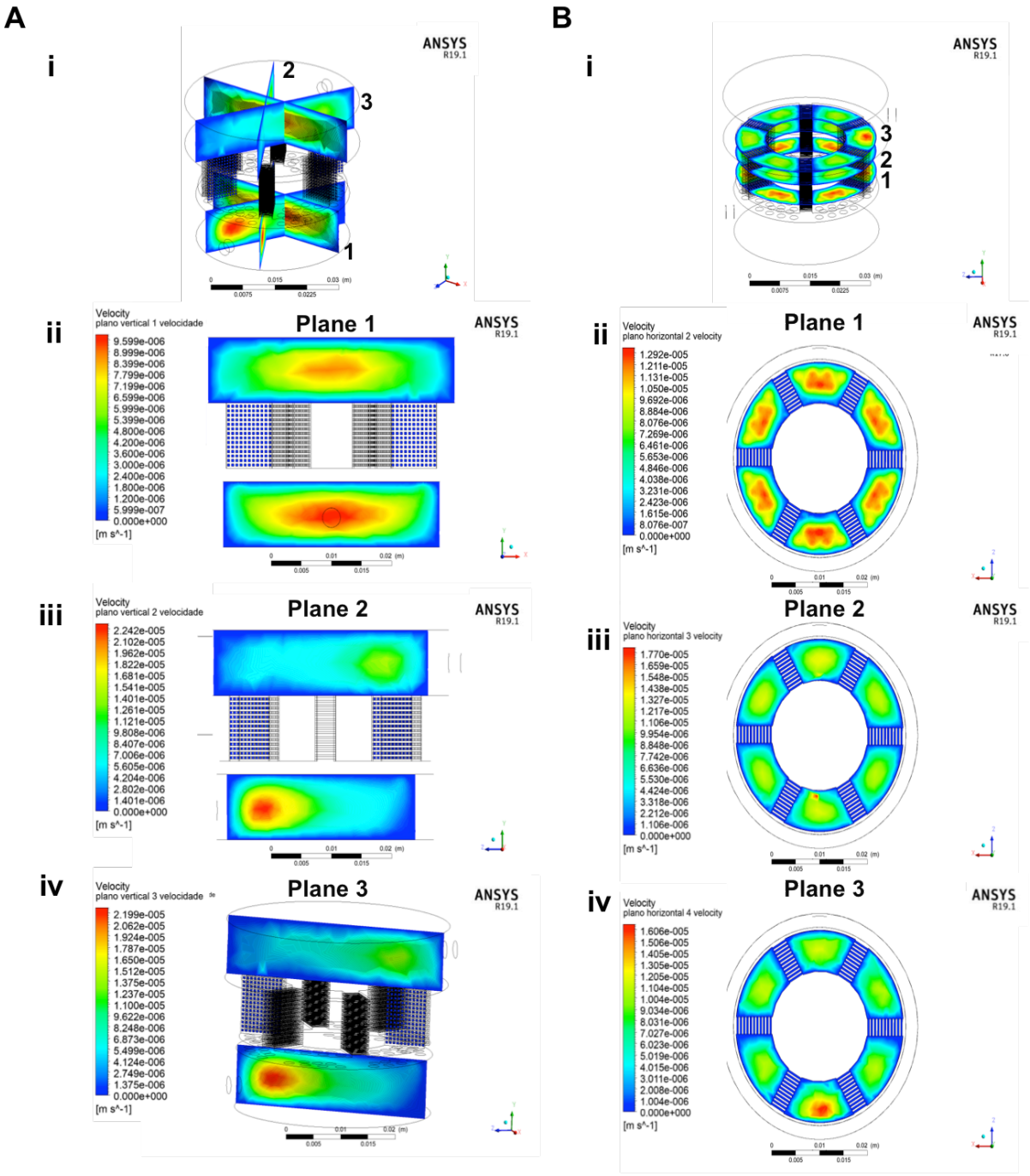

Supplementary Figure V.2. CFD modelling predicts linear fluid velocities distribution inside the bioreactor vessel. Additional vertical (A) and horizontal (B) planes (three each) were defined to further assess the fluid velocity distributions in different regions of the bioreactor (i). Fluid velocity distributions and respective values for the different vertical/horizontal planes considered (A, B (ii-iv)).

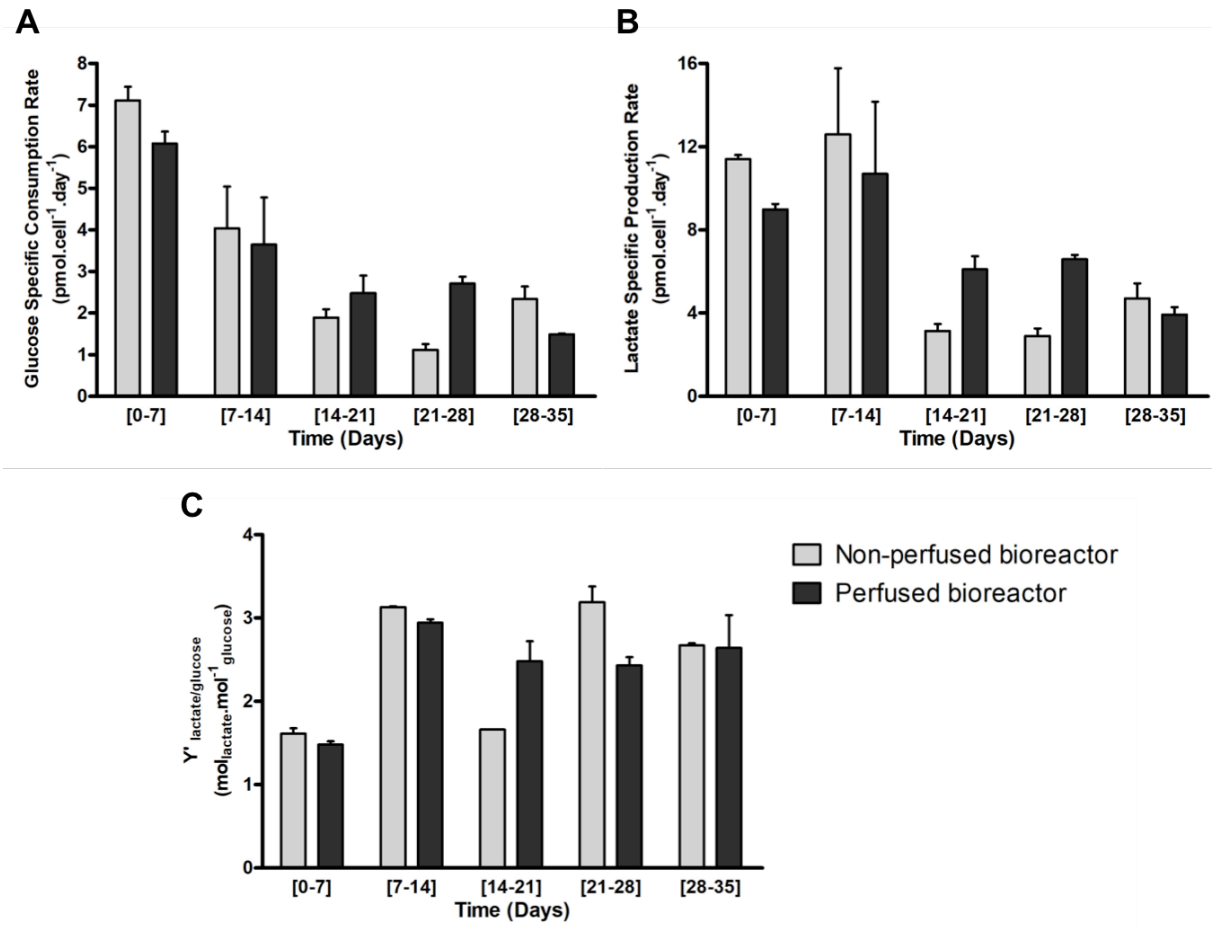

Supplementary Figure V.3. Metabolic analyses throughout all the culture (hBMSC expansion in PCL scaffolds (days 0-14) and hBMSC-PCL constructs culture in non-perfused/perfused bioreactor under chondrogenic differentiation conditions (days 14-35). Glucose specific consumption rate (A) and lactate specific production rate (B) by cells for different time intervals. Apparent yield of lactate from glucose ($Y_{Lac/Gluc}$) for defined culture time intervals (C). Results are expressed as mean ± SEM of three (n=3) independent experiments.

Chapter VI

ECM DECORATED POROUS PCL SCAFFOLDS FOR BONE TISSUE ENGINEERING

CHAPTER VI – Extracellular matrix decorated porous poly (ε-caprolactone) scaffolds for bone tissue engineering

Outline

The clinical demand for tissue-engineered bone is growing due to the increase of non-union fractures and delayed healing in an aging population. Herein, we present a method combining advanced manufacturing techniques with cell-derived extracellular matrix (ECM) to generate structurally well-defined bioactive scaffolds for bone tissue engineering (BTE).

In this work, highly porous three-dimensional poly (ε-caprolactone) (PCL) scaffolds with desired size and architecture were fabricated by fused deposition modeling/melt-extrusion and subsequently decorated with human mesenchymal stem/stromal cell (MSC)-derived ECM produced in-situ. The successful deposition of MSC-derived ECM onto PCL scaffolds (PCL-MSC ECM) was confirmed after decellularization using scanning electron microscopy, elemental analysis and immunofluorescence. The presence of MSC-derived ECM within the PCL scaffolds significantly enhanced MSC attachment and proliferation, with and without osteogenic medium supplementation. Additionally, under osteogenic induction, PCL-MSC ECM scaffolds promoted significantly higher calcium deposition and elevated relative expression of bone-specific genes, particularly osteopontin, when compared to pristine scaffolds.

Overall, the favorable effect of MSC-derived ECM in MSC osteogenic differentiation represents a promising strategy relying on a personalized BTE approach for the fabrication of patient defect-tailored scaffolds with enhanced biological performance and osteoinductive properties, resulting from the closer mimicry of the native bone niche.

VI.1. Introduction

The clinical demand for tissue-engineered bone has increased in recent years, due to the large number of medical conditions that require clinical intervention in an aging population. Each year in the United States alone, approximately 8 million people develop fractures, of which 5-10% fail to heal under standard treatment, resulting in non-union fractures (Holmes, 2017). The most common clinical procedures available to address these needs still rely on autologous and allogeneic bone grafts, however, these approaches are accompanied by side effects, and are limited for a wide-scale application due to the scarcity of the grafts (Chiarello et al., 2013). Therefore, new promising solutions for bone repair are being developed. In particular, bone tissue engineering (BTE) offers the possibility of generating new bone tissue by combining stem cells or osteoprogenitor cells, differentiation-inducing molecules, and 3D biomaterial scaffolds, with great promise of improvements in tissue functionality. However, despite the extensive amount of research on BTE and recent technological developments in biomaterial science, challenges still remain in achieving functional and mechanically competent bone growth (Gordeladze et al., 2017).

Personalized medicine in bone, cartilage or osteochondral repair relies in bioengineered products that are customized to perfectly fit the shape, structure and dimensions of the defect site. Additionally, cells isolated from the patient can be further integrated in a personalized BTE (or CTE) approach, representing an autologous strategy that reduces risk of immune rejection and inflammation (Neves et al., 2016; Roseti et al., 2017). The success of the implementation of BTE approaches in personalized medicine depends on the application of high-precision equipment for the automated, reproducible, and scalable production of functional bone tissue constructs.

Additive manufacturing (AM) techniques such as fused deposition modelling (FDM)/melt-extrusion and 3D printing have been used to fabricate scaffolds for BTE applications, offering advantages in controlling scaffold structural properties such as pore size, porosity and mechanical strength (Roseti et al., 2017). Additionally, AM techniques can be successfully implemented for personalized BTE by acquiring bone defect data and generating a 3D Computer Aided Design (CAD) model of both the anatomical structure in the patient and of the biomaterial scaffold for implantation in the defect site. Based on these CAD models a precise scaffold can be manufactured, seeded with cells and placed into the patient's defect to promote bone regeneration (Figure VI.1 A) (Melchels et al., 2012; Mota et al., 2015). FDM often works with easy to process, biodegradable and biocompatible synthetic polymers such as polycaprolactone (PCL) or polylactic acid (PLA). These materials, alone or in combination with osteoinductive minerals, have been widely applied in BTE approaches (Hajiali et al., 2018; Hutmacher et al., 2001; Poh et al., 2016; Roseti et al., 2017; Xiong et al., 2002). The

US Food and Drug Administration (FDA) has approved PCL-based scaffolds fabricated by FDM for craniofacial bone repair applications after their performance has been demonstrated in clinical pilot studies (Low et al., 2009; Schantz et al., 2006). PCL scaffolds have been extensively used to regenerate hard tissues like bone due to their mechanical properties and slow biodegradation rate. However, this synthetic material lacks bioactive sites and proteins, hampering cell attachment and differentiation, in particular limiting osteoinductive properties present in the native bone niche (Benders et al., 2013).

Different strategies have been employed to improve the biological response and osteoinductive properties of scaffolds through a better mimicry of the bone ECM. Such approaches include modification of the scaffold's surface with ECM components (e.g., collagen, fibronectin and vitronectin) (Ku et al., 2005; Kundu and Putnam, 2006; Won et al., 2015) or the introduction of cell-binding motifs, such as Arg-Gly-Asp (RGD) peptide (Guler et al., 2017). However, these proteins and peptides are not easily processed within the scaffold material or often fail to achieve the molecular complexity of the native ECM. While decellularized tissue-ECM scaffolds can more closely mimic tissue complexity, the application of decellularized tissue-ECM in BTE is limited by its fast degradation, weak mechanical properties and source tissue variability and scarcicity (Bracaglia and Fisher, 2015; Hoshiba et al., 2010).

Cell-derived ECM is a promising alternative approach as it serves as a reservoir of multiple cytokines and growth factors, better mimicing the *in vivo* microenvironment of cells (Bourgine et al., 2014; Hynes, 2009). Decellularized ECM from mesenchymal stem/stromal cells (MSC) has been able to promote MSC proliferation and osteogenic differentiation (Lai et al., 2010). Autologous or allogeneic cell-derived ECM can also be deposited in three-dimensional (3D) synthetic scaffolds to generate constructs with improved cellular activities, resulting in a closer mimicry of the native niche while maintaining adequate structural and mechanical properties (Cheng et al., 2014; Hoshiba et al., 2010). In fact, 3D cell-derived ECM scaffolds have been developed by cell-derived ECM deposition on different organic and inorganic materials. Cell-derived ECM –PCL electrospun scaffolds (Thibault et al., 2010), - titanium implants (Datta et al., 2005) and - ceramic scaffolds (Kim et al., 2017; Tour et al., 2011) have been previously applied in BTE approaches and these show improvement in scaffold bioactivity and osteogenic properties.

In the current study, we developed an extrusion-based 3D porous PCL scaffolds with controlled architecture, porosity and high interconnectivity, and decorated them with human bone marrow MSC – derived ECM, produced in-situ, in an effort to enhance the biological performance and osteoinductive capacity of the scaffold. Our hypothesis is that by providing a 3D synthetic scaffold with good mechanical support containing MSC-derived ECM environmental cues, we could recreate a niche closely mimicking the *in vivo* bone ECM. This

niche would then be capable of promoting different cellular processes, such as cell attachment, proliferation and osteogenic differentiation. The MSC-derived ECM PCL scaffolds developed were characterized in terms of their structure and presence of ECM components. Additionally, their ability to promote MSC osteogenic differentiation in comparison to pristine PCL scaffolds was evaluated by assessing cellular proliferation, calcium production, osteogenic staining and marker genes expression.

VI.2. Material & Methods

VI.2.1. Cell culture

Human bone marrow MSC (hBMSC) were obtained from Lonza (Basel-Switzerland). hBMSC were thawed and plated at a cell density of 3000 cells/cm^2 on tissue culture flasks (CELLTREAT® Scientific Products, MA) using low-glucose Dulbecco's Modified Eagle Medium (DMEM, Gibco, Grand Island, NY) supplemented with 10% fetal bovine serum (FBS, Gibco) and 1% penicillin-streptomycin (Pen-strep, Gibco), and kept at 37 ºC and 5% CO_2 in a humidified atmosphere. Medium renewal was performed every 3-4 days. All the experiments were performed using cells between passages 3 and 5.

VI.2.2. Fabrication of 3D porous PCL scaffolds

PCL (MW 50000 Da, CAPA™ 6500, Perstorp Caprolactones, UK) scaffolds were fabricated in a layer-by-layer approach using an in-house developed FDM equipment, the Bioextruder, as previously reported in the literature (Domingos et al., 2012; Moura et al., 2015). Briefly, the PCL filament material was melted and extruded through a nozzle guided by a robotic device with computer-controlled motion. PCL scaffolds with the desired size, structure and architecture, and with a selected 0-90º lay-down pattern were obtained in accordance to the three-dimensional models designed in CAD software (SolidWorks, Dassault Systèmes, S.A.).

VI.2.3. Generation of cell-derived ECM decorated PCL scaffolds

Prior to cell culture, PCL scaffolds were sterilized by UV exposure (1 h each side of the scaffold), and through 70% ethanol washing. Afterwards, the scaffolds were rinsed three times with a phosphate buffered saline (PBS, Gibco) + 1% penicillin/streptomycin solution and incubated with culture media for 1 h. Cell-derived ECM decorated PCL scaffolds (PCL-MSC ECM) were generated by a pre-culture of hBMSC on the 3D PCL scaffolds followed by

a complete scaffold decellularization (Figure VI.1 B). hBMSC were harvested and seeded onto the PCL scaffolds (1.2×10^5 cells/scaffold) and placed in an ultra-low attachment 24-well plate (Corning, NY). The scaffolds were then incubated for 2 h without culture media to allow initial cell attachment. Standard MSC growth medium consisting in DMEM + 10% FBS + 1% Pen-strep was added to each scaffold and the culture medium was changed every 3-4 days. After 14 days of culture to allow for hBMSC distribution through the entire scaffold, the medium was discarded and the scaffolds were rinsed twice with PBS. Afterwards, the cell-scaffold samples were decellularized following a previously reported protocol (Kang et al., 2012; Matsubara et al., 2004) by exposure to a 20 mM ammonium hydroxide (NH_4OH) + 0.5% Triton X-100 (Sigma-Aldrich, St. Louis, MO) solution for 5 min at room temperature. The ECM decorated PCL scaffolds (PCL-MSC ECM) were then gently washed three times with PBS. Samples were collected for immunofluorescence staining, scanning electron microscopy (SEM) and elemental analysis, as described in the following sections, to confirm the efficiency of the decellularization protocol.

VI.2.4. Characterization of cell-derived ECM decorated PCL scaffolds

VI.2.4.1. Immunofluorescent staining

The efficiency of scaffold decellularization treatment was assessed by cell morphology/immunocytochemistry analysis before and after decellularization. Thus, scaffolds were washed twice with PBS, fixed with 4% paraformaldehyde (PFA; Santa Cruz Biotechnology, Dallas, TX) for 20 min and then permeabilized with 0.1% Triton X-100 for 10 min. Afterwards, the scaffolds were incubated with phalloidin (dilution 1:250 - 2 µg/ml, Sigma) for 45 min in the dark, washed twice with PBS and counterstained with DAPI (1.5 µg/ml, Sigma) for 5 min. After washing twice with PBS, scaffolds before and after the decellularization process were imaged by fluorescent microscopy (Olympus IX51 Inverted Microscope: Olympus America Inc., Melville, NY).

Immunofluorescent staining for fibronectin and laminin was performed to investigate the presence of relevant ECM protein components and their distribution pattern on the decellularized PCL-MSC ECM scaffolds. Accordingly, PCL-MSC ECM scaffolds were washed with PBS and fixed with 4% PFA for 20 min at room temperature. Then, the scaffolds were washed three times with 1% bovine serum albumin (BSA) solution in PBS for 5 min. PCL-MSC ECM scaffolds were permeabilized and blocked with a solution of 0.3%Triton X-100, 1% BSA and 10% donkey serum in PBS at room temperature for 45 min, and incubated overnight at 4ºC with mouse anti-human primary antibodies for laminin and fibronectin (10 µg/ml in 0.3% Triton X-100, 1% BSA, 10% donkey serum solution, R&D systems,

Minneapolis, MN). After washing with 1% BSA in PBS, a NorthernLights™ 557-conjugated anti-mouse IgG secondary antibody (dilution 1:200 in 1% BSA PBS, R&D systems) was added to the samples and incubated in the dark for 1 h at room temperature. Finally, the cell nuclei were counterstained with DAPI (1.5 µg/ml, Sigma) for 5 min and then washed with PBS. The immunofluorescence staining was observed by fluorescence microscopy.

VI.2.4.2. Scanning electron microscopy (SEM) analysis

Prior to imaging, scaffold samples were fixed with 4% PFA for 20 min, washed thoroughly with PBS and dehydrated sequentially in 20%, 40%, 60%, 80%, 95% and 100% (v/v) ethanol solutions for 20 min each time. Then, samples were mounted on a holder and sputter-coated with a thin layer of 60% gold-40% palladium. The morphological and structural characterization of the PCL-MSC ECM and PCL scaffolds was performed using a field emission scanning electron microscope (FE-SEM, FEI-Versa 3D Dual Beam, Hillsboro). Samples were imaged at several magnifications using an accelerating voltage 3 kV.

VI.2.4.3. Energy dispersive X-ray (EDX) analysis

Carl Zeiss Supra field emission scanning electron microscope (FESEM, Hillsboro, USA) was used to conduct EDX analysis on the pristine PCL and PCL-MSC ECM scaffolds. The analysis was performed using an acceleration voltage of 10 kV and a spot size of 120 µm. The presence of specific elements on the EDX spectra of each sample was analyzed using INCA Microanalysis Suite software.

VI.2.5. hBMSC seeding, proliferation and differentiation on PCL-MSC ECM scaffolds

hBMSC were seeded on PCL-MSC ECM and PCL scaffolds (control) at a density of 1×10^5 cells per scaffold and incubated for 2 h at 37 ºC/5% CO_2 before adding culture media to promote initial cell attachment. In order to assess the effects of MSC-ECM presence on the biological performance and osteoinductive capacity of PCL scaffolds, four different experimental groups were considered (Figure VI.1 B): (1) PCL DMEM and (2) PCL-MSC ECM DMEM scaffold groups were cultured under standard expansion media consisting of DMEM supplemented with 10% FBS + 1% Pen-strep, while (3) PCL OSTEO and (4) PCL-MSC ECM OSTEO scaffold groups were cultured with osteogenic differentiation medium, composed by DMEM supplemented with 10% FBS, 10 mM β-glycerophosphate (Sigma-Aldrich), 10 nM dexamethasone (Sigma-Aldrich), 50 µg/mL ascorbic acid (Sigma-Aldrich)

and 1% Pen-strep. Scaffold-cell constructs of the different experimental groups were cultured during 21 days and medium renewal was performed every 3-4 days.

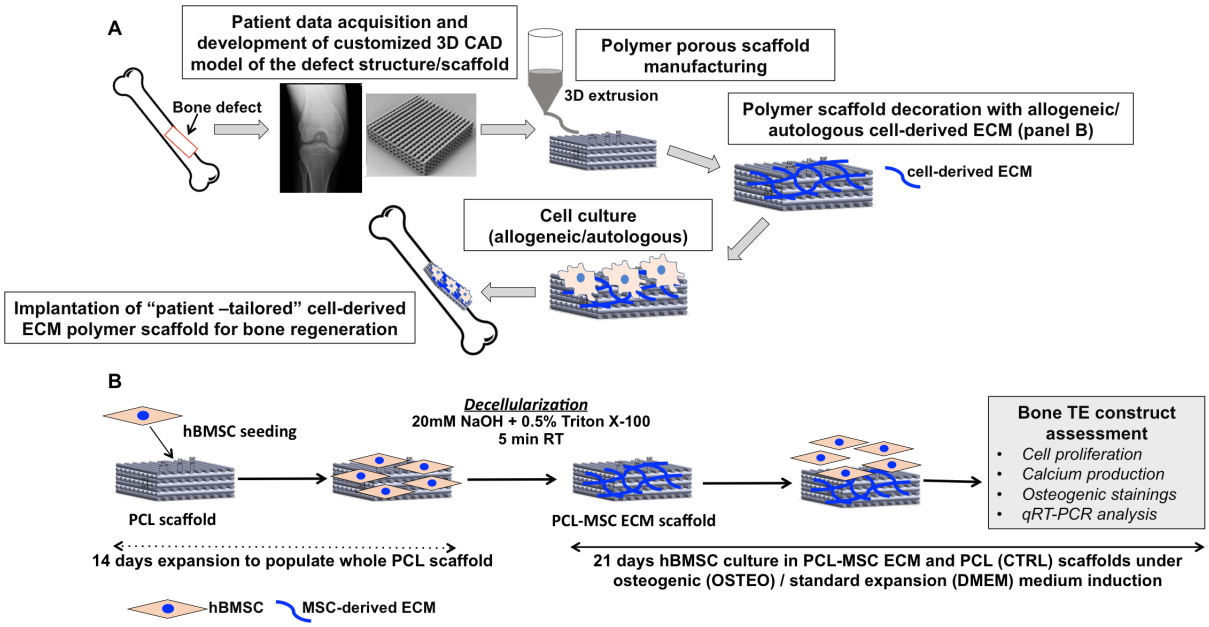

Figure VI.1. Schematic representation of a personalized patient-tailored bone tissue engineering approach combining additive manufacturing of polymer scaffolds and subsequent decoration with cell-derived ECM to improve scaffold's biological performance (A). Scheme of the experimental plan for the generation of PCL-MSC ECM scaffolds and evaluation of their ability to promote MSC proliferation and osteogenic differentiation (B).

VI.2.6. Cell viability and proliferation assay

The metabolic activity of hBMSC in the different experimental scaffold groups was evaluated using AlamarBlue® cell viability reagent (ThermoFischer Scientific, USA) on days 1, 7, 14 and 21 following the manufacturer's guidelines. Briefly, a 10% AlamarBlue® solution in culture medium was added to the scaffolds and incubated at 37 ºC in 5% CO_2 chamber for 3 h. Fluorescence intensity was measured in a microplate reader (SpectraMax M5, Molecular Devices, USA) at an excitation/emission wavelength of 560/590 nm and compared to a calibration curve to access the equivalent number of cells in each scaffold. Scaffolds without seeded cells (for each experimental group) were used as blank controls in the fluorescence intensity measurements. Four scaffolds (n=4) were analyzed for each experimental group and fluorescence values of each sample were measured in triplicates.

VI.2.7. Cell morphology assessment and elemental analysis

The morphology of hBMSC after 21 days of culture on PCL-MSC ECM and PCL scaffolds under the four different experimental conditions was analyzed by SEM. The previously fixed (4% PFA for 20 min) cell-scaffold constructs were stained with 1% (v/v) osmium tetroxide (Sigma-Aldrich) solution for 30 min and washed twice with PBS. Afterwards, samples were dehydrated using ethanol gradient solutions (20%, 40%, 60%, 80%, 95% and 100% (v/v)) for 20 min each and finally dried in a critical point dryer (supercritical Automegasamdri 915B, Tousimis, USA) in 100% isopropanol. Dried samples were then mounted, sputter-coated and imaged using the above-mentioned procedure. EDX analysis was performed using the parameters specified in the previous section to assess for calcium deposition (typical marker of osteogenic differentiation) by hBMSC cultured for 21 days under different experimental conditions.

VI.2.8. Calcium quantification assay

Calcium content quantification was performed after 14 and 21 days of hBMSC-scaffold culture for the four different experimental groups. Samples were washed with PBS and incubated with a 6 M HCl solution (Sigma-Aldrich) under agitation overnight at 4 ºC to remove and dissolve the calcium. The supernatant was then collected and used for total calcium quantification according to the manufacturer's instructions in the calcium colorimetric assay kit (Sigma-Aldrich). Absorbance at 575 nm was measured for each scaffold on a plate reader (SpectraMax M5, Molecular Devices, USA), and normalized to the total number of cells. Note that acellular scaffolds for each experimental group were used as blank controls. Three scaffolds (n=3) were analyzed for each condition and absorbance values of each sample were measured in triplicates. Finally, the absorbance values obtained for each blank control were subtracted from the respective sample group and total calcium was calculated using a calcium standard calibration curve.

VI.2.9. Osteogenic staining

After 21 days of culture, samples from the different experimental groups were assessed for osteogenic differentiation using ALP/Von Kossa and Xylenol orange stainings. For the ALP staining, cell culture medium was removed, samples were washed once with PBS, and fixed with 4% PFA for 20 min. Afterwards, samples were rinsed in miliQ water during 5 min and incubated with Fast Violet solution (Sigma-Aldrich) and Naphthol AS-MX Phosphate Alkaline solution (Sigma-Aldrich) in a final concentration of 4% for 45 min at room

temperature in the dark. In the case of Von Kossa staining, the scaffolds were washed twice with miliQ water and incubated with 2.5% silver nitrate solution (Sigma-Aldrich) for 30 min at room temperature protected from light. Finally, samples were washed three times with miliQ water and imaged using a fluorescence microscope (Olympus IX51 Inverted Microscope, NY USA). A 20 mM volume of Xylenol orange solution (Sigma-Aldrich) was added to previously fixed samples and incubated for 1 h at room temperature in the dark to visualize the mineral deposits on the different experimental groups. Scaffolds were then washed three times with PBS and twice with miliQ water and the fluorescent staining was observed by fluorescence microscopy.

VI.2.10. RNA extraction and real-time quantitative PCR analysis

Total RNA was extracted using the RNeasy Mini Kit (QIAGEN, Hilden, Germany). Briefly, the scaffolds were first incubated in lysis buffer with 200 rpm agitation for 30 min at 4 ºC. Afterwards, total RNA was isolated according to the manufacturer's protocol and quantified using a Nanodrop (ND-1000 Spectrophotometer, Nanodrop Technologies). cDNA was synthesized from the purified RNA using iScript™ Reverse Transcription Supermix (Bio-Rad, Hercules, CA USA) according to manufacturer's guidelines. Reaction mixtures (20 µl) were incubated in a thermal cycler (Veriti Thermal Cycler, Applied Biosystems, CA USA) with the following temperature protocol: 5 min at 25 ºC, 20 min at 46 ºC and 1 min at 95 ºC. The quantitative reverse transcription-polymerase chain reaction (RT-qPCR) was performed using PowerUp SYBR® Green Master Mix (Applied Biosystems) and the StepOnePlus real-time PCR equipment (Applied Biosystems). All reactions were carried out in accordance with the manufacturer's guidelines and using the following temperature protocol: denaturation step at 95 ºC for 10 min, followed by 40 cycles of 95 ºC (amplification step) for 15 s and 60 ºC for 1 min (annealing and extension). All samples were assayed in triplicate and the results were analyzed using the $2^{-\Delta\Delta Ct}$ method. Target genes (collagen type I (*COL I*), runt-related transcription factor (*Runx2*), alkaline phosphatase (*ALP*) and osteopontin (*OPN*)) expression was primarily normalized to the housekeeping gene glyceraldehyde 3-phosphate dehydrogenase (*GAPDH*) and then determined as a fold-change relative to the baseline expression of target gene measured in the PCL scaffolds in DMEM. The primer sequences used in the RT-qPCR analysis are summarized in Table VI.1.

Table VI.1. Forward and reverse primer gene sequences used for RT-qPCR analysis.

Gene	Fwd sequence	Rev sequence
GAPDH	5'-AACAGCGACACCCACTCCTC-3'	5'-CATACCAGGAAATGAGCTTGACAA-3'
COL I	5'-CATCTCCCCTTCGTTTTTGA-3'	5'-CCAAATCCGATGTTTCTGCT-3'
Runx2	5'-AGATGATGACACTGCCACCTCTG-3'	5'-GGGATGAAATGCTTGGGAACT-3'
ALP	5'-ACCATTCCCACGTCTTCACATTT-3'	5'-AGACATTCTCTCGTTCACCGCC-3'
OPN	5'-TGTGAGGTGATGTCCTCGTCTGTAG-3'	5'-ACACATATGATGGCCGAGGTGA-3'

VI.2.11. Statistical analysis

Results are presented as mean values ± standard deviation (SD). Each experiment was conducted in triplicate (n=3), unless specified differently. The statistical analysis of the data was performed using one-way ANOVA, followed by Tukey post-hoc test. GraphPad Prism version 7 software was used in the analysis and data was considered to be significant when p-values obtained were less than 0.05 (95% confidence intervals) (*$p < 0.05$, **$p < 0.01$, ***$p < 0.001$).

VI.3. Results

VI.3.1. Cell-derived ECM decorated PCL scaffolds production and characterization

The efficiency of the decellularization method used to generate PCL-MSC ECM scaffolds was assessed and is presented in Figure VI.2. Prior to decellularization treatment, immunofluorescence staining of F-actin (labeled by phalloidin in red) and nucleus (labeled by DAPI in blue) confirmed the presence of well-defined cell nuclei distributed throughout the scaffold (Figure VI.2 A and C). After decellularization by exposure to a 20 mM NH_4OH in 0.5% Triton X-100 solution, the residual DAPI staining (Figure VI.2 B) indicated that most of the cellular nuclei were disrupted and confirms the efficiency of decellularization. The presence of ECM protein components on the scaffolds after decellularization was demonstrated by immunofluorescent staining of fibronectin (Figure VI.2 D) and laminin (Figure VI.2 E).

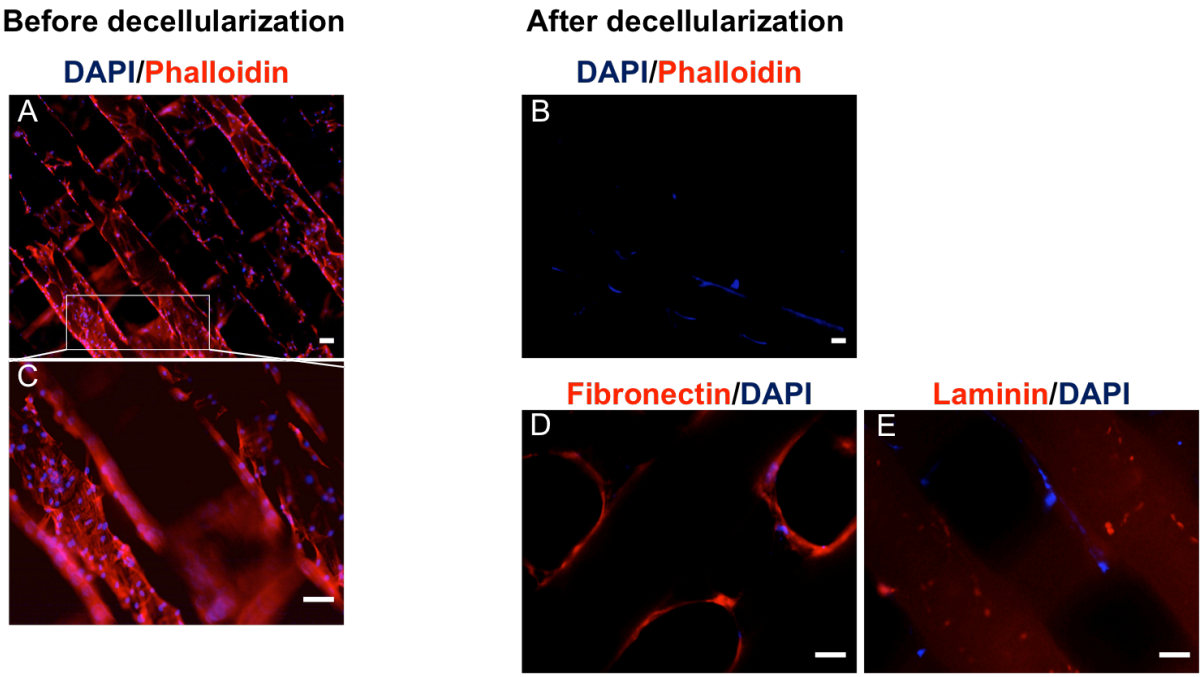

Figure VI.2. Characterization of the decellularization process to generate PCL-MSC ECM scaffolds. Fluorescence images of DAPI/Phalloidin staining before (A, C) and after (B) scaffold treatment with 20 mM NaOH + 0.5% Triton X-100 solution confirm the efficiency of the decellularization method used. The presence of ECM protein components Fibronectin (D) and Laminin (E) on PCL-MSC ECM scaffolds was confirmed by immunofluorescence staining. DAPI stains cell nuclei blue and phalloidin stains actin-rich cell cytoskeleton red. Scale bar: 100 µm.

The PCL-MSC ECM scaffolds were also analyzed by SEM and EDX and compared to the pristine PCL scaffolds (Figure VI.3). In contrast to the smooth regular surface observed in pristine PCL scaffold [Figure VI.3 (A, B – top view), (E, F-side view)], SEM micrographs showed clearly the presence of cell-derived ECM on the surface of the PCL-MSC ECM scaffold [Figure VI.3 (C, D – top view), (G, H-side view)]. The EDX spectra (Figure VI.3 I and J) demonstrated that, compared to PCL pristine scaffold, PCL-MSC ECM scaffold contained nitrogen, in addition to the carbon and oxygen constituents of PCL. In combination with SEM analysis (Figure VI.3) and fibronectin/laminin immunofluorescence staining (Figure VI.2 D and E), this result demonstrates the presence of ECM components on PCL-MSC ECM scaffolds after the decellularization treatment.

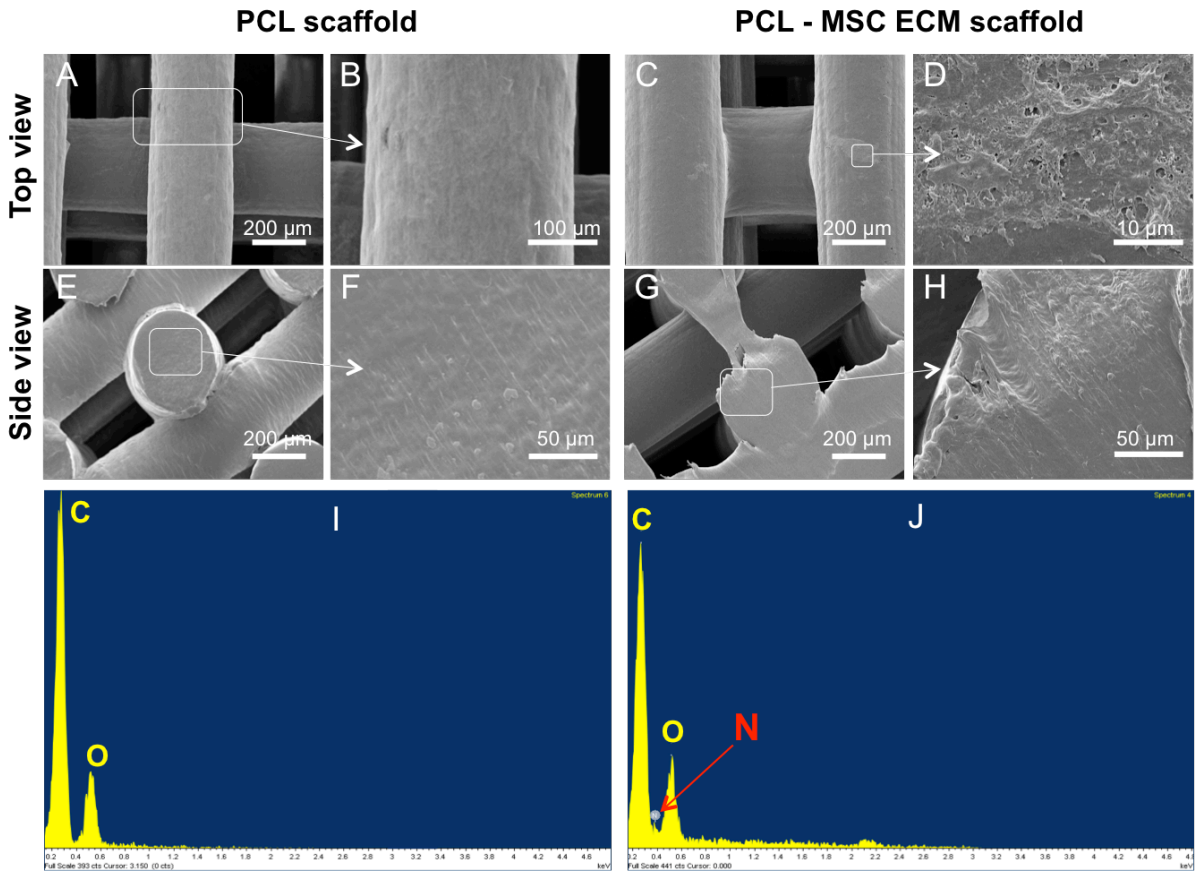

Figure VI.3. SEM morphological analysis of PCL (A, B, E and F) and PCL-MSC ECM scaffolds (C, D, G and H). The absence/presence of MSC-derived ECM in the PCL scaffold (pristine PCL *vs.* PCL-MSC ECM) was confirmed by top view (A, B / C, D) and side view (E, F / G, H) SEM micrographs, respectively. EDX spectrograms of pristine PCL (I) and PCL-MSC ECM scaffold (J). The nitrogen peak identified in PCL-MSC ECM spectrogram (J) suggests the presence of cell-derived ECM in addition to PCL material. The inserts (white box) in the images A, C, E and G identify the scaffold region that is showed in a higher magnification in images B, D, F and H, respectively. Scale bars values of SEM micrographs are depicted in the figure.

VI.3.2. Effects of PCL-MSC ECM scaffolds on cell proliferation

The metabolic activity of hBMSC cultured on PCL-MSC ECM and PCL scaffolds with standard expansion medium (DMEM+10% FBS) and osteogenic differentiation medium was measured by AlamarBlue® assay throughout the 21 days of culture and converted to equivalent cell numbers to assess the effect of MSC-derived ECM deposited onto PCL scaffolds on cell proliferation (Figure VI.4). After the first day of culture, PCL-MSC ECM scaffolds demonstrated a higher equivalent number of cells compared to pristine PCL scaffolds, suggesting that MSC-derived ECM had a positive impact on cell adhesion. A statistically significant ($p < 0.05$) increase in cell number was obtained when cells were cultured on PCL-MSC ECM scaffolds compared to pristine PCL scaffold under expansion media. At day 7, cells cultured on PCL-MSC ECM scaffolds reached higher and statistically

significant (p < 0.001) equivalent cell numbers compared with PCL scaffolds both under standard expansion and osteogenic differentiation media, demonstrating the efficiency of PCL-MSC ECM scaffolds in promoting cell proliferation. The number of cells increased continuously during incubation in all experimental groups during the 21 days of culture. Significant differences in cell numbers between PCL-MSC ECM scaffolds and their pristine PCL counterparts were evident throughout all the culture. These results clearly demonstrated that the deposition of decellularized ECM onto PCL scaffolds enhanced hBMSC attachment and proliferation, both under expansion media and osteogenic differentiation media.

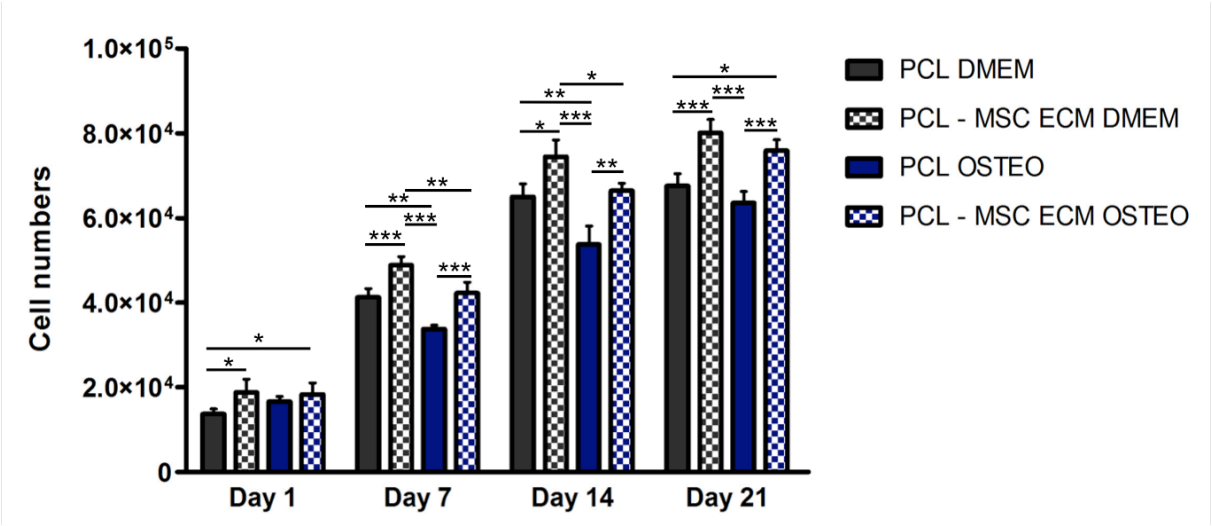

Figure VI.4. Proliferation of hBMSC cultured on PCL-MSC ECM and pristine PCL scaffolds for 21 days under standard DMEM + 10% FBS + 1% Anti-Anti medium and osteogenic differentiation medium. Results are expressed as mean ± SD; n=4; * p < 0.05, ** p < 0.01, *** p < 0.001.

VI.3.3. Effects of PCL-MSC ECM scaffolds on osteogenic gene expression

RT-qPCR analysis was performed to assess bone-specific gene expression after hBMSC culture on PCL-MSC ECM scaffolds. hBMSC cultured on PCL-MSC ECM scaffolds without osteogenic induction (PCL-MSC ECM DMEM) showed significantly higher expression of *COL I* (p < 0.01) (Figure VI.5 A), *Runx2* (p < 0.001) (Figure VI.5 B) and *ALP* (p < 0.01) (Figure VI.5 C) genes after 21 days compared with MSC cultured on pristine PCL scaffolds. Interestingly, hBMSC cultured on PCL-MSC ECM DMEM demonstrated statistically significant (p < 0.01) higher expression levels of *COL I* and *Runx2* compared with hBMSC cultured on pristine PCL scaffolds with osteogenic differentiation induction medium and similar to the ones verified for PCL-MSC ECM OSTEO group. These results suggest that the incorporation of MSC-derived ECM onto PCL scaffolds produced an effect powerful enough to support alone (i.e., in the absence of osteogenic inductive soluble factors) the upregulation

of certain osteogenic genes expression levels to values higher than the ones expressed by hBMSC cultured on pristine PCL scaffolds under osteogenic induction medium. Importantly, a statistically significant ($p < 0.01$) enhancement in *OPN* gene expression (Figure VI.5 D) was only observed when hBMSC were cultured under osteogenic differentiation conditions onto PCL-MSC ECM scaffolds.

These data illustrate that MSC-derived ECM combined with PCL scaffolds can enhance osteogenesis compared to PCL pristine scaffolds, as suggested by the higher mRNA expression levels of *Col I*, *Runx2*, *ALP* and *OPN*.

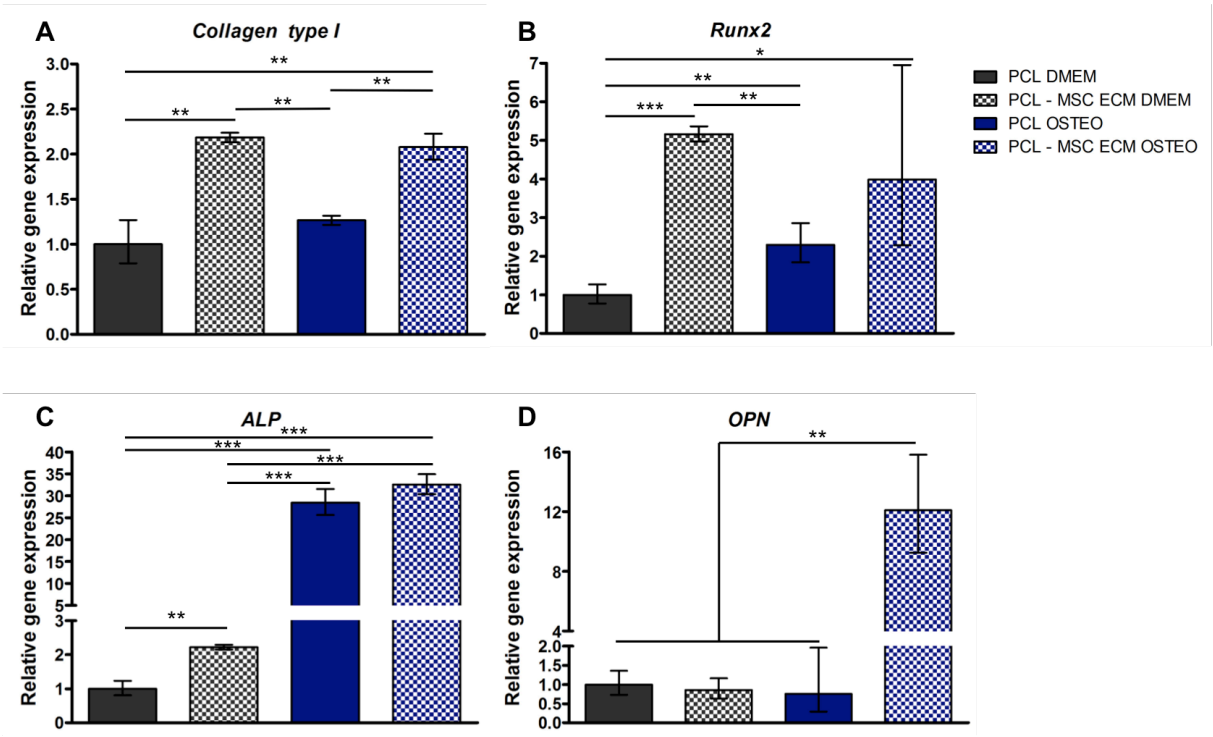

Figure VI.5. Osteogenic marker gene expression analysis by RT-qPCR after 21 days of hBMSC culture on PCL-MSC ECM / PCL scaffolds under osteogenic differentiation medium and standard expansion medium. Expressions of *Collagen type I* (A), *Runx2* (B), *ALP* (C) and *OPN* (D) were normalized to the endogenous gene *GAPDH* expression and calculated as a fold-change relative to the baseline expression of target gene measured in the PCL DMEM experimental group. Results are expressed as mean ± SD; n=3; * $p < 0.05$, ** $p < 0.01$, *** $p < 0.001$.

VI.3.4. Effects of PCL-MSC ECM scaffolds on mineralization and bone ECM production

SEM morphological evaluation of the final tissue constructs obtained after 21 days of hBMSC culture on PCL-MSC ECM and pristine PCL scaffolds with and without osteogenic induction demonstrated the presence of cells surrounded by secreted ECM [Figure VI.6 (A-H)]. As it is possible to observe clearly on Figure VI.6 G and H, the presence of mineralized particles was more evident on the constructs cultured under osteogenic induction.

Additionally, EDX analysis [Figure VI.6 (I-L)] of the different experimental groups confirmed the presence of calcium element in the PCL-MSC ECM (Figure VI.6 L) and PCL (Figure VI.6 K) scaffolds cultured in the presence of osteogenic medium.

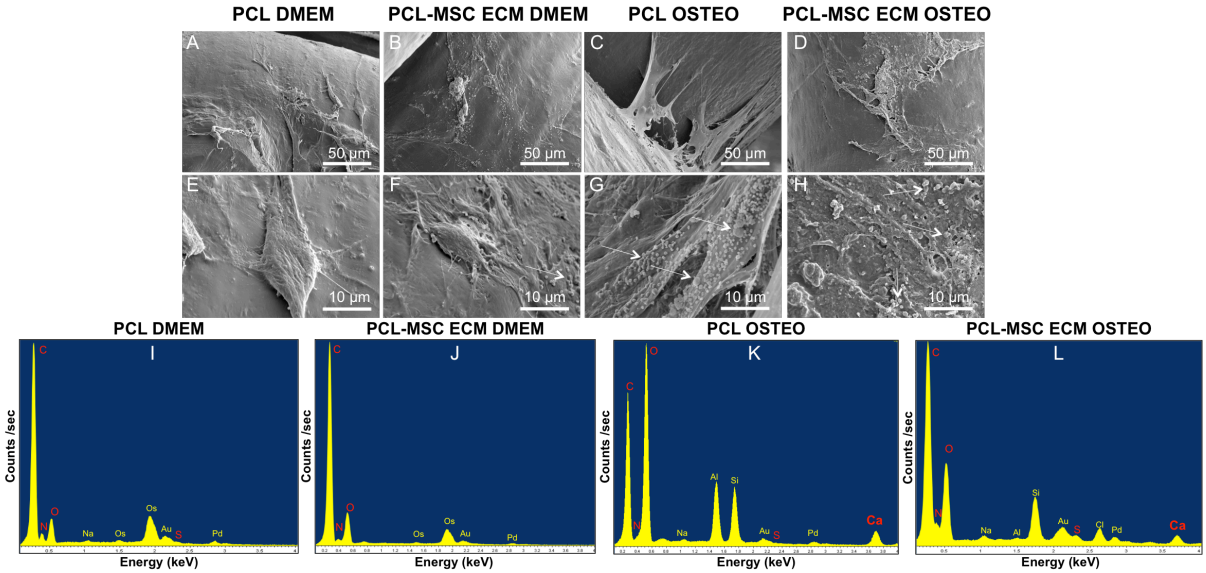

Figure VI.6. SEM images at two different magnifications of hBMSC cultured on PCL-MSC ECM and pristine PCL scaffolds for 21 days under osteogenic differentiation medium and standard expansion medium (A-H). White arrows highlight the presence of mineralized nodules after 21 days of culture on PCL-MSC ECM/PCL scaffolds. Scale bars values of SEM micrographs are depicted in the figure. EDX spectrograms (I-J) obtained after analysis of the different sample groups confirm the presence of calcium secreted by cells cultured on PCL-MSC ECM/PCL scaffolds exposed to osteogenic medium induction. Relevant elements are presented in red. Elements labelled with yellow colour correspond to contaminants from sample sputter coating and SEM microscope environment.

ALP/Von Kossa and Xylenol Orange staining were performed to evaluate the hBMSC osteogenic differentiation on PCL-MSC ECM and pristine PCL scaffolds. ALP [Figure VI.7 (B-E)] and Von Kossa [Figure VI.7 (F-I)] staining confirmed ALP activity (red areas in Figure VI.7 D and E) as well as the presence of mineral deposits (darker regions highlighted by white arrows in Figure VI.7 H and I), in all scaffolds cultured in osteogenic differentiation media. Interestingly, the amount of mineral deposits observed increased considerably in PCL-MSC ECM OSTEO group (Figure VI.7 I). Xylenol Orange fluorescent stain was used to further observe the mineralized deposits of calcium produced by hBMSC cultured on PCL-MSC ECM and PCL scaffolds [Figure VI.7 (J-M)]. When hBMSC were cultured on both scaffolds (with and without ECM) under standard expansion medium, few deposits of calcium were observed surrounding the construct (Figure VI.7 J and K). Although no dramatic differences between cells cultured onto PCL and PCL-MSC ECM scaffolds were observed after 21 days using Xylenol Orange stain, these results demonstrate that osteogenic induction promoted the increase of calcium deposition by hBMSC (Figure VI.7 L and M). Therefore, this qualitative data confirmed the successful differentiation of hBMSC into osteoblasts in both

PCL-MSC ECM and pristine PCL scaffolds when cultured in osteogenic differentiation medium.

Calcium content (Figure VI.7 A)] was also assessed after 14 and 21 days of culture under different experimental conditions to evaluate the effects of PCL-MSC ECM scaffolds on mineralization. After 14 days, the amount of cell-secreted calcium by cells cultured onto PCL-MSC ECM and PCL scaffolds under osteogenic medium induction was significantly increased compared to their respective scaffold counterparts cultured under expansion conditions. In fact, the amount of calcium produced by cells cultured onto PCL scaffolds was higher than the value observed for PCL-MSC ECM scaffolds when both were cultured under osteogenic induction conditions, however this difference was not statistically significant. As expected, hBMSC cultured for 21 days on PCL-MSC ECM and PCL scaffolds under osteogenic differentiation medium produced significantly higher calcium levels compared with hBMSC cultured on scaffolds under expansion conditions. Moreover, under expansion conditions, the presence of MSC-ECM on the PCL scaffolds demonstrated no significant effect on calcium production. Importantly, under osteogenic differentiation medium, cells cultured in PCL-MSC ECM produced significantly ($p < 0.05$) more calcium when compared to pristine PCL scaffold, suggesting that ECM deposition on PCL scaffolds might enhance mineralization by hBMSC after osteogenic induction. These results are concordant with the observations shown by SEM images/EDX spectrograms (Figure VI.6), ALP/Von Kossa [Figure VI.7 (F-I)] and Xylenol Orange [Figure VI.7 (J-M)] stainings.

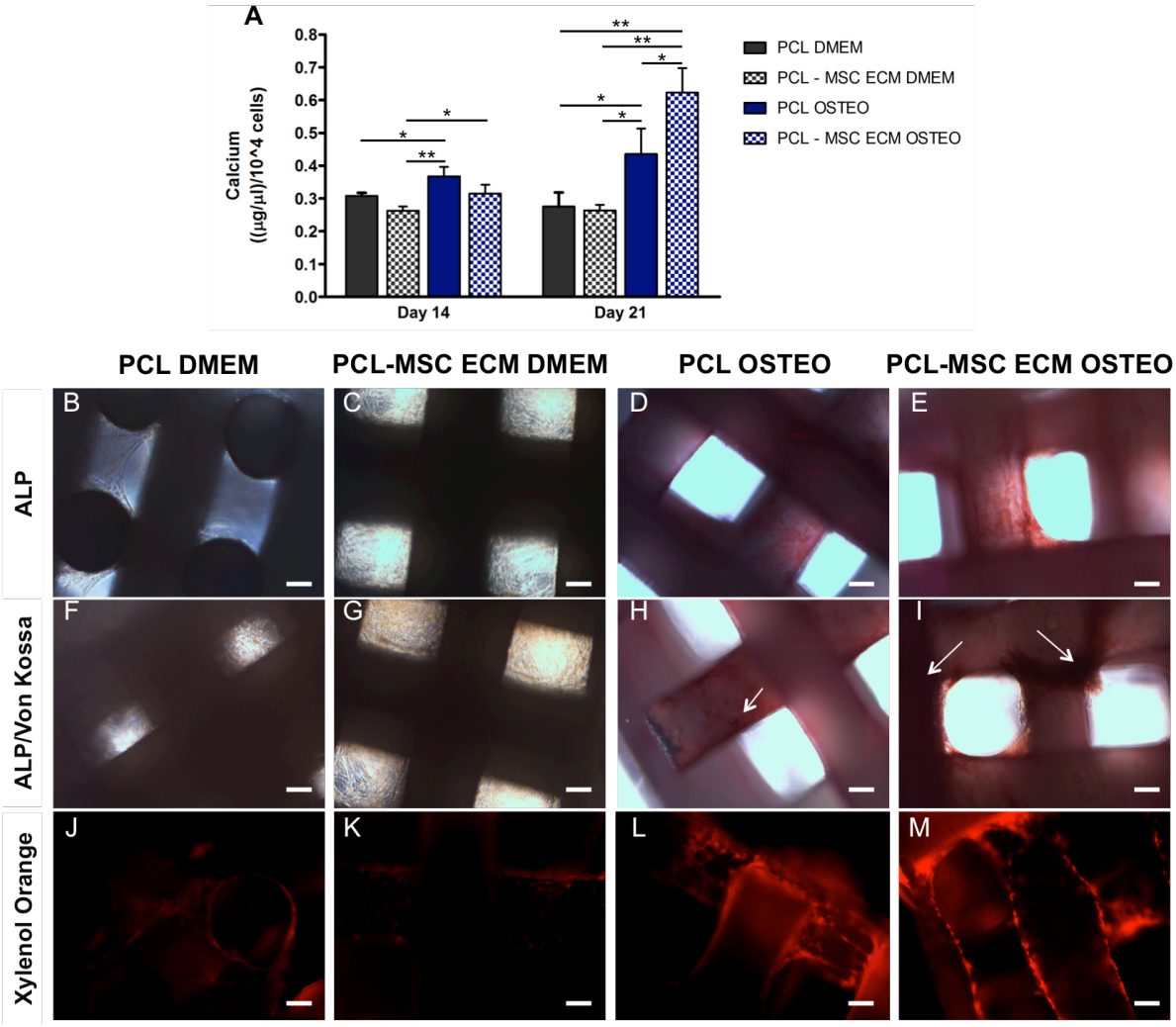

Figure VI.7. Osteogenic differentiation of hBMSC cultured on PCL-MSC ECM scaffolds. Calcium deposition quantification assay of hBMSC seeded on PCL-MSC ECM and pristine PCL scaffolds after 14 and 21 days culture under osteogenic differentiation medium and standard expansion medium (A). Results are expressed as mean ± SD; n=3; * $p < 0.05$, ** $p < 0.01$. ALP (B-E), ALP/Von Kossa (F-I) and Xylenol Orange (J-M) osteogenic stainings of hBMSC cultured for 21 days under osteogenic differentiation medium and standard expansion medium. ALP staining confirms ALP activity of cells by a red staining. Von kossa evaluates the presence of calcium deposits (dark areas highlighted by the white arrows). Xylenol Orange fluorescent staining further confirms the presence of calcium deposits, which stain in red. Scale bar: 100 µm.

VI.4. Discussion

The use of cell-derived ECM integrated with biomaterial scaffolds has appeared as a promising strategy for BTE applications (Fitzpatrick and McDevitt, 2015; Zhang et al., 2016). In this study, we combine AM technology with the concept of decellularized ECM produced in-situ to generate cell-derived ECM polymer-based scaffolds with a defined structure and enhanced bioactivity and osteoinductive properties. We aimed that by providing a closer mimicry of the native bone niche, through the incorporation of MSC-derived ECM, it is possible to improve MSC osteogenic differentiation while maintaining the advantages of polymeric scaffold such as a controlled and defined structure and good mechanical support.

PCL scaffolds used in this work were produced by FDM with controlled size and architecture (pore size of 390 μm / 0-90º lay-down pattern). These scaffolds are previously characterized as presenting a high porosity (56.6%), high interconnectivity (99.7%), and a compressive modulus of 30 MPa (Silva et al., 2017). Similar PCL scaffolds, fabricated using the same AM technique, have been tested for BTE using MG-63 cells (Patrício et al., 2014) and hBMSC (Endres et al., 2003). However, the performance of the PCL scaffold was limited by the suboptimal biological interaction between cells and synthetic material. Herein, we aimed to improve this interaction through the decoration of the PCL scaffold with MSC-derived ECM. After in-situ decoration with decellularized MSC-ECM, no apparent changes in scaffold architecture were observed by SEM analysis, suggesting that the appropriate mechanical properties of the support were maintained. Accordingly, a previous study performed with PCL scaffolds fabricated by selective laser sintering showed no significant effect of 2 weeks cell culturing on the scaffold's compressive modulus (Eosoly et al., 2012).

The deposition of MSC-derived ECM on PCL scaffolds was confirmed by SEM and EDX analysis and by immunofluorescence staining of relevant ECM proteins. Because of their important role in promoting cell attachment, growth and differentiation, fibronectin and laminin have been often selected as biomarkers for the presence of ECM on the scaffolds (Kleinman et al., 2003; Matsubara et al., 2004). Positive immunofluorescent staining for fibronectin and laminin was clearly observed in PCL-MSC ECM scaffolds, however the staining associated with these two proteins was not homogeneously spread along the scaffold microfibers. A similar observation was made by Kim et al (Kim et al., 2015), when assessing fibronectin distribution in human lung fibroblasts-derived ECM coated PLGA/PLA mesh scaffolds. SEM micrographs and EDX spectra analyzed in comparison with the ones obtained for the pristine PCL scaffold, further demonstrated the presence of deposited ECM on PCL-MSC ECM scaffolds. The presence of a nitrogen peak after decellularization in the PCL-MSC ECM scaffolds is in accordance with previous studies using bone-derived ECM or

rat BMSC-derived ECM to enhance the biological performance of polymeric/ceramic scaffolds, respectively (Kim, B. et al., 2017, Kim, J.Y. et al., 2018).

PCL-MSC ECM scaffolds enhanced significantly cell attachment and proliferation when compared with pristine PCL scaffolds, both under standard expansion and osteogenic induction. Previous studies have also shown increased cell numbers as a result of decellularized ECM incorporation in biomaterial scaffolds (Harvestine et al., 2016; Kim et al., 2017, 2015; Noh et al., 2016; Pati et al., 2015). In fact, Kim et al (Kim et al., 2017) showed improved proliferation of MC3T3-E1 osteoblast cells when cultured in rat BMSC-derived ECM coated biphasic calcium phosphate scaffolds, while Noh et al (Noh et al., 2016) reported higher umbilical cord blood-derived MSC cell numbers when cultured in a PLGA/PLA mesh scaffold coated with cell-derived ECM deposited by type I collagen overexpressing cells. This stimulatory effect in cell proliferation might be explained by the presence of bioactive molecules such as growth factors and cytokines within or recruited by the deposited decellularized-ECM. Recent proteomic studies have demonstrated the presence of adhesive molecules and growth factor binding proteins in cell-derived ECM generated from human BMSC (Ragelle et al., 2017). Moreover, fibroblast growth factor-2 (FGF-2), which was shown to promote proliferation of BMSC, was also identified in decellularized cartilage-ECM (Rothrauff et al., 2017; Solchaga et al., 2010). This evidence is in accordance with our observations and might provide an explanation for the higher hBMSC proliferative potential when cultured in PCL-MSC ECM scaffolds.

Gene expression analysis, supporting the role of MSC-ECM on hBMSC osteogenic differentiation, was verified by the upregulation of bone-specific marker genes. In *COL I* and *Runx2*, this effect was predominant enough that hBMSC cultured in PCL-MSC ECM scaffolds without osteogenic supplementation presented significantly higher expressions than the ones cultured in PCL scaffolds under osteogenic induction. However, despite some signs of hBMSC osteogenic differentiation provided by the calcium production and mineralized nodules observed in PCL-MSC ECM DMEM group, the levels were considerably lower than the ones obtained for scaffolds cultured in osteogenic medium. In fact, *Runx2* is an early bone differentiation marker, and its expression is upregulated in immature osteoblasts and downregulated in mature osteoblasts because it is not essential to maintain the expression of the major bone matrix protein genes (Komori, 2010). It is possible that osteogenic supplementation induced a later MSC osteogenic differentiation stage, explaining the lower *Runx2* expression in PCL-MSC ECM and PCL scaffolds after 21 days of culture in osteogenic media. The significantly higher *OPN* expression observed for PCL-MSC ECM scaffolds cultured under osteogenic induction compared to all other experimental groups, and more importantly the signifficantly higher calcium content measured for this condition at day 21 of culture, suggest that a synergistic effect of PCL-MSC ECM scaffolds and

osteogenic supplementation is important for a more mature MSC osteoblast differentiation state. Similar trends in OPN expression were previously reported when comparing human nasal tissue MSC-derived ECM coated scaffolds with their pristine PCL scaffold counterparts (Pati et al., 2015). Moreover, we believe that the observed upregulation of OPN gene expression in PCL-MSC ECM scaffolds cultured in osteogenic media is stimulating mineralization. In fact, previous studies have already reported the inductive effect of OPN on mineralization (Boskey, 1995; Gericke et al., 2005; Zurick et al., 2013).

Our results suggest a positive role of MSC-derived ECM decoration of PCL scaffolds in hBMSC osteogenic differentiation. Qualitative osteogenic staining showed clearly higher ALP activity and calcium deposition when both scaffold types were cultured under osteogenic medium, confirming the results observed for *ALP* gene expression and calcium content. However, substantial differences between the PCL-MSC ECM OSTEO and PCL OSTEO groups were not observed, which is in accordance with previous studies that reported similar qualitative observations of the osteogenic stainings between ECM-derived and non-ECM scaffolds (Kim et al., 2017; Pati et al., 2015). In terms of calcium deposition by cells, all scaffolds promoted calcium production and no significant differences were observed between PCL-MSC ECM and pristine PCL scaffolds when cultured in standard expansion medium with nearly constant values at all the time points assessed. Under osteogenic induction, both PCL-MSC ECM and PCL scaffolds promoted a significant increase in calcium production, however a significant enhancement promoted by the MSC-ECM presence compared to pristine PCL was only observed after 21 days, which is in agreement with previously published data for BMSCs cultured in different cell-derived ECM hybrid scaffold configurations (Kang et al., 2011). In fact, the results of the calcium quantification assay are concordant with the ones obtained from osteogenic staining, SEM analysis and EDX spectra after 21 days of culture. SEM images suggest the presence of mineralized nodules in PCL-MSC ECM and PCL scaffolds cultured under osteogenic induction, which is supported by the identification of calcium element in the respective EDX spectrograms. Fu et al obtained similar results, where they demonstrated the presence of mineralized modules after MSC osteogenic differentiation in both ECM-decorated PLLA and PLLA nanofiber mesh scaffolds (Fu et al., 2018). The mineralized nodules were also noticeable in lower abundance in PCL-MSC ECM scaffolds cultured under standard expansion conditions, suggesting a stimulatory effect of ECM in hBMSC osteogenesis, even in the absence of osteogenic culture supplements. Such observation is in agreement with the work of Thibault et al (Thibault et al., 2010), which showed that the osteogenic differentiation of MSC cultured onto ECM-containing constructs was maintained even in the absence of dexamethasone. Additionally, Datta and co-workers have also reported that MSC-derived ECM decoration of titanium scaffolds promotes the osteogenic differentiation of MSC, even in the absence of osteogenic

induction (Datta et al., 2006). However, our observations suggest that hBMSC osteogenic differentiation was enhanced by the synergistic effect of PCL-MSC ECM scaffolds and osteogenic induction medium, as supported by the elevated bone-specific markers gene expression and calcium levels.

In summary, we successfully established a method to fabricate MSC-derived ECM-decorated 3D PCL scaffolds with defined structure and enhanced biological performance. The presence of ECM components on the PCL scaffold was confirmed by SEM/EDX and immunofluorescence analysis. PCL-MSC ECM scaffolds promoted significant cell proliferation both under standard expansion and osteogenic differentiation conditions. The decellularized PCL-MSC ECM scaffolds showed improved osteoinductive properties as clearly supported by the significantly higher calcium deposition and osteogenic relative gene expressions, particularly the higher expression of the osteogenic marker *OPN*, observed at day 21 when compared to pristine PCL scaffolds under osteogenic medium. This strategy combining AM techniques and in-situ decellularized ECM production is promising for BTE applications as it allows the scalable and automated fabrication of “patient-tailored” scaffolds that perfectly fit in the bone defect site, and have also enhanced bioactivity and osteoinductivity as a result of closer mimicry of the native bone niche.

VI.5. References

Benders, K.E.M., Weeren, P.R. van, Badylak, S.F., Saris, D.B.F., Dhert, W.J.A., Malda, J., (2013). Extracellular matrix scaffolds for cartilage and bone regeneration. Trends Biotechnol. 31, 169–176.

Boskey, A.L., (1995). Osteopontin and Related Phosphorylated Sialoproteins: Effects on Mineralization. Ann. N. Y. Acad. Sci. 760, 249–256.

Bourgine, P.E., Scotti, C., Pigeot, S., Tchang, L.A., Todorov, A., Martin, I., (2014). Osteoinductivity of engineered cartilaginous templates devitalized by inducible apoptosis. Proc. Natl. Acad. Sci. 111, 17426–17431.

Bracaglia, L.G., Fisher, J.P., (2015). Extracellular Matrix-Based Biohybrid Materials for Engineering Compliant, Matrix-Dense Tissues. Adv. Healthc. Mater. 4, 2475–2487.

Cheng, C.W., Solorio, L.D., Alsberg, E., (2014). Decellularized tissue and cell-derived extracellular matrices as scaffolds for orthopaedic tissue engineering. Biotechnol. Adv. 32, 462–484.

Chiarello, E., Cadossi, M., Tedesco, G., Capra, P., Calamelli, C., Shehu, A., Giannini, S., (2013). Autograft, allograft and bone substitutes in reconstructive orthopedic surgery. Aging Clin. Exp. Res. 25, 101–103.

Datta, N., Holtorf, H.L., Sikavitsas, V.I., Jansen, J.A., Mikos, A.G., (2005). Effect of bone extracellular matrix synthesized in vitro on the osteoblastic differentiation of marrow stromal cells. Biomaterials 26, 971–977.

Datta, N., Pham, Q.P., Sharma, U., Sikavitsas, V.I., Jansen, J.A., Mikos, A.G., (2006). In vitro generated extracellular matrix and fluid shear stress synergistically enhance 3D osteoblastic differentiation. Proc. Natl. Acad. Sci. 103, 2488–2493.

Domingos, M., Chiellini, F., Gloria, A., Ambrosio, L., Bartolo, P., Chiellini, E., (2012). Effect of process parameters on the morphological and mechanical properties of 3D Bioextruded poly(ε-caprolactone) scaffolds. Rapid Prototyp. J. 18, 56–67.

Endres, M., Hutmacher, D.W., Salgado, A.J., Kaps, C., Ringe, J., Reis, R.L., Sittinger, M., Brandwood, A., Schantz, J.T., (2003). Osteogenic Induction of Human Bone Marrow-Derived Mesenchymal Progenitor Cells in Novel Synthetic Polymer–Hydrogel Matrices. Tissue Eng. 9, 689–702.

Eosoly, S., Vrana, N.E., Lohfeld, S., Hindie, M., Looney, L., (2012). Interaction of cell culture with composition effects on the mechanical properties of polycaprolactone-hydroxyapatite scaffolds fabricated via selective laser sintering (SLS). Mater. Sci. Eng. C 32, 2250–2257.

Fitzpatrick, L.E., McDevitt, T.C., (2015). Cell-derived matrices for tissue engineering and regenerative medicine applications. Biomater. Sci. 3, 12–24.

Fu, Y., Liu, L., Cheng, R., Cui, W., (2018). ECM decorated electrospun nanofiber for improving bone tissue regeneration. Polymers (Basel). 10, 272.

Gericke, A., Qin, C., Spevak, L., Fujimoto, Y., Butler, W.T., Sørensen, E.S., Boskey, A.L., (2005). Importance of phosphorylation for osteopontin regulation of biomineralization. Calcif. Tissue Int. 77, 45–54.

Gordeladze, J.O., Haugen, H.J., Lyngstadaas, S.P., Reseland, J.E., (2017). Bone tissue engineering: state of the art, challenges, and prospects., Tissue Engineering for Artificial Organs: Regenerative Medicine, Smart Diagnostics and Personalized Medicine, 525-551.

Guler, Z., Silva, J.C., Sezai Sarac, A., (2017). RGD functionalized poly(ε-caprolactone)/poly(m-anthranilic acid) electrospun nanofibers as high-performing scaffolds for bone tissue engineering RGD functionalized PCL/P3ANA nanofibers. Int. J. Polym. Mater. Polym. Biomater. 66, 139–148.

Hajiali, F., Tajbakhsh, S., Shojaei, A., (2018). Fabrication and properties of polycaprolactone composites containing calcium phosphate-based ceramics and bioactive glasses in bone tissue engineering: a review. Polym. Rev. 58, 164–207.

Harvestine, J.N., Vollmer, N.L., Ho, S.S., Zikry, C.A., Lee, M.A., Leach, J.K., (2016). Extracellular Matrix-Coated Composite Scaffolds Promote Mesenchymal Stem Cell Persistence and Osteogenesis. Biomacromolecules 17, 3524–3531.

Holmes, D., (2017). Non-union bone fracture: A quicker fix. Nature 550, S193.

Hoshiba, T., Lu, H., Kawazoe, N., Chen, G., (2010). Decellularized matrices for tissue engineering. Expert Opin. Biol. Ther. 10, 1717–1728.

Hutmacher, D.W., Schantz, T., Zein, I., Ng, K.W., Teoh, S.H., Tan, K.C., (2001). Mechanical properties and cell cultural response of polycaprolactone scaffolds designed and fabricated via fused deposition modeling. J. Biomed. Mater. Res. 55, 203–216.

Hynes, R.O., (2009). The extracellular matrix: Not just pretty fibrils. Science. 326, 1216–1219.

Kang, Y., Kim, S., Bishop, J., Khademhosseini, A., Yang, Y., (2012). The osteogenic differentiation of human bone marrow MSCs on HUVEC-derived ECM and β-TCP scaffold. Biomaterials 33, 6998–7007.

Kang, Y., Kim, S., Khademhosseini, A., Yang, Y., (2011). Creation of bony microenvironment with CaP and cell-derived ECM to enhance human bone-marrow MSC behavior and delivery of BMP-2. Biomaterials 32, 6119–6130.

Kim, B., Ventura, R., Lee, B.T., (2017). Functionalization of porous BCP scaffold by generating cell-derived extracellular matrix from rat bone marrow stem cells culture for bone tissue engineering. J. Tissue Eng. Regen. Med. 12, 1256–1267.

Kim, I.G., Hwang, M.P., Du, P., Ko, J., Ha, C.W., Do, S.H., Park, K., (2015). Bioactive cell-derived matrices combined with polymer mesh scaffold for osteogenesis and bone healing. Biomaterials 50, 75–86.

Kim, J.Y., Ahn, G., Kim, C., Lee, J.S., Lee, I.G., An, S.H., Yun, W.S., Kim, S.Y., Shim, J.H., (2018). Synergistic Effects of Beta Tri-Calcium Phosphate and Porcine-Derived Decellularized Bone Extracellular Matrix in 3D-Printed Polycaprolactone Scaffold on Bone Regeneration. Macromol. Biosci. 18, 1–10.

Kleinman, H.K., Philp, D., Hoffman, M.P., (2003). Role of the extracellular matrix in morphogenesis. Curr. Opin. Biotechnol. 14, 526–532.

Komori, T., (2010). Regulation of osteoblast differentiation by runx2, in: Advances in Experimental Medicine and Biology - Osteoimmunology, 43-49.

Ku, Y., Chung, C.P., Jang, J.H., (2005). The effect of the surface modification of titanium using a recombinant fragment of fibronectin and vitronectin on cell behavior. Biomaterials 26, 5153–5157.

Kundu, A.K., Putnam, A.J., (2006). Vitronectin and collagen I differentially regulate osteogenesis in mesenchymal stem cells. Biochem. Biophys. Res. Commun. 347, 347–357.

Lai, Y., Sun, Y., Skinner, C.M., Son, E.L., Lu, Z., Tuan, R.S., Jilka, R.L., Ling, J., Chen, X.-D., (2010). Reconstitution of Marrow-Derived Extracellular Matrix Ex Vivo: A Robust Culture System for Expanding Large-Scale Highly Functional Human Mesenchymal Stem Cells. Stem Cells Dev. 19, 1095–1107.

Low, S.W., Ng, Y.J., Yeo, T.T., Chou, N., (2009). Use of Osteoplug polycaprolactone implants as novel burr-hole covers. Singapore Med. J. 50, 777-780.

Matsubara, T., Tsutsumi, S., Pan, H., Hiraoka, H., Oda, R., Nishimura, M., Kawaguchi, H., Nakamura, K., Kato, Y., (2004). A new technique to expand human mesenchymal stem cells using basement membrane extracellular matrix. Biochem. Biophys. Res. Commun. 313, 503–508.

Melchels, F.P.W., Domingos, M.A.N., Klein, T.J., Malda, J., Bartolo, P.J., Hutmacher, D.W., (2012). Additive manufacturing of tissues and organs. Prog. Polym. Sci. 37, 1079–1104.

Mota, C., Puppi, D., Chiellini, F., Chiellini, E., (2015). Additive manufacturing techniques for the production of tissue engineering constructs. J. Tissue Eng. Regen. Med. 9, 174–190.

Moura, C.S., Da Silva, C.L., Bártolo, P.J., Ferreira, F.C., (2015). Combination of 3D extruded-based poly (ε-caprolactone) scaffolds with mesenchymal stem/stromal cells: Strategy optimization. Procedia Eng. 110, 122–127.

Neves, L.S., Rodrigues, M.T., Reis, R.L., Gomes, M.E., (2016). Current approaches and future perspectives on strategies for the development of personalized tissue engineering therapies. Expert Rev. Precis. Med. Drug Dev. 1, 93–108.

Noh, Y.K., Du, P., Kim, I.G., Ko, J., Kim, S.W., Park, K., (2016). Polymer mesh scaffold combined with cell-derived ECM for osteogenesis of human mesenchymal stem cells. Biomater. Res. 20, 6.

Pati, F., Song, T.H., Rijal, G., Jang, J., Kim, S.W., Cho, D.W., (2015). Ornamenting 3D printed scaffolds with cell-laid extracellular matrix for bone tissue regeneration. Biomaterials 37, 230–241.

Patrício, T., Domingos, M., Gloria, A., D'Amora, U., Coelho, J.F., Bártolo, P.J., (2014). Fabrication and characterisation of PCL and PCL/PLA scaffolds for tissue engineering. Rapid Prototyp. J. 20, 145–156.

Poh, P.S.P., Hutmacher, D.W., Holzapfel, B.M., Solanki, A.K., Stevens, M.M., Woodruff, M.A., (2016). In vitro and in vivo bone formation potential of surface calcium phosphate-coated polycaprolactone and polycaprolactone/bioactive glass composite scaffolds. Acta Biomater. 30, 319–333.

Ragelle, H., Naba, A., Larson, B.L., Zhou, F., Prijić, M., Whittaker, C.A., Del Rosario, A., Langer, R., Hynes, R.O., Anderson, D.G., (2017). Comprehensive proteomic characterization of stem cell-derived extracellular matrices. Biomaterials 128, 147–159.

Roseti, L., Parisi, V., Petretta, M., Cavallo, C., Desando, G., Bartolotti, I., Grigolo, B., (2017). Scaffolds for Bone Tissue Engineering: State of the art and new perspectives. Mater. Sci. Eng. C 78, 1246–1262.

Rothrauff, B.B., Yang, G., Tuan, R.S., (2017). Tissue-specific bioactivity of soluble tendon-derived and cartilage-derived extracellular matrices on adult mesenchymal stem cells. Stem Cell Res. Ther. 8, 133.

Schantz, J.T., Lim, T.C., Ning, C., Swee, H.T., Kim, C.T., Shih, C.W., Hutmacher, D.W., (2006). Cranioplasty after trephination using a novel biodegradable burr hole cover: Technical case report. Neurosurgery 58.

Silva, J.C., Moura, C.S., Alves, N., Cabral, J.M.S., Ferreira, F.C., (2017). Effects of different fibre alignments and bioactive coatings on mesenchymal stem/stromal cell adhesion and proliferation in poly (ε-caprolactone) scaffolds towards cartilage repair. Procedia Manuf. 12, 132–140.

Solchaga, L.A., Penick, K., Goldberg, V.M., Caplan, A.I., Welter, J.F., (2010). Fibroblast Growth Factor-2 Enhances Proliferation and Delays Loss of Chondrogenic Potential in Human Adult Bone-Marrow-Derived Mesenchymal Stem Cells. Tissue Eng. Part A 16, 1009–1019.

Thibault, R.A., Scott Baggett, L., Mikos, A.G., Kasper, F.K., (2010). Osteogenic Differentiation of Mesenchymal Stem Cells on Pregenerated Extracellular Matrix Scaffolds in the Absence of Osteogenic Cell Culture Supplements. Tissue Eng. Part A 16, 431–440.

Tour, G., Wendel, M., Tcacencu, I., (2011). Cell-Derived Matrix Enhances Osteogenic Properties of Hydroxyapatite. Tissue Eng. Part A 17, 127–137.

Won, J.-E., Mateous-Timoneda, M.A., Castano, O., Planell, J.A., Seo, S.-J., Lee, E.-J., Han, C.-M., Kim, H.-W., (2015). Fibronectin immobilization on to robotic-dispensed nanobioactive glass/polycaprolactone scaffolds for bone tissue engineering. Biotechnol. Lett. 37, 935–942.

Xiong, Z., Yan, Y., Wang, S., Zhang, R., Zhang, C., (2002). Fabrication of porous scaffolds for bone tissue engineering via low-temperature deposition. Scr. Mater. 46, 771–776.

Zhang, W., Zhu, Y., Li, J., Guo, Q., Peng, J., Liu, S., Yang, J., Wang, Y., (2016). Cell-Derived Extracellular Matrix: Basic Characteristics and Current Applications in Orthopedic Tissue Engineering. Tissue Eng. Part B Rev. 22, 193–207.

Zurick, K.M., Qin, C., Bernards, M.T., (2013). Mineralization induction effects of osteopontin, bone sialoprotein, and dentin phosphoprotein on a biomimetic collagen substrate. J. Biomed. Mater. Res. - Part A 101, 1571–1581.

Chapter VII

COAXIAL ALIGNED NANOFIBERS FOR CONTROLLED KARTOGENIN RELEASE TOWARDS IMPROVED MSC CHONDROGENIC DIFFERENTIATION

CHAPTER VII – Coaxial aligned nanofibers for controlled kartogenin release towards improved MSC chondrogenic differentiation

Outline

Electrospinning is a valuable technology for cartilage tissue engineering (CTE) due to its ability to produce fibrous scaffolds mimicking the nanoscale and alignment of collagen fibers present within the superficial zone of articular cartilage. Coaxial electrospinning allows the fabrication of core-shell fibers able to incorporate and release bioactive molecules (e.g. drugs or growth factors) in a controlled manner. Herein, we used coaxial electrospinning to produce coaxial poly(glycerol sebacate) (PGS)/poly(caprolactone) (PCL) aligned nanofibers (core:PGS/shell:PCL). The obtained scaffolds were characterized in terms of their structure, chemical composition, thermal properties, mechanical performance and *in vitro* degradation kinetics, in comparison to monoaxial PCL aligned fibers and respective non-aligned controls. All the electrospun scaffolds produced presented average fiber diameters within the nanometer-scale and the core-shell structure of the composite fibers was clearly confirmed by TEM. Additionally, fiber alignment significantly increased (>2-fold) the elastic modulus of both coaxial and monoxial scaffolds. Kartogenin (KGN), a small molecule known to promote mesenchymal stem/stromal cells (MSC) chondrogenesis, was loaded into the core PGS solution to generate coaxial PGS-KGN/PCL nanofibers. The KGN release kinetics and scaffold biological performance were evaluated in comparison to KGN-loaded monoaxial nanofibers and respective non-loaded controls. Coaxial PGS-KGN/PCL nanofibers showed a more controlled and sustained KGN release over 21 days than monoaxial PCL-KGN nanofibers. When cultured with human bone marrow MSC in incomplete chondrogenic medium (without TGF-β3), KGN-loaded scaffolds enhanced significantly cell proliferation and chondrogenic differentiation, as suggested by the increased sGAG amounts and chondrogenic markers gene expression levels. Overall, these findings highlight the potential of using coaxial PGS-KGN/PCL aligned nanofibers as a bioactive scaffold for CTE applications, particularly, targetting the regeneration of the superficial zone of articular cartilage.

VII.1. Introduction

Articular cartilage is a highly organized tissue comprised by four distinct zones (superficial, middle, deep and calcified zone), each with specific chondrocyte and extracellular matrix (ECM) organization and orientation (Klein et al., 2009). It has been reported that initial stages of osteoarthritis (OA) and age-associated weakening can lead to degradation of the superficial zone of articular cartilage (located around 200 μm in depth). Damage of the superficial zone results in abnormal mechanical performance of the tissue and stimulates an immune response triggered by the release of collagen molecules into the synovial fluid. In healthy functional articular cartilage, the superficial zone consists in a very polarized dense organization of nanoscale collagen type II fibrils, which are oriented parallel to the articular surface and populated with flattened chondrocytes (Hunziker et al., 2002; Mow and Guo, 2002). In comparison with the other zones of articular cartilage, the superficial zone presents the higher amounts of collagen and the lowest concentration of glycosaminoglycans (GAGs) (Klein et al., 2007). The superficial layer is the main responsible for the tissue resistance to shear and tensile forces generated during articular movement, due to the high tensile strength provided by the aligned collagen fibers. It also provides a frictionless surface to assure smooth articulation and functions as an effective barrier at the joint surface, isolating the cartilage from the immune system (Mikos and Temenoff, 2000; Mow and Guo, 2002).

Electrospinning has been used in cartilage tissue engineering (CTE) applications due to its ability to fabricate fibrous scaffolds with high porosity and large surface areas mimicking the nanometer scale and alignment of the collagen fibrils present in the native articular cartilage ECM (Braghirolli et al., 2014; Wise et al., 2009). Coaxial electrospinning, a development of the traditional method, uses a spinneret composed by two concentrically aligned nozzles (each one fed with a different casting solution) to fabricate fibers with a core-sheath structure. Coaxial electrospinning allows the encapsulation of nonspinnable polymers or drugs/biomolecules in the fiber core, promoting their protection and controlled-release (Sperling et al., 2016). The use of coaxial electrospun fibers in drug delivery and tissue engineering strategies has been recently reviewed (Pant et al., 2019; Ding et al., 2019). Regarding CTE strategies, coaxial electrospun fibers incorporating growth factors have been used to enhance the chondrogenic differentiation of mesenchymal stem/stromal cells (MSC) (Man et al., 2014; Wang et al., 2017).

In the present study, we used a coaxial electrospinning to produce coaxial aligned nanofibers of poly (glycerol sebacate) (PGS, core)/polycaprolactone (PCL, shell) (Figure VII.1). PGS is a biodegradable and biocompatible elastomeric material synthesized through the polycondensation reaction of glycerol and sebacic acid, which are both FDA-approved

(Loh et al., 2015). PCL is a slow-degrading biocompatible aliphatic polyester that offers a high tensile strength, thermal stability and chemical versatility. Additionally, PCL previously received FDA approval as drug delivery and medical devices (Low et al., 2009; Woodruff and Hutmacher, 2010). Recently, PCL and PGS were blended to produce porous scaffolds by salt-leaching method for CTE applications (Liu et al., 2019). Importantly, PCL and PGS were also combined to produce blended electrospun fibers for cardiac and corneal regeneration (Masoumi et al., 2014; Vogt et al., 2019; Salehi et al., 2017).

The coaxial aligned PGS/PCL nanofibers produced were used to promote the sustained release of a small molecule kartogenin (KGN). KGN was shown to promote the chondrogenic differentiation of human bone marrow mesenchymal stem/stromal cells (hBMSC), exhibited chondroprotective effects *in vitro* and reduced cartilage degeneration after intra-articular injection in OA mouse models (Johnson et al., 2012). KGN functions by interacting with the actin-binding protein filamin A, disrupting its balance with the transcription factor core-binding factor β (CBFβ). CBFβ enters the nucleus and interacts with RUNX1 to form the CBFβ-RUNX1 complex that activates the transcription of chondrogenesis-related proteins and enhances cartilage ECM synthesis (Cai et al., 2019; Johnson et al., 2012). Recently, several groups have used biomaterial platforms to promote the sustained release of KGN towards improved cartilage regeneration (Fan et al., 2018; Hu et al., 2017; Kang et al., 2014; Shi et al., 2016). However, the use of coaxial electrospun aligned fibers to promote KGN controlled delivery for CTE applications is currently underexplored.

Herein, our aim was to develop coaxial PGS/PCL electrospun aligned nanofibers able to promote a sustained release of KGN while being compatible with the size and alignment of natural ECM in the superficial zone of articular cartilage. These fibers were characterized in terms of their structural, chemical, thermal and mechanical properties and *in vitro* biodegradation. The *in vitro* release kinetics of KGN from coaxial PGS/PCL and monoaxial PCL aligned nanofibers was evaluated for 21 days. In addition, the ability of KGN-loaded electrospun scaffolds to promote hBMSC chondrogenic differentiation in the absence of the chondrogenic cytokine TGF-β3 was evaluated in comparison to the respective non-loaded controls by assessing typical cartilage-ECM production and gene expression.

VII.2. Material & Methods

VII.2.1. Materials

Polycaprolactone (PCL, MW 80000 Da), 2,2,2-trifluoroethanol (TFE), sodium hydroxide (NaOH), dimethylsulfoxide (DMSO), isopropanol, sebacic acid and glycerol were purchased from Sigma-Aldrich (St. Louis, Missouri USA). PGS pre-polymer was synthesized based in previously reported protocols (Rai et al., 2013; Wang et al., 2002). Briefly, sebacic acid and glycerol (in a 1:1 equimolar ratio) were reacted at 120ºC for 3 h under a nitrogen atmosphere to generate a pre-polycondensed polymer, following by a crosslinking step at 120ºC under vacuum for 48 h. Kartogenin (KGN, MW 321.84 g/mol) was obtained from Tocris Bioscience.

VII.2.2. Fabrication of coaxial PGS/PCL electrospun nanofibers

Polymer casting solutions for coaxial electrospinning were prepared by dissolving PCL in TFE at 10% w/v (shell solution) and PGS in TFE at 80% w/v (core solution). The solutions were mixed overnight at room temperature to achieve homogeneity. The core-shell fibers were fabricated using an electrospinning apparatus (Figure VII.1 A) equipped with a coaxial spinneret (MEEC, Ogori, Fukuoka, Japan), as previously described (Hou et al., 2016). Core PGS and shell PCL solutions were loaded into syringes placed in a mechanical syringe pump (NE-1000, New Era Pump System Inc., Wantang, NY USA) and connected by PTFE tubing to the coaxial spinneret. The diameters of the inner and outer needles in the coaxial spinneret were 0.64 mm and 2.5 mm, respectively. The controlled flow rates of the core and shell solutions were 50 µL/min and 180 µL/min, respectively. A high voltage source (Spellman CZE1000R, Hauppauge, NY USA) was used to apply a voltage of 20 kV, creating a potential difference between the needle and copper collectors placed at a distance of 17 cm from the needle tip. Monoaxial PCL fibers were fabricated using the same process parameters, with a needle with 0.64 mm diameter and a flow rate of 180 µL/min. The non-aligned and aligned fibers were produced on different electrospinning collectors: a round copper plate for non-aligned fibers (Figure VII.1 B) and a two parallel copper plates (separated by 2 cm) collector was used to align fibers (Figure VII.1 C and D). All the fiber groups were produced under the similar ambient conditions (temperature and relative humidity varied between 21-23ºC and 25-35%, respectively). Prior to further use, the fibers were dried in a desiccator to remove any remaining solvents.

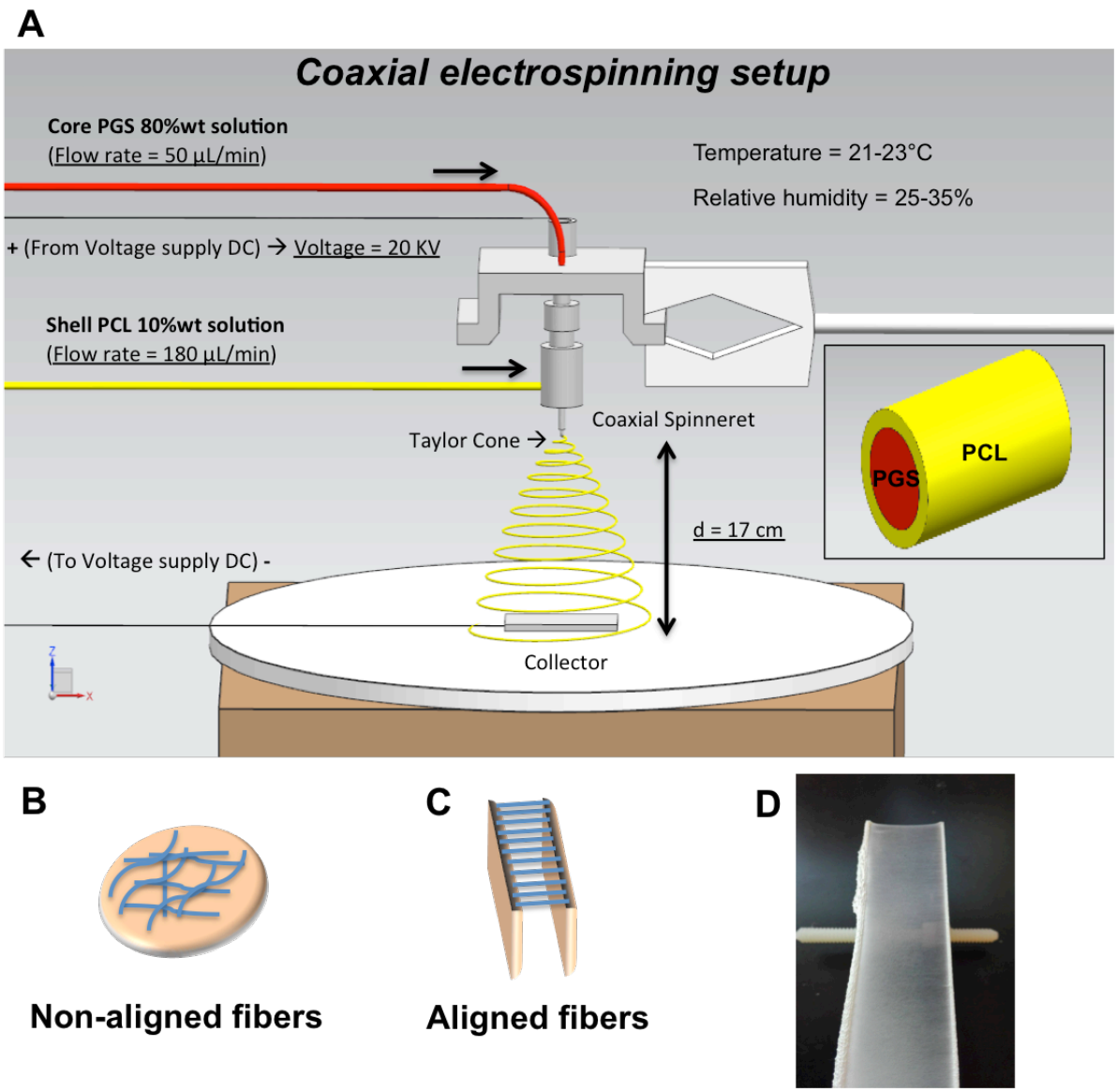

Figure VII.1. Coaxial electrospinning setup and parametes used for the fabrication of coaxial aligned PGS/PCL nanofibers (A). Non-aligned nanofibers were produced in a round aluminum foil-coated copper collector plate (B) and aligned nanofibers were recovered in a two parallel copper plate collector (C, D).

VII.2.3. Characterization of coaxial PGS/PCL electrospun nanofibers

VII.2.3.1. SEM analysis and fiber diameter measurements

The structural characterization of the non-aligned/aligned coaxial PGS/PCL and monoxial PCL fibers was performed using a field emission scanning electron microscope (FE-SEM, FEI-Versa 3D Dual Beam, Hillsboro). Prior to imaging, samples were mounted on a holder and sputter-coated with a thin layer of 60% gold-40% palladium. Samples were imaged at several magnifications using an accelerating voltage of 3-5 kV. The average fiber diameters and subsequent distributions of both non-aligned/aligned monoaxial PCL and coaxial

PGS/PCL fibers were determined by measuring 100 individual fibers per condition from at least 5 different SEM images using the ImageJ software (ImageJ 1.51f, National Institutes of Health, USA). In addition, the mats were cross-sectioned in liquid nitrogen, sputter-coated with thin layer of 60% gold-40% palladium and imaged by SEM to assess the core-shell structure of the fibers.

VII.2.3.2. TEM analysis

The core-shell nature of coaxial PGS/PCL electrospun nanofibers was confirmed by TEM. For that, coaxial PGS/PCL nanofibers were spun directly on lacey carbon coated 200 mesh copper grids and imaged using a JEOL-JEM-2011 TEM (JEOL Ltd., Tokyo, Japan) operating at an accelerating voltage of 200 kV.

VII.2.3.3. X-ray diffraction (XRD) analysis

X-ray diffraction (XRD) analysis was used to confirm the presence of both PCL and PGS materials in the constitution of coaxial PGS/PCL electrospun fibers. Thus, coaxial PGS/PCL and monoaxial PCL fiber mats as well as PCL and PGS raw polymers were evaluated using a Bruker D8-DISCOVER X-ray diffractometer equipped with a $Cu_{K\alpha}$ radiation source and a pyrolytic graphite monochromator.

VII.2.3.4. ATR-FTIR analysis

A Spectrum One FTIR Spectrometer (PerkinElmer, USA) working in the Attenuated total reflectance – Fourier transform infrared (ATR-FTIR) mode was used to collect the spectra of both coaxial PGS/PCL and monoaxial PCL electrospun fibers in the spectral region 4000-650 cm^{-1} and with a resolution of 4 cm^{-1}. Characteristic peaks were identified by comparison with the spectra of PCL and PGS raw polymers.

VII.2.3.5. Differential scanning calorimetric (DSC) analysis

Pre-weighed samples of coaxial PGS/PCL fibers, monoaxial PCL fibers and respective PCL, PGS raw polymers were hermetically sealed in aluminum pans and submitted to healing and cooling cycles between -50ºC and 100ºC at a constant heating rate of 5ºC/min using a TA Instruments DSC-Q100 equipment (New Castle, Delaware USA) under nitrogen supply. The thermal properties of the samples, namely the melting and crystallization

temperatures were determined using the Universal Analysis software V4.7A (TA Instruments).

VII.2.3.6. Mechanical tensile testing

The mechanical properties of non-aligned/aligned monoaxial PCL and coaxial PGS/PCL electrospun scaffolds were assessed under uniaxial tensile testing using a mechanical tester (Instron® Model 5544) with a 10 N load cell and at a constant displacement rate of 10 mm/min. For each fiber mat condition, five different test specimens (n=5) were prepared in a rectangular shape with a length of 15 mm, width of 10 mm and a thickness of 0.2 mm. Bluehill® 2 software was used to collect and process the experimental data from the tensile tests. Young's elastic moduli were calculated from the initial 0-15% linear in the stress-strain curve. Ultimate tensile strength (UTS) was measured from the highest peak of the stress-strain curves.

VII.2.3.7. *In vitro* accelerated degradation study

Monoaxial PCL and coaxial PGS/PCL aligned electrospun mats were cut into 15 mm x 7 mm x 0.2 mm and subjected to a accelerated degradation assay by incubation with 5 mL of 0.5 mM NaOH solution in PBS (Gibco) at 37ºC for different time periods (7, 14 and 21 days). Upon incubation at each degradation timepoint, electrospun scaffolds were rinsed gently with PBS and dried under vacuum. The samples weight (n=3) was measured and the percentage of weight loss was determined by dividing the obtained weight loss to the initial dry weight of each sample (before incubation).

VII.2.4. *In vitro* kartogenin (KGN) release assay

KGN was dissolved in a mixture of DMSO:TFE (volume ratio 20:80) under agitation overnight and then combined with the polymer casting solutions at a final concentration of 2mg/mL to fabricate two different groups of aligned electrospun nanofibers following the procedure described in subsection 2.2: coaxial PGS-KGN/PCL (core solution: PGS 80%-KGN 0.2% w/v and shell solution: PCL 10% w/v) and monoaxial PCL-KGN (solution: PCL 10%-KGN 0.2% w/v). KGN-loaded electrospun scaffolds (15 mm x 7 mm x 0.2 mm) were weighed, immersed in 1 mL of PBS (pH 7.4) and placed on a shaker (100 rpm) at 37ºC with a humidified atmosphere to mimic physiological conditions. At each sampling time, the total volume of PBS was collected and replaced with the same volume of fresh PBS to determine the release kinetics of KGN from the electrospun scaffolds. The amount of KGN released

from each electrospun scaffold was evaluated using HPLC (Agilent 1200 LC system, EC-C18 reverse phase column) and normalized to the scaffold initial weight. *In vitro* release was measured from five scaffolds (n=5) at different time-points during 21 days (0, 1, 3, 6, 12, 24, 48, 72, 120, 168, 216, 288, 360, 432 and 504 h).

VII.2.5. hBMSC seeding and culture on KGN-loaded electrospun aligned nanofibers

As the goal of this study is to fabricate electrospun fibers able to mimic the alignment and nanometer scale of the collagen fibers present in the superficial layer of native articular cartilage, we performed the *in vitro* cell culture experiments using coaxial PGS/PCL aligned and monoaxial PCL aligned nanofibers with or without loaded KGN.

Previous to cell seeding, the electrospun scaffolds were sterilized by UV exposure for 3 h, placed in ultra-low cell attachment 24-well plates and washed three times with PBS+1% Pen-Strep solution. Afterwards, the nanofiber scaffolds were soaked in culture medium and incubated at 37ºC for 1 h.

Human bone marrow MSC (hBMSC) were purchased from Lonza (Basel-Switzerland), thawed and expanded on tissue culture flasks (CELLTREAT® Scientific Products, MA) using low-glucose Dulbecco's Modified Eagle Medium (DMEM, Gibco, Grand Island, NY) supplemented with 10% fetal bovine serum (FBS, Gibco) and 1% penicillin-streptomycin (Pen-strep, Gibco), and kept at 37 ºC and 5% CO_2 in a humidified atmosphere until scaffold seeding. Complete medium renewal was performed every 3-4 days and all the experimental assays were performed using cells in passage 3 or 4.

hBMSC were seeded on the electrospun nanofiber scaffolds at a density of 50000 cells per scaffold and incubated for 2 h at 37ºC and 5% CO_2 without culture medium to favor initial cell attachment. Afterwards, incomplete chondrogenic medium composed by high glucose DMEM (Thermo Fisher Scientific) with 100nM dexamethasone (Sigma-Aldrich), 50 µg/mL ascorbic acid 2-phosphate (Sigma-Aldrich), 40 µg/mL L-proline (Sigma-Aldrich), 1mM sodium pyruvate (Gibco), ITS™+ Premix supplement (6.25 µg/mL bovine insulin; 6.25 µg/mL transferrin; 6.25 µg/mL selenous acid; 5.33 µg/mL linoleic acid; 1.25 µg/mL BSA, Corning), Pen-strep (100 U/mL penicillin; 100 µg/mL streptomycin) was added to all the scaffolds. The cultures were conducted during 21 days at 37ºC and 5% CO_2 under low oxygen conditions (hypoxia – 5% O_2 to mimic the hypoxic environment of articular cartilage) and the chondrogenic culture medium (without TGF-β3) was fully renewed every 3-4 days.

The metabolic activity of hBMSC on the monoaxial/coaxial KGN-loaded aligned nanofibers and respective controls was evaluated using AlamarBlue® cell viability reagent (ThermoFischer Scientific, USA) on days 3, 7, 14 and 21 following the manufacturer's guidelines. Briefly, a 10% (v/v) AlamarBlue® solution in culture medium was added to the

scaffolds and incubated at 37 ºC in 5% CO_2 chamber for 3 h. Fluorescence intensity values were measured in a microplate reader (SpectraMax M5, Molecular Devices, USA) at an excitation/emission wavelength of 560/590 nm and compared to a calibration curve to access the equivalent number of viable cells present in each scaffold. Acellular scaffolds (for each experimental group) were used as blank controls in the fluorescence intensity measurements. Three independent scaffolds (n=3) were analyzed for each experimental group and fluorescence values of each sample were measured in triplicates.

VII.2.6. Assessment of hBMSC chondrogenic differentiation on KGN-loaded aligned electrospun nanofibers

VII.2.6.1. Cell morphology evaluation by SEM

The morphology of the cells cultured for 21 days on monoaxial/coaxial KGN-loaded aligned nanofibers and respective controls was observed by SEM. The samples were fixed with 4% PFA for 20 min, stained with 1% (v/v) osmium tetroxide (Sigma-Aldrich) solution for 30 min and washed twice with PBS. Afterwards, samples were dehydrated using ethanol gradient solutions (20%, 40%, 60%, 80%, 95% and 100% (v/v)) for 20 min each and finally dried in a critical point dryer (supercritical Automegasamdri 915B, Tousimis, USA) in 100% isopropanol. Dried samples were mounted, sputter-coated and imaged using the above-mentioned SEM procedure.

VII.2.6.2. sGAG content quantification (DMMB assay)

At days 14 and 21 of differentiation, the electrospun scaffolds were collected, washed with PBS and digested in a 125 µg/mL papain enzyme (from papaya latex, Sigma-Aldrich) solution (50 mM sodium phosphate, 2 mM N-acetyl cysteine, 2 mM EDTA, all from Sigma-Aldrich, pH 6.5) at 60ºC overnight (16-18 h). The sulfated GAG (sGAG) produced by cells on the electrospun scaffolds was quantified using 1,9-dimethylmethylene blue (DMMB, Sigma-Aldrich) assay. The digested samples were mixed with a DMMB solution (16 mg DMMB in 0.3% w/v glycine, 0.27% sodium chloride in distilled water, pH 3.0) in 96-well plates and the absorbance was measured at 525 nm. The sGAG amounts were extrapolated from a calibration curve generated using chondroitin 6-sulfate (sodium salt from shark cartilage, Sigma-Aldrich) standards and normalized to the equivalent number of cells present in each scaffold. Three scaffolds (n = 3) were used for each experimental group and the absorbance values were measured in triplicate. Acellular electrospun scaffolds for each experimental group were used as blank controls.

VII.2.6.3. RNA extraction and real-time quantitative PCR (RT-qPCR) analysis

Total RNA was extracted from the final constructs (day 21) using the RNeasy Mini Kit (QIAGEN, Hilden, Germany). Briefly, the samples were first incubated in lysis buffer with 200 rpm agitation for 30 min at 4 ºC. Afterwards, total RNA was isolated according to the manufacturer's protocol and quantified using a Nanodrop (ND-100 Spectrophotometer, Nanodrop Technologies). cDNA was synthesized from the purified RNA using iScript™ Reverse Transcription Supermix (Bio-Rad, Hercules, CA USA) following the manufacturer's guidelines. The reaction mixtures with a total volume of 20 µL were incubated in a thermal cycler (Veriti Thermal Cycler, Applied Biosystems, CA USA) for 5 min at 25ºC, 20 min at 46ºC and 1 min at 95ºC and then were maintained at 4ºC.

Real time quantitative PCR (RT-qPCR) analysis was performed using the TaqMan® Fast Advanced Master Mix (Applied Biosystems) and StepOnePlus real-time PCR system (Applied Biosystems) according to the manufacturer's protocol. Reactions were run in triplicate using the TaqMan® Gene Expression Assays (20X) (Thermo Fisher Scientific) presented in Table VII.1. The obtained CT values were normalized against the expression of housekeeping gene *GAPDH* and the analysis was performed using the $2^{-\Delta\Delta Ct}$ method. Results for target gene expressions in the different experimental groups are presented as fold-change expression levels relative to hBMSC before scaffold seeding (day 0).

Table VII.1. TaqMan assays used for RT-qPCR analysis.

Targe Genes	ID numbers
GAPDH	Hs02758991_g1
COL1A1	Hs00164004_m1
COL2A1	Hs00264051_m1
Sox9	Hs00165814_m1
ACAN	Hs00153936_m1
PRG4	Hs00981633_m1

VII.2.6.4. Immunofluorescence analysis

After 21 days of differentiation, the medium was removed and the electrospun scaffolds were washed with PBS and fixed with PFA 4% for 20 min. The samples were then washed twice with PBS and permeabilized and blocked with a solution of 0.3% Triton X-100 (Sigma-Aldrich), 1% BSA (Sigma-Aldrich) and 10% Goat serum (ThermoFischer Scientific) in PBS at room temperature for 30 min. A solution containing primary antibody for collagen II (1:200 in

blocking solution, mouse collagen II monoclonal antibody 6B3, ThermoFisher Scientific) was incubated with the samples overnight at 4ºC. Afterwards the samples were washed once with 1% BSA solution (in PBS) and incubated with the secondary antibody Goat anti-mouse IgG AlexaFluor 488 (1:150 in 1% BSA (in PBS) solution, ThermoFisher Scientific) for 1 h at room temperature and protected from light. Finally, the samples were counterstained with DAPI (Sigma-Aldrich) for 5 min at room temperature, washed with PBS and imaged using a confocal microscope (Zeiss LSM 510META Spectral Confocal).

VII.2.7. Statistical analysis

Results are presented as mean values ± standard deviation (SD) of 3 independent experiments (n=3), unless specified differently. The statistical analysis of the data was performed using one-way ANOVA, followed by Tukey post-hoc test. GraphPad Prism version 7 software was used in the analysis and data was considered to be significant when *p*-values obtained were less than 0.05 (95% confidence intervals, $*p < 0.05$).

VII.3. Results

VII.3.1. Coaxial PGS/PCL electrospun nanofibers scaffold structural characterization

Coaxial PGS/PCL and monoaxial PCL aligned nanofibers as well as their respective non-aligned controls were produced using the electrospinning apparatus and conditions shown in Figure VII.1. SEM micrographs (Figure VII.2 A) showed that all the electrospun scaffolds were highly porous and interconnected, which favors oxygen and media diffusion through the scaffold and provides a higher surface area for cell adhesion. Figure VII.2 B presents the average fiber diameter and respective distributions for all the conditions studied. Importantly, all the electrospun scaffolds presented average fiber diameters in the nanometer scale (505-738 nm), which is advantageous to mimic the structural features of *in vivo* articular cartilage ECM. Interestingly, both coaxial PGS/PCL and monoaxial PCL aligned nanofibers presented slightly lower average fiber diameters than their non-aligned counterparts. The core-shell structure of the fibers was confirmed by TEM (Figure VII.3), as it is possible to clearly discriminate between two different materials, PGS in the core and PCL in the shell (Figure VII.3 B), as opposed to PCL monoaxial fiber (Figure VII.3 A). The coaxial structure was also observed by SEM analysis of cross-sectioned fibers (Figure VII.3 C).

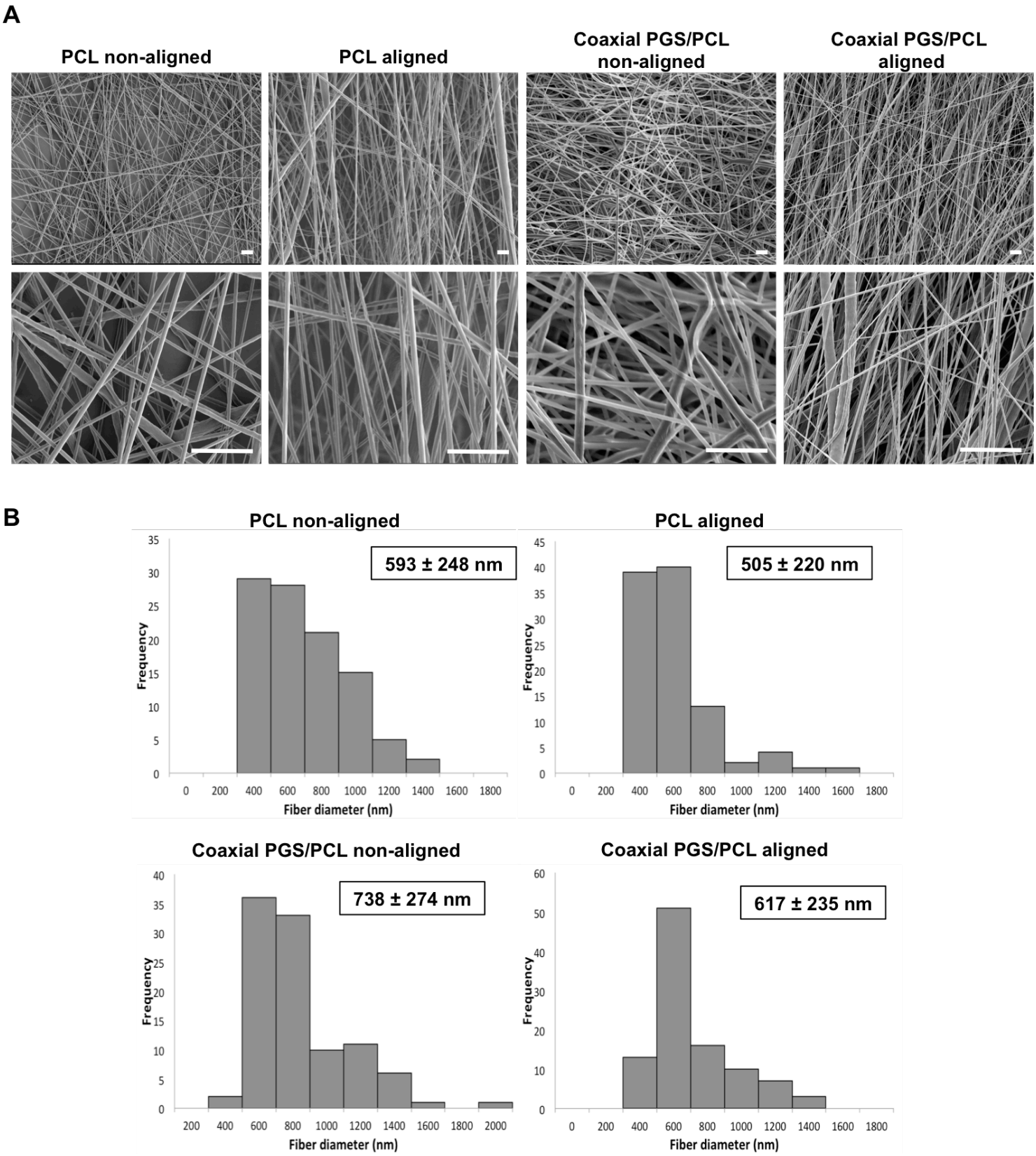

Figure VII.2. SEM images (at two different magnifications) of the non-aligned/aligned monoxial PCL and coaxial PGS/PCL nanofibers (A) and respective fiber diameter distribution histograms (B). Average fiber diameters are presented as mean ± SD of 100 individual fibers. Scale bar: 5 μm.

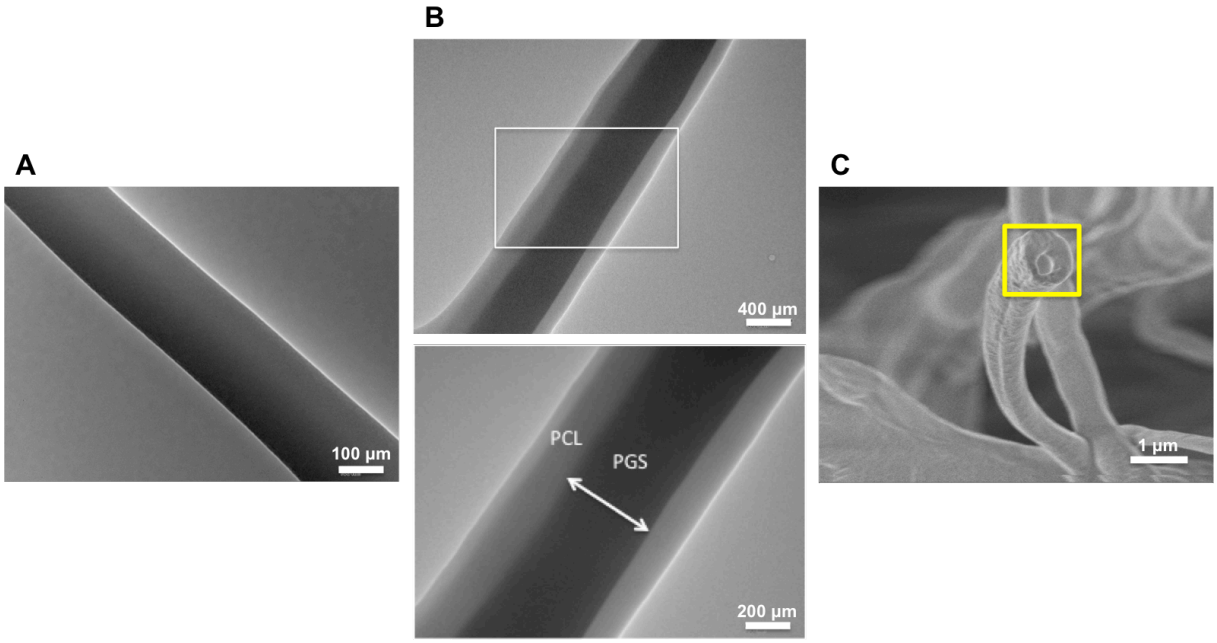

Figure VII.3. Confirmation of the core-shell structure of the produced electrospun nanofibers. TEM images of monoaxial PCL nanofibers (A) and of coaxial PGS/PCL nanofibers (B). The bottom image in B corresponds to a magnification of the top image (white box). The core-shell structure of coaxial PGS/PCL nanofibers was further confirmed by SEM analysis of cross-sectioned fibers, highlighted by the yellow box (C). Scale bars are depicted in the figure.

VII.3.2. Chemical, thermal, mechanical and biodegradation properties of coaxial PGS/PCL electrospun nanofibers scaffolds

The chemical characterization of the coaxial PGS/PCL nanofibers in comparison with PCL nanofibers as well as with the PGS pre-polymer and pure polymer PCL was performed by XRD (Figure VII.4 A) and FTIR analysis (Figure VII.4 B). XRD spectra of both PCL polymer and nanofibers show the presence of two peaks at 21.3º and 23.7º, while the PGS polymer exhibits two peaks at 19.3º and 23º. The XRD spectra for the coaxial PGS/PCL nanofibers present three peaks including the two major peaks of the PCL spectra and a peak at 19.3º that can be assigned to the PGS portion, thereby confirming the presence of both PCL and PGS polymers in their constitution. The presence of both PGS and PCL in the coaxial electrospun scaffolds was also confirmed by FTIR analysis. Both PGS and PCL (polymer and nanofibers) showed very similar major IR peaks at approximately 2943 cm^{-1} (CH_2 stretching-asymmetric), 2864 cm^{-1} (CH_2 stretching-symmetric), 1725 cm^{-1} (ester carbonyl bond stretching) and 1187 cm^{-1} (carbon-oxygen bond stretching). Despite being slightly masked by other peaks higher amplitude, the PGS spectra showed an additional hydroxyl group peak at 3450 cm^{-1}, which was not present in PCL. The coaxial PGS/PCL nanofibers presented all the mentioned peaks, suggesting the composite nature of the fibers.

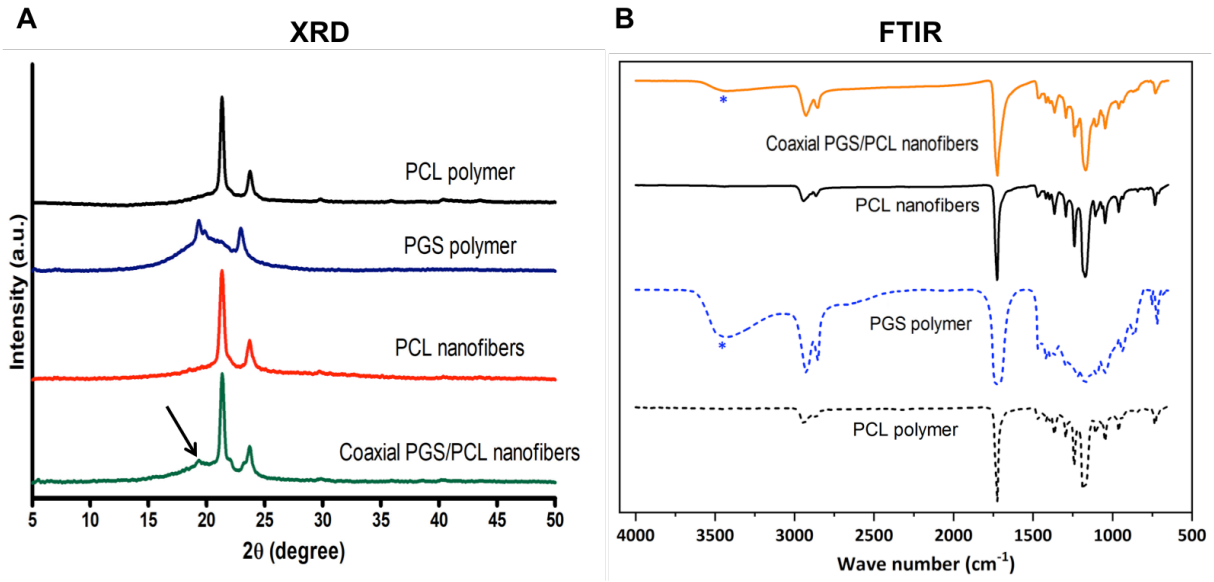

Figure VII.4. XRD (A) and FTIR (B) analysis of coaxial PGS/PCL nanofibers, monoxial PCL nanofibers and respective PGS and PCL polymers. The black arrow and blue asterisk highlight the characteristic peaks that confirmed the presence of both PCL and PGS in the coaxial electrospun nanofibers.

The thermal properties of the fabricated electrospun scaffolds were also assessed using DSC analysis (Figure VII.5). DSC thermograms of heating (Figure VII.5 A) and cooling (Figure VII.5 B) cycles for the electrospun scaffolds and respective individual polymers also supported the composite nature of the coaxial nanofibers. Indeed, the coaxial PGS/PCL nanofibers exhibit two distinct melting temperatures (T_m) ($T_{m\text{-}PCL}$=52.90ºC and $T_{m\text{-}PGS}$ 13.45ºC) and crystallization temperatures (T_c) ($T_{c\text{-}PCL}$=27.28ºC and $T_{c\text{-}PGS}$=-7.77ºC) indicating the presence of both polymers in its constitution. All the melting and crystallization temperatures calculated are summarized in Figure VII.5 C.

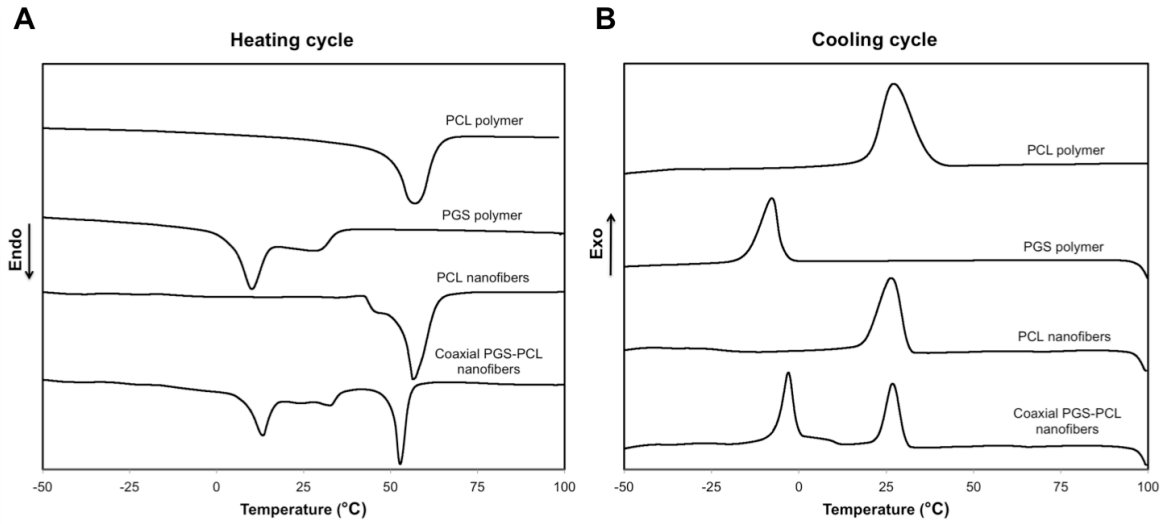

C

Sample	$T_{m\text{-}PCL}$(°C)	$T_{c\text{-}PCL}$(°C)	$T_{m\text{-}PGS}$(°C)	$T_{c\text{-}PGS}$(°C)
PCL polymer	57.07	27.17	-	-
PGS polymer	-	-	10.17	-7.77
PCL nanofibers	56.60	26.49	-	-
Coaxial PGS/PCL nanofibers	52.90	27.28	13.45	-3.06

Figure VII.5. DSC thermograms (heating (A) and cooling (B) cycles) of coaxial PGS/PCL nanofibers, monoxial PCL nanofibers and respective pure PGS and PCL polymers. Melting (T_m) and crystallization (T_c) temperatures determined for all the samples tested (C).

The analysis of the mechanical performance of the electrospun scaffolds under tensile testing is shown in Figure VII.6. In order to assess the effect of the fiber alignment on the scaffold mechanical properties, non-aligned coaxial and monoaxial nanofibers were also considered in the analysis. Representative stress-strain curves for all the conditions tested are presented in Figure VII.6 A. Fiber alignment resulted in a significant increase ($p < 0.05$) in the elastic modulus in both monoaxial (9.90 ± 0.87 MPa in PCL aligned *vs.* 4.02 ± 0.88 MPa in PCL non-aligned) and coaxial (11.78 ± 0.73 MPa in coaxial PGS/PCL aligned *vs.* 5.06 ± 1.51 MPa in coaxial PGS/PCL non-aligned) configurations. It is also possible to observe that the addition of PGS in the core of coaxial fibers resulted in an increase in the elastic modulus when compared to the respective monoaxial counterparts, however such increase was not statistically significant (Figure VII.6 B). Regarding the UTS, aligned fibers also presented higher values than the non-aligned counterparts, however significant differences were only observed for monoaxial PCL fibers (5.36 ± 0.76 MPa in PCL aligned *vs.* 2.85 ± 0.47 MPa in PCL non-aligned and 2.98 ± 0.20 MPa in coaxial PGS/PCL aligned *vs.* 2.33 ± 0.26 MPa in coaxial PGS/PCL non-aligned) (Figure VII.6 C).

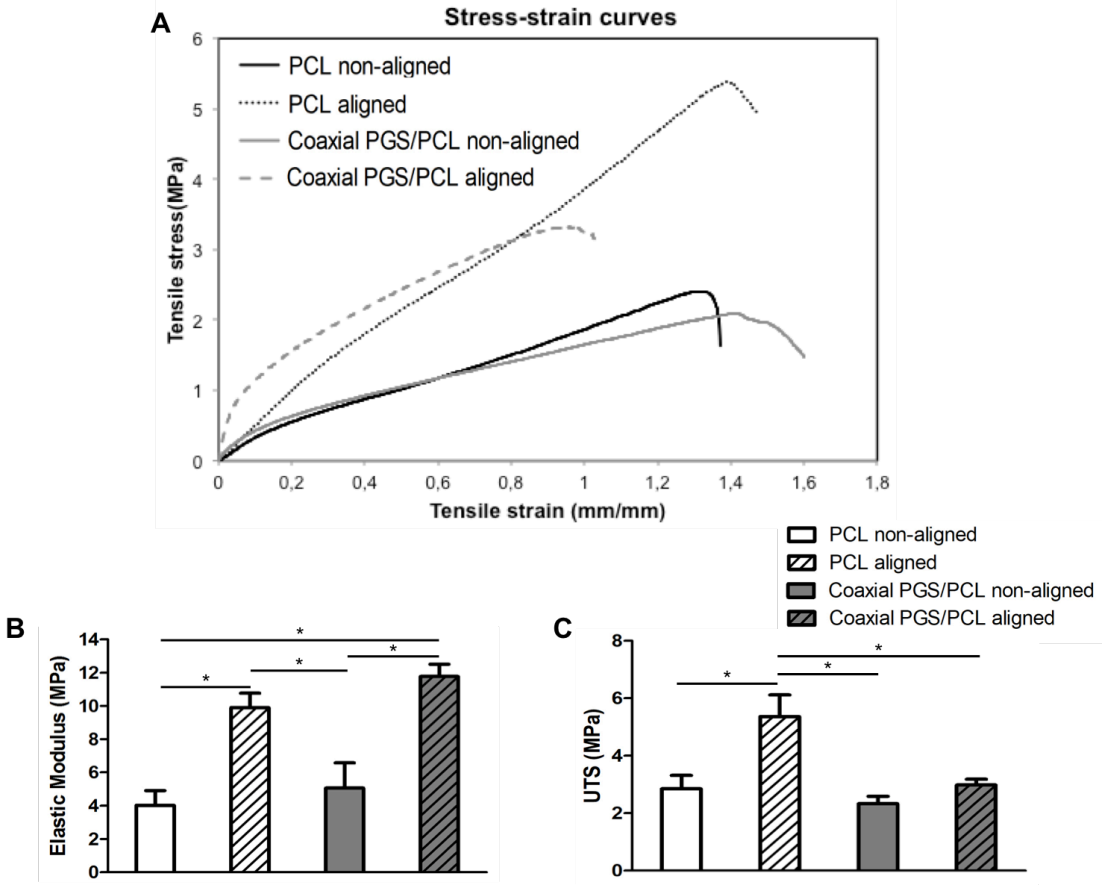

Figure VII.6. Mechanical properties of aligned/non-aligned monoaxial PCL and coaxial PGS/PCL electrospun scaffolds: Representative stress-strain curves (A), elastic modulus (B) and ultimate tensile strength (C). Results are presented as mean ± SD of five independent specimens (n=5). *$p < 0.05$.

The degradation of coaxial PGS/PCL and monoaxial PCL aligned electrospun scaffolds was studied under accelerated conditions (in 0.5 mM NaOH solution) for 21 days (Figure VII.7). After 21 days, monoaxial PCL electrospun scaffolds showed only a residual mass loss (2.3 ± 1.4%), confirming the reported slow-degradation behavior of the PCL polymer. In contrast, coaxial PGS/PCL nanofibers showed a higher degradation rate, reaching a weight loss of 23 ± 1.6% at the end of the experiment (Figure VII.7 A). This is in accordance with SEM images of the samples before (day 0) and after the accelerated degradation assay (day 21), in which a considerable deterioration of the fibers was observed in coaxial PGS/PCL electrospun scaffolds (Figure VII.7 B).

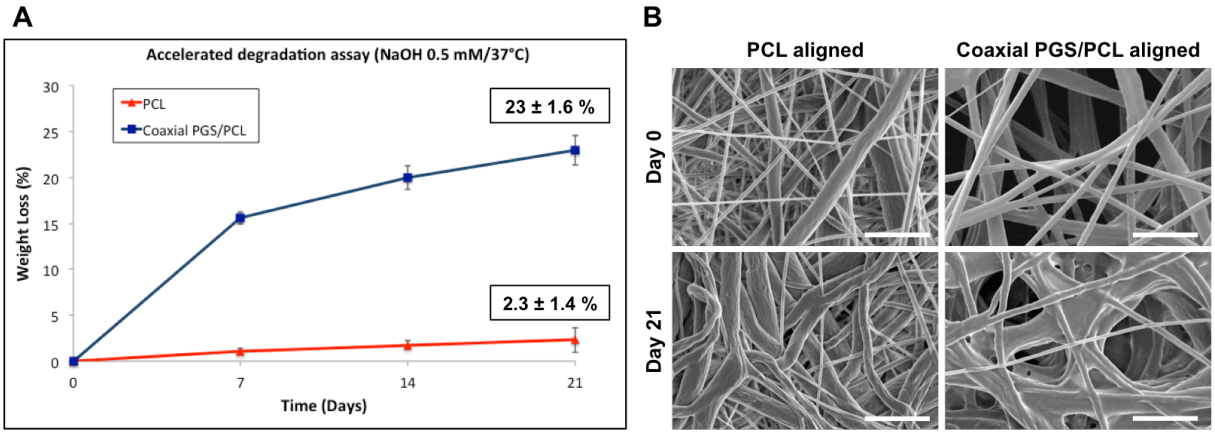

Figure VII.7. *In vitro* accelerated degradation of monoaxial PCL and coaxial PGS/PCL aligned electrospun scaffolds: Percentage of weigth loss evaluated after 7, 14 and 21 days soaking in NaOH 0.5 mM solution (in PBS) at 37ºC (A) and SEM images of the electrospun scaffolds before (day 0) and at the end of the degradation assay (day 21) (B). Results are presented as mean ± SD of three independent samples (n=3). Scale bar: 5 µm.

VII.3.3. KGN release profile from monoaxial/coaxial electrospun scaffolds

KGN (Figure VII.8 B) was loaded into the core PGS solution to produce coaxial PGS-KGN/PCL aligned nanofibers and also into the PCL solution to generate monoaxial PCL-KGN aligned nanofibers (Figure VII.8 A). The addition of KGN did not result in any meaningful changes on the structure of the nanofibrous scaffolds fabricated. The produced scaffolds were assessed for the *in vitro* release kinetics of KGN during 21 days. For both scaffold types, the KGN release profile was characterized by an initial burst release until 24 h, followed by a relatively slow and nearly linear release. As it is possible to observe in Figure VII.8 C, coaxial nanofibers allowed a more controlled release and an alleviated burst release than the monoaxial nanofibers. During the 21 days of the *in vitro* study, a total of 0.32 ± 0.03 µg KGN/mg of scaffold and 1.11 ± 0.44 µg KGN/mg of scaffold were released from the coaxial PGS-KGN/PCL and monoaxial PCL-KGN nanofibers, respectively.

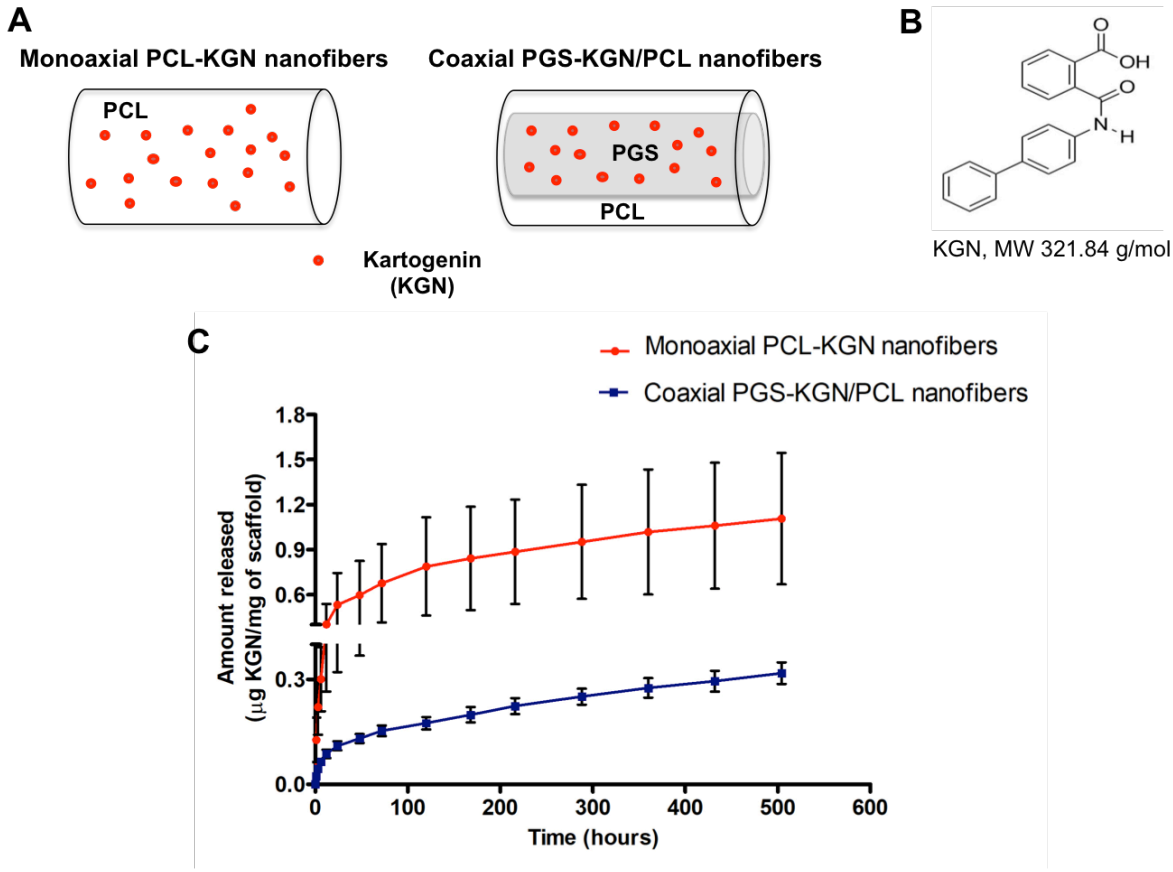

Figure VII.8. *In vitro* release of KGN from monoaxial PCL and coaxial PGS/PCL aligned nanofibers for 21 days at 37ºC, pH = 7.4 and 100 rpm: Schematic representation of the coaxial PGS-KCN/PCL and monoaxial PCL-KGN fibers (A), chemical structure of KGN (B), and amount of KGN released as a function of time and normalized to the weight of the scaffold. Results are presented as mean ± SD of five independent scaffolds (n=5).

VII.3.4. Effects of KGN-loaded electrospun aligned nanofibers on cell proliferation and morphology

The effects of KGN release on hBMSC proliferation (Alamar Blue assay) were evaluated *in vitro* using both coaxial PGS-KGN/PCL and monoaxial PCL-KGN aligned nanofibers in comparison to non-loaded controls (Figure VII.9 A). At the end of the experiment (day 21), both coaxial PGS-KGN/PCL and monoaxial PCL-KGN aligned nanofibers showed significantly higher ($p < 0.05$) equivalent cell numbers than the scaffolds without KGN. The coaxial PGS-KGN/PCL electrospun scaffolds also showed improved hBMSC proliferation in comparison to PCL-KGN, however, such increase was not statistically significant. Interestingly, coaxial PGS-KGN/PCL scaffolds presented a significantly enhanced hBMSC proliferation in comparison with coaxial PGS/PCL scaffolds since earlier stages of the culture (from day 7 onwards). The morphology of hBMSCs on the different electrospun scaffolds tested (at day 21) was analyzed by SEM and can be observed in Figure VII.9 B.

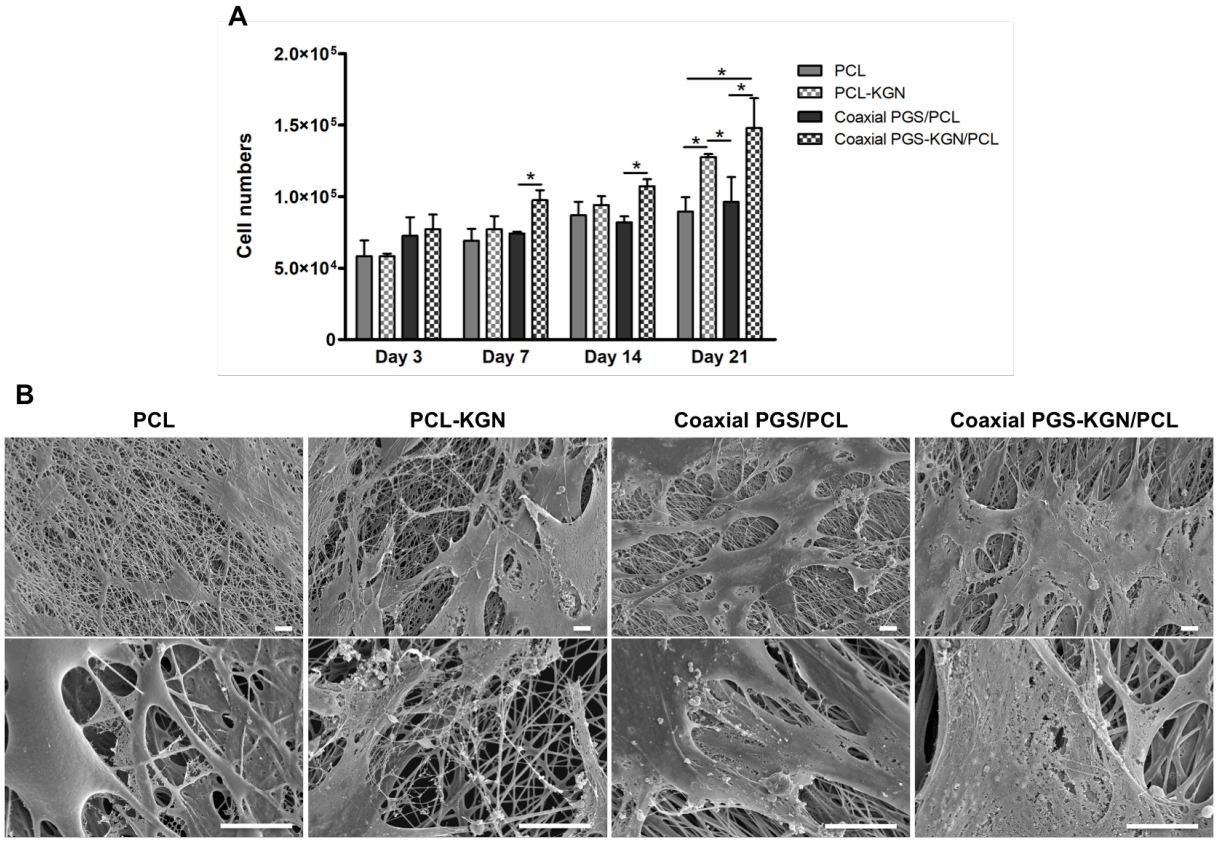

Figure VII.9. Effects of KGN-loaded monoaxial and coaxial aligned nanofibers on hBMSC proliferation and morphology: Cell proliferation assay (A) and SEM images showing hBMSC morphology on all the electrospun scaffolds tested (at day 21) (B). Results are presented as mean ± SD (n=3). *p < 0.05. Scale bar: 10 μm.

VII.3.5. hBMSC chondrogenic differentiation on KGN-loaded electrospun aligned nanofibers

The ability of KGN-loaded coaxial and monoaxial electrospun scaffolds to promote hBMSC chondrogenesis was evaluated by assessing cartilage-like ECM production and the expression of chondrogenic gene markers. As shown in Figure VII.10, all the scaffolds tested supported GAG production (Figure VII.10 A) over time and stained positively for the presence of collagen II (Figure VII.10 B), both main components of articular cartilage ECM. At day 14, higher amounts of GAG were observed for PCL-KGN electrospun scaffolds (7.92 ± 1.32 μg sGAG/10^5 cells) compared to all other groups. After 21 days of chondrogenic differentiation, PCL, PCL-KGN, coaxial PGS/PCL and coaxial PGS-KGN/PCL electrospun scaffolds afforded sGAG amounts of 7.50 ± 1.96 μg/10^5 cells, 9.74 ± 1.93 μg/10^5 cells, 5.09 ± 2.04 μg/10^5 cells and 10.12 ± 1.91 μg/10^5 cells, respectively. Despite both KGN-loaded scaffolds affording higher sGAG amounts than the scaffolds without KGN, a statistically

significant (p < 0.05) enhancement was just observed for the coaxial PGS-KGN/PCL scaffolds compared to non-loaded counterparts.

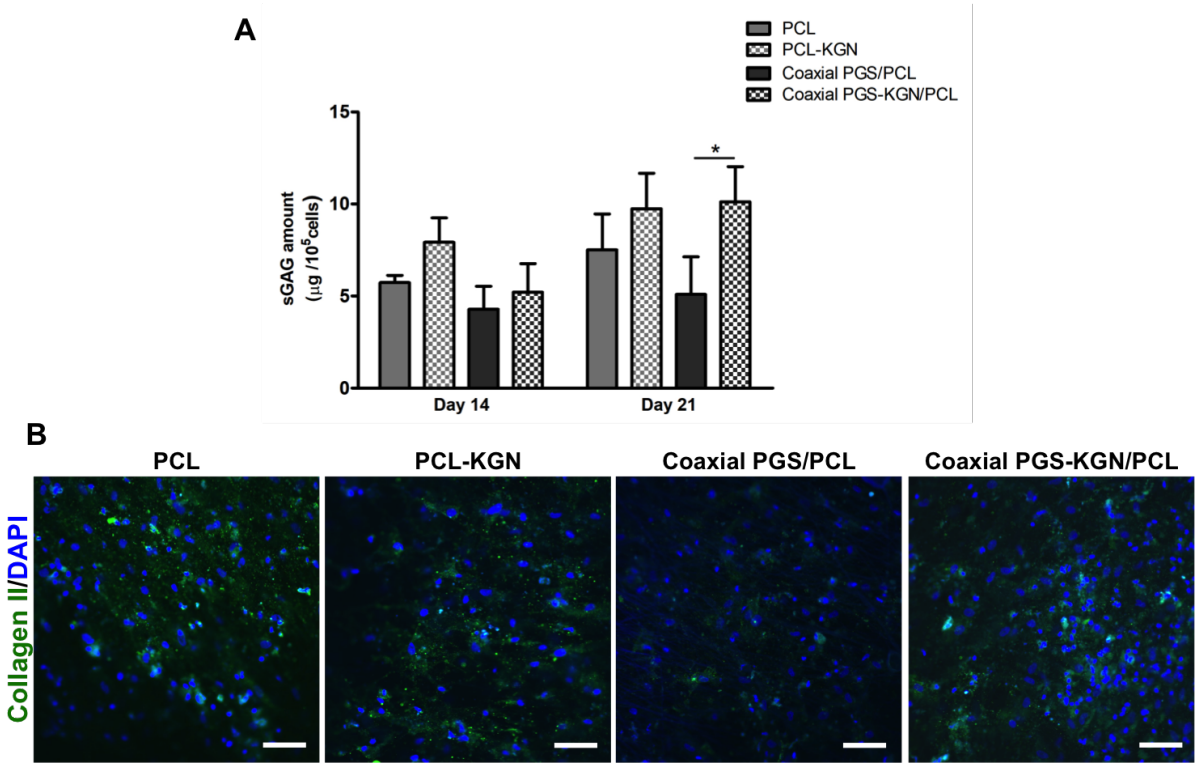

Figure VII.10. Effects of KGN-loaded monoaxial and coaxial aligned nanofibers on cartilage ECM production: sGAG amounts produced after 14 and 21 days of hBMSC chondrogenic differentiation on the electrospun scaffolds (A) and immunofluorescence analysis to evaluate the presence of collagen II on the electrospun scaffolds (at day 21) (B). For the immunofluorescence analysis, samples were counterstained with DAPI. Results are presented as mean ± SD (n=3). *p < 0.05. Scale bar: 50 µm.

Gene expression in the different groups of electrospun scaffolds was evaluated at the end of the differentiation protocol (day 21) by RT-qPCR analysis (Figure VII.11). All the scaffolds showed no significant upregulation of *COL1A1* gene (Figure VII.11 A), a fibrocartilage marker, in comparison to the control (hBMSC at day 0). Regarding *COL2A1* (Figure VII.11 B), *Sox9* (Figure VII.11 C) and *ACAN* (Figure VII.11 D) gene expression, KGN-loaded electrospun scaffolds demonstrated significantly higher (p < 0.05) expressions in comparison to the non-loaded electrospun scaffolds. Moreover, no statistically significant differences were observed between coaxial PGS-KGN/PCL and monoaxial PCL-KGN electrospun scaffolds. It is noteworthy that all the electrospun scaffolds resulted in significant upregulation of the PRG4 gene (Figure VII.11 E), which encodes for lubricin/superficial zone protein (SZP) present in the superficial layer of articular cartilage and responsible for the lubrication at the joint surface.

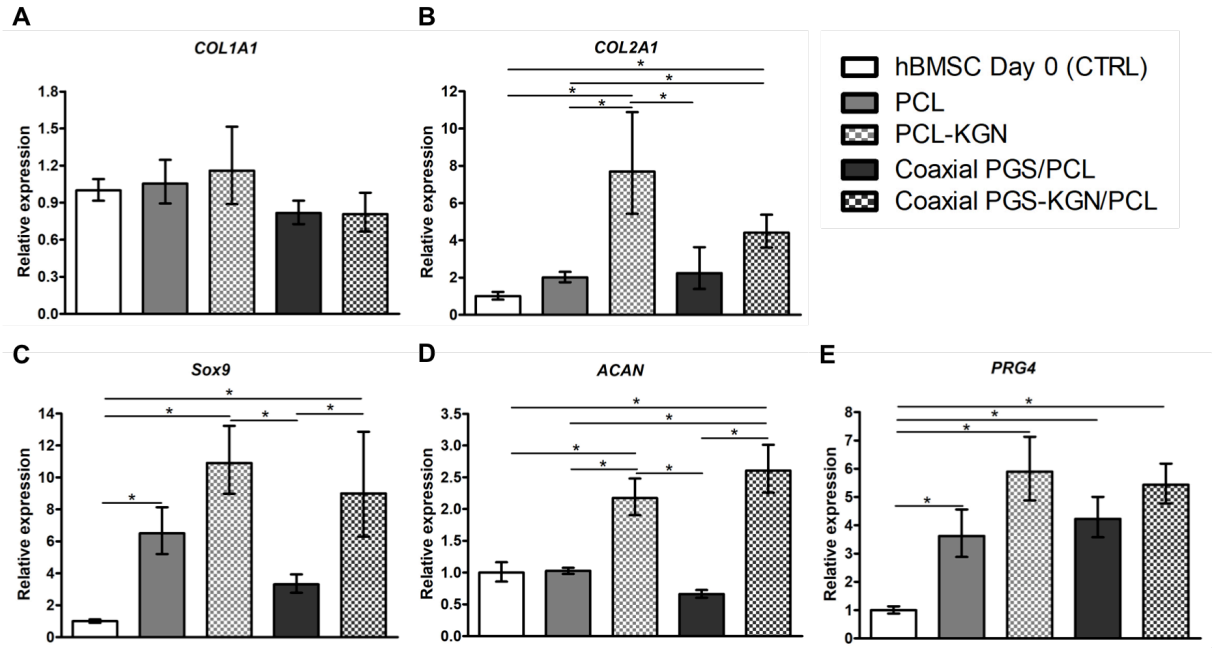

Figure VII.11. Effects of KGN-loaded monoaxial and coaxial aligned nanofibers on the gene expression of hBMSC evaluated by RT-qPCR analysis after 21 days of chondrogenic differentiation. Expressions of *COL1A1* (A), *COL2A1* (B), *Sox9* (C), *ACAN* (D) and *PRG4* (E) were normalized to the endogenous gene *GAPDH* expression and calculated as a fold-change relative to the baseline expression of the control sample (hBMSC before scaffold seeding at day 0). Results are presented as mean ± SD; n=3; * $p < 0.05$.

VII.4. Discussion

The fabrication of biomimetic scaffolds that can recapitulate the structural features of articular cartilage ECM is crucial for successful tissue regeneration. Biodegradable electrospun nanofiber scaffolds have been explored to mimic the size, alignment and mechanical properties of the collagen fibers present in the superficial zone of articular cartilage (Wise et al., 2009). Moreover, electrospun nanofibers have been explored in combination with MSCs for CTE applications (Alves Da Silva et al., 2010; Reboredo et al., 2016; Shafiee et al., 2011). However, despite all the advantages of electrospun scaffolds, they seem to be insufficient to fully regulate cellular behavior. Hence, the integration of bioactive molecules with electrospun fibers has been explored to improve scaffold's biological performance (Ji et al., 2011).

Synthetic polymers are commonly used to produce electrospun scaffolds for CTE due to their versatility, superior mechanical properties and higher consistency across batches (Cheng et al., 2019). Despite PGS emergence as a promising scaffold material for tissue engineering applications, processing of PGS fibrous scaffolds is challenging due to the high temperature and vacuum conditions necessary for the PGS pre-polymer synthesis. In

addition, due to its low molecular weight, PGS pre-polymer itself has low solution viscosity even at high concentrations and therefore cannot be directly electrospun to generate stable fibers (Ifkovits et al., 2008). Strategies used to overcome this limitation include blending with other synthetic or natural materials or the adoption of coaxial fiber configuration, encapsulating PGS in the core (Hou et al., 2017; Kharaziha et al., 2013; Sant et al., 2011; Yi and La Van, 2008).

In this study, we used coaxial electrospinning to fabricate core-shell PGS/PCL aligned nanofiber scaffolds able to mimic the structural features of cartilage ECM, promote the delivery of a chondroinductive small molecule and support cell culture. All the electrospun scaffolds produced were comprised of fibers in the nanometer scale, which was previously shown to be advantageous for MSC chondrogenic differentiation (Schagemann et al., 2013; Wise et al., 2009). Schagemann and colleagues observed enhanced hBMSC chondrogenic differentiation in PCL nanofibrous scaffolds with fiber diameters of approximately 400 nm in comparison to PCL microfibrous scaffolds (Schagemann et al., 2013). The core-shell structure of the coaxial PGS/PCL scaffolds produced was clearly observed by SEM and TEM. The composite nature of the coaxial fibers produced was further confirmed by XRD, FTIR and DSC analysis, which was in accordance with previously reported characterizations (Gaharwar et al., 2014; Salehi et al., 2014).

The coaxial PGS/PCL aligned nanofibrous scaffolds had an elastic modulus of approximately 11.8 ± 0.7 MPa, which is slightly higher, but close to values previously reported for PGS-PCL blend aligned scaffolds (Gaharwar et al., 2014; Masoumi et al., 2014). We observed that the core-shell configuration of the coaxial fibers presented a much lower effect on the electrospun scaffold's elastic modulus than fiber alignment. In fact, coaxial PGS/PCL and monoaxial PCL aligned nanofiber scaffolds showed 2.3-fold and 2.5-fold higher elastic modulus than its respective non-aligned counterparts. This is corroborated by a previous work, in which it was reported that aligned PCL scaffolds afforded a 2.2-fold higher elastic modulus compared to randomly oriented scaffolds (Kim, 2008). Additionally, Gaharwar *et al*. also observed similar behavior for aligned PGS-PCL blend microfibrous scaffolds (Gaharwar et al., 2014). Importantly, our coaxial PGS/PCL scaffold had an elastic modulus under tensile testing within the range of the tensile modulus described for healthy cartilage (5-25 MPa), which varies considerably based on tissue location as result of zonal collagen distribution (Mow and Guo, 2002). In addition, as previously reported by Hou and colleagues for non-aligned coaxial PGS/PCL electrospun microfibers, there is an advantageous possibility of tuning the scaffolds mechanical properties by varying the amount of PGS present in the fiber core (Hou et al., 2017).

The degradation of both coaxial PGS/PCL and monoaxial PCL aligned nanofibers was evaluated *in vitro* for 21 days under accelerated hydrolytic conditions. PCL and PGS have

considerably different biodegradation rates. While the fast degrading PGS is reported to be completely resorbed in the body within 60 days, PCL has a resident time *in vivo* of more than 2 years (Sun et al., 2006; Wang et al., 2003). Accordingly, Masoumi et al. showed that the degradation rate of PCL-PGS blend electrospun scaffolds was highly dependent on the PGS content (Masoumi et al., 2014). After 21 days under accelerated hydrolytic degradation, coaxial PGS/PCL nanofibers afforded a much higher weight loss (23%) than the residual weight loss verified for monoaxial PCL nanofibers (2.3%). In the first 7 days, a higher degradation rate was observed for the coaxial fibers, possibly due to a fast hydrolytic degradation of the encapsulated PGS. From day 7 onwards, a nearly linear mass loss suggests *in vitro* degradation by surface erosion, which is the predominant mechanism described for both PGS and PCL polymers (Bartnikowski et al., 2019; Pomerantseva et al., 2009). Previously, Hou *et al*. reported a weight loss of 26% for coaxial PGS/PCL microfibers after 12 days under accelerated degradation conditions, however, the NaOH solution used was twice as concentrated as the one used in this work (Hou et al., 2017). Nevertheless, direct comparisons between different studies are difficult as the degradation is dependent on many factors including scaffold structural features (e.g. fiber diameter) (You et al., 2004).

The integration of chondroinductive factors such as proteins or small molecules with biomimetic electrospun scaffolds appears to be a promising route for improved CTE strategies. Small molecules (e.g. KGN) offer important advantages over protein growth factors, such as high stability and lower cost (Lo et al., 2014). KGN has been described as a promising drug for cartilage regeneration *in vivo*. However, after injection, small molecules like KGN are quickly cleared through the lymphatic system, limiting its local effects and compromising its therapeutic effectiveness. Therefore, different drug delivery systems have been recently developed to achieve the sustained and localized delivery of KGN (Cai et al., 2019; Fan et al., 2018; Hu et al., 2017; Kang et al., 2014; Li et al., 2016; Shi et al., 2016; Zhu et al., 2019, 2017). We speculated that coaxial aligned electropsun nanofibers able to release KGN in a controlled manner would promote hBMSC chondrogenesis, and therefore, promising for improved CTE strategies, particularly for the regeneration of the superficial zone. KGN incorporation did not result in any meaningful change in the structure of the electrospun scaffolds, which is in agreement with a recent study using KGN-encapsulating fibrous membranes to enhance rotator cuff tendon-bone healing (Zhu et al., 2019). Coaxial PGS-KGN/PCL aligned nanofibers promoted a much more controlled *in vitro* release of KGN than monoaxial PCL-KGN aligned nanofibers. This observation results from the fact that in the coaxial configuration, KGN is confined in the core region of the nanofibers and needs to first disperse through the shell polymer before exits the fiber. In contrast, in the monoaxial PCL-KGN nanofibers, KGN is randomly distributed throughout the nanofiber and possibly located on the fiber surface, which might explain the initial burst release observed.

The bioactivity of the released KGN was assessed through the evaluation of KGN-loaded electrospun scaffolds ability to promote hBMSC growth and chondrogenesis. Both coaxial PGS-KGN/PCL and PCL-KGN aligned nanofibers significantly promoted the proliferation of hBMSC in comparison to non-loaded scaffolds. These results are in agreement with previous studies reporting the enhancing effect of KGN supplementation in hBMSC growth (Johnson et al., 2012; Spakova et al., 2018). Additionally, Zhu and colleagues reported improved proliferation of human adipose-derived MSC in the presence of KGN delivered from a chitosan-hyaluronic acid hydrogel, which also supports our observations (Zhu et al., 2017). Importantly, our results demonstrated that after 21 days of differentiation in the absence of TGF-β3, both coaxial/monoaxial KGN-loaded electrospun scaffolds promoted sGAG production and chondrogenic gene expression when compared to the respective non-loaded scaffolds. In agreement, previous studies showed that KGN supplementation either as culture media additive or through nanoparticle-mediated delivery promotes increased sGAG production during the chondrogenic differentiation of hBMSC in micromass cultures without TGF-β3 (Kang et al., 2014; Xu et al., 2016). Regarding the upregulation of chondrogenic markers in hBMSC-seeded KGN-loaded scaffolds, similar trends were observed in previous studies using different KGN-delivery systems combined with human MSC (Kang et al., 2014; Zhu et al., 2017). In agreement to our results, Zhu et al. recently reported enhanced expressions of *ACAN*, *COL2* and *Sox9* genes in rat bone MSC cultured in aligned KGN-encapsulated PCL membranes in comparison to the membranes without KGN (Zhu et al., 2019). Moreover, our observations are also supported by the results from Yin *et al*., which observed significantly increased *Sox9* and *COL2* expressions in rabbit BMSC cultured on KGN-loaded P(LLA-CL)/collagen nanofibrous scaffolds (Yin et al., 2017).

In summary, we have successfully fabricated and characterized coaxial PGS/PCL aligned electrospun scaffolds able to mimic the nanoscale and alignment of collagen fibers present in articular cartilage ECM. The coaxial PGS/PCL aligned nanofibers produced were able to promote a much more sustained release of KGN in comparison to monoaxial PCL aligned scaffolds. Importantly, KGN-loaded aligned nanofiber scaffolds promoted significantly the proliferation and chondrogenic differentiation of hBMSC, favoring cartilage-like ECM production and gene expression, in the absence of chondrogenic cytokine TGF-β3. Overall, our results highlight the potential of KGN-loaded coaxial aligned nanofibers for the development of novel biomimetic MSC-based strategies to regenerate articular cartilage, particularly for the repair of defects in its superficial zone.

VII.5. References

Alves Da Silva, M.L., Martins, A., Costa-Pinto, A. R., Costa, P., Faria, S., Gomes, M., Reis, R.L., Neves, N.M., (2010). Cartilage tissue engineering using electrospun PCL nanofiber meshes and MSCs. Biomacromolecules 11, 3228–3236.

Bartnikowski, M., Dargaville, T.R., Ivanovski, S., Hutmacher, D.W., (2019). Degradation mechanisms of polycaprolactone in the context of chemistry, geometry and environment. Prog. Polym. Sci. 96, 1–20.

Braghirolli, D.I., Steffens, D., Pranke, P., (2014). Electrospinning for regenerative medicine: A review of the main topics. Drug Discov. Today 19, 743–753.

Cai, G., Liu, W., He, Y., Huang, J., Duan, L., Xiong, J., Liu, L., Wang, D., (2019). Recent advances in kartogenin for cartilage regeneration. J. Drug Target. 27, 28–32.

Cheng, A., Schwartz, Z., Kahn, A., Li, X., Shao, Z., Sun, M., Ao, Y., Boyan, B.D., Chen, H., (2019). Advances in Porous Scaffold Design for Bone and Cartilage Tissue Engineering and Regeneration. Tissue Eng. - Part B Rev. 25, 14–29.

Ding, Y., Li, W., Zhang, F., Liu, Z., Ezazi, N.Z., Liu, D., Santos, H.A., (2019). Electrospun Fibrous Architectures for Drug Delivery, Tissue Engineering and Cancer Therapy, Adv. Funct. Mater. 29, 1802851.

Fan, W., Li, J., Yuan, L., Chen, J., Wang, Z., Wang, Y., Guo, C., Mo, X., Yan, Z., (2018). Intra-articular injection of kartogenin-conjugated polyurethane nanoparticles attenuates the progression of osteoarthritis. Drug Deliv. 25, 1004–1012.

Gaharwar, A.K., Nikkhah, M., Sant, S., Khademhosseini, A., (2014). Anisotropic poly (glycerol sebacate) - poly (caprolactone) electrospun fibers promote endothelial cell guidance. Biofabrication 7, 015001.

Hou, L., Udangawa, W.M.R.N., Pochiraju, A., Dong, W., Zheng, Y., Linhardt, R.J., Simmons, T.J., (2016). Synthesis of Heparin-Immobilized, Magnetically Addressable Cellulose Nanofibers for Biomedical Applications. ACS Biomater. Sci. Eng. 2, 1905–1913.

Hou, L., Zhang, X., Mikael, P.E., Lin, L., Dong, W., Zheng, Y., Simmons, T.J., Zhang, F., Linhardt, R.J., (2017). Biodegradable and Bioactive PCL-PGS core-shell fibers for tissue engineering. ACS Omega 2, 6321–6328.

Hu, Q., Ding, B., Yan, X., Peng, L., Duan, J., Yang, S., Cheng, L., Chen, D., (2017). Polyethylene glycol modified PAMAM dendrimer delivery of kartogenin to induce chondrogenic differentiation of mesenchymal stem cells. Nanomedicine Nanotechnology, Biol. Med. 13, 2189–2198.

Hunziker, E.B., Quinn, T.M., Häuselmann, H.-J., (2002). Quantitative structural organization of normal adult human articular cartilage. Osteoarthr. Cartil. 10, 564–72.

Ifkovits, J.L., Padera, R.F., Burdick, J.A., (2008). Biodegradable and radically polymerized elastomers with enhanced processing capabilities. Biomed. Mater. 3, 034104.

Ji, W., Sun, Y., Yang, F., van den Beucken, J.J.J.P., Fan, M., Chen, Z., Jansen, J.A., (2011). Bioactive electrospun scaffolds delivering growth factors and genes for tissue engineering applications. Pharm. Res. 28, 1259–1272.

Johnson, K., Zhu, S., Tremblay, M.S., Payette, J.N., Wang, J., Bouchez, L.C., Meeusen, S., Althage, A., Cho, C.Y., Wu, X., Schultz, P.G., (2012). A stem cell-based approach to cartilage repair. Science. 336, 717–721.

Kang, M.L., Ko, J.Y., Kim, J.E., Im, G. Il, (2014). Intra-articular delivery of kartogenin-conjugated chitosan nano/microparticles for cartilage regeneration. Biomaterials 35, 9984–9994.

Kharaziha, M., Nikkhah, M., Shin, S.R., Annabi, N., Masoumi, N., Gaharwar, A.K., Camci-Unal, G., Khademhosseini, A., (2013). PGS:Gelatin nanofibrous scaffolds with tunable mechanical and structural properties for engineering cardiac tissues. Biomaterials 34, 6355–6366.

Kim, G.H., (2008). Electrospun PCL nanofibers with anisotropic mechanical properties as a biomedical scaffold. Biomed. Mater. 3, 025010.

Klein, T.J., Chaudhry, M., Bae, W.C., Sah, R.L., (2007). Depth-dependent biomechanical and biochemical properties of fetal, newborn, and tissue-engineered articular cartilage. J. Biomech. 40, 182–190.

Klein, T.J., Malda, J., Sah, R.L., Hutmacher, D.W., (2009). Tissue Engineering of Articular Cartilage with Biomimetic Zones. Tissue Eng. Part B Rev. 15, 143–157.

Li, X., Ding, J., Zhang, Z.-Z., Yang, M., Yu, J.-K., Wang, J., Chang, F., Chen, X., (2016). Kartogenin-Incorporated Thermogel Supports Stem Cells for Significant Cartilage Regeneration. ACS Appl. Mater. Interfaces 8, 5148–5159.

Liu, Y., Tian, K., Hao, J., Yang, T., Geng, X., Zhang, W., (2019). Biomimetic poly(glycerol sebacate)/polycaprolactone blend scaffolds for cartilage tissue engineering. J. Mater. Sci. Mater. Med. 30, 53.

Lo, K.W., Jiang, T., Gagnon, K.A., Nelson, C., Laurencin, C.T., (2014). Small-molecule based musculoskeletal regenerative engineering. Trends Biotechnol. 32, 74–81.

Loh, X.J., Abdul Karim, A., Owh, C., (2015). Poly(glycerol sebacate) biomaterial: synthesis and biomedical applications. J. Mater. Chem. B 3, 7641–7651.

Low, S.W., Ng, Y.J., Yeo, T.T., Chou, N., (2009). Use of Osteoplug polycaprolactone implants as novel burr-hole covers. Singapore Med. J. 50, 777–780.

Man, Z., Yin, L., Shao, Z., Zhang, X., Hu, X., Zhu, J., Dai, L., Huang, H., Yuan, L., Zhou, C., Chen, H., Ao, Y., (2014). The effects of co-delivery of BMSC-affinity peptide and rhTGF-β1 from coaxial electrospun scaffolds on chondrogenic differentiation. Biomaterials 35, 5250–5260.

Masoumi, N., Larson, B.L., Annabi, N., Kharaziha, M., Zamanian, B., Shapero, K.S., Cubberley, A.T., Camci-Unal, G., Manning, K.B., Mayer, J.E., Khademhosseini, A., (2014). Electrospun PGS:PCL Microfibers Align Human Valvular Interstitial Cells and Provide Tunable Scaffold Anisotropy. Adv. Healthc. Mater. 3, 929–939.

Mikos, A.G., Temenoff, J.S., (2000). Review: tissue engineering for regeneration of articular cartilage. Biomaterials 21, 431–440.

Mow, V.C., Guo, X.E., (2002). Mechano-Electrochemical Properties Of Articular Cartilage: Their Inhomogeneities and Anisotropies. Annu. Rev. Biomed. Eng. 4, 175–209.

Pant, B., Park, M., Park, S.-J., (2019). Drug Delivery Applications of Core-Sheath Nanofibers Prepared by Coaxial Electrospinning: A Review. Pharmaceutics. 11, 305.

Pomerantseva, I., Krebs, N., Hart, A., Neville, C.M., Huang, A.Y., Sundback, C.A., (2009). Degradation behavior of poly(glycerol sebacate). J. Biomed. Mater. Res. - Part A 91A, 1038–1047.

Rai, R., Tallawi, M., Barbani, N., Frati, C., Madeddu, D., Cavalli, S., Graiani, G., Quaini, F., Roether, J.A., Schubert, D.W., Rosellini, E., Boccaccini, A.R., (2013). Biomimetic poly(glycerol sebacate) (PGS) membranes for cardiac patch application. Mater. Sci. Eng. C 33, 3677–3687.

Reboredo, J.W., Weigel, T., Steinert, A., Rackwitz, L., Rudert, M., Walles, H., (2016). Investigation of Migration and Differentiation of Human Mesenchymal Stem Cells on Five-Layered Collagenous Electrospun Scaffold Mimicking Native Cartilage Structure. Adv. Healthc. Mater. 5, 2191–2198.

Salehi, S., Czugala, M., Stafiej, P., Fathi, M., Bahners, T., Gutmann, J.S., Singer, B.B., Fuchsluger, T.A., (2017). Poly (glycerol sebacate)-poly (ε-caprolactone) blend nanofibrous scaffold as intrinsic bio- and immunocompatible system for corneal repair, Acta Biomater. 50, 370-380.

Salehi, S., Fathi, M., Javanmard, S.H., Bahners, T., Gutmann, J.S., Ergün, S., Steuhl, K.P., Fuchsluger, T.A., (2014). Generation of PGS/PCL blend nanofibrous scaffolds mimicking corneal stroma structure. Macromol. Mater. Eng. 299, 455–469.

Sant, S., Hwang, C.M., Lee, S.-H., Khademhosseini, A., (2011). Hybrid PGS–PCL microfibrous scaffolds with improved mechanical and biological properties. J. Tissue Eng. Regen. Med. 5, 283–291.

Schagemann, J.C., Paul, S., Casper, M.E., Rohwedel, J., Kramer, J., Kaps, C., Mittelstaedt, H., Fehr, M., Reinholz, G.G., (2013). Chondrogenic differentiation of bone marrow-derived mesenchymal stromal cells via biomimetic and bioactive poly-ε-caprolactone scaffolds. J. Biomed. Mater. Res. - Part A 101, 1620–1628.

Shafiee, A., Soleimani, M., Chamheidari, G.A., Seyedjafari, E., Dodel, M., Atashi, A., Gheisari, Y., (2011). Electrospun nanofiber-based regeneration of cartilage enhanced by mesenchymal stem cells. J. Biomed. Mater. Res. - Part A 99A, 467–478.

Shi, D., Xu, X., Ye, Y., Song, K., Cheng, Y., Di, J., Hu, Q., Li, J., Ju, H., Jiang, Q., Gu, Z., (2016). Photo-cross-linked scaffold with kartogenin-encapsulated nanoparticles for cartilage regeneration. ACS Nano 10, 1292–1299.

Spakova, T., Plsikova, J., Harvanova, D., Lacko, M., Stolfa, S., Rosocha, J., (2018). Influence of kartogenin on chondrogenic differentiation of human bone Marrow-Derived MSCs in 2D culture and in Co-Cultivation with OA osteochondral explant. Molecules 23, 1–16.

Sperling, L.E., Reis, K.P., Pranke, P., Wendorff, J.H., (2016). Advantages and challenges offered by biofunctional core-shell fiber systems for tissue engineering and drug delivery. Drug Discov. Today 21, 1243–1256.

Sun, H., Mei, L., Song, C., Cui, X., Wang, P., (2006). The in vivo degradation, absorption and excretion of PCL-based implant. Biomaterials 27, 1735–1740.

Vogt, L., Rivera, L.R., Liverani, L., Piegat, A., El Fray, M., Boccaccini, A.R., (2019) Poly(ε-caprolactone)/poly(glycerol sebacate) electrospun scaffolds for cardiac tissue engineering using benign solvents, Mater. Sci. Eng. C. 103, 109712.

Wang, C., Hou, W., Guo, X., Li, J., Hu, T., Qiu, M., Liu, S., Mo, X., Liu, X., (2017). Two-phase electrospinning to incorporate growth factors loaded chitosan nanoparticles into electrospun fibrous scaffolds for bioactivity retention and cartilage regeneration. Mater. Sci. Eng. C 79, 507–515.

Wang, Y., Ameer, G.A., Sheppard, B.J., Langer, R., (2002). A tough biodegradable elastomer. Nat. Biotechnol. 20, 602–606.

Wang, Y., Kim, Y.M., Langer, R., (2003). In vivo degradation characteristics of poly (glycerol sebacate). J. Chem. Phys. 66, 192–197.

Wise, J.K., Yarin, A.L., Megaridis, C.M., Cho, M., (2009). Chondrogenic Differentiation of Human Mesenchymal Stem Cells on Oriented Nanofibrous Scaffolds: Engineering the Superficial Zone of Articular Cartilage. Tissue Eng. Part A 15, 913–921.

Woodruff, M.A., Hutmacher, D.W., (2010). The return of a forgotten polymer - Polycaprolactone in the 21st century. Prog. Polym. Sci. 35, 1217–1256.

Xu, J., Li, J., Lin, S., Wu, T., Huang, H., Zhang, K., Sun, Y., Yeung, K.W.K., Li, G., Bian, L., (2016). Nanocarrier-Mediated Codelivery of Small Molecular Drugs and siRNA to Enhance Chondrogenic Differentiation and Suppress Hypertrophy of Human Mesenchymal Stem Cells. Adv. Funct. Mater. 26, 2463–2472.

Yi, F., La Van, D.A., (2008). Poly(glycerol sebacate) nanofiber scaffolds by core/shell electrospinning. Macromol. Biosci. 8, 803–806.

Yin, H., Wang, J., Gu, Z., Feng, W., Gao, M., Wu, Y., Zheng, H., He, X., Mo, X., 2017. Evaluation of the potential of kartogenin encapsulated poly(L-lactic acid-co-caprolactone)/collagen nanofibers for tracheal cartilage regeneration. J. Biomater. Appl. 32, 331–341.

You, Y., Min, B.M., Lee, S.J., Lee, T.S., Park, W.H., (2004). In vitro degradation behavior of electrospun polyglycolide, polylactide, and poly(lactide-co-glycolide). J. Appl. Polym. Sci. 95, 193–200.

Zhu, Q., Ma, Z., Li, H., Wang, H., He, Y., (2019). Enhancement of rotator cuff tendon-bone healing using combined aligned electrospun fibrous membranes and kartogenin. RSC Adv. 9, 15582–15592.

Zhu, Y., Tan, J., Zhu, H., Lin, G., Yin, F., Wang, L., Song, K., Wang, Y., Zhou, G., Yi, W., (2017). Development of kartogenin-conjugated chitosan-hyaluronic acid hydrogel for nucleus pulposus regeneration. Biomater. Sci. 5, 784–791.

Chapter VIII

HIERARCHICAL TRI-LAYERED SCAFFOLD CONCEPT FOR CARTILAGE TISSUE ENGINEERING

CHAPTER VIII – Hierarchal tri-layered scaffold concept for cartilage tissue engineering

Outline

Articular cartilage self-repair is limited by the intrinsic absence of vasculature and low chondrocyte density and proliferation capacity. Cartilage defects treatment upon injury, wear and tear, or degenerative arthritic disease require surgical procedures that are unable to generate functional repaired tissue with structure and mechanical performance similar to the native tissue. With the development of tissue engineering, it was predicted that articular cartilage would be one of the first tissues to be successfully regenerated due to its avascular nature and because it was composed by a single cell type. However, this prediction proved wrong and the fabrication of functional engineered cartilage tissues remains elusive mainly due to the challenging task of reproducing the complex hierarchical and organized structure of the native cartilage tissue. Mature articular cartilage is composed of four distinct zones (calcified zone, deep zone, middle or transitional zone and superficial zone), each one with specific cell density/phenotype, extracellular matrix composition, collagen fibers orientation and mechanical properties.

In the current study, we introduced a novel hierarchical tri-layered scaffold with the aim of reproducing the complex architecture and zone-dependent properties of native articular cartilage. The scaffold concept developed consists in a 3D-extruded porous polycaprolactone (PCL) scaffold as deep zone layer, a GAG-based hydrogel in the middle zone and aligned PCL/Gelatin nanofibers as superficial zone layer. The structure and different layer integration was observed macroscopically and by scanning electron microscopy. The ability of the hierarchical scaffold to support human bone marrow stem/stromal cells (hBMSC) culture and chondrogenic differentiation was determined by assessing cell metabolic activity, sGAG production and the expression of chondrogenic gene markers in comparison to scaffolds corresponding to each one of the individual layers. Additionally, immunofluorescence analysis showed that the hierarchical scaffold was capable of supporting cartilage-specific protein expression.

While further characterization of the final engineered tissues is still necessary to assess the full potential of the concept presented, our results suggest that the hierarchical tri-layered scaffold was able to support MSC chondrogenic differentiation. Thus, this biomimetic strategy represents a promising approach for the repair of full-thickness osteochondral defects and to be used as a more structurally reliable *in vitro* model for disease modeling and drug screening.

VIII.1. Introduction

Articular cartilage defects can occur for a variety of reasons including traumatic injuries, chronic repetitive microtrauma or age-related degeneration. Additionally, cartilage defects normally do not self-repair due to the typical avascular, aneural and relatively hypocellular structure of the articular cartilage tissue. Cartilage lesions can be classified into microfractures (damage of the collagen network of the articular surface) as well as chondral or osteochondral defects. Chondral defects are macroscopic defects caused by trauma or from degeneration of previous existent microfracture that normally extend to the subchondral bone, originating osteochondral defects (Camarero-Espinosa et al., 2016; Mano and Reis, 2007). Traditionally, cartilage defects have been graded into five groups following the Outerbridge classification (Grade 0 – healthy tissue; Grade I – superficial lesions, soften and swollen cartilage; Grade II – cartilage presents fissures that have a diameter ≤ 1.27 cm; Grade III – cartilage presents fissures that have a diameter ≥ 1.27 cm and Grade IV – cartilage injury extend through the tissue and reach the subchondral bone) (Outerbridge, 1961). Cartilage defects if untreated or filled with improper repaired tissue often lead to osteoarthritis.

The current methods used for the clinical management of cartilage defects include bone marrow stimulation techniques (i.e., microfracture and arthroscopic debridement), osteochondral auto-/allo-grafts (i.e., mosaicplasty) and autologous chondrocyte implantation (ACI). However, these regeneration techniques have several limitations such as donor site morbidity, insufficient or inappropriate defect filing (fibrocartilaginous tissue), and inefficiency in producing hyaline-like repaired tissue with sufficient functionality (Huang et al., 2016). As a result of the search for new alternatives for cartilage repair, tissue engineering strategies combining cells, biomaterial scaffolds and biological signals have been proposed with the promise of generating functional tissue with native-like structure and mechanical performance. When tissue engineering was first described by Langer and Vacanti over twenty years ago (Langer and Vacanti, 1993), it was predicted that articular cartilage would be one of the first tissues to be successfully engineered due to the presence of a single cell type and its lack of vasculature. However, cartilage regeneration remains challenging mainly due to the failure in replicating the highly complex hierarchical structure of articular cartilage (Huey et al., 2012).

From the articulating surface to the subchondral bone, articular cartilage multi-zonal structure can be divided into four distinct zones (the superficial or tangential zone; the middle or transitional zone; the deep or radial zone and the calcified zone), each one with different ECM composition and orientation, cell phenotypes and mechanical properties (Klein et al., 2009). The superficial zone (surface to 10-20% of cartilage thickness) is composed by

densely packed collagen fibers that align parallel to the articular surface and are responsible for the high tensile strength observed in this region. This zone presents a higher density (compared with the other zones) of flattened and elongated chondrocytes, high levels of collagen II and low amounts of GAGs (Hunziker et al., 2002; Klein et al., 2007). It is also noteworthy that the chondrocytes in the superficial zone secrete proteoglycan 4 (PRG4), also known as lubricin or superficial zone protein (SZP), which works as a boundary lubricant at the joint surface (Flannery et al., 1999). The middle zone (40-60% of total cartilage thickness) is characterized by random collagen fibers and an aggrecan-rich ECM. The chondrocytes in this region are present in a lower cell density and have a rounded shape (Camarero-Espinosa and Cooper-White, 2017; Knudson and Knudson, 2001). Under the middle zone, resides the deep zone (20-50% of total cartilage thickness), which contains a higher concentration of GAGs, lower collagen II concentration, and lower chondrocyte density in comparison to the other zones of articular cartilage. In this region, the collagen fibers and elongated chondrocytes are arranged perpendicularly to the subchondral bone (Bhosale and Richardson, 2008; Correia et al., 2015). Moreover, the cells in this zone secrete less collagen II, and collagen X and collagen I are also present in small amounts (Eyre and Wu, 1995). The base of the deep zone is a calcified zone, which can be identified by the presence of the tidemark. The calcified zone works as an interface between the cartilage and the subchondral bone and contains high levels of collagen X (Redler et al., 1975). This zone-varying ECM composition and organization dictates the mechanical properties of the articular cartilage. In fact, as GAG amounts increase from the superficial zone to the deep zone, the water content and swelling pressure also increase, resulting in a corresponding increase in compressive modulus (Klein et al., 2007). In addition to zone-specific mechanical properties, other studies have already reported zone-specific gene expression (Grogan et al., 2013), protein distribution patterns (Müller et al., 2014), and GAG type/sulfation levels (Kuiper and Sharma, 2015).

Cartilage tissue engineering (CTE) strategies creating homogeneous engineered tissues have not been able to generate functional repaired tissue. Therefore, CTE strategies are now focused on the reproduction *in vitro* of the architectural features and organization of native articular cartilage. In addition, the increased evidence that support from the subchondral bone is essential for cartilage repair suggests that CTE approaches should also consider how to achieve a better integration of bone-cartilage interface (Gomoll et al., 2010; Yan et al., 2015).

In the recent years, different approaches aiming to fabricate engineered tissues with cartilage-like hierarchical stratified structure and zone-varying properties have been developed (Atesok et al., 2016; Correia et al., 2015). These approaches include the use of multi-layered scaffolds with varying fiber orientation (McCullen et al., 2012), pore size (Zhang

et al., 2013), protein content (Zhu et al., 2014), and polymer form (Steele et al., 2014); or multi-layered hydrogels with zone-varying compositions (Nguyen et al., 2011; Zhu et al., 2017) and with encapsulated zone-specific chondrocytes (Ng et al., 2009).

In the current study, we propose a new hierarchical tri-layered scaffold concept aiming to provide a closer mimicry of the native articular cartilage structure and zone-varying properties. The proposed hierarchical tri-layered scaffold consists in a 3D-extruded porous polycaprolactone (PCL) scaffold as deep zone layer, a GAG-based hydrogel as the middle zone layer and aligned PCL/Gelatin nanofibers as the superficial zone layer. Our concept will be validated by assessing the ability of the hierarchical scaffold to support MSC chondrogenic differentiation, taking into consideration the cell density ratio and the hypoxic nature of native articular cartilage tissue.

VIII.2. Material & Methods

VIII.2.1. Cell culture

Human bone marrow MSC (hBMSC) were purchased from Lonza (Basel-Switzerland). hBMSC were thawed and expanded on tissue culture flasks (CELLTREAT® Scientific Products, MA) using low-glucose Dulbecco's Modified Eagle Medium (DMEM, Gibco, Grand Island, NY) supplemented with 10% fetal bovine serum (FBS, Gibco) and 1% penicillin-streptomycin (Pen-strep, Gibco), and kept at 37 ºC and 5% CO_2 in a humidified atmosphere until scaffold seeding. Complete medium renewal was performed every 3-4 days and all the experimental assays were performed using cells between passages 3 and 5.

VIII.2.2. Fabrication of hierarchical tri-layered scaffold

VIII.2.2.1. Deep zone layer (DL) – 3D extruded porous PCL scaffold

Poly (ε-caprolactone) (PCL, MW 50000 Da, CAPA™ 6500, Perstorp Caprolactones, UK) scaffolds were fabricated using in-house developed melt-extrusion equipment and characterized as previously described (Figure VIII.1A) (Domingos et al., 2009; Silva et al., 2017). 3D porous PCL scaffolds with a 0-90º lay-down pattern, 390 μm pore size and dimensions of 7 mm x 7 mm x 3 mm were used as the deep zone layer of the hierarchical tri-layered scaffold.

VIII.2.2.2. Middle zone layer (ML) – HyStem-CS hydrogel system

The middle zone layer of the hierarchical scaffold consisted of a GAG-based hydrogel system with encapsulated hBMSCs. HyStem hydrogel kit (ESI BIO, Biotime Inc., CA USA) is fully chemically defined and is composed of sterile thiol-modified hyaluronan (Glycosil), a thiol-reactive PEGSSDA crosslinker and degassed, deionized water (DG water). Chondroitin sulfate (CS, Sigma-Aldrich), which is the main GAG in the articular cartilage, was combined with the HyStem hydrogel following the manufacturer's guidelines to provide a closer mimicry of the native tissue biochemistry. Briefly, Glycosil was dissolved in DG water and combined with a previously prepared CS solution (in distilled water) to generate a final HyStem-CS 1% (w/v) hydrogel (Figure VIII.1B). The mixture obtained was then used to resuspend the hBMSC pellet for cell encapsulation. The PEGSSDA cross-linker solution was added to the Glycosil-CS mixture with cells in a 1:4 volume ratio and mixed well by pipetting to form the hydrogel. The gelation of the final HyStem-CS hydrogel with encapsulated hBMSCs was completed within 30 min.

VIII.2.2.3. Superficial zone layer (SL) – Aligned PCL/Gelatin nanofibers

PCL (Mn=80000 Da, Sigma-Aldrich) and Gelatin (Sigma-Aldrich) were dissolved (70:30 ratio) at 10% w/v in 1,1,1,3,3,3-hexafluoro-2-propanol (HFIP, Sigma-Aldrich) with agitation overnight. The nanofibrous electrospun scaffolds were fabricated by electrospinning (Figure VIII.1C). PCL/Gelatin solution was loaded into a syringe placed in a mechanical syringe pump (NE-1000, New Era Pump System Inc.) and connected by PTFE tubing to a 23G metallic needle (0.64 mm diameter). A flow rate of 1 mL/h and an applied voltage of 20 kV (generated by a high power source Spellman CZE1000R) were used in the process. The aligned nanofibers were produced in a two parallel copper plates collector placed at 18 cm distance from the needle tip. All the nanofibers scaffolds were fabricated under the same process parameters and with controlled ambient conditions (temperature = 20-22ºC and relative humidity = 20-25%). The aligned nanofiber scaffolds produced were used as the superficial zone layer of the hierarchical scaffolds to mimic the alignment and nanoscale nature of the collagen fibers in native articular cartilage (Figure VIII.1 C).

VIII.2.3. SEM analysis

The structural features of the hierarchical tri-layered scaffold as well as of each individual layer were observed using a field emission scanning electron microscope (FE-SEM, FEI-Versa 3D Dual Beam, Hillsboro). The samples were mounted on a holder, sputter-coated

with a thin layer of 60% gold-40% palladium and imaged using an accelerating voltage of 5 kV. The average fiber diameters and distributions of the aligned PCL/Gelatin nanofibers (superficial zone layer) were determined by measuring 100 individual fibers per condition from at least 5 different SEM images using the ImageJ software (ImageJ 1.51f, National Institutes of Health, USA).

VIII.2.4. hBMSC chondrogenic differentiation on hierarchical tri-layered scaffolds and respective individual layers

Before performing the cell culture assays, 3D PCL scaffolds and PCL/Gelatin nanofibrous scaffolds were sterilized by UV exposure for 3 h, washed three times with PBS+1% Pen-strep solution and conditioned with culture medium for 1 h at 37ºC. Based on previous studies reporting a cell density ratio of 3:2:1 for the superficial:middle:deep zone in normal adult articular cartilage (Hunziker et al., 2002; Ren et al., 2016), 150000, 100000, and 50000 hBMSCs were seeded/encapsulated in aligned PCL/Gelatin nanofibers, HyStem-CS hydrogels and porous PCL scaffolds, respectively (Figure VIII.1 E). hBMSCs were first seeded on PCL scaffolds and aligned PCL/gelatin nanofibers and incubated without culture media for 1 h to promote initial cell adhesion. During this period, other group of hBMSCs was harvested and encapsulated in HyStem-CS hydrogels. Before full gelation was achieved (≈15-20 min), HyStem-CS hydrogels with encapsulated cells (middle zone layer) were placed on top of the PCL scaffolds (deep zone layer) previously seeded with cells. Afterwards, using sterile tweezers, the cell-seeded aligned PCL/Gelatin nanofibers (superficial zone layer) were placed on the top of fully cross-linked HyStem-CS hydrogels (Figure VIII.1 D). The hierarchical scaffolds were then incubated for 30 min without culture medium to not disrupt the whole scaffold initial assembly. The individual layers were seeded/encapsulated with 300000 hBMSCs for comparison studies with the hierarchical tri-layered scaffold. All scaffolds were cultured with chondrogenic media composed by high glucose DMEM (ThermoFisher Scientific) with 100 nM dexamethasone (Sigma-Aldrich), 50 µg/mL ascorbic acid 2-phosphate (Sigma-Aldrich), 40 µg/mL L-proline (Sigma-Aldrich), 1 mM sodium pyruvate (Gibco), ITS^{TM}+ Premix supplement (6.25 µg/mL bovine insulin; 6.25 µg/mL transferrin; 6.25 µg/mL selenous acid; 5.33 µg/mL linoleic acid; 1.25 µg/mL BSA, Corning), Pen-strep (100 U/mL penicillin; 100 µg/mL streptomycin) and 10 ng/mL TGF-β3 (R&D Systems) and maintained at 37ºC/5% CO_2 under hypoxic conditions (5% O_2) for 21 days. The chondrogenic medium was changed very carefully every 3-4 days. A schematic representation of the hierarchical scaffold assembly process is presented in Figure VIII.1 D.

VIII.2.5. Cell metabolic activity (Alamar Blue assay)

The metabolic activity of cells in the hierarchical scaffolds and respective individual layers was evaluated using AlamarBlue® cell viability reagent (ThermoFischer Scientific, USA) on days 3, 7, 14 and 21 following the manufacturer's guidelines. Briefly, a 10% (v/v) AlamarBlue® solution prepared in culture medium was added to the samples and incubated at 37ºC in 5% CO_2 incubator for 3 h. The fluorescence intensity of three (n=3) independent samples per condition was measured in a microplate reader (SpectraMax M5, Molecular Devices, USA) at an excitation/emission wavelength of 560/590 nm and the fluorescence intensity values of each sample were measured in triplicate. Acellular scaffolds (for each experimental group) were used as blank controls and subtracted from the values obtained in the cell-scaffold constructs.

VIII.2.6. sGAG content quantification (DMMB assay)

At the end of the differentiation protocol (day 21), hierarchical scaffolds and individual scaffold layers were collected, washed with PBS and digested in a 125 µg/mL papain enzyme (from papaya latex, Sigma-Aldrich) solution (50 mM sodium phosphate, 2 mM N-acetyl cysteine, 2 mM EDTA, all from Sigma-Aldrich, pH 6.5) at 60ºC overnight (16-18 h). The amount of cell-produced sulfated GAG (sGAG) on the tissue constructs was quantified using the 1,9-dimethylmethylene blue (DMMB, Sigma-Aldrich) assay. In this assay, the digested samples were mixed with a DMMB solution (16 mg DMMB in 0.3% w/v glycine, 0.27% sodium chloride in distilled water, pH 3.0) in 96-well plates and the absorbance was measured at 525 nm. The absorbance values were compared to chondroitin 6-sulfate (sodium salt from shark cartilage, Sigma-Aldrich) standards to estimate the sGAG amounts present in each scaffold. Two scaffolds (n=2) were used for each experimental group and the absorbance values were measured in triplicate. Acellular hierarchical scaffolds and each individual layer scaffolds were used as blank controls and subtracted from the values obtained in the cell-scaffold constructs.

VIII.2.7. RNA extraction and real-time quantitative PCR (RT-qPCR) analysis

Total RNA was isolated from the final tissue constructs (day 21) generated by differentiating hBMSCs in the hierarchical tri-layered scaffolds and respective individual layers using the RNeasy Mini kit (Quiagen, Hilden, Germany). Samples were first incubated in lysis buffer with agitation for 30 min at 4°C, followed by the total RNA extraction protocol according to the manufacturer's guidelines. Isolated RNA was quantified using a Nanodrop

(ND-100 Spectrophotometer, Nanodrop Technologies) and cDNA was synthesized from the purified RNA using iScript™ Reverse Transcription Supermix (Bio-Rad, Hercules, CA USA) following the manufacturer's guidelines. The reaction mixtures with a total volume of 20 µL were incubated in a thermal cycler (Veriti Thermal Cycler, Applied Biosystems, CA USA) for 5 min at 25ºC, 20 min at 46ºC and 1 min at 95ºC and then were maintained at 4ºC.

The real time quantitative PCR (RT-qPCR) analysis was performed using the TaqMan® Fast Advanced Master Mix (Applied Biosystems) and StepOnePlus real-time PCR system (Applied Biosystems) following the manufacturer's protocol. Reactions were run in triplicate using TaqMan® Gene Expression Assays (20X) (Thermo Fisher Scientific) specified in Table VIII.1. CT values were normalized against the expression of housekeeping gene *GAPDH* and the analysis was performed using the $2^{--\Delta\Delta Ct}$ method. Results for gene expressions in the final tissue constructs are presented as fold-change expression levels relative to hBMSC before scaffold seeding (day 0).

Table VIII.1. TaqMan assays used for RT-qPCR analysis.

Targe Genes	ID numbers
GAPDH	Hs02758991_g1
COL2A1	Hs00264051_m1
Sox9	Hs00165814_m1
ACAN	Hs00153936_m1
PRG4	Hs00981633_m1
COL10A1	Hs00166657_m1

VIII.2.8. Immunofluorescence analysis of hierarchical scaffolds

After 21 days of chondrogenic differentiation, hierarchical scaffolds were fixed with 4% PFA for 20 min and washed with PBS. Afterwards, scaffolds were included in Tissue-Tek® O.C.T. Compound (VWR), frozen in liquid nitrogen and stored at -80ºC. The OCT blocks were sliced into 15 µm sections using a microtome cryostat (Microm HM 505E Cryostat, GMI, MN USA) at -20ºC and mounted in glass slides. The slides were washed twice in PBS (5 min each wash) and washed with 0.1 M glycine (Sigma-Aldrich) solution in PBS for 10 min at room temperature to remove PFA residues. Samples were permeabilized with 0.1% Triton-X (Sigma-Aldrich) solution in PBS for 10 min and incubated with a blocking solution (10% FBS in TBST – 20 mM Tris-HCl pH 8.0 (Sigma-Aldrich), 150 mM NaCl (Sigma-Aldrich), 0.05% (v/v) Tween-20 (Sigma-Aldrich)) for 30 min at room temperature and the slices were dried with a tissue. For immunofluorescence analysis, the slides were incubated with primary

antibodies (in blocking solution) for collagen II (1:200, mouse collagen II monoclonal antibody 6B3, ThermoFisher Scientific), and aggrecan (1:400, mouse aggrecan monoclonal antibody BC-3, ThermoFisher Scientific) overnight at 4ºC. Afterwards, the slides were washed three times with TBST (5 min each wash) and incubated with secondary antibodies Goat anti-mouse IgG- AlexaFluor 546 (1:500, ThermoFisher Scientific) for 45 min in the dark at room temperature. The slides were then washed with TBST (3 washes, 5 min each), counterstained with DAPI for 5 min at room temperature, washed again with TBST and mounted with Mowiol (Sigma-Aldrich). Finally, the immunostaining in the hierarchical scaffolds was observed using a confocal microscope (Zeiss LSM 710).

VIII.2.9. Data analysis

Results are presented as mean values ± standard deviation (SD) of three replicate samples (n=3), unless otherwise specified.

VIII.3. Results

VIII.3.1. Fabrication and structural assessment of hierarchical tri-layered scaffold

In this work, we combined different scaffold fabrication technologies to produce a hierarchical tri-layered scaffold that can resemble the architecture of native articular cartilage. The scaffold individual layers namely, 3D-extruded PCL scaffold, HyStem-CS hydrogel and aligned PCL/Gelatin nanofibers were produced as described in section VIII.2.2. Figure VIII.1 presents a schematic overview of the individual layers scaffold fabrication and of the whole cell-seeded hierarchical scaffold assembly (as described in section VIII.2.4).

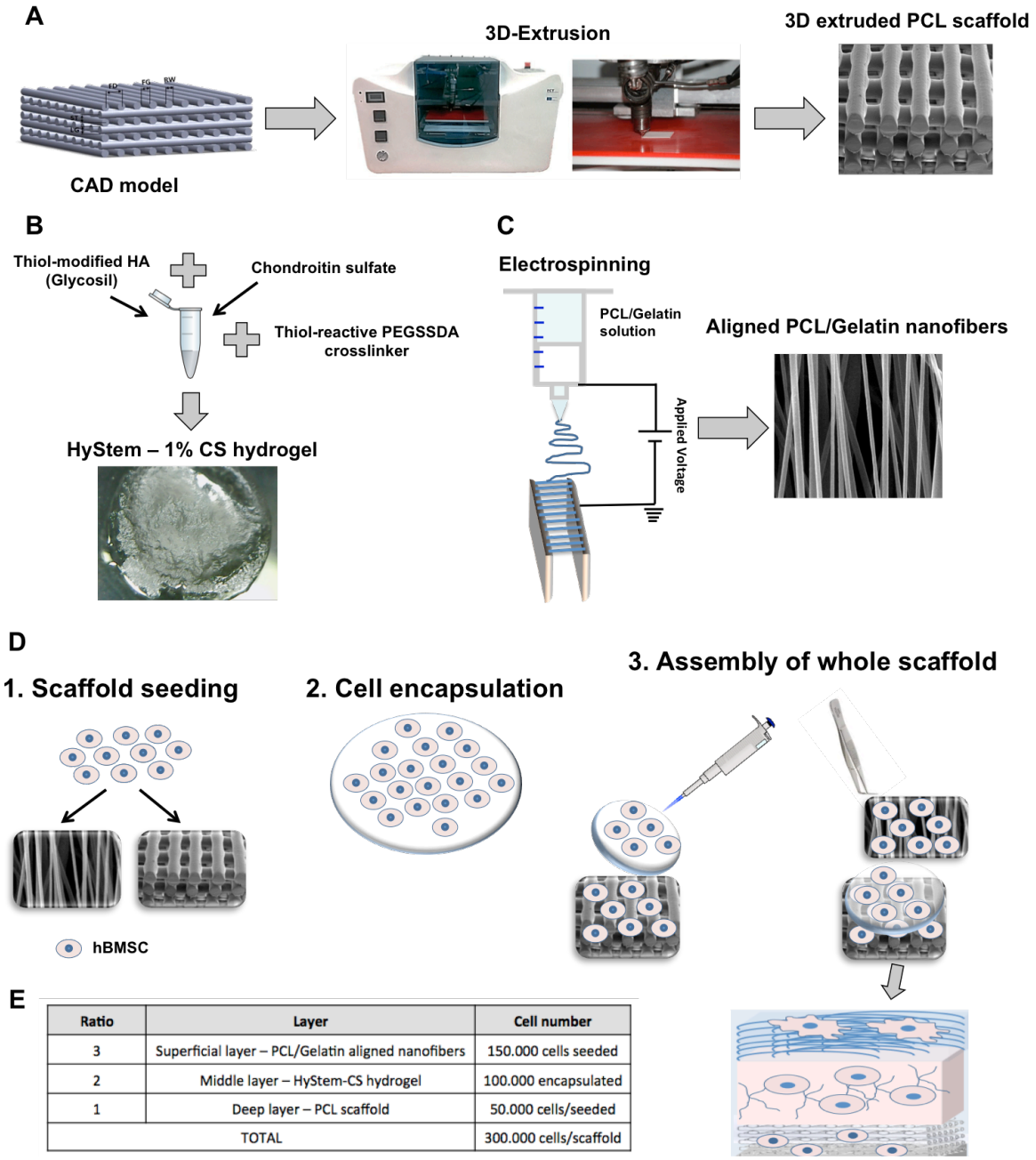

Ratio	Layer	Cell number
3	Superficial layer – PCL/Gelatin aligned nanofibers	150.000 cells seeded
2	Middle layer – HyStem-CS hydrogel	100.000 encapsulated
1	Deep layer – PCL scaffold	50.000 cells/seeded
TOTAL		300.000 cells/scaffold

Figure VIII.1. Schematic overview of the hierarchical tri-layered scaffold fabrication. 3D porous PCL scaffolds were produced by melt-extrusion based in previously designed CAD models and used as deep zone layer (A). Chondroitin sulfate was combined with the components of the HyStem hydrogel kit (thiol-modified HA and thiol-reactive PEGSSDA cross-linker) to generate HyStem-CS hydrogel to be used as the middle zone layer (B). Electrospinning was used to fabricate aligned PCL/Gelatin nanofibers (superficial zone layer). To produce the cell-scaffold constructs, hBMSC were firstly seeded on 3D porous PCL scaffolds and PCL/Gelatin nanofibers and incubated without media to promote initial cell attachment. Meanwhile, hBMSC were encapsulated in HyStem-CS hydrogels. Before full gelation, the hydrogel middle layer was placed on top of the deep zone layer and afterwards, the cell-seeded aligned nanofibrous scaffold was placed on the top of the middle zone layer generating the whole hierarchical scaffold structure (D). To better mimic the *in vivo* articular tissue, hBMSC were seeded/encapsulated according to a 3:2:1 cell density ratio previously described for superficial:middle:deep zones (E) (Hunziker et al., 2002; Ren et al., 2016).

SEM analysis shows the fabricated PCL/Gelatin aligned nanofibers with an average fiber diameter of 531 ± 159 nm (Figure VIII.2). Therefore, the electrospun scaffolds produced were promising for CTE strategies and for use as the superficial layer of the hierarchical scaffold due to their ability to mimic the alignment and nanoscale features of the native articular cartilage ECM.

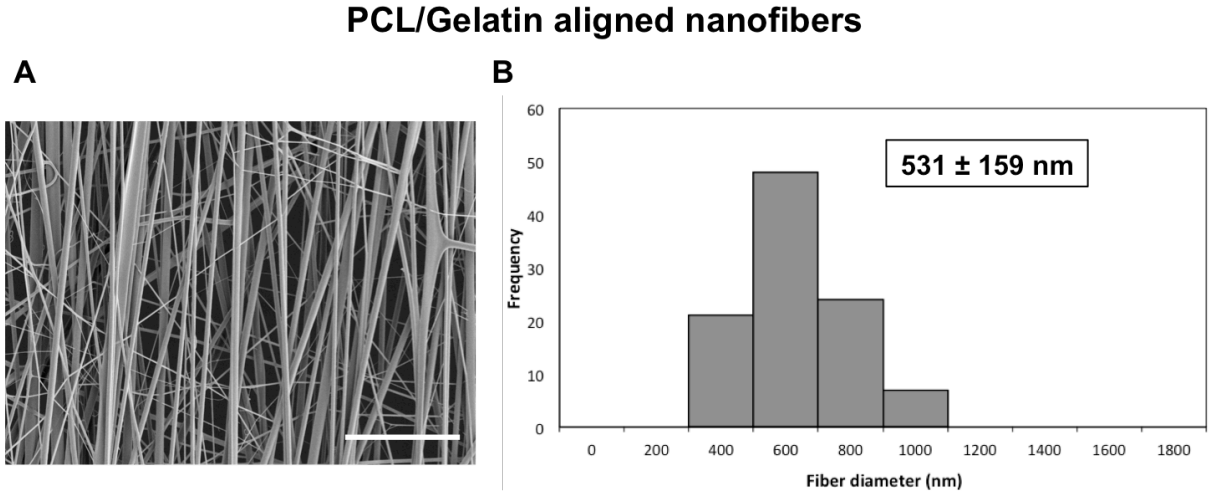

Figure VIII.2. SEM micrograph (A) and fiber diameter distributions (B) for the aligned PCL/Gelatin electrospun nanofibers fabricated to be used as superficial zone layer of the hierarchical tri-layered scaffold. Results are presented as mean ± SD (n=100 individual fibers). Scale bar: 10 μm.

Before the *in vitro* cell culture experiments, we assessed the procedure to fabricate and assemble the hierarchical tri-layered scaffold. Therefore, we produced acellular hierarchical scaffolds as shown in Figure VIII.3 D. We observed that, by placing the hydrogel layer (ML) on the top of the 3D PCL porous scaffold (DL) at the right gelation time, the gel was able to integrate with the scaffold pores and form stable bilayer hydrogel-scaffolds (Figure VIII.3 C). Afterwards, a mat of aligned PCL/Gelatin nanofibers (SL) was cut to meet the dimensions of the scaffold and placed on top of the hydrogel layer.

The structure of the assembled hierarchical scaffold was observed by SEM analysis. Figure VIII.4 presents a tilted top view and a side view of the hierarchical scaffold with the respective individual layers identified.

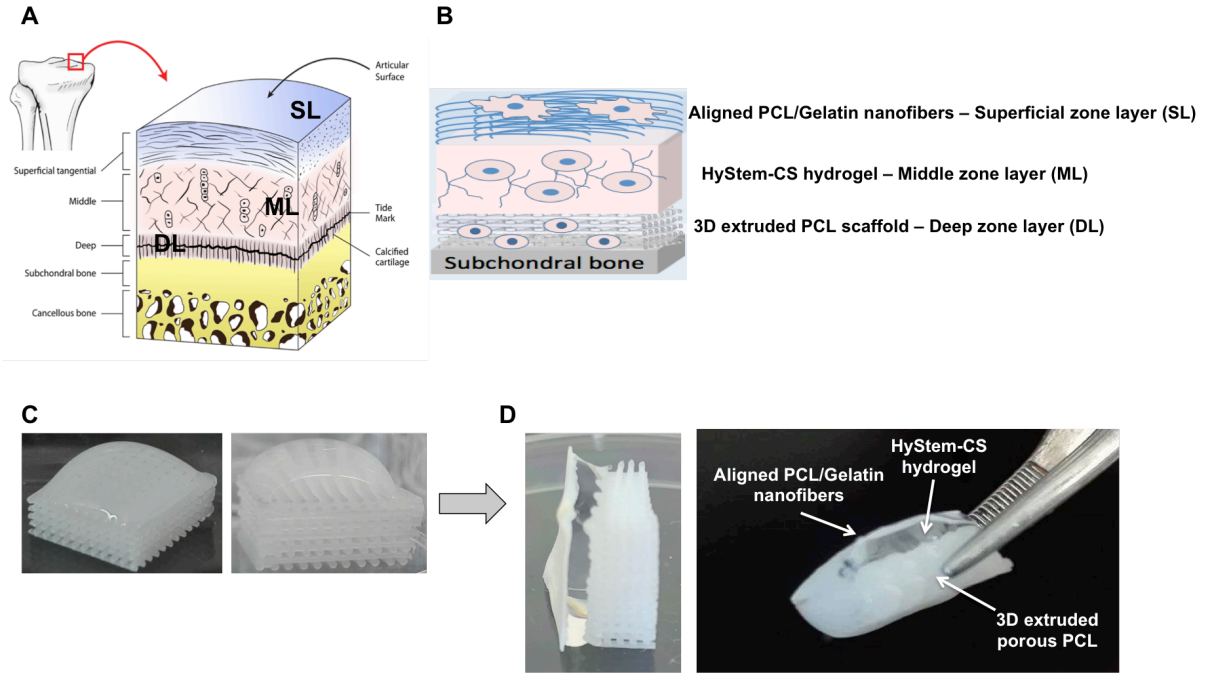

Figure VIII.3. Hierarchical scaffold assembly. The native structure of articular cartilage (A, adapted from Atesok *et al* 2016) was replicated *in vitro* by a tri-layered hierarchical scaffold (B) consisting in a 3D porous PCL scaffold layer mimicking the deep/calcified zone (DL); a GAG-based hydrogel as the middle zone layer (ML) and aligned PCL/Gelatin nanofibers to mimic the superficial/tangential zone (SL). Photographic images of the hydrogel-PCL bilayer construct (C) and of the whole tri-layered hierarchical scaffold (D).

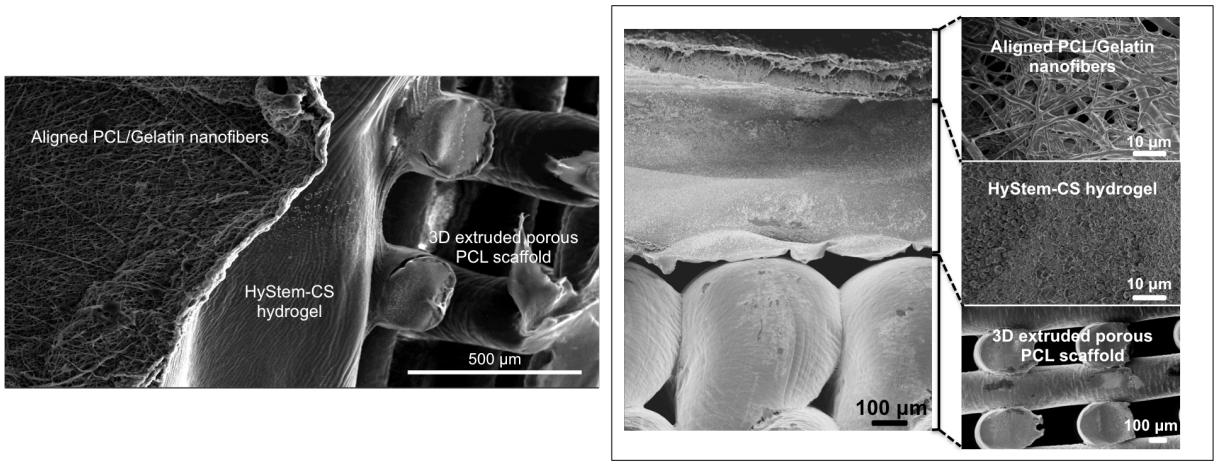

Figure VIII.4. SEM micrographic images (tilted top view on the left and lateral view on the right) of the whole tri-layered hierarchical scaffold with the respective individual layers identified. Scale bars are depicted in the images.

VIII.3.2. Evaluation of hBMSC chondrogenic differentiation on the hierarchical tri-layered scaffold and respective individual layers

The biological performance of the hierarchical scaffolds was assessed in comparison with the individual scaffold layers seeded with equal numbers of hBMSC. Thus, cell metabolic activity (Alamar Blue assay), sulfated GAG production (DMMB assay) and gene expression (RT-qPCR analysis) were evaluated. A cell density ratio of 3:2:1 for superficial:middle:deep layer was adopted during the production of the hBMSC-laden hierarchical constructs and all the cultures were performed under hypoxic conditions (5% O_2) to better mimic the *in vivo* articular cartilage niche.

The hierarchical scaffolds maintained a nearly intact structure during the 21 days of chondrogenic differentiation (Figure VIII.5 A). All the different scaffold conditions (hierarchical and individual layers) showed the presence of metabolically active hBMSC throughout the 21 days culture period. Nevertheless, higher cell metabolic activities were observed for the hierarchical scaffold and PCL/Gelatin aligned nanofibers (SL) (Figure VIII.5 B). At the end of the experiment (day 21), amounts of sulfated GAG produced were 16.04 ± 0.17 µg/scaffold, 11.18 ± 0.38 µg/scaffold, 17.12 ± 0.17 µg/scaffold and 19.66 ± 3.55 µg/scaffold for the deep layer, middle layer, superficial layer and hierarchical scaffold, respectively (Figure VIII.5 C).

After 21 days of hBMSC chondrogenic differentiation, RT-qPCR analysis was performed in all the final tissue constructs to evaluate the expression of the chondrogenic markers *COL2A1* (Figure VIII.6 A), *Sox9* (Figure VIII.6 C), *ACAN* (Figure VIII.6 D) and *PRG4* (Figure VIII.6 E) as well as the expression of the hypertrophic marker *COL10A1* (Figure VIII.6 B). The hierarchical scaffold showed upregulation of all chondrogenic markers in comparison to the control and increased *ACAN* expression levels when compared to all the individual layer scaffolds. Additionally, all the individual layers showed upregulation of all chondrogenic marker genes, with the exception of the HyStem-CS hydrogel (ML), in which *Sox9* and *ACAN* were downregulated. It is noteworthy that higher expressions of the hypertrophic marker *COL10A1* were detected in the PCL scaffold (DL) and in the hierarchical scaffold.

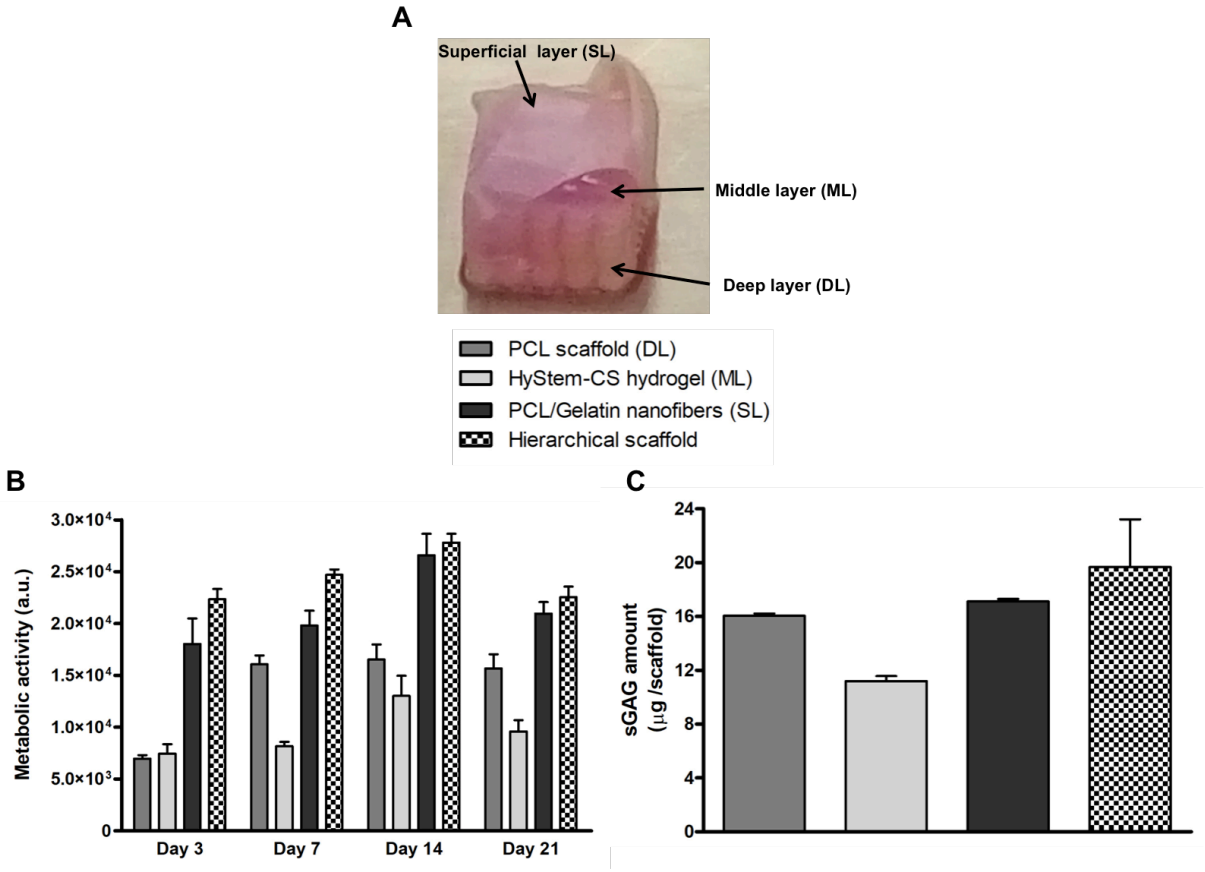

Figure VIII.5. Evaluation of the hierarchical scaffold biological performance: Hierarchical scaffold structure after 21 days of chondrogenic differentiation (A). Cell metabolic activity assessed by Alamar Blue assay throughout culture (B) and sGAG production evaluated by DMMB assay at the end of the experiment (C). Results are presented as mean ± SD (n=3 for metabolic activity assay and n=2 for GAG quantification assay).

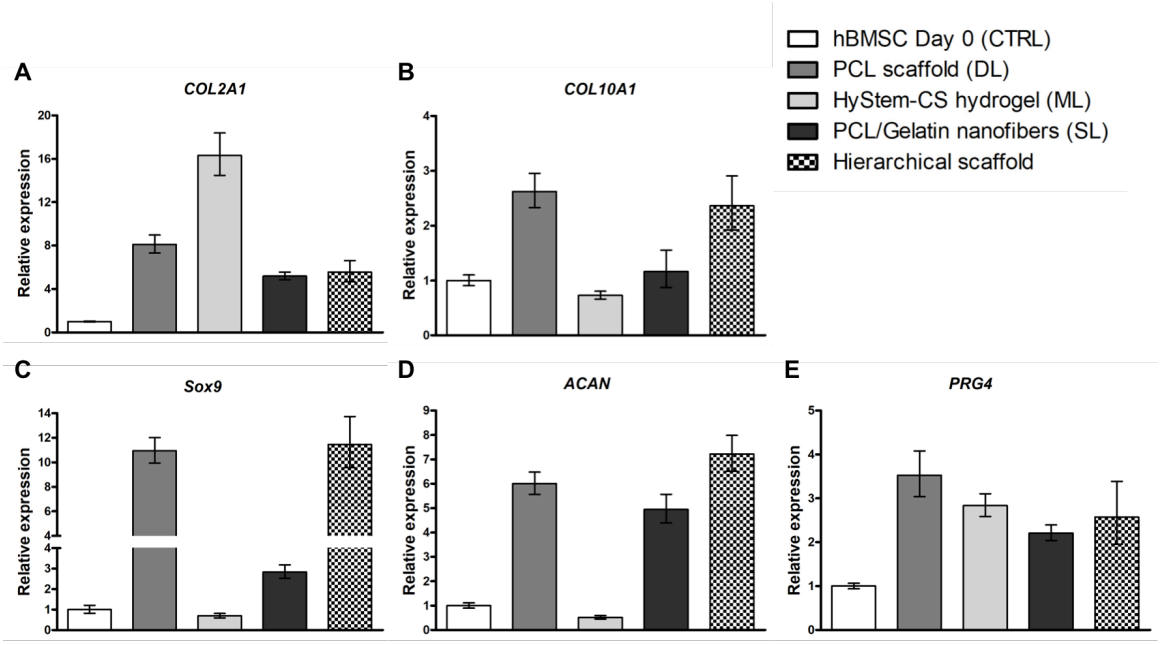

Figure VIII.6. Gene expression analysis (RT-qPCR) in the final hierarchical scaffold/individual layers tissue constructs. Expressions of *COL2A1* (A), *COL10A1* (B), *Sox9* (C), *ACAN* (D) and *PRG4* (E) were normalized to the *GAPDH* expression and calculated as a fold-change relative to the baseline expression of the control sample (hBMSC at day 0). Results are presented as mean ± SD (n=3).

The final hierarchical scaffold tissue constructs were also assessed by immunoflurescence analysis for the presence of the major cartilage components collagen II and aggrecan. After processing the hierarchical scaffold samples for immunofluorescence staining, we were not able to obtain slices containing the three layers of the scaffold. However, Figure VIII.7 shows immunofluorescence staining performed in slices containing the middle and superficial layers. The hierarchical scaffold samples stained positively for the presence of collagen II and aggrecan. Moreover, it is possible to identify the presence of collagen II within the PCL/Gelatin aligned nanofibers (SL) of the hierarchical scaffold (Figure VIII.7 A).

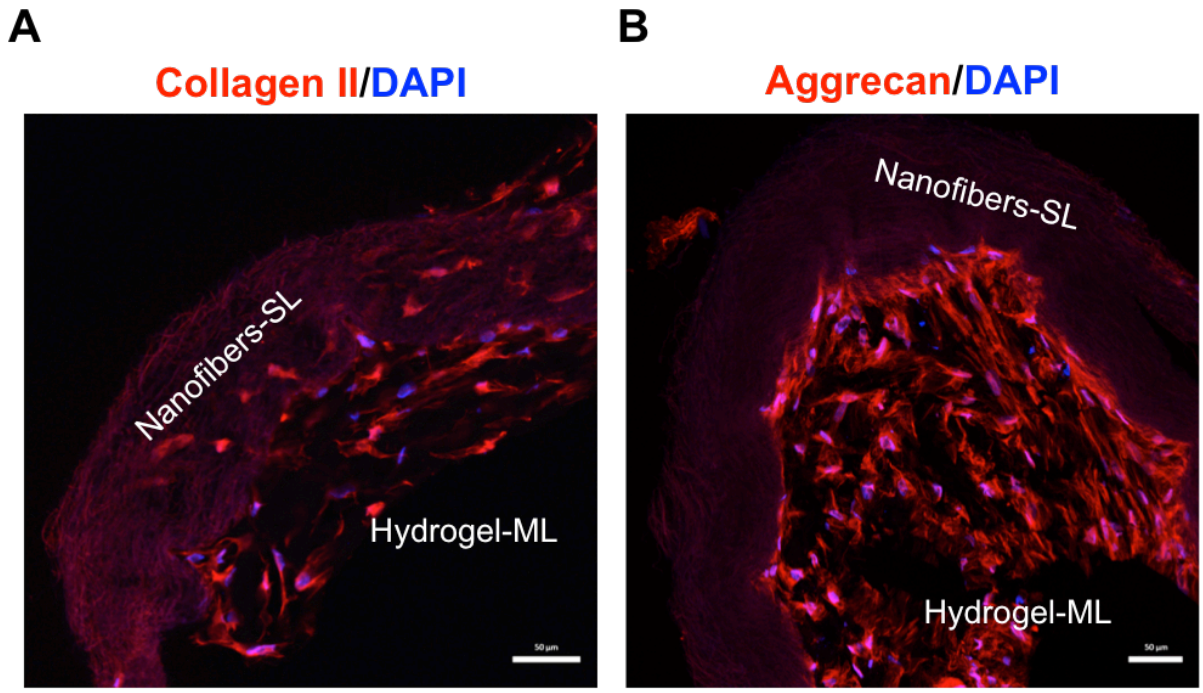

Figure VIII.7. Immunofluorescence analysis to evaluate the presence of collagen II (A) and aggrecan (B) on the final hierarchical scaffold constructs (day 21) (B). The samples were counterstained with DAPI. Scale bar: 50 μm.

VIII.4. Discussion

Despite significant advances in tissue engineering and regenerative medicine, obtaining engineered cartilage tissues with native-like properties and long-term functionality remains challenging. CTE strategies have encountered specific difficulties due to the complex hierarchical and multizonal structure of articular cartilage, with depth-varying ECM composition and organization, and consequently, depth-varying mechanical properties (Klein et al., 2007). Therefore, current CTE strategies are focused on the fabrication of multilayered and hierarchical scaffolds with structures and properties that mimic those found in the native tissue.

Major developments introduced by additive manufacturing (AM) techniques have significantly improved the control over the microarchitecture and mechanical properties of CTE scaffolds (Guo et al., 2016; Melchels et al., 2012). However, one of the main limitations of AM for CTE applications is its low resolution, making it impossible to fabricate scaffolds mimicking the nanoscale collagen fibers present in the superficial zone of articular cartilage. In contrast, conventional scaffold fabrication techniques lacking precision and reproducibility (in comparison to AM), such as electrospinning, have the ability to provide nanotopographical cues important for cell growth and differentiation. Therefore, combining AM tecnhologies such as FDM/melt-extrusion or bioprinting with electrospinning have the potential to fabricate hierarchical structures, with microscale/nanoscale features in a controlled manner, should be advantageous to mimic the zonal specificities of articular cartilage ECM (Giannitelli et al., 2015).

In the recent years, different CTE strategies have been developed aiming to produce multi-layered engineered cartilage tissues with native-like structure and function. Researchers have created multi-layered scaffolds or hydrogels by varying the biomaterial content, by using different cell populations in each layer or by creating gradients of biomolecules such as proteins and GAGs (Callahan et al., 2013; Chow et al., 2014; Correia et al., 2015; McCullen et al., 2012; Ng et al., 2009; Nguyen et al., 2011b; Zhu et al., 2014). The majority of these approaches have successfully created multilayered scaffolds with zone-specific properties and cell responses. However, they usually are creating compositional or mechanical gradients to induce the differentiation of cells towards the different zones of articular cartilage and do not focus in reproducing the architectural features of the native tissue in a single scaffold. In contrast, Steele *et al* followed a more structure-mimicking approach by combining different scaffold fabrication techniques to produce a bilayered 3D PCL scaffold composed by an aligned fiber zone to mimic the superficial zone deposited into a bulk porous particulate-template scaffold to allow chondrocyte infiltration and increased GAG production (Steele et al., 2014).

In the present study, we introduce a first concept for a novel tri-layered hierarchical scaffold aiming to provide a close mimicry of the native articular cartilage structure. Herein, we combine 3D-extrusion, hydrogel synthesis and electrospinning to achieve different micro/nano-scale topographies, compositions and mechanical support to meet the specificities of each zone of articular cartilage tissue. Thus, the proposed hierarchical scaffold consists in a 3D-extruded porous PCL scaffold as the deep zone layer, a GAG-based hydrogel as the middle zone layer and electrospun PCL/Gelatin aligned nanofibers as the superficial zone layer. PCL scaffolds were chosen to mimic the deep/calcified zone of articular cartilage due to their good mechanical support and slow biodegradation, which is important to match the slow regeneration of cartilage. In addition, 3D extruded PCL scaffolds have been widely used in both cartilage and bone repair, suggesting that this material is a good choice to place at the bone/cartilage interface (Chuenjitkuntaworn et al., 2016; Kim et al., 2010; Puppi et al., 2010; Williams et al., 2005). As middle layer, we selected a commercially available HA-based hydrogel (HyStem kit) that was previously used to promote MSC chondrogenic differentiation (Aleksander-Konert et al., 2016). Since CS is the major GAG found in adult cartilage, particularly in the middle zone, we added CS to the hydrogel system to promote a closer mimicry of the native tissue biochemical composition (Knudson and Knudson, 2001; Kuiper and Sharma, 2015). As the top layer of the hierarchical scaffold, we used aligned PCL/Gelatin nanofibers to resemble the size and orientation of the collagen fibers present in the superficial zone. Accordingly, He *et al* had previously shown the potential of PCL/Gelatin nanofibrous membranes combined with MSC-chondrocyte co-cultures for *in vivo* cartilage repair (He et al., 2015).

The great majority of the multi-layered scaffold CTE strategies use an equal number of cells to seed the different layers, which is not what happens in cartilage *in vivo*. In fact, previous studies have described a chondrocyte density gradient of 3:2:1 ratio for the superficial:middle:deep zones of articular cartilage (Hunziker et al., 2002). Other important feature of the *in vivo* articular cartilage niche is its hypoxic nature. Moreover, there is also a gradient in O_2 tension between the different zones of articular cartilage, with reported values of 6% O_2 in the superficial zone and 1% O_2 in the deep zone (Zhou et al., 2004). Considering the abovementioned differences, the hierarchical scaffold ability to promote hBMSC chondrogenic differentiation was evaluated in comparison with the individual layer scaffolds, following a biomimetic cell density gradient and under hypoxic conditions (5% O_2).

The hierarchical scaffolds produced were able to support hBMSC chondrogenic differentiation, as suggested by preliminary experiments reporting increased sGAG amounts, upregulation of chondrogenic marker genes and expression of cartilage-specific proteins. Regarding gene expression, the different scaffold groups showed upregulation of chondrogenic marker genes, with the exception of the HyStem-CS hydrogel. Indeed,

unexpectedly, the HyStem-CS hydrogel layer showed downregulation of *Sox9* and *ACAN* expressions. Nevertheless, this layer was the one with the highest *COL2A1* expression and with the lowest expression of *COL10A1*, indicating reduced hypertrophy compared to the other groups. In fact, *COL10A1* expression was increased in the PCL scaffold (DL), which is consistent with the higher collagen X amounts reported for the deep zone of human articular cartilage (Eyre and Wu, 1995; van der Kraan and van den Berg, 2012). In the hierarchical scaffold, also composed of the PCL scaffold, *COL10A1* was also upregulated in comparison to the other layers. This increase might be related with the higher stiffness of the deep layer scaffold in comparison to the other layers. Concordantly, Zhu and colleagues reported an effect of hydrogel stiffness in promoting chondrocyte hypertrophy (Zhu et al., 2017).

Herein, we present the first proof of concept use of this hierarchical scaffold and, therefore, some limitations of the current study need to be addressed in future research. First, the preliminary results presented here need to be confirmed using other experimental assays. Additionally, the mechanical properties of the final hierarchical scaffold tissue constructs need to be evaluated and compared to those of native cartilage tissue. Noteworthy, it is possible to tailor the mechanical properties of the whole hierarchical scaffold by modulating the pore geometry and fiber organization of the deep layer PCL scaffold (Olubamiji et al., 2016). Further immunohistochemical/histological assays should be performed to assess if the appropriate ECM is being generated in the respective layers of the hierarchical scaffold. In the current study, the assembly of the whole cell-laden hierarchical scaffold was performed manually by a laborious and time-consuming process. Therefore, future research should focus on the development of an integrated technology based on the combination of AM-based extrusion, bioprinting and electrospinning enabling the continuous production and assembly of the hierarchical tissue constructs in a more automated and reproducible manner.

Despite the need for further developments, our results highlight the potential of biomimetic hierarchical scaffold strategies for CTE focusing on the repair of full thickness cartilage or osteochondral defects (Grade III or IV) or as more reliable 3D *in vitro* models for disease modeling and drug screening.

VIII.5. References

Aleksander-Konert, E., Paduszyński, P., Zajdel, A., Dzierzewicz, Z., Wilczok, A., (2016). In vitro chondrogenesis of Wharton's jelly mesenchymal stem cells in hyaluronic acid-based hydrogels. Cell. Mol. Biol. Lett. 21, 11.

Atesok, K., Doral, M.N., Karlsson, J., Egol, K.A., Jazrawi, L.M., Coelho, P.G., Martinez, A., Matsumoto, T., Owens, B.D., Ochi, M., Hurwitz, S.R., Atala, A., Fu, F.H., Lu, H.H., Rodeo, S.A., (2016). Multilayer scaffolds in orthopaedic tissue engineering. Knee Surgery, Sport. Traumatol. Arthrosc. 24, 2365–2373.

Bhosale, A.M., Richardson, J.B., (2008). Articular cartilage: structure, injuries and review of management. Br. Med. Bull. 87, 77–95.

Callahan, L.A.S., Childers, E.P., Bernard, S.L., Weiner, S.D., Becker, M.L., (2013). Maximizing phenotype constraint and extracellular matrix production in primary human chondrocytes using arginine-glycine-aspartate concentration gradient hydrogels. Acta Biomater. 9, 7420–7428.

Camarero-Espinosa, S., Cooper-White, J., (2017). Tailoring biomaterial scaffolds for osteochondral repair. Int. J. Pharm. 523, 476–489.

Camarero-Espinosa, S., Rothen-Rutishauser, B., Foster, E.J., Weder, C., (2016). Articular cartilage: From formation to tissue engineering. Biomater. Sci. 4, 734–767.

Chow, L.W., Armgarth, A., St-Pierre, J.-P., Bertazzo, S., Gentilini, C., Aurisicchio, C., McCullen, S.D., Steele, J.A.M., Stevens, M.M., (2014). Peptide-Directed Spatial Organization of Biomolecules in Dynamic Gradient Scaffolds. Adv. Healthc. Mater. 3, 1381–1386.

Chuenjitkuntaworn, B., Osathanon, T., Nowwarote, N., Supaphol, P., Pavasant, P., (2016). The efficacy of polycaprolactone/hydroxyapatite scaffold in combination with mesenchymal stem cells for bone tissue engineering. J. Biomed. Mater. Res. - Part A 104, 264–271.

Correia, C.R., Reis, R.L., Mano, J.F., (2015). Multiphasic, multistructured and hierarchical strategies for cartilage regeneration, in: Engineering Mineralized and Load Bearing Tissues. pp. 143–160.

Domingos, M., Dinucci, D., Cometa, S., Alderighi, M., Bártolo, P.J., Chiellini, F., (2009). Polycaprolactone Scaffolds Fabricated via Bioextrusion for Tissue Engineering Applications. Int. J. Biomater. 2009, 239643.

Eyre, D.R., Wu, J.J., (1995). Collagen structure and cartilage matrix integrity. J. Rheumatol. 82–85.
Flannery, C.R., Hughes, C.E., Schumacher, B.L., Tudor, D., Aydelotte, M.B., Kuettner, K.E., Caterson, B., (1999). Articular cartilage superficial zone protein (SZP) is homologous to megakaryocyte stimulating factor precursor and is a multifunctional proteoglycan with potential growth-promoting, cytoprotective, and lubricating properties in cartilage metabolism. Biochem. Biophys. Res. Commun. 254, 535–541.

Giannitelli, S.M., Mozetic, P., Trombetta, M., Rainer, A., (2015). Combined additive manufacturing approaches in tissue engineering. Acta Biomater. 24, 1–11.

Gomoll, A.H., Madry, H., Knutsen, G., van Dijk, N., Seil, R., Brittberg, M., Kon, E., (2010). The subchondral bone in articular cartilage repair: Current problems in the surgical management. Knee Surgery, Sport. Traumatol. Arthrosc. 18, 434–447.

Grogan, S.P., Duffy, S.F., Pauli, C., Koziol, J.A., Su, A.I., D'Lima, D.D., Lotz, M.K., (2013). Zone-specific gene expression patterns in articular cartilage. Arthritis Rheum. 65, 418–428.

Guo, T., Lembong, J., Zhang, L.G., Fisher, J.P., (2016). Three-Dimensional Printing Articular Cartilage: Recapitulating the Complexity of Native Tissue . Tissue Eng. Part B Rev. 23, 225–236.

He, X., Feng, B., Huang, C., Wang, H., Ge, Y., Hu, R., Yin, M., Xu, Z., Wang, W., Fu, W., Zheng, J., (2015). Electrospun gelatin/polycaprolactone nanofibrous membranes combined with a coculture of bone marrow stromal cells and chondrocytes for cartilage engineering. Int. J. Nanomedicine 10, 2089–2099.

Huang, B.J., Hu, J.C., Athanasiou, K.A., (2016). Cell-based tissue engineering strategies used in the clinical repair of articular cartilage. Biomaterials 98, 1–22.

Huey, D.J., Hu, J.C., Athanasiou, K.A., (2012). Unlike bone, cartilage regeneration remains elusive. Science. 338, 917–921.

Hunziker, E.B., Quinn, T.M., Häuselmann, H.-J., (2002). Quantitative structural organization of normal adult human articular cartilage. Osteoarthr. Cartil. 10, 564–72.

Kim, H.J., Lee, J.H., Im, G. Il, (2010). Chondrogenesis using mesenchymal stem cells and PCL scaffolds. J. Biomed. Mater. Res. - Part A 92, 659–666.

Klein, T.J., Chaudhry, M., Bae, W.C., Sah, R.L., (2007). Depth-dependent biomechanical and biochemical properties of fetal, newborn, and tissue-engineered articular cartilage. J. Biomech. 40, 182–190.

Klein, T.J., Malda, J., Sah, R.L., Hutmacher, D.W., (2009). Tissue Engineering of Articular Cartilage with Biomimetic Zones. Tissue Eng. Part B Rev. 15, 143–157.

Knudson, C.B., Knudson, W., (2001). Cartilage proteoglycans. Semin. Cell Dev. Biol. 12, 69–78.

Kuiper, N.J., Sharma, A., 2015. A detailed quantitative outcome measure of glycosaminoglycans in human articular cartilage for cell therapy and tissue engineering strategies. Osteoarthr. Cartil. 23, 2233–2241.

Langer, R., Vacanti, J.P., (1993). Tissue Engineering. Science. 260, 920–926.

Mano, J.F., Reis, R.L., (2007). Osteochondral defects: Present situation and tissue engineering approaches. J. Tissue Eng. Regen. Med. 1, 261–273.

McCullen, S.D., Autefage, H., Callanan, A., Gentleman, E., Stevens, M.M., (2012). Anisotropic Fibrous Scaffolds for Articular Cartilage Regeneration. Tissue Eng. Part A 18, 2073–2083.

Melchels, F.P.W., Domingos, M. a N., Klein, T.J., Malda, J., Bartolo, P.J., Hutmacher, D.W., (2012). Additive manufacturing of tissues and organs. Prog. Polym. Sci. 37, 1079–1104.

Müller, C., Khabut, A., Dudhia, J., Reinholt, F.P., Aspberg, A., Heinegård, D., Önnerfjord, P., (2014). Quantitative proteomics at different depths in human articular cartilage reveals unique patterns of protein distribution. Matrix Biol. 40, 34–45.

Ng, K.W., Ateshian, G.A., Hung, C.T., (2009). Zonal Chondrocytes Seeded in a Layered Agarose Hydrogel Create Engineered Cartilage with Depth-Dependent Cellular and Mechanical Inhomogeneity. Tissue Eng. Part A 15, 2315–2324.

Nguyen, L.H., Kudva, A.K., Guckert, N.L., Linse, K.D., Roy, K., (2011). Unique biomaterial compositions direct bone marrow stem cells into specific chondrocytic phenotypes corresponding to the various zones of articular cartilage. Biomaterials 32, 1327–1338.

Olubamiji, A.D., Izadifar, Z., Si, J.L., Cooper, D.M.L., Eames, B.F., Chen, D.X.B., (2016). Modulating mechanical behaviour of 3D-printed cartilage-mimetic PCL scaffolds: Influence of molecular weight and pore geometry. Biofabrication 8, 025020.

Outerbridge, R.E., (1961). The etiology of chondromalacia patellae. J. Bone Joint Surg. Br. 43, 752–757.

Puppi, D., Chiellini, F., Piras, A.M., Chiellini, E., (2010). Polymeric materials for bone and cartilage repair. Prog. Polym. Sci. 35, 403–440.

Redler, I., Mow, V.C., Zimny, M.L., Mansell, J., (1975). The ultrastructure and biomechanical significance of the tidemark of articular cartilage. Clin. Orthop. Relat. Res. 112, 357–362.

Ren, X., Wang, F., Chen, C., Gong, X., Yin, L., Yang, L., (2016). Engineering zonal cartilage through bioprinting collagen type II hydrogel constructs with biomimetic chondrocyte density gradient. BMC Musculoskelet. Disord. 17, 1–10.

Silva, J.C., Moura, C.S., Alves, N., Cabral, J.M.S., Ferreira, F.C., (2017). Effects of different fibre alignments and bioactive coatings on mesenchymal stem/stromal cell adhesion and proliferation in poly (ε-caprolactone) scaffolds towards cartilage repair. Procedia Manuf. 12, 132–140.

Steele, J.A.M., McCullen, S.D., Callanan, A., Autefage, H., Accardi, M. a., Dini, D., Stevens, M.M., (2014). Combinatorial scaffold morphologies for zonal articular cartilage engineering. Acta Biomater. 10, 2065–2075.

van der Kraan, P.M., van den Berg, W.B., (2012). Chondrocyte hypertrophy and osteoarthritis: Role in initiation and progression of cartilage degeneration? Osteoarthr. Cartil. 20, 223–232.

Williams, J.M., Adewunmi, A., Schek, R.M., Flanagan, C.L., Krebsbach, P.H., Feinberg, S.E., Hollister, S.J., Das, S., (2005). Bone tissue engineering using polycaprolactone scaffolds fabricated via selective laser sintering. Biomaterials 26, 4817–4827.

Yan, L., Oliveira, J.M., Oliveira, A.L., Reis, R.L., (2015). Current Concepts and Challenges in Osteochondral Tissue Engineering and Regenerative Medicine. ACS Biomater. Sci. Eng. 1, 183–200.

Zhang, Q., Lu, H., Kawazoe, N., Chen, G., (2013). Preparation of collagen porous scaffolds with a gradient pore size structure using ice particulates. Mater. Lett. 107, 280–283.

Zhou, S., Cui, Z., Urban, J.P.G., (2004). Factors influencing the oxygen concentration gradient from the synovial surface of articular cartilage to the cartilage-bone interface: A modeling study. Arthritis Rheum. 50, 3915–3924.

Zhu, D., Tong, X., Trinh, P., Yang, F., (2017). Mimicking Cartilage Tissue Zonal Organization by Engineering Tissue-Scale Gradient Hydrogels as 3D Cell Niche. Tissue Eng. Part A 24, 1–10.

Zhu, Y., Wan, Y., Zhang, J., Yin, D., Cheng, W., (2014). Manufacture of layered collagen/chitosan-polycaprolactone scaffolds with biomimetic microarchitecture. Colloids Surfaces B Biointerfaces 113, 352–360.

Chapter IX

FINAL REMARKS AND FUTURE DIRECTIONS

CHAPTER IX - FINAL REMARKS AND FUTURE DIRECTIONS

As a result of the growing aging population and, consequently, the increasing number of cases of joint degenerative diseases such as osteoarthritis, there is an urgent need for new tissue engineering approaches that can actually produce hyaline-like cartilage repaired tissue. This would represent an improvement over the current surgical methods used that often generate fibrocartilage, which compromises the functionality of the repaired tissue.

Despite the great number of research studies and the major developments that have been made in the field of cartilage tissue engineering (CTE), an engineered cartilage tissue with native-like structural and mechanical properties and with long-term functionality has not yet been obtained, which has limited the clinical translation of these approaches. One major issue in CTE has been an inability to reproduce the highly complex stratified structure of articular cartilage tissue *in vitro*. Since tissue functionality is dictated by its zone-varying structure and adequate microenvironment, recent approaches have been mainly focused on mimicking the *in vivo* features of articular cartilage structure and niche to improve the quality of the resulting engineered tissues.

In this thesis, based on what is currently known about the articular cartilage biochemical composition, structure and *in vivo* microenvironment, we explored different CTE strategies for the *in vitro* production of engineered cartilage tissues. We combined MSCs, biodegradable scaffolds and specific "*in vivo*-like" chemical/physical/environmental stimuli to enhance the chondrogenic potential of cells and, therefore, generate improved tissue constructs.

The main findings and contributions arising from this PhD thesis work are summarized below:

GAGs are a major component or articular cartilage and, therefore, are critical in the evaluation of the quality of engineered tissues. However, very little information is available about the GAG composition of cells, cell-derived ECM and engineered tissues relevant for CTE applications. Thus, we proposed to use a highly selective and accurate LC-MS/MS method to determine the GAG disaccharide composition of different types of decellularized cell-derived ECM and their corresponding human cell sources (chondrocytes, hBMSC and hSMSC) routinely used in CTE approaches. Significant differences in GAG composition and disaccharide sulfation patterns were observed between the different cell-derived ECM generated as well as between the different cell sources. We also observed the effects of the decellularization method used on the relative GAG disaccharide composition. Furthermore, we also used the same LC-MS/MS method to study the GAG remodeling during the chondrogenic differentation of hBMSC and hSMSC under normoxic and hypoxic environments. We observed that hBMSC and hSMSC were impacted differently by hypoxia

in terms of chondrogenic gene expression and average GAG disaccharide composition. Nevertheless, in terms of GAG composition and regardless the oxygen tension, all the final MSC-based microtissues were primarily composed of CS, the predominant GAG in articular cartilage, which is in agreement with the observed in chondrocyte-based microtissues.

Based on the native biochemical composition of articular cartilage and on the results obtained from the LC-MS/MS analysis, we used CS and HA as culture medium additives to provide additional chemical cues for the MSC (hBMSC and hSMSC) chondrogenic differentiation in custom-made 3D porous PCL scaffolds. While previous studies have reported a positive effect of CS and HA supplementation on BMSC chondrogenesis in different culture systems (Chen et al., 2011; Christiansen-Weber et al., 2018; Schwartz et al., 2011), to the best of our knowledge, this is the first report exploring the effects of GAG supplementation using hSMSC. Indeed, we showed that GAG supplementation, particularly with HA, promoted the chondrogenic differentiation of both hBMSC and hSMSC in PCL scaffolds as suggested by increased sGAG production and elevated chondrogenic markers expression. Nevertheless, differences were observed between the two MSC sources, namely the suggestion of reduced tissue hypertrophy in hSMSC-derived engineered tissues, in comparison to the ones generated using hBMSC.

Another contribution of this thesis was the development of a fully customizable perfusion bioreactor platform capable of enhancing the chondrogenic differentiation of hBMSCs in PCL scaffolds. We demonstrated the benefits of a perfusion culture since the final perfused hBMSC-PCL constructs presented higher sGAG production, higher chondrogenic marker genes expression, abundant cartilage-specific protein expression and reduced hypertrophy comparing to non-perfused constructs. This study highlighted the potential of additive manufacturing (AM) for developing fully personalized CTE strategies and more reliable *in vitro* models.

In our final hierarchical scaffold concept, the 3D extruded PCL scaffold will target the regeneration of the deep and calcified zones at the bone/cartilage interface. Thus, we thought it would be interesting to evaluate the scaffold's potential to promote MSC osteogenic differentiation. We showed that the decoration of the PCL scaffold structure with MSC-derived ECM is an efficient strategy to enhance its bioactivity and osteoinductive properties as demonstrated by the improvements in cell proliferation and osteogenesis when compared to pristine PCL scaffolds. The combination of AM technology for the fabrication of scaffolds designed to perfectly fit the patient's bone defect with autologous cell-derived ECM/cells have the potential to generate scaffolds with improved biological performance for personalized bone tissue engineering strategies.

Within the scope of this thesis, we also fabricated and characterized KGN-loaded coaxial aligned nanofibers addressing the regeneration of the superficial layer of articular cartilage. A

coaxial configuration allowed a much more controlled KGN release than the monoaxial fibers and both KGN-loaded scaffolds showed improved MSC chondrogenic differentiation. Our results showed that the biological performance of electropsun scaffolds mimicking the nanometer scale and alignment of native articular cartilage ECM can be improved through the incorporation of the chondroinductive drug KGN, highlighting the potential of these scaffolds for MSC-based CTE strategies, particularly, to repair defects in the articular cartilage superficial zone.

Importantly, as final contribution, this thesis introduced the concept of using a hierarchical tri-layered scaffold to mimic the multi-zonal stratified structure of articular cartilage with zone-dependent cell density and phenotype, ECM composition and mechanical properties. While further characterization studies of the hierarchical scaffold and the resultant engineered tissues are needed, our results suggest the ability of the scaffold to support MSC chondrogenic differentiation. Upon appropriate modifications and testing, this hierarchical tri-layered scaffold could represent a promising approach for the regeneration of full-thickness cartilage defects and be used as a reliable *in vitro* model for disease modeling and drug screening.

Limitations of the study and possible future directions:

During the timeframe of this PhD thesis, several new questions were raised and study limitations could be identified as opportunities for future research. Thus, in the following paragraphs, we summarize some of the limitations/open questions that remain to be addressed and suggest possible future research lines:

- We provided a GAG and disaccharide compositional analysis for the different cell-derived ECM produced and respective cell sources. Moreover, the cell-derived matrices produced were also assessed qualitatively in terms of their structure (SEM) and for the presence of most common ECM proteins (collagen I, fibronectin and laminin). Due to the highly complex combination of macromolecules present in ECM, it is likely that we have missed relevant information about other ECM components that could vary between the different cell-derived ECM studied. Further studies should include the compositional GAG analysis of other cell types. We believe that this analysis should be complemented with proteomic tools to provide a more comprehensive and complete characterization of the cell-derived ECM matrisome. Efforts are also needed to provide information about the complete ECM composition of healthy/diseased tissues as well as of cell-derived matrices, with the purpose of identifying possible new biomarkers for diagnosis and as a guide for designing the

next generation ECM-biomimetic scaffolds for tissue engineering applications (Naba et al., 2016; Ragelle et al., 2017).

- In this thesis, we studied GAG remodeling during the differentiation of hBMSC and hSMSC towards cartilage under different oxygen tension culturing conditions (21% O_2 and 5% O_2). Although we used undifferentiated and differentiated chondrocytes (under the same conditions) as controls, the inclusion of a human articular cartilage sample as a final control in the analysis would be helpful for evaluating the MSC-based cartilage microtissues produced. In addition, we believe that complementing the LC-MS/MS approach with a transcriptomic analysis of the cartilage microtissues generated would provide important information not only about how oxygen tension affects the regulation of chondrogenic genes, but also how it affects the expression of genes involved in the biosynthesis of specific GAG types.

- Besides expanding the analysis to other cell sources able to generate chondrogenic-like tissues (e.g., adipose stem/stromal cells, induced pluripotent stem cells (iPSC), periosteum-derived cells), another future direction of this work could be the use of our LC-MS/MS method to analyze differences in the GAG and disaccharide composition between healthy and diseased cartilage tissues (e.g., affected with OA) as well as from cells (chondrocytes, MSC / iPSC) isolated/derived from these tissues. The identified differences may provide insightful information about OA disease mechanism, which remains poorly understood. Furthermore, it would be also interesting to apply this method to evaluate the GAG composition of scaffold-based engineered cartilage tissues, however, an optimization of protocols for GAG isolation and purification might be required.

- GAG (CS and HA) supplementation as culture medium additives enhanced the chondrogenic differentiation of both hBMSC and hSMSC in 3D porous PCL scaffolds. However, our studies were performed considering just a single concentration for each GAG type (based in physiological values reported for cartilage and synovial fluid in human knee) and the synergistic effect of HA and CS was not evaluated. Therefore, further studies optimizing HA and CS concentrations to achieve higher MSC chondrogenic potential are needed. Studies on the evaluation of the synergistic effect of GAGs in comparison to single GAG supplementation also need to be considered. In addition, as proposed by Wu and colleagues, GAG supplementation strategies (mainly with high MW HA) can be further explored to prepare non-Newtonian culture medium that can recreate better the biochemistry and biomechanics of the synovial

fluid and possibly, provide a improved environment for the development of engineered cartilage tissue (Wu et al., 2017). It is also important to note that only one form of CS was studied in this thesis. There are multiple forms of CS and the impact of CS composition and possible CS sequence will eventually need to be considered.

- The extruded perfusion bioreactor developed in this thesis allows the study of the effect of fluid-induced shear stress stimuli on the hBMSC chondrogenesis in PCL scaffolds. However, the actual values of shear stress experienced by the tissue constructs were not predicted and further computational modeling studies are required to provide such information. Moreover, all the *in vitro* culture experiments were performed at a single flow rate. Thus, a study varying flow rate stimulation values should be performed to determine the ideal bioreactor operating conditions required to maximize the chondrogenic potential of hBMSC. Additionally, as articular cartilage motion consists of a combination of compressive, tensile and shear deformations, future research should focus on the development of novel AM-based bioreactors enabling the simultaneous and controlled application of multiple mechanical stimuli to enhance the quality and functionality of the engineered cartilage tissues.

- Another future direction for this work could be exploring the use of MSC-derived ECM decorated scaffolds for CTE applications (similar to chapter VI). Due to their chondrogenic potential and because they are joint native cells, hSMSC or chondrocytes could also be used to produce the cell-derived ECM on the surface of the scaffolds. Moreover, other scaffold configurations with cell-derived ECM to promote the MSC chondrogenic differentiation could be considered, such as cell derived ECM-loaded electrospun fibers (Carvalho et al., 2019) or hydrogels incorporating cell-derived ECM particles.

- Aiming to mimic the size and alignment of ECM fibers present in the superficial zone of articular cartilage, we developed coaxial PGS/PCL aligned nanofibers able to allow the controlled release of the chondroinductive drug KGN. We demonstrated that these scaffolds were able to promote hBMSC chondrogenic differentiation in the absence of TGF-β3-supplemented medium. However, a comparison with KGN supplemented in the culture medium as well as the evaluation of possible positive synergistic effects of TGF-β3 and KGN released from the nanofibers was not assessed and should be addressed in future studies. Additionally, a deeper

understanding of the relation between scaffold biodegradation, KGN release kinetics and tissue formation should be pursued.

- With the objective of mimicking *in vitro* the stratified multi-zonal architecture of articular cartilage, we introduced a novel concept for a hierarchical tri-layered scaffold and showed its ability to support hBMSC chondrogenic differentiation. Nevertheless, more characterization experiments are required to evaluate the full potential of the scaffold, namely, the assessment of the mechanical properties of the final engineered cartilage tissue and further immunofluorescence/histological assays to evaluate if the proper zone specific-ECM is being produced in the respective layer of the hierarchical scaffold. In this initial proof of concept study, the assembly of the different layers into a whole hierarchical scaffold was performed manually in a laborious process. Therefore, future research should work towards the development of new integrated AM equipment capable of producing and assembling the different layers of the hierarchical scaffold in a fast, sterile and reproducible manner. One possibility could be a system combining extrusion for the production of deep zone layer PCL scaffolds; stereolithography allowing for the encapsulation of cells and subsequent polymerization in a GAG-based hydrogel (middle zone layer); electrospinning apparatus to produce aligned nanofibers (superficial zone layer) and a bioprinting system for seeding cells in the deep zone layer and superficial zone layer scaffolds. While many technological hurdles will probably arise before such system could be used, we believe the ongoing developments in the field of additive biomanufacturing will make sucess possible in a relatively short timeframe. In fact, the successful combination of different AM-based approaches has been reported (Giannitelli et al., 2015; Lee et al., 2016). Furthermore, based on our findings in this thesis, the biological performance of the hierarchical tri-layered scaffold could be improved. For example, a second generation of the hierarchical scaffold could be comprised by MSC-derived ECM decorated PCL scaffolds for the deep zone layer and aligned coaxial PGS-KGN/PCL nanofibers as superficial zone layer. For a more complete *in vitro* mimicry of the native articular cartilage structure and microenvironment, the hierarchical scaffold could be combined with an AM-based bioreactor able to provide different mechanical stimuli to recreate articular motion stresses and with GAG-supplemented medium simulating the biochemical signaling and viscosity of the synovial fluid. As future lines of research, other cell sources (e.g. hSMSC or chondrocytes) can also be tested with this system and the use of iPSC-derived from arthritic tissues can be exploited to generate more reliable *in vitro* disease models.

- Throughout this thesis, some hypertrophy in the final hBMSC-based engineered cartilage tissues was suggested by the upregulation of *COLX* gene. Indeed, the tendency of MSC to undergo hypertrophic differentiation has also been reported by other groups (Mueller and Tuan, 2008; Somoza et al., 2014). Possible strategies that are being adopted to prevent the formation of engineered hypertrophic cartilage tissue include the use of articular cartilage-derived progenitor cells (Levato et al., 2017) or co-culture systems of MSC and articular chondrocytes (Bian et al., 2011; Fischer et al., 2010). Thus, possible future work might include testing these cells and co-cultures in our scaffold-based approaches. Additionally, as this thesis focused mainly on the *in vitro* fabrication of engineered cartilage tissues, *in vivo* studies were not performed. However, we understand that *in vivo* animal testing of the scaffold-based engineered cartilage tissues produced should be considered in the future to assess their potential to repair cartilage defects as well as possible inflammatory responses.

References

Bian, L., Zhai, D.Y., Mauck, R.L., Burdick, J.A., (2011). Coculture of Human Mesenchymal Stem Cells and Articular Chondrocytes Reduces Hypertrophy and Enhances Functional Properties of Engineered Cartilage. Tissue Eng. Part A 17, 1137–1145.

Carvalho, M.S., Silva, J.C., Udangawa, R.N., Cabral, J.M.S., Ferreira, F.C., da Silva, C.L., Linhardt, R.J., Vashishth, D., (2019). Co-culture cell-derived extracellular matrix loaded electrospun microfibrous scaffolds for bone tissue engineering. Mater. Sci. Eng. C 479–490.

Chen, W.C., Yao, C.L., Chu, I.M., Wei, Y.H., (2011). Compare the effects of chondrogenesis by culture of human mesenchymal stem cells with various type of the chondroitin sulfate C. J. Biosci. Bioeng. 111, 226–231.

Christiansen-Weber, T., Noskov, A., Cardiff, D., Garitaonandia, I., Dillberger, A., Semechkin, A., Gonzalez, R., Kern, R., (2018). Supplementation of specific carbohydrates results in enhanced deposition of chondrogenic-specific matrix during mesenchymal stem cell differentiation. J. Tissue Eng. Regen. Med. 12, 1261–1272.

Fischer, J., Dickhut, A., Rickert, M., Richter, W., (2010). Human articular chondrocytes secrete parathyroid hormone-related protein and inhibit hypertrophy of mesenchymal stem cells in coculture during chondrogenesis. Arthritis Rheum. 62, 2696–2706.

Giannitelli, S.M., Mozetic, P., Trombetta, M., Rainer, A., (2015). Combined additive manufacturing approaches in tissue engineering. Acta Biomater. 24, 1–11.

Lee, S.-J., Nowicki, M., Harris, B., Zhang, L.G., (2016). Fabrication of a Highly Aligned Neural Scaffold via a Table Top Stereolithography 3D Printing and Electrospinning. Tissue Eng. Part A 23, 491–502.

Levato, R., Webb, W.R., Otto, I.A., Mensinga, A., Zhang, Y., van Rijen, M., van Weeren, R., Khan, I.M., Malda, J., (2017). The bio in the ink: cartilage regeneration with bioprintable hydrogels and articular cartilage-derived progenitor cells. Acta Biomater. 61, 41–53.

Mueller, M.B., Tuan, R.S., (2008). Functional characterization of hypertrophy in chondrogenesis of human mesenchymal stem cells. Arthritis Rheum. 58, 1377–1388.

Naba, A., Clauser, K.R., Ding, H., Whittaker, C.A., Carr, S.A., Hynes, R.O., (2016). The extracellular matrix: Tools and insights for the “omics” era. Matrix Biol. 49, 10–24.

Ragelle, H., Naba, A., Larson, B.L., Zhou, F., Prijić, M., Whittaker, C.A., Del Rosario, A., Langer, R., Hynes, R.O., Anderson, D.G., (2017). Comprehensive proteomic characterization of stem cell-derived extracellular matrices. Biomaterials 128, 147–159.

Schwartz, Z., Griffon, D.J., Fredericks, L.P., Lee, H.-B., Weng, H.-Y., (2011). Hyaluronic acid and chondrogenesis of murine bone marrow mesenchymal stem cells in chitosan sponges. Am. J. Vet. Res. 72, 42–50.

Somoza, R.A., Welter, J.F., Correa, D., Caplan, A.I., (2014). Chondrogenic Differentiation of Mesenchymal Stem Cells: Challenges and Unfulfilled Expectations. Tissue Eng. Part B Rev. 20, 596–608.

Wu, Y., Stoddart, M.J., Wuertz-Kozak, K., Grad, S., Alini, M., Ferguson, S.J., 2017. Hyaluronan supplementation as a mechanical regulator of cartilage tissue development under joint-kinematic mimicking loading. J. R. Soc. Interface 14, 20170255.

LIST OF PUBLICATIONS

Oral Communications

26th Annual Meeting of the European Orthopaedic Research Society (EORS 2018), Galway, Ireland, 25th-28th September 2018, **J.C. Silva**, C.S. Moura, G. Borrecho, A.P. Alves de Matos, J.M.S. Cabral, R.J. Linhardt and F.C. Ferreira, *"Extruded perfusion bioreactor: a versatile custom-made platform to study shear stress in cartilage tissue engineered constructs"*

12th European Symposium on Biochemical Engineering Sciences (ESBES 2018), Lisboa, Portugal, 9th-12th September 2018, **J.C. Silva**, C.S. Moura, G. Borrecho, A. Alves de Matos, J.M.S. Cabral, R.J. Linhardt and F.C. Ferreira, *"Extruded perfusion bioreactors as a customizable culture platform to study fluid shear stress stimuli in articular cartilage tissue engineered constructs"*

254th American Chemical Society National Meeting & Exposition, Washington, DC, 20th-24th August 2017, **J.C. Silva**, R.N. Udangawa, F.F. Garrudo, P.E. Mikael, F.C. Ferreira and R.J. Linhardt, *"Biodegradable aligned core-shell nanofibers for articular cartilage tissue engineering"*

254th American Chemical Society National Meeting & Exposition, Washington, DC, 20th-24th August 2017, F.F. Garrudo, **J.C. Silva**, C.A.V. Rodrigues, J.M.F. Morgado, R.J. Linhardt and F.C. Ferreira, *"Polybenzimidazole electrospun nanofibers for neural cell culture"*

International Conference on Sustainable and Intelligent Manufacturing (RESIM 2016), CDRSP- Polytechnic Institute of Leiria, Marinha Grande - Portugal, 14th-17th December 2016, **J.C. Silva,** C.S. Moura, N.M. Alves, J.M.S. Cabral and F.C. Ferreira, *"Effects of different fibre alignments and bioactive coatings on mesenchymal stem/stromal cell adhesion, proliferation and chondrogenesis in poly (ε-caprolactone) scaffolds"*

5th Advanced Course on Regenerative Medicine, Center for Rapid and Sustainable Product Development – Polytechnic Institute of Leiria, Marinha Grande – Portugal, 11th December 2015, **J.C. Silva**, C.S Moura, J.M.S. Cabral, R.J. Linhardt and F.C. Ferreira, *"Integrated approach combining mesenchymal stem cells, hierarchical scaffolds and bioreactors for cartilage repair"*

Soft Matter in Biomedicine, Lisboa, Portugal, 12th October 2018, **J.C. Silva**, C.S. Moura, G. Borrecho, A. Alves de Matos, J.M.S. Cabral, R.J. Linhardt and F.C. Ferreira, *"Extruded scaffolds and perfusion bioreactors to study shear stress stimuli in cartilage tissue engineered constructs"*

cMDIS Fall Symposium, New York, USA, 7th December 2018, F.F. Garrudo, C. Chapman, P. Hoffman, **J.C. Silva**, R.N. Udangawa, P.E. Mikael, C.A.V. Rodrigues, J.M.F. Morgado, F.C. Ferreira and R.J. Linhardt, *"Conductive Polyaniline-PCL fibers for neuron regeneration"*

Poster Communications

26th Annual Meeting of the European Orthopaedic Research Society (EORS 2018), Galway, Ireland, 25th-28th September 2018, **J.C. Silva**, X. Han, P.E. Mikael, K. Xia, J.M.S. Cabral, F.C. Ferreira and R.J. Linhardt, *"Glycosaminoglycan disaccharide changes during chondrogenic differentiation of human bone marrow/synovial-derived mesenchymal stem cells under different oxygen tensions"*

26th Annual Meeting of the European Orthopaedic Research Society (EORS 2018), Galway, Ireland, 25th-28th September 2018, **J.C. Silva**, M.S. Carvalho, R.N. Udangawa, C.S. Moura, J.M.S. Cabral, C.L. da Silva, F.C. Ferreira, D. Vashishth and R. J. Linhardt, *"Extracellular matrix decorated porous polycaprolactone scaffolds for bone tissue engineering"*

Biomedical Engineering Society Annual Meeting (BMES 2018), Atlanta-Georgia, USA, 17th-20th October 2018, F.F. Garrudo, C. Chapman, R.N. Udangawa, **J.C. Silva**, P. Hoffman, P.E. Mikael, C.A.V. Rodrigues, J.M.S. Cabral, J.M.F. Morgado, F.C. Ferreira and R.J. Linhardt, *"Conductive PCL-PANI fibers for neural tissue regeneration"*

254th American Chemical Society National Meeting & Exposition, Washington, DC, 20th-24th August 2017, **J.C. Silva**, C.S. Moura, G. Borrecho, A.P. Alves de Matos, J.M.S. Cabral, R.J. Linhardt and F.C. Ferreira, *"Effects of chondroitin sulfate and hyaluronic acid supplementation in the chondrogenic differentiation of bone-marrow derived mesenchymal stem cells on poly (ε-caprolactone) scaffolds towards cartilage repair"*

254th American Chemical Society National Meeting & Exposition, Washington, DC, 20th-24th August 2017, F.F. Garrudo, Y. Yu, **J.C. Silva**, P.E. Mikael, C.A.V. Rodrigues, F.C. Ferreira and R.J. Linhardt, *"Glycosaminoglycan profile change in differentiating ReN-VM cells"*

2nd International Congress of CiiEM – Translational Research and Innovation in Human and Health Sciences, Monte da Caparica-Portugal, 11th-13th June 2017, **J.C. Silva**, C.S. Moura, G. Borrecho, P. Henriques, A.P. Alves de Matos, J.M.S. Cabral, R.J. Linhardt and F.C. Ferreira, *"Mesenchymal stem cells combined with 3D extruded scaffolds and glycosaminoglycan supplementation as an integrated strategy towards cartilage repair: biochemical, structural and morphological analysis"*

European Chapter Meeting of the Tissue Engineering and Regenerative Medicine International Society (TERMIS –EU 2016), Uppsala, Sweden, 28th June-1st July 2016, **J.C. Silva**, C.S. Moura, T. Viana, J.M.S. Cabral and F.C. Ferreira, *"Poly (ε-caprolactone) scaffolds combined with extruded perfusion bioreactor prototypes as an integrated platform for articular cartilage tissue engineering"*

Meeting of the Portuguese Society for Neuroscience SPN 2019, Lisboa-Portugal, 30th May-01st June 2019, F.F. Garrudo, P.E. Mikael, R.N. Udangawa, C.A. Chapman, P. Hoffman, **J.C. Silva**, C.A.V. Rodrigues, J.M.S. Cabral, J.M.F. Morgado, F.C. Ferreira and R.J. Linhardt, *"Harnessing electricity for neural stem cells"*

IST PhD Open Days, Instituto Superior Técnico, Lisboa – Portugal, 9th-12th November 2015, **J.C. Silva**, *"Hierarchical scaffolds integrated with extruded bioreactors for cartilage repair"*

Conference Abstracts in Peer-Reviewed International Scientific Journals

J.C. Silva, C.S. Moura, G. Borrecho, A.P. Alves de Matos, J.M.S. Cabral, R.J. Linhardt and F. C. Ferreira, “Extruded perfusion bioreactor: a versatile custom-made platform to study shear stress in cartilage tissue engineered constructs”, ***Orthopaedic Proceedings*** 100-B: Suppl. 15, page 111, 2018, (doi: 10.1302/1358-992X.2018.15.111).

J.C. Silva, C.S. Moura, G. Borrecho, P. Henriques, A.P. Alves de Matos, J.M.S. Cabral, R.J. Linhardt and F.C. Ferreira, "Mesenchymal stem cells combined with 3D extruded scaffolds and glycosaminoglycan supplementation as an integrated strategy towards cartilage repair: biochemical, structural and morphological analysis", ***Annals of Medicine*** 50, page S51, 2018, (doi: abs/10.1080/07853890.2018.1427445).

J.C. Silva, C.S. Moura, T. Viana, J.M.S. Cabral and F.C. Ferreira, "Poly (ε-caprolactone) scaffolds combined with extruded perfusion bioreactor prototypes as an integrated platform for articular cartilage tissue engineering", ***European cells & materials*** 31 Suppl. 1, page P101, 2016.

Articles in Peer-Reviewed International Scientific Journals

J.C. Silva, M.S. Carvalho, X. Han, K. Xia, P.E. Mikael, J.M.S. Cabral, F.C. Ferreira and R.J. Linhardt, “Compositional and structural analysis of glycosaminoglycans in cell-derived extracellular matrices”*,* ***Glycoconjugate Journal***, 36, 141-154 2019, (doi: 10.1007/s10719-019-09858-2).

M.S. Carvalho*, **J.C. Silva***, R.N. Udangawa, J.M.S. Cabral, F.C. Ferreira, C.L. da Silva, R.J. Linhardt and D. Vashishth, “Co-culture cell-derived extracellular matrix loaded electrospun microfibrous scaffolds for bone tissue engineering”*,* ***Materials Science and Engineering: C***, 99, 479-490, 2019, (doi: 10.1016/j.msec.2019.01.127), *These authors contributed equally.

J.C. Silva, C.S. Moura, N.M. Alves, J.M.S. Cabral and F.C. Ferreira, “Effects of different fibre alignments and bioactive coatings on mesenchymal stem/stromal cell adhesion and proliferation in poly (ε-caprolactone) scaffolds towards cartilage repair”, ***Procedia Manufacturing***, 12, 132-140, 2017, (doi: 10.1016/j.promfg.2017.08.034).

F.F. Garrudo, C.A. Chapman, P. Hoffman, R. N. Udangawa, **J.C. Silva**, P.E. Mikael, C.A.V. Rodrigues, J.M.S. Cabral, J.M.F. Morgado, F.C. Ferreira and R.J. Linhardt, “Polyaniline-polycaprolactone blended nanofibers for neural cell culture”, ***European Polymer Journal***, 117, 28-37, 2019, (doi: 10.1016/j.eurpolymj.2019.04.048).

M.S. Carvalho, **J.C. Silva**, J.M.S. Cabral, C.L. da Silva and D. Vashishth, “Cultured cell-derived extracellular matrices to enhance the osteogenic differentiation and angiogenic properties of human mesenchymal stem/stromal cells”, ***Journal of Tissue Engineering and Regenerative Medicine***, 13, 1544-1558, 2019, (doi: 10.1002/term.2907).

J.C. Silva, C.S. Moura, G. Borrecho, A.P. Alves de Matos, C.L. da Silva, J.M.S. Cabral, P.J. Bártolo, R.J. Linhardt and F.C. Ferreira, "Extruded bioreactor perfusion culture supports the chondrogenic differentiation of human mesenchymal stem/stromal cells in 3D porous poly (ε-caprolactone) scaffolds", ***Biotechnology Journal*** (accepted, in press).

F.F. Garrudo, R.N. Udangawa, P. Hoffman, L. Sordini, C.A. Chapman, P.E. Mikael, F.A. Ferreira, **J.C. Silva**, C.A.V. Rodrigues, J.M.S. Cabral, J.M.F. Morgado, F.C. Ferreira and R.J. Linhardt, "Polybenzimidazole nanofibers for neural stem cell culture", ***Materials Today Chemistry*** (accepted, in press).

J.C. Silva, C.S. Moura, G. Borrecho, A.P. Alves de Matos, J.M.S. Cabral, R.J. Linhardt and F.C. Ferreira, "Effects of glycosaminoglycan supplementation in the chondrogenic differentiation of bone marrow- and synovial-derived mesenchymal stem/stromal cells on 3D-extruded poly (ε-caprolactone) scaffolds", (submitted to *International Journal of Polymeric Materials and Polymeric Biomaterials*).

J.C. Silva*, M.S. Carvalho*, R.N. Udangawa, C.S. Moura, J.M.S. Cabral, C.L. da Silva, F.C. Ferreira, D. Vashishth and R.J. Linhardt, "Extracellular matrix decorated polycaprolactone scaffolds for improved mesenchymal stem/stromal cell osteogenesis: A patient-tailored bone tissue engineering approach", (submitted to *Journal of Biomedical Materials Research: Part B-Applied Biomaterials*), *These authors contributed equally.

J.C. Silva, X. Han, T.P. Silva, K. Xia, P.E. Mikael, J.M.S. Cabral, F.C. Ferreira and R.J. Linhardt, "Glycosaminoglycan remodeling during chondrogenic differentiation of human bone marrow / synovial-derived mesenchymal stem/stromal cells under normoxia and hypoxia", (submitted to *Journal of Cellular Biochemistry*).

J.C. Silva, R.N. Udangawa, J. Chen, C.D. Mancinelli, F.F. Garrudo, P.E. Mikael, J.M.S. Cabral, F.C. Ferreira and R.J. Linhardt, "Kartogenin-loaded coaxial PGS/PCL aligned nanofibers for cartilage tissue engineering", (submitted to *Materials Science and Engineering: C*).

M.S. Carvalho, **J.C. Silva**, C. Hoff, J.M.S. Cabral, R.J. Linhardt, C.L. da Silva and D. Vashishth, "Loss and rescue of osteocalcin and osteopontin regulate mesenchymal stem/stromal cell osteogenesis and angiogenic potential", (submitted to *Journal of Cellular Physiology*).

C.S. Moura, **J.C. Silva**, S. Faria, P.R. Fernandes, C.L. da Silva, J.M.S. Cabral, R.J. Linhardt, P.J. Bártolo and F.C. Ferreira, "Chondrogenic differentiation of mesenchymal stem/stromal cells on 3D porous poly (ε-caprolactone) scaffolds: effects of material alkaline treatment and chondroitin sulfate supplementation", (submitted to *Journal of Bioscience and Bioengineering*).

J.C. Silva, C.D. Mancinelli, R.N. Udangawa, M. Sorci, K. Xia, F. Zhang, F.C. Ferreira and R.J. Linhardt, "Fabrication of low molecular weight heparin-loaded porous polycaprolactone nanofibers for tissue engineering applications", (in preparation).

APPENDIX - Effects of different fiber alignments and bioactive coatings on mesenchymal stem/stromal cell adhesion and proliferation in poly (ε-caprolactone) scaffolds towards cartilage repair

Throughout this thesis, we used 3D extruded PCL scaffolds as a support platform to induce MSC chondrogenic (Chapters IV and VIII) and osteogenic (Chapter VI) differentiation. Herein, we provide a preliminary study of the effects of scaffold fiber alignment and of the use bioadhesive coatings on MSC adhesion and proliferation in PCL scaffolds.

Outline

In this work, 3D biodegradable PCL scaffolds with high porosity and interconnectivity were produced by extrusion and characterized in terms of their structural and mechanical properties. The effects of scaffold fiber alignment (0-45º and 0-90º) and of different adhesive coatings (Fibronectin, Gelatin and commercially available CellStart™) on hBMSCs adhesion, migration and proliferation were evaluated using AlamarBlue™ assay. Fibronectin and CellStart™ coated PCL scaffolds presented an improvement in cell adhesion of approximately 2-fold relatively to the non-treated scaffolds, independently of fiber alignment. In overall, all the conditions studied promoted hBMSCs growth and migration on the fabricated PCL scaffolds, without affecting their chondrogenic differentiation and extracellular matrix deposition.

A.1. Introduction

As a result of the lack of effective treatments for cartilage lesions caused by trauma or by the action of degenerative diseases such as osteoarthritis and rheumatoid arthritis, Tissue Engineering (TE) strategies combining cells and biomaterial scaffolds, are gaining notoriety as they carry the promise of generating mature and functional tissue with appropriate structure and mechanical properties (Vinatier et al., 2009). In terms of cell source, stem cells, particularly MSC have been widely used in cartilage TE strategies (Tan et al., 2017; Fellows et al., 2016).

The emergence of Additive Manufacturing (AM) techniques, such as fused deposition modeling (FDM)/melt extrusion, a technique used in this work, was quite important to foster many successful developments in regenerative medicine field, particularly for cartilage TE. AM techniques offered the possibility of producing tailor-made scaffolds in a rapid and controlled manner with the desired size, shape and architecture to completely fit in the

patient's defect site (Melchels et al., 2012). The application of AM techniques to TE approaches mainly consists in acquiring data of the anatomical structure that needs repair to generate a 3D CAD model of both the anatomical structure and of the biomaterial scaffold designed to be placed in patient's defect site. Then, the scaffold is manufactured and seeded with cells, and afterwards implanted into the patient to promote tissue regeneration (Mota et al., 2015). FDM or melt extrusion is a commercially available AM technique, in which thin thermoplastic filaments or granules are melted by heating and guided by a robotic device with computer-controlled motion, to generate the 3D object. In this process, the material leaves the extruder in a hot liquid form and solidifies immediately upon cooling on the top of the previously formed layer. Therefore, each layer works as substrate for the next layer and must be maintained at a temperature just below the solidification point of the thermoplastic material to assure good interlayer adhesion (Melchels et al., 2012; Murphy et al., 2014). AM technologies often use synthetic polymeric materials, such as PCL, which was used in this study. PCL is a linear aliphatic polyester with a low melting point (≈60ºC) and a high thermal stability over 350ºC (Domingos et al., 2012). Therefore, this thermoplastic polymer is easy to process, chemically versatile and structurally stable, reasons that make PCL a suitable material for the manufacturing of 3D TE scaffolds with a highly interconnected pore network. Additionally, PCL is also a biodegradable and biocompatible material, previously approved by the FDA for the production of *in vivo* medical and drug carrier devices (Domingos et al., 2012; van Uden et al., 2015).

Cell adhesion to the biomaterial scaffold structure is the initial requirement for any TE strategy (Camarero-Espinosa et al., 2016). However, as AM techniques usually employ the use of synthetic materials lacking bioadhesive sites, lower cell attachments may occur and compromise the success of the procedure. Several approaches have been used to enhance cell adhesion to PCL scaffolds, including changing scaffold porosity (Salerno et al., 2016) and pore size (Phipps et al., 2012; Moura et al., 2015), controlling fiber orientation (Chang et al., 2013) and using surface modification approaches such as coating the scaffold structure with extracellular matrix (ECM) molecules containing cell-binding motifs (Guariano et al., 2011; Yeo et al., 2012; Chen et al., 2014). In contrast, chondrogenic differentiation requires MSC condensation, which can be inhibit by materials that promote too much cell stretching upon their adhesion to scaffolds, implying that a compromise between cell adhesion and condensation is required for TE cartilage repair strategies (Ng et al., 2017).

The objective of this work was to study the effect of different PCL scaffold fiber alignments (0-45º/0-90º) and of different standard cell culture bioadhesive coatings in promoting hBMSC adhesion and proliferation towards the development of an optimized and integrated TE strategy for cartilage regeneration.

A.2. Materials & Methods

A.2.1. PCL scaffold fabrication and characterization

PCL (MW 50.000 Da, Sigma-Aldrich) scaffolds with both fiber orientations (0-45º and 0-90º) were produced by FDM using a Bioextruder machine as previously described (Moura et al., 2015; Silva et al., 2016). The scaffolds were then structurally characterized by scanning electron microscopy (SEM, Hitachi model S2400) and by micro-computed tomography analysis (μ-CT, Scansky 1174v2, Brucker version 1.1). For SEM analysis, scaffold samples were coated with a 45 nm gold/palladium layer using a sputter coater (Quorum Technologies model E5100). PCL scaffolds of both architectures with dimensions 5 mm x 5 mm x 3 mm were also assessed in terms of their mechanical properties under compressive testing using an Instron (model 5544) machine equipped with a 2 kN load cell and a 50 mm diameter cylindrical compression plate and operating with an extension rate of 1 mm/min. For each scaffold configuration, 5 scaffold samples were tested. The results of the tests were then analyzed using the Bluehill® 3 software. The Young's/compressive modulus of elasticity was calculated by the slope of the initial linear region of the stress-strain curve, in which the compressive stress is defined as the compressive load per unit area of the minimal original cross section carried by the test specimen at any given moment and the compressive strain corresponds to the change in length per unit of original length along the longitudinal axis.

A.2.3. PCL scaffold coating and wettability/contact angle assessment

PCL scaffolds of both configurations were firstly sterilized (12 h UV treatment and ethanol 70% (v/v, Merck) washing) and then submitted to the different surface modification protocols by completely submersing the samples in the respective adhesive coating solutions: (i) human-derived Fibronectin 5 μg/mL (Sigma-Aldrich) solution in Phosphate buffered saline (PBS, Gibco) for 1 h at 37ºC; (ii) Gelatin 0.2% w/v (Sigma-Aldrich) solution in PBS for 1 h at 37ºC; and (iii) CellStart™ 1:200 diluted (Life Technologies) solution in PBS for 1 h at 37ºC). The scaffold samples were coated right before the cell culture studies or otherwise maintained at 4ºC until usage. Wettability was measured by the contact angle, which is defined by the intersection of the liquid-solid interface. When the contact angle is lower than 90º the material is considered hydrophilic while above 90º is hydrophobic. To study the effect of the different surface coatings on PCL's wettability, films were produced by dissolving PCL in chloroform (Merck) and by promoting solvent evaporation overnight inside a chemical flow hood. Afterwards, PCL films were treated with the different coating solutions and the contact angle was measured using a DSA25B goniometer (Krüss) at 2 different time points (t = 0 sec and t = 30 sec). For that, a sessile drop of distilled water was added on the top of the films

and the results were analyzed using the software Drop Shape Analysis 4 version 2.1. For each condition, 5 measurements were performed.

A.2.3. hBMSC seeding and culture on PCL scaffolds

For the in vitro cell culture studies, $6x10^4$ hBMSCs (passage 5) were seeded on the top of each sterile and coated PCL scaffold, which were previously placed in a 24-well ultra-low attachment plate (VWR). Cells were left to incubate at 37ºC/5% CO_2 for 90 min in order to promote initial cell adhesion. Afterwards, culture medium was added to completely immerse the scaffold. These cultures were composed by 2 stages: an expansion phase during the first 2 weeks followed by a chondrogenic differentiation phase for 3 weeks. During the expansion stage, scaffolds were cultured in Dulbecco's modified Eagle's medium (DMEM, Gibco) with 10% fetal bovine serum (FBS, Life Technologies), and 1% antibiotic-antimycotic (Anti-Anti, Gibco) solution, while during chondrogenesis, scaffold samples were cultured using the StemPro Chondrogenesis Differentiation kit (Gibco) and 1% anti-anti solution. Throughout all the experiment, medium was fully replaced each 3-4 days and all samples were cultured inside an incubator under hypoxic conditions (37ºC/5% CO_2 and 5% O_2) to promote MSC chondrogenic differentiation.

A.2.4. Evaluation of hBMSCs adhesion, proliferation and chondrogenic differentiation

Cell adhesion (Day 1 after seeding) and cell proliferation (Days 1, 7, 14, 21, 28 and 35) were assessed using the AlamarBlue™ indirect cell quantification assay (AB, Invitrogen), following the manufacturer's guidelines. Briefly, scaffold samples were incubated 2.5 h in an AB solution (1:10 v/v diluted in culture media), and afterwards, the fluorescence intensity was measured in a multiplate fluorometer (Infinite 200 PRO, TECAN) with an excitation wavelength of 560 nm and an emission wavelength of 590 nm. Cell quantification is reported as equivalent cell numbers, which were estimated through correlation between 590 nm light absorbance fluorescence intensity values with counted cells cultivated in standard tissue culture polystyrene well plates (BD falcon). Note that cell proliferation during the first day of culture could also contribute to report "cell adhesion" percentages, considering that the population doubling time for MSC was observed to occur at values higher than 24 h (Baksh et al., 2007).

At the end of the experiment (Day 35), PCL scaffolds were dehydrated using an ethanol gradient solution treatment (20%/40%/60%/90% and 96% v/v for 30 min each) and analyzed by SEM as described above. Additionally, the chondrogenic differentiation of hBMSCs in the different conditions was assessed by Alcian Blue (Sigma-Aldrich) staining, which labels sulfated glycosaminoglycans (sGAG). For that, samples were washed once with PBS, fixed

with 2% PFA for 20 min and incubated with a 1% Alcian Blue solution (in 0.1N HCl) for 1 h. Afterwards, scaffolds were rinsed twice with PBS, washed once with distilled water and observed under a light microscope (LEICA® DMI3000B).

A.2.5. Statistical analysis

Data are presented as mean ± standard deviation (SD). The statistical analysis was performed using the analytical features of GraphPad Prism 7. Statistical significant differences between two independent sets of samples (conditions) were assessed by an unpaired t-test, in which p-value represents the probability that the null hypothesis is true, in the particular case the null hypothesis is the values compared to be similar to each other, considering that measured values follow a Gaussian distribution. Statistically significant values were considered for p-value < 0.05 (*p <0.05, **p <0.01 and ***p <0.001). For the cell culture studies, triplicates of each condition were used (same donor). In the mechanical testing and contact angle measurements, 5 samples of each condition were used.

A.3. Results & Discussion

PCL scaffolds (Figure A.1-A) with different fiber alignments (0-45º and 0-90º) were fabricated by extrusion and their structure was characterized by SEM (Figure A.1-B) and by µ-CT (Figure A.1-C). Using µ-CT analysis, important scaffold features such as porosity, interconnectivity and surface area to volume ratio were estimated (Table A.1). Both scaffold configurations presented high interconnectivities, which is of great importance for efficient nutrient supply and waste removal in a TE strategy.

Table A.1. Properties of PCL scaffolds estimated by µ-CT analysis.

Scaffold features	***0-45º***	***0-90º***
Porosity (%)	52.4	56.6
Surface area to volume ratio (mm^{-1})	22.7	21.2
Interconnectivity (%)	98.8	99.7

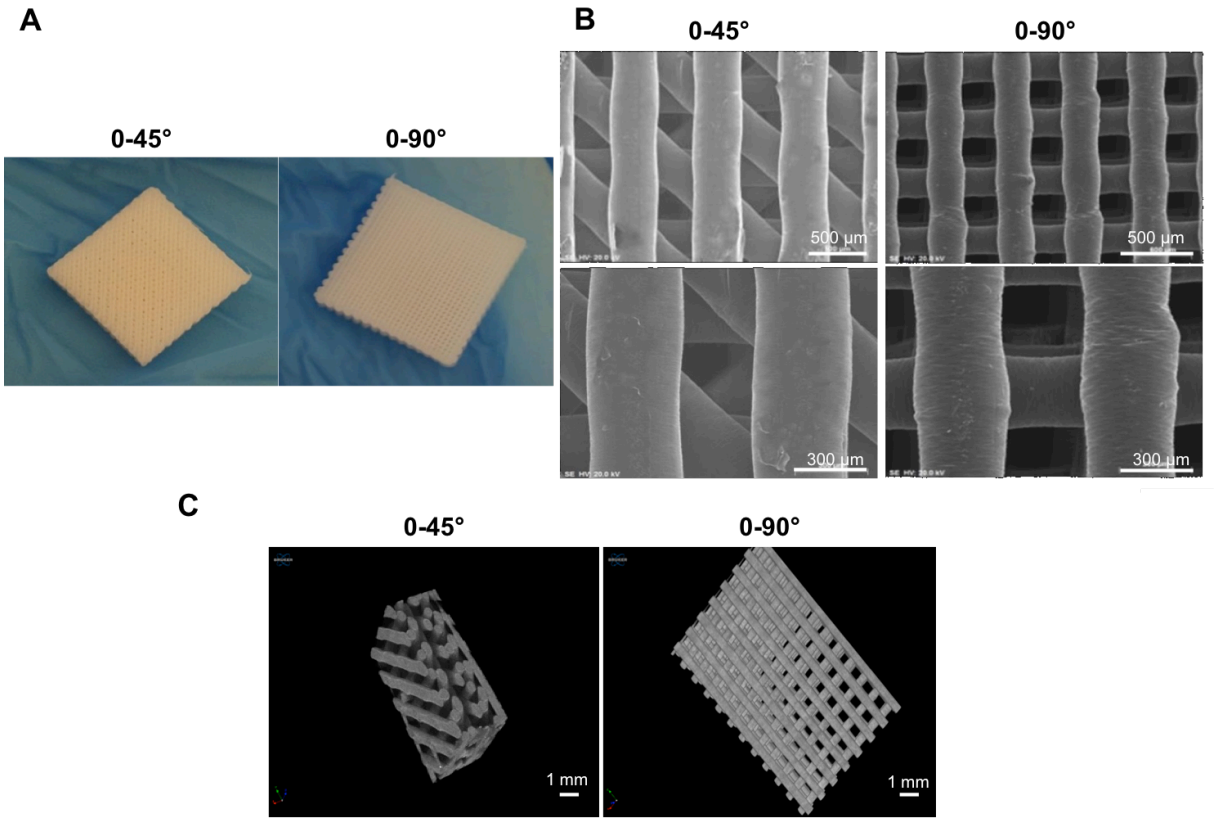

Figure A.1. Characterization of PCL scaffolds fabricated with different fiber orientations (0-45º and 0-90º). Gross view of the scaffolds (A). SEM (B) and 3D reconstructed µ-CT images (C) of scaffolds with different fiber alignments. Scale bars are depicted in the image.

The manufactured scaffolds were also characterized in terms of their mechanical properties (Young's compressive modulus) under compressive testing in the apparatus shown in Figure A.2-A. As represented in Figure A.2-B, PCL scaffolds with 0-45º angle between fibers present slightly higher compressive modulus (35 ± 3 MPa) compared to 0-90º PCL scaffolds (30 ± 1 MPa), which may be explained by their lower porosity.

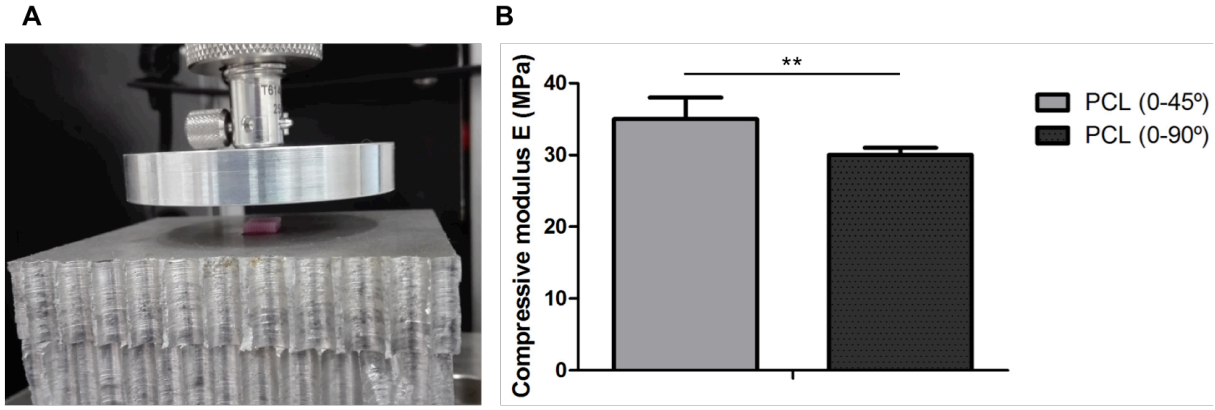

Figure A.2. Compressive mechanical testing of PCL scaffolds with different fiber alignments (0-45º/0-90º): experimental apparatus (A) and compressive modulus (B); n=5; ** p<0.01.

The effect of the different surface coatings on PCL material wettability was studied by measuring the water contact angle in PCL films (Figure A.3). The untreated PCL films presented a contact angle superior to 90º, which corresponds to a hydrophobic behaviour as previously reported in the literature (Ku et al., 2010). After treatment with the different bioadhesive coatings, all the conditions promoted a decrease in the contact angle for values lower than 90º, making the scaffold surface hydrophilic, which may lead to higher cell adhesions. Such effect was significantly more evident when Fibronectin and CellStart™ coatings were used.

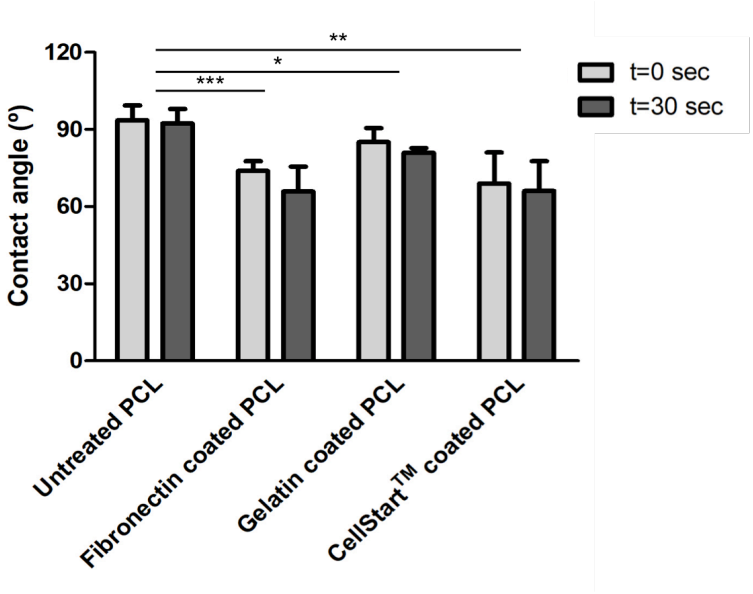

Figure A.3. Contact angle values for the different surface coatings studied in PCL films; n=5; *p<0.05, **p<0.01, ***p<0.001 relative to untreated PCL.

The percentage of hBMSCs adhesion (Figure A.4) to both PCL scaffold configurations treated with the different surface coatings was evaluated at day 1 by calculating the ratio between the number of viable equivalent cells in the scaffold (estimated indirectly using the AlamarBlue™ assay) and the number of cells seeded at the beginning of the experiment. Fibronectin and CellStart™ treatments promoted a statistically significant improvement in cell adhesion of approximately 2-fold relatively to the untreated PCL samples for both fiber alignments. However, when the Gelatin coating was used no significant improvement was noticed. These findings are coherent with the results shown in Figure A.4, as lower contact angles (more hydrophilic material) often correspond to higher cell adhesions. Moreover, no significant differences in cell adhesion were observed between scaffolds with different fiber alignments submitted to the same coating protocol.

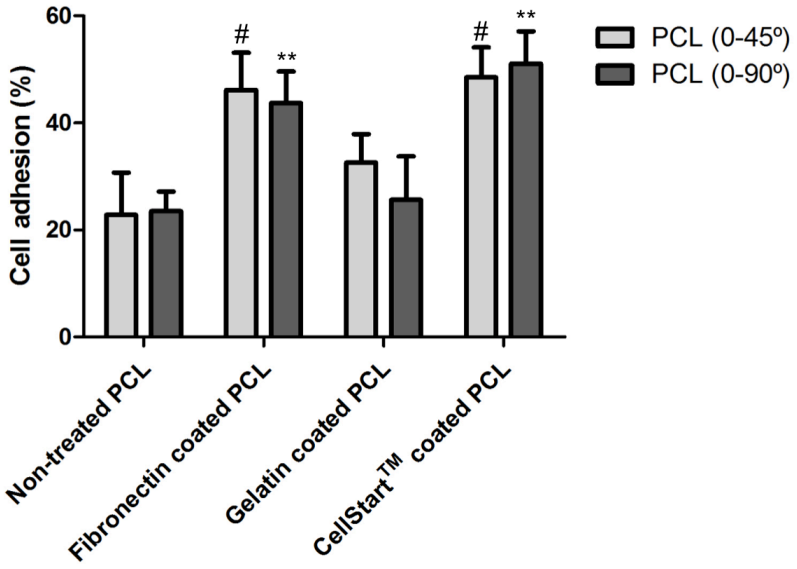

Figure A.4. hBMSCs adhesion to PCL scaffolds treated with different surface coatings; n=3; ** $p<0.01$, relative to untreated PCL (0-90º) and # $p<0.05$ relative to untreated PCL (0-45º).

Concerning the cell proliferation studies (Figure A.5), all the conditions tested supported hBMSC growth throughout the culture period. In the case of the 0-45º PCL scaffolds (Figure A.5-A), no relevant differences were observed in the final cell numbers for the different surface coatings tested. Regarding the 0-90º PCL scaffolds (Figure A.5-B), Fibronectin coated samples presented a noticeable higher final number of cells per scaffold compared to the remaining conditions. As it is possible to observe in Figure A.4 and Figure A.5, higher initial cell adhesions did not result necessarily in higher final equivalent cell numbers at the end of the culture. An explanation for this may be related with the long culture period employed in this work (35 days), in which the hBMSC were capable of recover from lower cell attachments and proliferate to populate the whole scaffold structure. However, for shorter *ex vivo* culture periods, a high initial cell adhesion to the scaffold structure might be crucial for the success of the TE strategy.

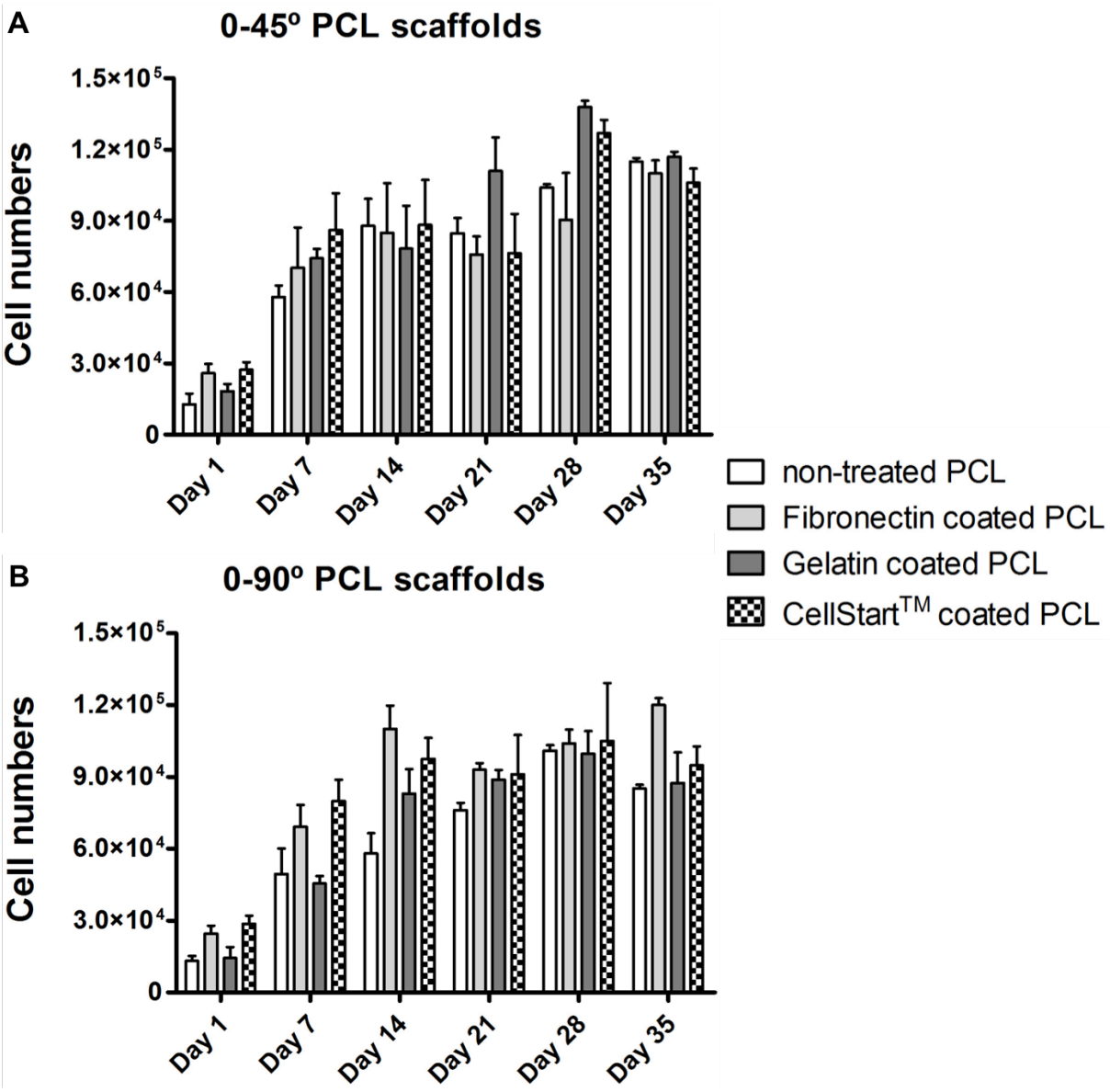

Figure A.5. hBMSC equivalent numbers (Alamar Blue assay) throughout 5 weeks of culture (expansion during the first 2 weeks followed by chondrogenic differentiation for 3 weeks) in 0-45º (A) and 0-90º (B) PCL scaffolds treated with different adhesive surface coatings; n=3.

At the end of the experiment, all hBMSC-PCL constructs were imaged by SEM (Figure A.6) and assessed for chondrogenic differentiation using the Alcian Blue staining protocol (Figure A.7). As it is possible to observe in Figure A.7, all the conditions stained positive for sGAG, major components of cartilage tissue. Further studies including RT-qPCR analysis of chondrogenic gene markers and histological/immunohistochemistry assessment of the final tissue-constructs will be required for a more complete evaluation of the effects of the scaffold fiber alignments and surface adhesive coatings studied on MSC chondrogenic potential.

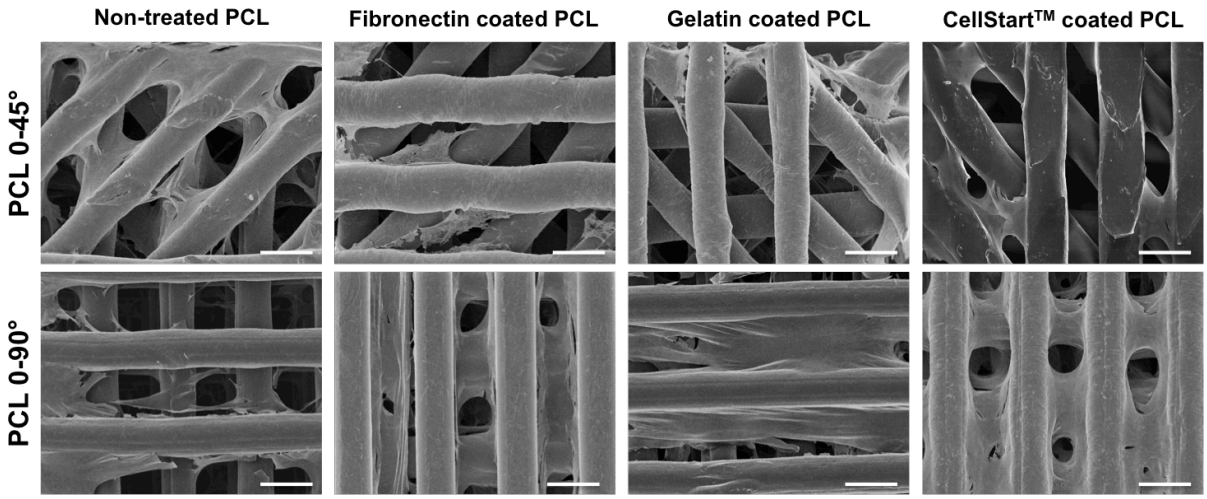

Figure A.6. SEM analysis (at the end of the experiment) of hBMSC-PCL tissue constructs obtained with the different scaffold fiber orientations and adhesive surface coatings. Scale bars: 500 μm.

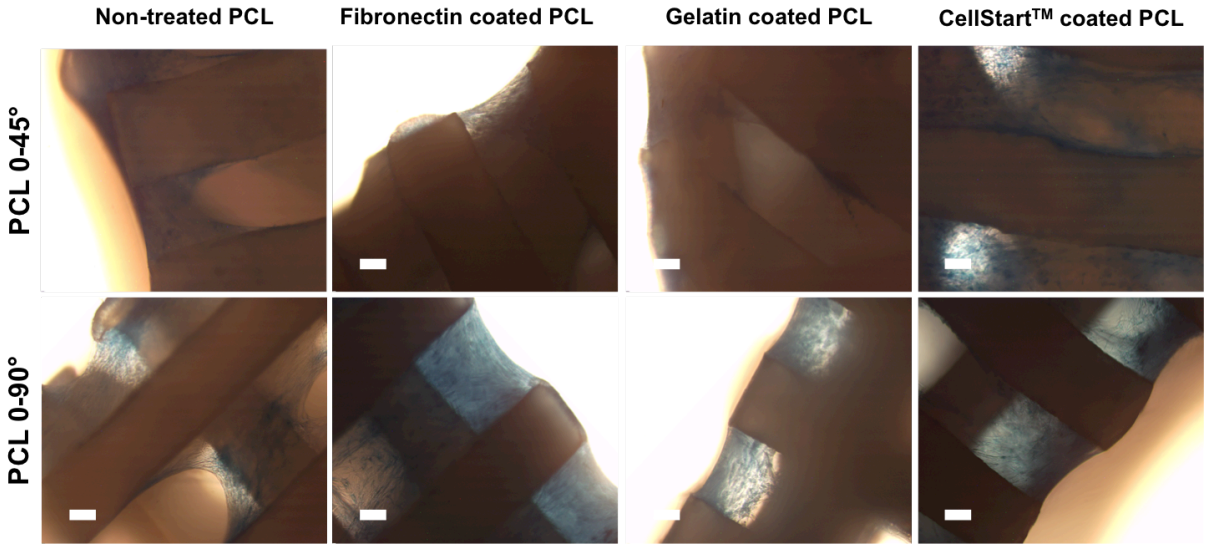

Figure A.7. Alcian Blue staining (at the end of the experiment) identifying the presence of sGAG in the hBMSC-PCL tissue constructs obtained with the different scaffold fiber orientations and adhesive surface coatings. Scale bars: 100 μm.

In conclusion, 3D highly interconnected PCL scaffolds with two different fiber alignments (0-45º and 0-90º) were successfully fabricated and characterized in terms of their structural and mechanical properties. With the objective of enhancing hBMSC adhesion to the produced PCL scaffolds, three different standard coatings containing adhesive proteins/motifs were tested. Cell adhesion to PCL scaffolds was increased by approximately 2-fold relatively to the untreated condition by using Fibronectin and CELLstart™ coating protocols, independently of the scaffold architecture. These results seemed to be correlated with the ones obtained after contact angle assessment of the coated and untreated PCL material, as more hydrophilic samples (lower contact angle) correspond to higher cell adhesions in the *in vitro* culture studies. However, such correlation between improved

adhesion and lower contact angle was not observed for gelatin coating suggesting that specificity of the biological motives also play a role in mediating cell adhesion. Despite the differences observed in the initial cell adhesion, all the conditions tested supported hBMSC proliferation, migration and chondrogenic differentiation.

A.4. References

Baksh, D., Yao, R., Tuan, R.S., (2007). Comparison of Proliferative and Multilineage Differentiation Potential of Human Mesenchymal Stem Cells Derived from Umbilical Cord and Bone Marrow, Stem Cells. 25, 1384–1392.

Camarero-Espinosa, S., Cooper-White, J., (2017). Tailoring Biomaterial Scaffolds for Osteochondral Repair. Int. J. Pharm. 532, 476–489.

Chang, J.C., Fujita, S., Tonami, H., Kato, K., Iwata, H., Hsu, S., (2013). Cell orientation and regulation of cell-cell communication in human mesenchymal stem cells on different patterns of electrospun fibers. Biomed. Mater. 8, 055002.

Chen, C.H., Lee, M.Y., Shyu, V.B.H., Chen, Y.C., Chen, C.T., Chen, J.P., (2014). Surface modification of polycaprolactone scaffolds fabricated via selective laser sintering for cartilage tissue engineering, Mater. Sci. Eng. C. 40, 389–397.

Domingos, M., Chiellini, F., Gloria, A., Ambrosio, L., Bartolo, P., Chiellini, E., (2012). Effect of process parameters on the morphological and mechanical properties of 3D Bioextruded poly(ε-caprolactone) scaffolds. Rapid Prototyp. J. 18, 56–67.

Fellows, C.R., Matta, C., Zakany, R., Khan, I.M., Mobasheri, A., (2016). Adipose, Bone Marrow and Synovial Joint-Derived Mesenchymal Stem Cells for Cartilage Repair. Front. Genet. 7, 1–20.

Guarino, V., Alvarez-Perez, M., Cirillo, V., Ambrosio, L., (2011). hMSC interaction with PCL and PCL/gelatin platforms: A comparative study on films and electrospun membranes, J. Bioact. Compat. Polym. 26, 144–160.

Ku, S.H., Park, C.B., (2010). Human endothelial cell growth on mussel-inspired nanofiber scaffold for vascular tissue engineering, Biomaterials. 31, 9431–9437.

Melchels, F.P.W., Domingos, M.A.N., Klein, T.J., Malda, J., Bartolo, P.J., Hutmacher, D.W., (2012). Additive manufacturing of tissues and organs. Prog. Polym. Sci. 37, 1079–1104.

Mota, C., Puppi, D., Chiellini, F., Chiellini, E., (2015). Additive manufacturing techniques for the production of tissue engineering constructs. J. Tissue Eng. Regen. Med. 9, 174–190.

Moura, C.S., Da Silva, C.L., Bártolo, P.J., Ferreira, F.C., (2015). Combination of 3D extruded-based poly (ε-caprolactone) scaffolds with mesenchymal stem/stromal cells: Strategy optimization. Procedia Eng. 110, 122–127.

Murphy, S.V., Atala, A., (2014). 3D bioprinting of tissues and organs. Nat. Biotechnol. 32, 773–785.

Ng, J.J., Wei, Y., Zhou, B., Bernhard, J., Robinson, S., Burapachaisri, A., Guo, X.E., Vunjak-Novakovic, G., (2017). Recapitulation of physiological spatiotemporal signals promotes in vitro formation of phenotypically stable human articular cartilage. Proc. Natl. Acad. Sci. 114, 2556–2561.

Phipps, M.C., Clem, W.C., Grunda, J.M., Clines, G.A., Bellis, S.L., (2012). Increasing the pore sizes of bone-mimetic electrospun scaffolds comprised of polycaprolactone, collagen I and hydroxyapatite to enhance cell infiltration. Biomaterials. 33, 524–534.

Salerno, A., Guarnieri, D., Iannone, M., Zeppetelli, S., Netti, P.A., (2010). Effect of micro- and macroporosity of bone tissue three-dimensional-poly(epsilon-caprolactone) scaffold on human mesenchymal stem cells invasion, proliferation, and differentiation in vitro. Tissue Eng. Part A. 16, 2661–2673.

Silva, J.C., Moura, C.S., Viana, T., Cabral, J.M.S., Ferreira, F.C., (2016). Poly (ε-caprolactone) scaffolds combined with extruded perfusion bioreactor prototypes as an integrated platform for articular cartilage tissue engineering. Eur. Cell. Mater. 31, P125.

Tan, A.R., Hung, C.T., (2017). Concise review: Mesenchymal stem cells for functional cartilage tissue engineering: taking cues from chondrocyte-based constructs. Stem Cells Transl. Med. 6, 832–842.

van Uden, S., Silva-Correia, J., Correlo, V.M., Oliveira, J.M., Reis, R.L., (2015). Custom-tailored tissue engineered polycaprolactone scaffolds for total disc replacement. Biofabrication. 7, 015008.

Vinatier, C., Mrugala, D., Jorgensen, C., Guicheux, J., Noël, D., (2009). Cartilage engineering: a crucial combination of cells, biomaterials and biofactors. Trends Biotechnol. 27, 307–314.

Yeo, M.G., Kim, G.H., (2012). Preparation and characterization of 3D composite scaffolds based on rapid-prototyped PCL/β-TCP struts and electrospun PCL coated with collagen and HA for bone regeneration. Chem. Mater. 24, 903–913.